DNA-mediated Charge Transport in DNA Repair

Thesis by
Amie Kathleen Boal

In Partial Fulfillment of the Requirements for the Degree of Doctor of Philosophy

California Institute of Technology
Pasadena, California
2008
(Defended May 1, 2008)

ACKNOWLEDGEMENTS

I must first acknowledge my research advisor, Prof. Jacqueline Barton. Jackie, without your guidance and inspiration, none of this work would have been possible. It has been incredibly exciting to work on these projects and I have really appreciated your passion and enthusiasm for them and for all of the science that goes on in your lab. I have learned so much in the time that I've been here, not the least of which how to be a good scientist. Thank you for your constant support, kindness, and confidence in me.

I would also like to thank my thesis committee, Profs. Carl Parker, Nate Lewis, and Harry Gray, for their feedback and suggestions during my examinations. I very much appreciate their support and kindness, but willingness to ask tough questions and provide constructive criticism.

I am extremely endebted to the numerous collaborators who have provided the materials, advice, and experimental expertise to complete the projects in this thesis. I would like to especially thank Prof. Dianne Newman and Prof. Jeffrey Gralnick. Their interest in this project has allowed us to think about things on an entirely different level – and our relationship with them really demonstrated, for me, the power of collaboration with people whose area of expertise is far different than my own. And I am very grateful that Jeff was willing to spend so much time teaching me to be a bit of a biologist - the skills I learned will definitely be useful in the future. Thank you also to Prof. Sheila David and her students Alison Livingston, Valerie O'Shea, and Olga Lukianova for providing us with many, many aliquots of MutY and *A. fulgidus* UDG and valuable advice on how to work with these proteins. I also very much appreciate the protein samples provided to us by Prof. Tim O'Connor and I'm very grateful that he allowed me to spend a few weeks

working in his lab learning to purify protein with his technician, Dave Baker. And thank you to Jana Rudolf and Prof. Malcolm White for their gift of XPD samples.

I have also been very fortunate to have the opportunity to work very closely with several members of the Barton group. Eylon Yavin was contributed heavily to the EPR spectroscopy work in this thesis and it was wonderful to be able to share the excitement of those results with him. Alon Gorodetsky was kind enough to perform very important graphite electrochemistry experiments on our proteins. Alon's enthusiasm is nothing short of infectious and I am so glad that he was willing to take that project on. I am extremely grateful to Joey Genereux for his very thorough work on more accurate models for different damage detection schemes in cellular environments. Joey's contributions to this project have certainly made me think about how our work fits into a larger context. And I very much appreciate the AFM studies by Pam Sontz which required a truly heroic effort making big DNAs and counting proteins (and thanks to Maria DeRosa, whose idea inspired that work).

One of the best things about working for Jackie is the wonderful group of people she attracts to her laboratory. Certainly all of the people I have interacted with here have contributed, in some way or another, to my scientific development and general wellbeing during my time here, but I will only mention a few here. I feel very lucky to have been paired with Elizabeth Boon upon my arrival at Caltech – she very kindly trained me to do experiments and answered my many questions. Liz, Sarah Delaney, and Jae Yoo were especially welcoming to me and invited me to run the LA Marathon with them my first year. Jon Hart, Donato Ceres, and Greg Drummond were extremely helpful in solving scientific problems in my first few years in the group. Sarah Delaney, Melanie O'Neill, Maria DeRosa, and Anne Petitjean all offered me much needed support during my candidacy exam preparations and afterwards. It has helped me immensely to be able to

commiserate with my classmates, Katy Augustyn, Fangwei Shao, and Irv Lau - I have missed you all very much this last year! I am also very grateful to my colleagues in "south central" Noyes, Cindy Puckett, Fangwei Shao, Christine Romano, and Paul Lee for making our part of the lab a pleasant and fun place to work. And a special thank you to Paul for listening to all of my stories about my dog and for good conversations about science and "science." Thank you to Mi Hee Lim and Marisa Buzzeo for help and advice in figuring out what to do next with my life – and for being, along with Eddie Merino, awesome postdoc role models. Thank you also to Eddie for organizing our summer softball team and encouraging everyone to play.

I very much appreciate the opportunity to work with two wonderful SURF students, Tatyana Shatova and Andrea Dubin. Both of you were great, willing students and fun to hang out with during the summer! I have no doubt that both of you have illustrious scientific careers in front of you.

I also would like to thank my undergraduate advisor, Prof. Dan O'Leary, at Pomona College. It was in his classes and research laboratory that I began to realize that I might want to be a chemist, a researcher, and a teacher. I will be forever grateful that he asked me to work in his lab and his passion for excellent teaching and research will always be something that I strive to achieve in my career.

I am very lucky to have a supportive family. I would certainly not have made it to this point without the love and support of Ben Allen. Thanks for making my life easier in so many ways – by showing me how to do cool stuff on the computer, listening to the "woe is Amie" monologue from time to time, cooking me dinner every night, and being a brilliant scientist who helps me solve all of my problems in and out of the lab! And thank you for adopting Orson with me and making our little family complete - for the time being, at least! Thank you also to my parents for their encouragement and understanding of

the graduate student experience – and for all they have done to help me get a world-class education. And thank you to my little brothers, Ben and Willie, for being such interesting and accomplished people and for being willing to come and visit me from time to time. Even though we don't talk or see each other very often, I think of all of you (Mom, Dad, Ben, and Willie) everyday.

ABSTRACT

The double-helical structure of deoxyribonucleic acid (DNA) imparts upon this important biological molecule both the ability to store genetic information within a cell and also the capacity to serve as medium for charge transport. DNA-mediated charge transport is now a very well-studied phenomenon but biological roles for these reactions have not been explored. It has been demonstrated that DNA-mediated charge transport can funnel oxidative DNA damage to sites of low oxidation potential in a number of biologically relevant environments ranging from reconstituted nucleosome core particles, to isolated nuclei and mitochondria from HeLa cells. DNA-mediated charge transport may also play a role in transcriptional activation or repression as modulated by redox-active transcription factors. Here we examine how DNA-mediated charge migration could also provide a pathway for protein-protein communication among DNA repair enzymes, a pathway that might serve as a scheme for rapid lesion detection inside the cell.

DNA-mediated charge transport reactions are modulated by the structure and dynamics of the double helix. Particularly important for fast and efficient charge transport is the integrity of the base-pair π-stack of DNA. The presence of even a single mismatched base-pair causes a dramatic attenuation in the effectiveness of DNA-mediated charge transport. To examine the scope of base-pair structure perturbations that can hinder DNA charge transport, we have investigated a series of duplexes, each containing a single altered base, at DNA-modified electrodes. The efficiency of DNA charge transport in these systems is evaluated electrochemically by monitoring the reduction of an intercalative probe. These experiments reveal that a wide variety of damaged bases can

diminish charge migration through DNA, including those that result from oxidative damage events (8-oxo-guanine, 5-hydroxy-cytosine) and those associated with aberrant alkylation (O4-methyl-thymine, O6-methyl-guanine).

The remarkable sensitivity of charge transport reactions in DNA to a broad range of damaged bases inspired investigation of the role of DNA-mediated charge transport in DNA repair. A class of base excision repair glycosylases exists that contain [4Fe4S] clusters and the function of this cofactor in these enzymes is not well understood, though these clusters are often found in proteins involved in electron transfer reactions. We have used DNA-modified gold electrodes to investigate the properties of the [4Fe4S] cluster in these enzymes and discovered that MutY and Endonuclease III (EndoIII) are redox-active when bound to DNA with midpoint potentials in the 50−100 mV *versus* NHE range, typical of $[4Fe4S]^{2+/3+}$ processes. This redox activity furthermore requires a DNA-mediated path to the [4Fe4S] cluster. Studies of EndoIII on graphite electrodes show that the DNA-bound redox properties of the enzyme are similar to those observed on gold, while in the absence of DNA, the potential for the $[4Fe4S]^{2+/3+}$ couple is shifted positive by ~ 280 mV. This potential shift may indicate a differential binding affinity for DNA by the oxidized and reduced forms of EndoIII; the oxidized form could bind DNA as much as 3 orders of magnitude more tightly than the reduced form of the enzyme. The DNA-mediated redox activity observed in these proteins has prompted us to propose a model for how these proteins might use DNA charge transport as a fast and efficient damage detection method. In this model, a protein binds DNA and becomes oxidized. If the surrounding DNA is undamaged, DNA charge transport will allow another repair protein to reduce the first protein from a distance *via* the DNA base-pair stack. This reduced protein has diminished affinity for DNA and diffuses away; the charge transport

reaction has served as a scan of the intervening genomic region. If, instead, lesion sites are present in the vicinity of the initial protein, this protein is more likely to remain oxidized and tightly bound in the damaged area. Thus, this detection scheme would allow [4Fe4S] DNA repair enzymes to rapidly eliminate undamaged regions of the genome from their search while spending more time bound near lesions.

The DNA-bound redox activity of the [4Fe4S] cluster harbored by MutY has also been examined in solution. DNA-mediated oxidation of the [4Fe4S] cluster *via* a guanine radical intermediate leads to formation of the $[4Fe4S]^{3+}$ cluster as observed by electron paramagnetic resonance (EPR) spectroscopy and transient absorption spectroscopy. Furthermore, gel electrophoresis experiments indicate that MutY can quench guanine radicals, preventing formation of permanent oxidative guanine lesions. EPR experiments also demonstrate that degraded cluster products (e.g., $[3Fe4S]^{1+}$) are formed both by DNA-mediated oxidation and by oxidants in solution. In the latter case, signal intensities are increased in the presence of DNA. These results support the idea that the DNA-bound form of MutY is more easily oxidized than MutY free in solution. The fact that guanine radicals can oxidize MutY may be biologically relevant, as well. Guanine radicals are one of the first products of oxidative DNA damage, thus oxidation of MutY by a guanine radical could serve to not only directly repair this lesion, but also to activate a DNA-mediated charge transport search for damage in the genome in regions undergoing oxidative stress.

DNA-mediated charge transport may also be employed in a cooperative fashion among different [4Fe4S] cluster DNA repair enzymes, allowing them to help each other eliminate undamaged portions of the genome from their search. To explore this

possibility we have calculated that cooperative DNA CT makes possible for MutY, an extremely low copy number enzyme, a full scan of the *Escherichia coli* genome within the doubling time of the cell (~ 20 minutes). The genome scanning time also depends on the proportion of protein initially in the oxidized state, thus allowing the DNA repair response to adjust according to the conditions present in the cell. A simple processive scanning model for lesion detection by MutY is insufficient. This cooperativity between MutY and EndoIII was also tested experimentally in *E. coli.* Inactivation of EndoIII (*nth*-) in a MutY activity reporter strain yields a twofold increase in the mutation rate, indicating a loss of MutY activity in the absence of EndoIII. This loss of activity, or helper function, cannot be attributed to an overlapping substrate specificity. However, investigation of an EndoIII mutant (Y82A) that retains this defect in helper function also exhibits a 50% loss in signal intensity (compared to wt EndoIII) when examined on a DNA-modified electrode. Thus, helper function by EndoIII could involve DNA-mediated redox activity of the [4Fe4S] cluster in EndoIII. This work demonstrates a connection between *in vivo* cooperativity among DNA repair enzymes and DNA-mediated charge transport as well as a biological role for this chemistry in DNA repair.

TABLE OF CONTENTS

Appendix II. Inactivation of genes in *Escherichia coli*

LIST OF FIGURES

CHAPTER 7.

CHAPTER 8.

CHAPTER 9.

APPENDIX I.

APPENDIX II.

LIST OF TABLES

CHAPTER 1

Biological Contexts for DNA Charge Transport Chemistry

Adapted from Merino, E. J., Boal, A. K., and Barton, J. K. (2008) *Current Opinion in Chemical Biology* (*in press*), and Boal, A. K., Yavin, E., and Barton, J. K. (2007) *Journal of Inorganic Biochemistry* 101, 1913.

INTRODUCTION

The double helical structure adopted by B-form DNA, where a negatively charged sugar phosphate backbone surrounds a π-stacked array of heterocyclic aromatic base-pairs, allows it to serve as an efficient medium for long-range charge transport (CT) (*1*). This chemistry has now been well established as a property of DNA. DNA CT can be rapid and it can occur over long molecular distances if the reaction is initiated by oxidants or reductants that are intercalated or otherwise well coupled into the base-pair stack. The observation that even very subtle changes to the structure of the base-pair stack, for instance, the presence of a single mismatched or damaged base, can drastically attenuate the efficiency of DNA-mediated CT further highlights the importance of the DNA base pair π-stack in these reactions. While many features of DNA CT under a variety of experimental conditions have now been elucidated, the role of DNA CT in biological processes requires more consideration.

DNA Damage over Long Range

It was first shown that DNA CT can promote damage to DNA from a distance in a DNA assembly containing a tethered rhodium intercalator, a potent photooxidant, spatially separated from two low energy guanine doublets (*2*). Guanines are the bases that are most easily oxidized in DNA, and the 5'-Gs of guanine doublets have a particularly low oxidation potential (*3, 4*). Since then, long range oxidative DNA damage has been extensively characterized using a variety of photooxidants. It has become clear that electron holes, oxidizing equivalents injected into the DNA through a host of damaging agents, formed at any site along the DNA duplex will migrate to low energy guanine sites. The distance range over which holes can migrate and whether guanine

radicals, once generated, provide a chemical signal for oxidative stress throughout the genome via DNA-mediated CT are questions that need to be addressed (Figure 1.1).

This long range migration of charge was explored in DNA oligonucleotides of defined length and sequence using covalently tethered photooxidants as initiators of oxidative damage. With $[Rh(phi)_2bpy]^{3+}$ (phi = 9,10-phenanthrenequinone diimine) as the photooxidant, guanine doublet sites throughout the duplex show intense levels of damage even when the oxidant is located 200 Å away (*5*). CT over similar distances has also been observed with other photooxidants (*6*). Longer duplexes have not been systematically examined, but, given the very shallow distance dependences observed thus far, efficient DNA CT over greater distance regimes is likely possible. Recently, in a Rh-tethered assembly containing an extended adenine tract, the distance dependence of DNA CT was shown to be essentially flat, with no change in damage over 5 nm (*7)* (Figure 1.2). Therefore, holes can migrate over long molecular distances to form permanent DNA lesions far from the oxidant binding site. In all of these experiments, strong damage is observed at the 5'-G of GG sites. Thus, this damage pattern has become the hallmark of one electron oxidative damage arising through DNA CT.

While DNA CT proceeds over long distances, the reaction is exquisitely sensitive to mismatches, base lesions, and other perturbations to the DNA base pair stack (*1*). This was evident first in the finding that DNA bulges can interfere with long range oxidative damage. Intervening mismatches, particularly those where local stacking is highly perturbed, also attenuate long range oxidative damage. Thus, while DNA CT can occur over remarkably long distances, it is a reaction that is modulated by the intervening sequence-dependent structure and dynamics of DNA.

Figure 1.1. DNA charge transport (CT) in a biological environment. DNA CT could play a role in many cellular processes ranging from funneling oxidative DNA damage to regulatory or noncoding regions in the mitochondrion and nucleus to mediating protein signaling in DNA repair and transcriptional regulation pathways.

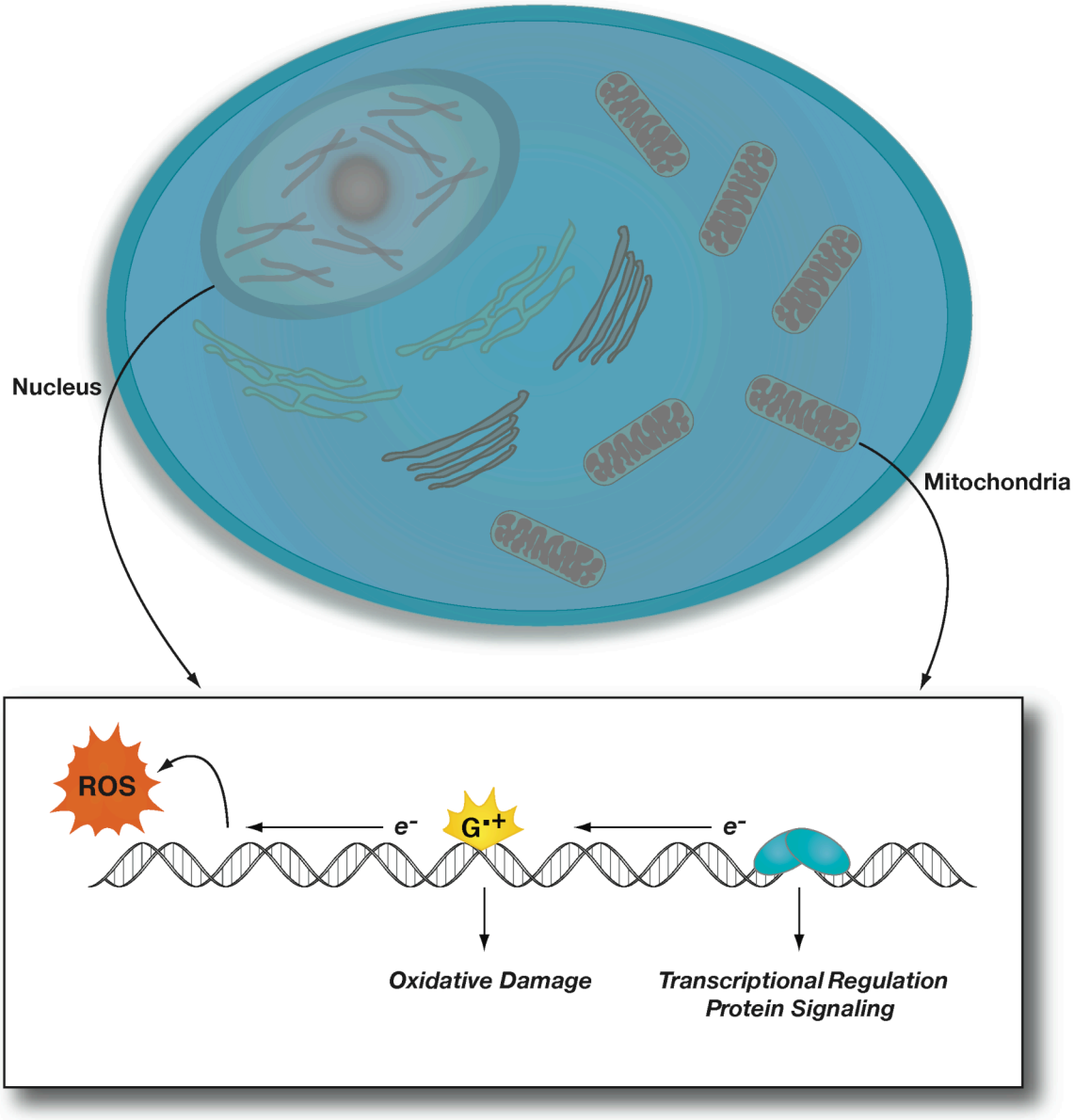

Figure 1.2. DNA CT in DNA damage. Upon irradiation, the intercalating Rh-oxidant accepts an electron (arrow) giving rise to an electron hole that is funneled to a low oxidation potential site, such as a guanine doublet, resulting in formation of a guanine radical (yellow). Guanine radicals can be quenched to generate oxidative DNA lesions.

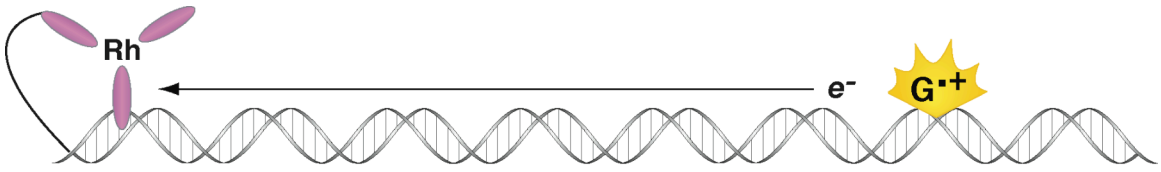

Interestingly, fewer experiments have been carried out to explore electron transfer through DNA (*8*). DNA-mediated electrochemistry, involving ground state DNA-mediated reductions, exhibits a very shallow distance dependence with a remarkable sensitivity to intervening mismatches and lesions (*9, 10*). Recent solution experiments, where electron and hole transfer are compared using the same DNA and photoactivated group demonstrate that electron transfers through DNA are similarly characterized by these two important features: (i) a shallow distance dependence and (ii) a sensitivity to perturbations in the base pair stack (*11*).

The constant assault on DNA by endogenous and exogenous oxidizing agents often leads to covalent modification of DNA, and due to DNA-mediated CT, these modifications may not necessarily arise at the site of first collision (*12*). Oxidative reactions in DNA have important implications for mutation and subsequent pathogenesis inside cells. The most common biological oxidant, iron, undergoes Fenton chemistry to produce hydroxyl radicals and other species that can readily react with the DNA bases. Additionally, radicals generated on the sugar-phosphate backbone can lead to hole formation on the DNA bases (*13*). Thus, once a hole is produced in double stranded DNA, DNA CT can funnel the hole to low oxidation potential sites, where the hole reacts irreversibly with O_2 and H_2O. Oxidative reactions of DNA bases with O_2 and H_2O leads to mutagenic DNA lesions (*12, 14*). Further oxidation of DNA base lesions yields products that bypass the repair machinery and exacerbate DNA damage.

Funneling Oxidative Damage to Specific DNA Regions

The involvement of DNA CT in promoting the formation of oxidative lesions suggests that DNA damage products may not be uniformly distributed within a genome but may instead be funneled to specific sites. This hypothesis is supported by analysis

of genomic DNA showing that introns and exons contain differential amounts of low oxidation potential sites (*15*). Further examination of eight eukaryotic genomes illustrates that DNA CT may drive the ultimate distribution of oxidative DNA lesions (*16*). For instance, exons contain a 50–fold decrease in oxidation prone guanine. Therefore protection of protein coding regions from DNA lesions may be due to their lack of low oxidation potential sites such that DNA CT can funnel damage out of the exons and into introns. Telomeres, the ends of chromosomes, also represent hot spots for DNA damage as they are of particularly high guanine content. Moreover, the DNA telomeres may also adopt quadruplex structures, and it has been shown that holes are preferentially shuttled to guanines within these structures (*17, 18*).

Whether DNA CT is important in funneling damage to discrete locations could be resolved by determining the location of oxidative lesions in a genome. Visualizing the sequence details of oxidative damage on a genome is difficult, however, due to their size and low copy number within the cell. Most methods only interrogate the total level of damaged DNA adducts by mass spectrometry as well as a variety of other techniques but do not yield the location in the sequence of the lesions produced. Ligation-mediated PCR has, however, been utilized to determine the sequence details of oxidative damage in DNA genomes (*19*). DNA CT was shown to occur in isolated nuclei from HeLa cells using ligation-mediated PCR in conjunction with $[Rh(phi)_2bpy]^{3+}$; the complex binds to DNA without sequence specificity, and upon photoactivation, either promotes strand breaks directly at the oxidant site or induces one electron oxidative damage (*20*). The pattern of oxidative lesions reveals hallmarks of DNA CT, with damage occurring predominately at guanine-rich low oxidation potential sites, the 5'-G of guanine doublets and triplets. Moreover, the results showed that while oxidative damage was found

preferentially at guanine doublets, the rhodium photooxidant was bound primarily at distant sites. Hence, the damage must have occurred through DNA-mediated CT. This work established that CT can occur in DNA within the nucleus.

Another biologically important target for oxidative stress is the mitochondrion. Mitochondria contain their own DNA and also harbor an abundance of reactive oxygen species as a result of their function in oxidative phosphorylation (*21*). Mutations in mitochondrial DNA have been found in a variety of tumors and are associated with other diseases, while other DNA perturbations, like large scale rearrangements, are common in mitochondrial DNA (*21*). Oxidative damage to extracted mitochondrial DNA (*22*), as well as to mitochondrial DNA within functioning mitochondria (*23*), promoted by the rhodium photooxidant reveals that DNA lesions can arise from a distance using DNA CT. Again, this damage from a distance was demonstrated by comparing sites of Rh binding *versus* guanine oxidation. The spatial separation between the Rh binding sites and one electron guanine oxidation sites is striking; oxidation can occur more than 70 bases away from the nearest bound oxidant. Again these data support long range CT through DNA within a cellular organelle, here the mitochondrion (Figure 1.3).

Some interesting biological consequences of DNA CT emerged from these studies. First, sites of base oxidation by DNA CT in mitochondrial DNA overlap with known mutational hot spots associated with cancers. The correlation between mutation frequency (*24*) and lesions produced suggests that DNA CT may be a major contributor to mitochondrial oxidative lesions *in vivo*. Secondly, one highly damaged position found is a regulatory element known as conserved sequence block II that is vital for DNA replication. Conserved sequence block II contains a seven guanosine repeat, the largest guanosine repeat on the mitochondrial genome. Positioning such a low oxidation

Figure 1.3. Funneling oxidative DNA damage *via* DNA CT in mitochondria. Each mitochondrion (blue/grey) harbors several mitochondrial genomes. Replication is regulated through a critical regulatory element termed conserved sequence block II (cyan). Upon irradiation with a Rh photooxidant, CT funnels damage to the regulatory element. Oxidation of the regulatory element could decrease the ability of oxidized genomes to be copied, thereby favoring replication of undamaged genomes.

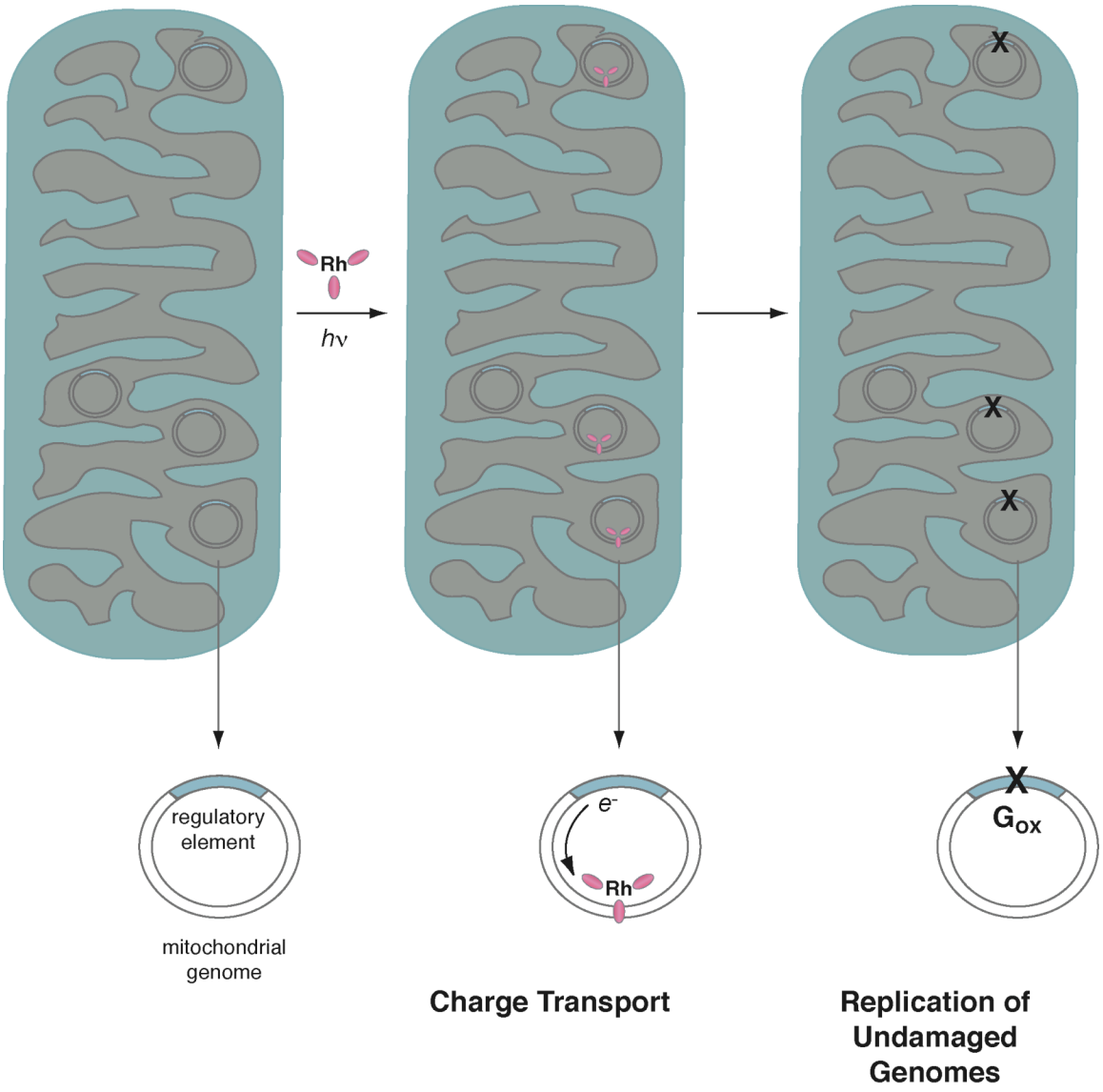

potential site as a regulatory element can be advantageous since each mitochondrion contains many copies of its genome. Funneling damage to a regulatory element, via DNA CT, could decrease the likelihood that damaged mitochondrial genomes will be replicated by the formation of an oxidative lesion that perturbs the replication machinery. These lesions might signal the level of damage in a particular genome, thus DNA CT may thus provide a protection mechanism to exclude damaged DNA from the replication cycle in mitochondria.

Long Range CT in the Presence of DNA-bound Proteins

Since it is apparent that DNA-mediated CT can take place in the crowded environment of a cell, it becomes important to ask systematically what are the effects of DNA-binding proteins on DNA CT? Moreover, within many organisms, DNA is packaged into chromatin or chromatin-like higher order structures via interactions with histone proteins. How does the nucleosome structure, containing DNA-bound histones, affect DNA CT?

Several studies of DNA CT in the presence of specific DNA-binding proteins have been carried out. Experiments to monitor CT through the DNA base pair stack is unaltered when a protein, such as a helix-turn helix protein, is bound in such a way that it induces little structural change in the DNA (*25*). Proteins that perturb the structure of DNA, however, have a profound effect on the yield of CT (*26*). Uracil DNA glycosylase, a DNA repair enzyme that flips uracil residues out of the base-pair stack, does not allow CT to proceed beyond the protein binding site. TATA-binding protein, a transcription factor that kinks the DNA helix by > 90 degrees, also diminishes CT efficiency to guanine doublets. This sensitivity of DNA-mediated CT to protein binding has actually led to the

application of DNA electrochemistry as a sensitive probe for DNA binding by base-flipping proteins as well as proteins like TATA-binding protein (*26, 27*).

In studies of long range oxidation, DNA-binding proteins have also been found to tune the oxidation potential of possible damage sites in DNA. For example, the restriction enzyme BamHI, which binds the DNA sequence 5'-GGATCC-3' inhibits damage at the guanine doublet located within its binding site (*28*). BamHI makes extensive hydrogen bonding contacts to the guanines in its restriction site and these interactions are proposed to change the ionization potential, making the guanines less susceptible to oxidation. The mechanisms that proteins employ to perturb DNA CT, structural alteration of the π-stack or modification of the electronic properties of specific bases, are interesting to consider in a biological context. One could imagine DNA-binding proteins, through a specific interaction, could insulate a particular sequence or a region of the genome, disallowing the propagation of DNA CT. Whether such protection is actually utilized within the cell has not yet been established.

A question of significant interest has been whether DNA CT can proceed within the nucleosome core particle (Figure 1.4). Experiments were first carried out on DNA using the intercalating photooxidant, $[Rh(phi)_2bpy]^{3+}$, in the presence and absence of bound histones (*29*). The 146 base pair DNA sequence employed in these studies was the same utilized for the crystal structure determination of the nucleosome core particle (*30*), which had a distinct kink in the DNA at its center in order to obtain consistent phasing of the DNA bound in the nucleosomes. We observed damage at all of the 5'-Gs of guanine doublets between the Rh, bound at the DNA terminus, and this central kink, both in the absence and presence of the histone proteins. Thus it appears that even

Figure 1.4. DNA CT in a nucleosome core particle. Photoactivation of a tethered Rh oxidant in histone-bound DNA generates oxidative damage at a distance in the nucleosome.

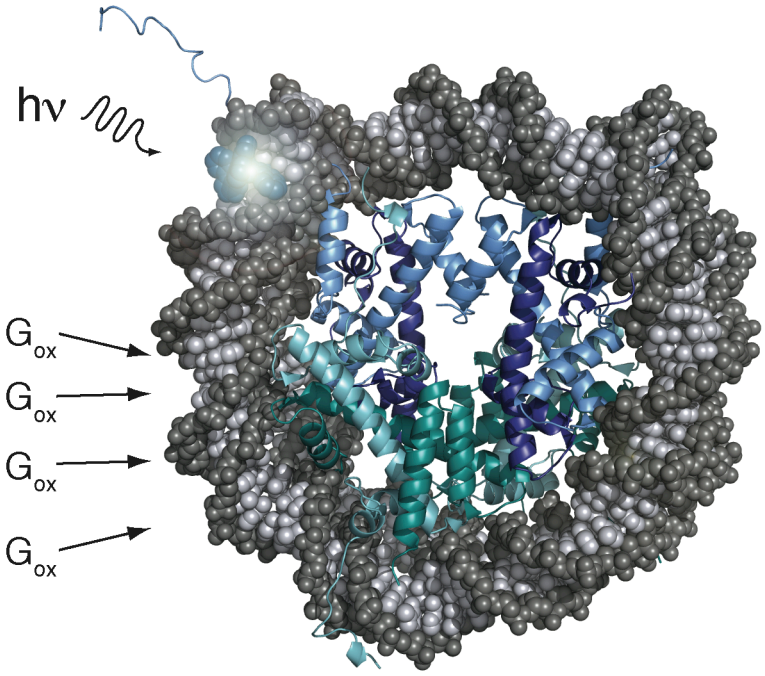

within the nucleosome, DNA CT may proceed. This long range CT within DNA in the nucleosome core particle was confirmed in similar experiments using tethered anthraquinone as the photooxidant (*31*). Some variations in relative intensities across the guanine doublets were observed for damage in the nucleosome versus that for the free DNA when comparing anthraquinone and the Rh intercalator. These variations may represent differences along the DNA in access to oxygen and water, required to make the irreversible damage products from the guanine radical, and possible tuning of local guanine oxidation potentials by the DNA-bound histones. Between Rh and anthraquinone as photooxidants, the small variations in guanine damage observed likely reflect differences in rates of back electron transfer for the two oxidants. Interestingly, anthraquinone-tethered nucleosomes were also recently utilized to show that DNA-protein crosslinking can result from long range DNA CT (*32*).

As indicated, DNA CT was found to occur in the mitochondrion, and here the DNA is also bound by its native suite of proteins (*23*). Mitochondrial DNA-protein interactions were found to be altered, perhaps also through crosslinking, as a result of oxidative damage arising via DNA CT. These results may resemble those seen in the nucleosome core particle. Importantly, in considering DNA being packaged in the nuclesome core particle, we generally consider that the DNA is being not only packaged but also protected from the assault of various damaging agents. Certainly these results show that within the nucleosome, the DNA is not protected from oxidative damage occurring *via* DNA-mediated CT.

Oxidation from a Distance of DNA-bound Proteins

Not only can proteins serve to modulate DNA CT, DNA-binding proteins can also participate in reactions at a distance through DNA-mediated CT. DNA-binding proteins

contain a variety of functional motifs with oxidation potentials similar to or lower than that of guanine (*33*). Guanine radicals generated with a ruthenium photooxidant can be transferred to aromatic amino acid side chains (tyrosine and tryptophan) present in positively charged peptides (Lys-Tyr-Lys and Lys-Trp-Lys) (*34*). Photolyase, an enzyme that uses CT to repair thymine dimer lesions in DNA, contains a flavin cofactor that can also be oxidized and reduced via the DNA π-stack when probed electrochemically on DNA-modified electrodes (*35*). Additionally, appropriately positioned thiols incorporated into the sugar-phosphate backbone can be oxidized in a DNA-mediated reaction (*36*).

Similarly, many DNA-binding proteins contain cysteine residues that are redox-active, and these too may be oxidized at a distance through DNA CT (*37*). One example is p53, a redox-modulated transcription factor that contains ten conserved cysteine residues in its DNA-binding domain (*38*). We prepared a DNA assembly containing a pendant photooxidant, and the consensus sequence for binding p53 (*37*). As illustrated in Figure 1.5, we observe that photoactivation of the anthraquinone promotes oxidative dissociation of p53 from the DNA. The presence of an intervening mismatch, moreover, inhibits this DNA-mediated reaction. Analysis of the p53 crystal structure reveals several candidates for thiol oxidation close to the DNA, and mass spectrometry of trypsin digests of p53 after photolysis is consistent with disulfide bond formation in the DNA-bound protein. Hence DNA-bound p53 can be oxidized from a distance and induced to dissociate from its target site from a distance through DNA-mediated CT.

The oxidation of p53 through DNA CT was also probed within the cellular environment. Human HCT cells were treated with the Rh photooxidant and irradiated to generate high levels of guanine radicals. A new oxidized form of p53 was detected via western blot that could be reversed by addition of exogenous thiols, consistent with

Figure 1.5. DNA CT leads to the oxidative dissociation of p53 (a tetramer) from its promoter, triggered from a distance.

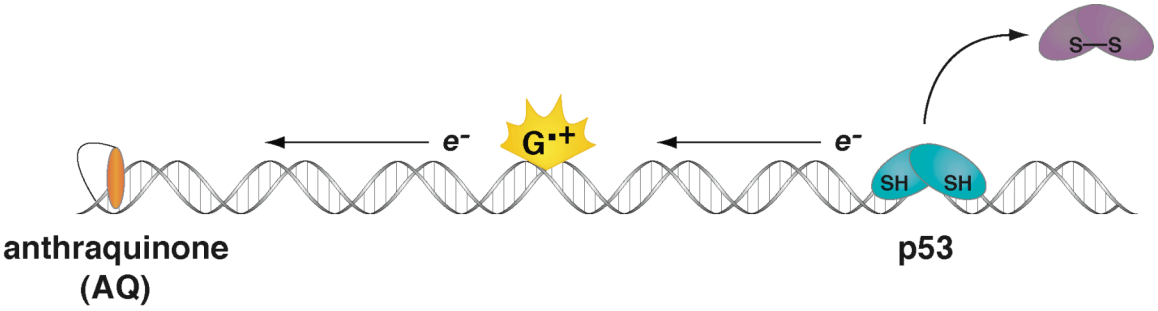

disulfide bond formation. In fact, the same oxidized p53 was produced upon addition of hydrogen peroxide. This oxidized p53 appears under conditions of oxidative stress.

The promoter sequences for p53 are diverse and can include those that control expression of important apoptotic or developmental genes. Biologically, p53 must distinguish between various promoters depending upon the cellular environment (*39*). Further investigation reveals that the DNA-mediated oxidation of p53 and subsequent dissociation is promoter specific (*37*). On a promoter involved in apoptosis, p21, p53 does not dissociate with photoactivation from a distance, although dissociation is observed on a promoter involved in DNA repair. We hypothesize that under high levels of oxidative stress, formation of guanine radicals via DNA CT occurs frequently, signaling that the DNA repair pathway is futile. When bound to DNA repair promoters, p53 oxidation followed by dissociation occurs, though p53 remains bound to promoters to activate cell cycle arrest under the high oxidative stress. Importantly, these results, taken together, provide a chemical rationale for the cellular response of p53 to oxidative stress through long range signaling using DNA-mediated CT.

The Possibility of DNA-mediated Signaling among Proteins

DNA repair proteins are another major class of DNA-binding proteins that could modulate or participate in DNA CT events. Given the well established sensitivity of DNA CT to a wide variety of damaged bases (*10*), it is interesting to consider that DNA repair proteins could harness CT to search DNA for damaged sites.

In base excision repair (BER), glycosylase enzymes are responsible for searching the genome for chemically modified bases and catalyzing their excision (*40*). These enzymes must first locate their substrate in a vast excess of undamaged DNA, flip the substrate into the active site of the protein, and catalyze scission of the N-glycosidic

bond between the errant base and the sugar-phosphate backbone. While much is known about the catalysis and substrate discrimination steps in this process, very little is known about the daunting initial search of the genome these enzymes must undertake. It has been demonstrated that many of these enzymes can move along the DNA helix in a processive manner (*41, 42*), but the *in vivo* relevance of this search mechanism as the primary mode of damage detection by DNA-binding proteins is disputed (*43-45*).

Many BER glycosylases contain a [4Fe4S] cluster (*46-48*), the function of which is unknown. Endonuclease III (EndoIII) was the first glycosylase discovered to contain this metal cofactor (*46*). EndoIII removes a wide variety of oxidized pyrimidines from DNA and contains the helix-hairpin-helix (HhH) recognition motif (*49-57*). MutY, structurally similar to EndoIII (*56-59*), is another BER glycosylase that contains a [4Fe4S] cluster (*58*). However, MutY instead removes adenine from 8-oxo-guanine:adenine mispairs (*60-72*).

The role of the [4Fe4S] cluster in these glycosylases is of great interest. Experiments were performed with EndoIII to determine the properties and function of the [4Fe4S] cluster (*46, 73*). Mossbauer and electron paramagnetic resonance (EPR) spectroscopy experiments confirmed that the protein contains the $[4Fe4S]^{2+}$ cluster when the protein is not bound to DNA. The cluster was unable to be oxidized by ferricyanide without degradation to the $[3Fe4S]^{1+}$ species as observed by EPR at 4K. Photoreduction of EndoIII did give rise to the $[4Fe4S]^{1+}$ cluster but with an estimated reduction potential of less than -600 mV versus NHE. Since it appeared that stable oxidation of the [4Fe4S] cluster was not possible, nor was reduction feasible in a biological environment, the cofactor was relegated to a structural role.

The [4Fe4S] cluster was analogously assigned a structural role in MutY. However, the David laboratory has since performed several experiments to investigate

the role of the cluster in this protein (*74-76*). They have developed a method to remove reversibly the cluster from the protein and discovered that the cofactor is not necessary for protein folding nor does it contribute to the thermal stability of the protein. Nonetheless, the [4Fe4S] cluster is necessary for DNA binding and enzyme activity. In addition, mutagenesis studies further highlight the necessity of the [4Fe4S] cluster for MutY repair. In these experiments, the cysteines that ligate the cluster are mutated to both coordinating (histidine and serine) and non-coordinating (alanine) residues leading to, in some cases, quite dramatic effects on the repair capacity of MutY.

Crystal structures are available for MutY and EndoIII both free and bound to DNA (*56-59, 77, 78*). These provide many clues about the environment of the cluster in both states. In each protein, the [4Fe4S] cluster is ligated by a unique cysteine motif (C-X_6-C-X_2-C-X_5-C). Some of these ligating residues are located in a loop termed the iron-sulfur cluster loop (FCL). This loop also contains many positively charged residues that interact with the DNA backbone. The overall structures of the free and DNA-bound proteins are similar (backbone RMSD = 1.3 – 2.1 Å); large conformational changes do not occur in the protein upon binding to DNA. In both MutY and EndoIII, the [4Fe4S] cluster is located ~ 13 Å from the nearest DNA backbone atom, and ~ 20 Å from both the center of the DNA helix and the glycosylase active site.

We have studied the DNA-mediated electron transfer properties of several repair proteins that contain [4Fe4S] clusters, a cofactor capable of being oxidized by guanine radicals (*79, 80*), using a variety of experimental techniques (*81, 82*). The electron lost upon oxidation of the $[4Fe4S]^{2+}$ cluster can be trapped in DNA by a uridine base modified with a nitroxide spin label. The resulting nitroxide radical species is detected with EPR spectroscopy (*81*). Similarly, a guanine radical cation, generated with a ruthenium photooxidant and monitored spectroscopically or with gel electrophoresis, can be

quenched by MutY, resulting in formation of a $[4Fe4S]^{3+}$ cluster (*82*). Importantly, guanine radicals are the first products of oxidative DNA damage inside the cell, and these results indicate that base radicals could provide the driving force *in vivo* to activate DNA-mediated CT signaling among [4Fe4S] BER glycosylases.

When investigated at DNA-modified electrodes, MutY and EndoIII are redox-active, displaying electrochemical signals with midpoint potentials (+50-100 mV versus NHE) typical of high-potential iron proteins, proteins that can adopt either the 2+ or 3+ cluster oxidation state (*79, 80*). These proteins exhibit dramatically smaller signals at electrodes containing an abasic site, indicating that CT to the [4Fe4S] cluster is DNA-mediated and requires an intact π-stack. We have also electrochemically examined EndoIII in the absence of DNA at a graphite electrode (*83*). The signal associated with the 2+/3+ redox couple in this situation is much less reversible and has a much more positive potential (~ 280 mV positive shift) indicating that EndoIII is both less easily oxidized and more unstable in the $[4Fe4S]^{3+}$ form when the protein is not bound to DNA. Furthermore, the positive potential shift allows us to estimate that the protein containing the $[4Fe4S]^{3+}$ cluster binds DNA much more tightly than the reduced form of EndoIII; the difference in K_d when comparing the $[4Fe4S]^{2+}$ and $[4Fe4S]^{3+}$ forms of EndoIII is at least 3 orders of magnitude.

A new role for the [4Fe4S] cluster in these glycosylase enzymes must now be considered. The presence of a redox-active [4Fe4S] cluster could allow DNA repair proteins to use DNA-mediated CT as a way to search quickly and efficiently for damaged bases in DNA (*79-83*). Figure 1.6 illustrates a model for how this search process might transpire. Here we propose that DNA CT could help reduce the search problem faced by these enzymes, allowing glycosylases to rapidly eliminate a search through genomic regions devoid of lesions and instead spend most of their time bound in the vicinity of

Figure 1.6. A model for DNA CT in DNA repair. DNA-mediated redox activity in a class of DNA repair proteins that contain a [4Fe4S] cluster could allow these enzymes to use DNA CT as a damage detection strategy. Under conditions of oxidative stress, guanine radicals are generated and these can oxidize the [4Fe4S] cluster in the repair enzyme (top). A second protein, upon binding to DNA, becomes oxidized and transfers its lost electron, in a DNA-mediated CT reaction, to the first DNA-bound protein. The first protein becomes reduced, subsequently loses affinity for DNA, and binds elsewhere. If a lesion is present between the two proteins (bottom), the CT reaction occurs much less efficiently, thus the proteins remain in the oxidized state and bound near the lesion. As illustrated here, DNA CT therefore serves to redistribute DNA repair enzymes away from undamaged DNA and into the vicinity of lesion sites, facilitating fast and efficient damage detection.

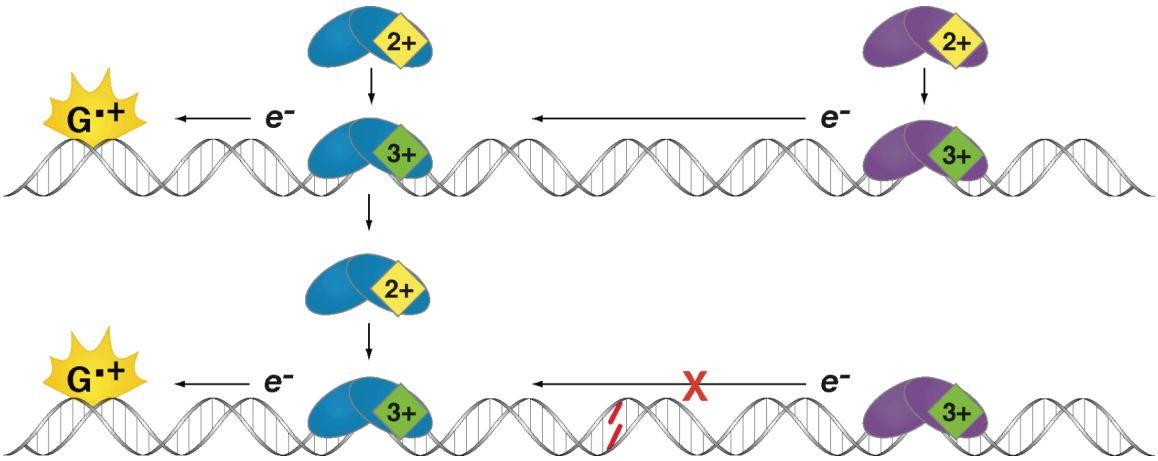

damaged sites. Importantly, we have shown that guanine radicals can readily oxidize the [4Fe4S] cluster in these proteins, indicating that this event could trigger a DNA CT signaling cascade among these proteins initiating the search for lesions. Hence, DNA-mediated CT could play a simultaneous role in funneling DNA damage to sites of low oxidation potential and recruiting proteins to find and repair that damage.

It is interesting to note that other organisms also contain BER repair proteins with an iron-sulfur cofactor (*47, 48*). Most notably, in a set of thermophilic organisms, there are uracil DNA glycosylase (UDG) homologs (*47*) as well as XPD (a nucleotide excision repair helicase) homologs that contain iron-sulfur clusters. The presence of a [4Fe4S] cluster in a thermophilic UDG is especially noteworthy given that the primary process that leads to uracil in DNA, cytosine deamination, has an enhanced rate at high temperatures (*84*). Yet these organisms do not display a higher mutation rate (*85*). Might the presence of this cofactor help fulfill this greater requirement for repair? One of these, *Archaeoglobus fulgidus* UDG, has been evaluated at DNA-modified electrodes and also exhibits DNA-mediated redox activity with a midpoint potential of +95 mV versus NHE (*80*).

The recent discovery that mutations in the human gene for MutY (*MUTYH*) can cause predisposition to colorectal cancer (*86*) underscores the need to understand how repair enzymes effectively find and repair DNA damage. Over 50 different missense and in-frame deletion mutations in *MUTYH* have been observed in colorectal cancer patients. Two of the most common mutations implicated in *MUTYH*-associated polyposis (MAP), Y165C and G382D, involve highly conserved positions in the protein. In *E. coli* MutY, the corresponding mutations (Y82C and G253D) lead to modest decreases in substrate binding affinity and rate of excision (*87*). In addition, structural studies show that Y82 and G253 interact with the DNA near the 8-oxo-guanine lesion site (*77, 78*). It is likely

that Y82 and G253 are involved in substrate recognition, but it is still not completely understood how all of the mutations implicated in MAP give rise to cancer and it is clear that defects in the rate of excision and substrate binding affinity may not account for all of the deficiencies observed with these mutants *in vivo* (*86, 87*). Futhermore, an increasing body of evidence indicates that finding the lesion is likely the limiting step for effective BER inside the cell (*89*) and it is, therefore, of critical importance to understand all of the strategies employed by these proteins to detect damage.

Is the redox activity of the [4Fe-4S] cluster relevant *in vivo*? MutY and Endo III have similar redox potentials and could cooperatively search for damage using DNA CT inside the cell (*80*). In this instance, if Endo III were inactivated, a decrease in the *in vivo* activity of MutY should be observed. The CC104 *E. coli* strain, which uses a mutation in *lacZ* to report the frequency of G:C to T:A transversion mutations, is often used as an indicator of MutY activity *in vivo* (*60, 90*). When the Endo III gene (*nth)* is knocked out in the CC104 genetic background, a small increase in the G:C to T:A mutation rate is observed (*91*). While this observed effect appears at first to be attributed to overlapping substrate specificity with MutY, *in vitro* evidence to support this idea is lacking (*55*). Could this relationship instead have something to do with the iron-sulfur cofactor harbored by each protein?

SUMMARY

Guanine radicals are one the first signals of oxidative stress inside a cell and DNA CT could provide a mechanism to disseminate these radicals in genomic DNA. Given that certain sequences have markedly low oxidation potentials, the lesions that result from this process may be unevenly distributed throughout the genome. Thus, inside the cell, DNA CT may play a major role in the DNA damage process by funneling damage to specific sites. However, many fundamental characteristics of DNA CT *in vivo* still need to be addressed. In particular, it is not known which sequences are prone to oxidative damage via DNA CT, nor is it fully understood which distance regimes are possible for DNA CT in biological environments.

Guanine radicals may also be important in mediating protein signaling processes. These DNA-based radicals may transfer to low oxidation potential sites in proteins, including amino acid side chains or protein-bound cofactors, eliciting a functional change in the protein. Here, DNA CT could serve as an antenna for DNA damage, allowing proteins to monitor oxidation events that occur far away and respond to them quickly. DNA CT could also provide a mechanism for protein-protein communication and, to this end, we have proposed that DNA repair enzymes could use DNA CT to cooperatively search for damage. Understanding the full range of DNA-binding proteins that could participate in these signaling pathways, and their associated cofactors, is a major focus of investigation.

REFERENCES

1. O'Neill, M.A., and Barton, J.K. (2005) *Charge Transfer in DNA: from Mechanism to Application.* Wagenknecht, H.A. Wiley-VCH, Ed., 27.

2. Hall, D.B., Holmlin, R.E., and Barton, J.K. (1996) *Nature 382*, 731.

3. Steenken, S., and Jovanovich, S. (1997) *J. Am. Chem. Soc. 119*, 617.

4. Saito, I., Takayama, M., Sugiyama, H., Nakatani, K., Tsuchida, A., Yamamoto, M. (1995) *J. Am. Chem. Soc. 117*, 6406.

5. Nunez, M.E., Hall, D.B., and Barton, J.K. (1999) *Chem. Biol. 6*, 85.

6. Ly, D., Sanil, L., and Schuster, G.B. (1999) *J. Am. Chem. Soc. 121*, 9400.

7. Augustyn, K.E., Genereux, J.C., and Barton, J.K. (2007) *Angew. Chim. Int. Ed. 46*, 5731.

8. Wagenknecht, H.A. (2003) *Angew. Chim. Int. Ed. 42*, 2454.

9. Boon, E.M., Ceres, D.M., Drummond, T.G., Hill, M.G., and Barton, J.K. (2000) *Nat. Biotechnol. 18*, 1096.

10. Boal, A.K., and Barton, J.K. (2005) *Bioconjug Chem 16*, 312.

11. Elias, B., Shao, F., and Barton, J.K. (2008) *J. Am. Chem. Soc. 130*, 1152.

12. Burrows, C.J., and Muller, J.G. (1998) *Chem. Rev. 98,* 1109.

13. Giese, B. (2000) *Acc. Chem. Res. 33*, 631.

14. Valko, M., Izakovic, M., Mazur, M., Rhodes, C.J., and Telser, J. (2004) *Mol. Cell. Biochem. 266,* 37.

15. Friedman, K.A., and Heller, A. (2001) *J. Phys. Chem. B 105,* 11859.

16. Friedman, K.A., and Heller A. (2004) *J. Am. Chem. Soc. 126*, 2368.

17. Delaney, S., and Barton, J.K. (2003) *Biochemistry 42*, 14159.

18. Szalai, V.A., Singer, M.J., and Thorp, H.H. (2002) *J. Am. Chem. Soc. 124,* 1625.

19. Besaratinia, A., and Pfeifer, G.P. (2006) *Carcinogenesis 27*, 1526.

20. Nunez, M.E., Holmquist, G.P., and Barton, J.K. (2001) *Biochemistry 40*, 12465.

21. Wallace, D.C. (2005) *Annu. Rev. Biochem. 39*, 359.

22. Merino, E.J., and Barton, J.K. (2007) *Biochemistry 46*, 2805.

23. Merino, E.J., and Barton, J.K. (2008) *Biochemistry 47*, 1511.

24. Tan, D.J., Bai, R.K., and Wong, L.J.C. (2002) *Cancer Res. 62,* 972.

25. Rajski, S.R., and Barton, J.K. (2001) *Biochemistry 40,* 5556.

26. Boon, E.M., Salas, J.E., and Barton, J.K. (2002) *Nat. Biotechnol. 20*, 282.

27. Gorodetsky, A.A., Ebrahim, A., and Barton, J.K. (2008) *J. Am. Chem. Soc. 130*, 2924.

28. Nakatani, K., Dohno, C., Ogawa, A., and Saito, I. (2002) *Chem. Biol. 9*, 361.

29. Nunez, M.E., Noyes, K.T., and Barton, J.K. (2002) *Chem. Biol. 9*, 403.

30. Luger, K., Mader, A., Richmond, R., Sargent, D., and Richmond, T.J. (1997) *Nature 389,* 251.

31. Bjorklund, C.C., and David, W.B. (2006) *Nucleic Acids Res. 34*, 1836.

32. Bjorklund, C.C., and Davis, W.B. (2007) *Biochemistry 46*, 10745.

33. Stubbe, J., Nocera, D.G., Yee, C.S., and Chang, M.C. (2003) *Chem. Rev. 103,* 2167.

34. Wagenknecht, H.A., Stemp, E.D.A., and Barton, J.K. (2000) *Biochemistry 39*, 5482.

35. DeRosa, M.C., Sancar, A., and Barton, J.K. (2005) *Proc. Natl. Acad. Sci. USA 102*, 10788.

36. Takada, T., and Barton, J.K. (2005) *J. Am. Chem. Soc. 127*, 12204.

37. Augustyn, K.E., Merino, E.J., and Barton, J.K (2007) *Proc. Natl. Acad. Sci. USA 104*, 18907.

38. Cho, Y., Gorina, S., Jeffrey, P.D., and Pavletich, N.P. (1994) *Science 265*, 346.

39. Prives, C., and Hall, P.A. (1999) *J. Pathol. 187*, 112.

40. David, S.S., and Williams, S.D. (1998) *Chem. Rev. 98*, 1221.

41. Blainey, P. C., van Oijen, A. M., Banerjee, A., Verdine, G. L., and Xie, X. S. (2006) *Proc. Natl. Acad. Sci. USA 103*, 5752.

42. Francis, A. W., and David, S. S. (2003) *Biochemistry 42*, 801.

43. Halford, S. E., and Szczelkun, M. D. (2002) *Eur. Biophys. J. 31*, 257.

44. Gowers, D. M., and Halford, S. E. (2003) *EMBO J. 22*, 1410.

45. Gerland, U., Moroz, J. D., and Hwa, T. (2002) *Proc. Natl. Acad. Sci. USA 99*, 12015.

46. Cunningham, R.P., Asahara, H., Bank, J.F., Scholes, C.P., Salerno, J.C., Surereus, K., Munck, E., McCracken, J., Peisach, J., and Emptage, M.H. (1989) *Biochemistry 28*, 4450.

47. Hinks, J. A., Evans, M. C. W., de Miguel, Y., Sartori, A. A., Jiricny, J., and Pearl, L. H. (2002) *J. Biol. Chem. 277*, 16936.

48. Rebeil, R., Sun, Y., Chooback, L., Pedraza-Reyes, M., Kinsland, C., Begley, T. P., and Nicholson, W. L. (1998) *J. Bacteriol. 180*, 4879.

49. Demple, B., and Linn, S. (1980) *Nature 287*, 203.

50. Katcher, H. L., and Wallace, S. S. (1983) *Biochemistry 22*, 4071.

51. Briemer, L. H., and Lindahl, T. (1984) *J. Biol. Chem. 259*, 5543.

52. Weiss, R. B., and Duker, N. J. (1986) *Nucleic Acids Res. 14*, 6621.

53. Boorstein, R. J., Hilbert, T. P., Cadet, J., Cunningham, R. P., and Teebor, G. W. (1989) *Biochemistry 28*, 6164.

54. Wagner, J. R., Blount, B. C., and Weinfeld, M. (1996) *Anal. Biochem. 233*, 76.

55. Dizdaroglu, M., Laval, J., and Boiteux, S. (1993) *Biochemistry 32*, 12105.

56. Kuo, C. F., McRee, D. E., Fisher, C. L., O'Handley, S. F., Cunningham, R. P., and Tainer, J. A. (1992) *Science 258*, 434.

57. Thayer, M. M., Ahern, H., Xing, D., Cunningham, R. P., and Tainer, J. A. (1995) *EMBO J. 14*, 4108.

58. Guan, Y., Manuel, R. C., Arvai, A. S., Parikh, S. S., Mol, C. D., Miller, J. H., Lloyd, S., and Tainer, J. A. (1998) *Nat. Struct. Biol. 5*, 1058.

59. Michaels, M. L., Pham, L., Nghiem, Y., Cruz, C., and Miller, J. H. (1990) *Nucleic Acids Res. 18*, 3841.

60. Nghiem, Y., Cabrera, M., Cupples, C. G., and Miller, J. H. (1988) *Proc. Natl. Acad. Sci. USA 85*, 2709.

61. Micheals, M. L., Cruz, C., Grollman, A. P., and Miller, J. H. (1992) *Proc. Natl. Acad. Sci. USA 89*, 7022.

62. Michaels, M. L., and Miller, J. H. (1992) *J. Bacteriol. 174*, 6321.

63. Michaels, M. L., Tchou, J., Grollman, A. P., and Miller, J. H. (1992) *Biochemistry 31*, 10964.

64. Gogos, A. , Cillo, J., Clarke, N. D., and Lu, A. L. (1996) *Biochemistry 35*, 16665.

65. Lu, A. L., Tsai-Wu, J. J., and Cillo, J. (1995) *J. Biol. Chem. 270*, 23582.

66. Manuel, R. C., Czerwinski, E. W., and Lloyd, R. S. (1996) *J. Biol. Chem. 271*, 16218.

67. Francis, A. W., Helquist, S. A., Kool, E. T., and David, S. S. (2003) *J. Am. Chem. Soc. 125*, 16235.

68. Chepanoske, C. L., Porello, S. L., Fujiwara, T., Sugiyama, H., and David, S. S. (1999) *Nucleic Acids Res. 27*, 3197.

69. Vidmar, J. J., and Cupples, C. G. (1993) *Can. J. Microbiol. 39*, 892.

70. Bulychev, N. V., Varaprasad, C. V., Dorman, G., Miller, J. H., Eisenberg, M., Grollman, A. P., and Johnson, F. (1996) *Biochemistry 35*, 13147.

71. Porello, S. L., Leyes, A. E., and David, S. S. (1998) *Biochemistry 37*, 14756.

72. Radicella, J. P., Clark, E. A., and Fox, M. S. (1998) *Proc. Natl. Acad. Sci. USA 85*, 9674.

73. Fu, W., O'Handley, S., Cunningham, R. P., and Johnson, M. K. (1992) *J. Biol. Chem. 267*, 16135.

74. Porello, S. L., Cannon, M. J., and David, S. S. (1998) *Biochemistry 37*, 6465.

75. Messick, T. E., Chmiel, N. H., Golinelli, M. P., Langer, M. R., Joshua-Tor, L., and David, S. S. (2002) *Biochemistry 41*, 3931.

76. Golinelli, M. P., Chmiel, N. H., and David, S. S. (1999) *Biochemistry 38*, 6997.

77. Fromme, J. C., and Verdine, G. L. (2003) *EMBO J. 22*, 3461.

78. Fromme, J. C., Banerjee, A., Huang, S. J., and Verdine, G. L. (2004) *Nature 427*, 652.

79. Boon, E.M., Livingston, A.L., Chmiel, N.H., David, S.S., and Barton, J.K. (2003) *Proc. Natl. Acad. Sci. USA 100*, 12543.

80. Boal, A.K., Yavin, E., Lukianova, O.A., O'Shea, V.L., David, S.S., and Barton, J.K. (2005) *Biochemistry 44*, 8397.

81. Yavin, E., Stemp, E.D.A., O'Shea, V.L., David, S.S., and Barton, J.K. (2006) *Proc. Natl. Acad. Sci. USA 103*, 3610.

82. Yavin, E., Boal, A.K., Stemp, E.D.A., Boon, E.M., Livingston, A.L., O'Shea, V.L., David, S.S., and Barton, J.K. (2005) *Proc. Natl. Acad. Sci. USA 102*, 3546.

83. Gorodetsky, A.A., Boal, A.K., and Barton, J.K. (2006) *J. Am. Chem. Soc. 128*, 12082.

84. Lindahl, T., and Nyberg, B. (1974) *Biochemistry 13*, 3405.

85. Jacobs, K. L., and Grogan, D. W. (1997) *J. Bacteriol. 179*, 3298.

86. Cheadle, J.P., and Sampson, J.R. (2007) *DNA Repair 6*, 274.

87. Al-Tassan, N., Chmiel, N.H., Maynard, J., Fleming, N., Livingston, A.L., Williams, G.T., Hodges, A.K., Davies, D.R., David, S.S., Sampson, J.R., and Cheadle, J.P. (2002) *Nat. Genet. 30*, 227.

88. Pope, M.A., Chmiel, N.H., and David, S.S. (2005) *DNA Repair 4*, 315.

89. Livingston, A.L., O'Shea, V.L., Kim, T., Kool, E.T., and David, S.S. (2008) *Nat. Chem. Biol. 4*, 51.

90. Cupples, C. G., and Miller, J. H. (1989) *Proc. Natl. Acad. Sci. USA 86*, 5345.

91. Tano, K., Iwamatsu, Y., Yasuhira, S., Utsumi, H., and Takimoto, K. (2001) *J. Radiat. Res. 42*, 409.

CHAPTER 2

Electrochemical Detection of Lesions in DNA

Adapted from Boal, A. K., and Barton, J. K. (2005) *Bioconjugate Chemistry 16*, 312.

INTRODUCTION

DNA is remarkably susceptible to chemical modification (*1-3*). Hydrolytic damage is the most common form of DNA base modification and often leads to deamination of cytosine and depurination. Oxidative damage results in a variety of base modifications, but 8-oxo-G is thought to be the most prevalent of these lesions. Non-enzymatic alkylation by endogenous and exogenous alkylating agents is also an important type of base damage (*2*). Modification of DNA bases can disrupt DNA replication and transcription by altering the base pairing properties of the DNA base and stalling the protein machinery associated with these processes. Base damage may also be an important indicator in the diagnosis and treatment of cancer, as high levels of damaged bases are often the result of exposure to carcinogens (*4*).

The base pair π-stack, formed when duplex DNA assumes a helical conformation, is capable of mediating charge transport (CT) (*5-9*). This chemistry is exquisitely sensitive to changes in base pair structure and dynamics; intervening mismatches in base pairing lead to a loss in the ability to transfer charge from an electron donor to an electron acceptor (*10*), as do bulges (*11*) or structural perturbations in base pair stacking induced by proteins (*12, 13*). While an *in vivo* role for DNA-mediated CT has yet to be established, it is interesting to consider that DNA-mediated CT may be involved in DNA damage and repair (*14*). Long range DNA-mediated CT provides a potential route for funneling oxidative damage to specific regions of the genome and insulating alternate regions (*14, 15*). We have proposed that DNA repair proteins may take advantage of the sensitivity of DNA-mediated CT to DNA structural modifications in order to scan the genome for damage as an efficient long range detection scheme (*14, 16*).

The remarkable sensitivity of DNA-mediated CT to perturbations in base pair stacking and dynamics suggested that this chemistry could be applied in the design of sensors that detect base pair mismatches and damage products. Our laboratory has developed one such sensor for the detection of single base mutations in duplex DNA (*17, 18*). In this device, a monolayer of thiol-terminated DNA oligonucleotide duplexes is assembled on a gold surface; a redox-active intercalator bound near the top of the film acts as the probe of DNA CT chemistry. The DNA-mediated reduction of the intercalator is easily monitored electrochemically if the DNA is fully Watson-Crick base paired. However, the presence of a single base pair mismatch or other structural perturbation within the base pair stack attenuates intercalator reduction. This sensor is unique in that it does not exploit differences in hybridization thermodynamics to detect mutations, but instead differences in electronic coupling within the π-stack. Greater sensitivity to perturbations in the π-stack is attained by coupling the DNA-mediated reduction of the intercalative probe into an electrocatalytic cycle with an oxidant in solution capable of re-oxidizing the intercalator. Figure 2.1 illustrates this cycle utilizing the intercalator methylene blue as the electrocatalyst for ferricyanide reduction. The integrity of the DNA π-stack is repeatedly probed via electron transfer in this catalytic cycle, and thus any perturbations in base pair stacking are amplified. Using this methodology, all single base mismatches in DNA, irrespective of sequence context or thermal stability, can be readily detected (*18*). Indeed recently, a full range of DNA-based biosensors have been developed (*19,20*).

Here we examine the scope of this methodology. We are interested in determining the primary factors governing the detection of DNA lesions by DNA charge transfer chemistry and the range of lesions that may be detected. How effective, for

Figure 2.1. Scheme for electrocatalysis at a DNA-modified electrode. MB^+ denotes methylene blue as the redox-active intercalative probe. MB^+ is reduced to leucomethylene blue (LB^+) in a DNA-mediated electron transfer process. Ferricyanide ($Fe(CN)_6^{3+}$) is oxidized by LB^+ to regenerate the redox-active intercalative probe.

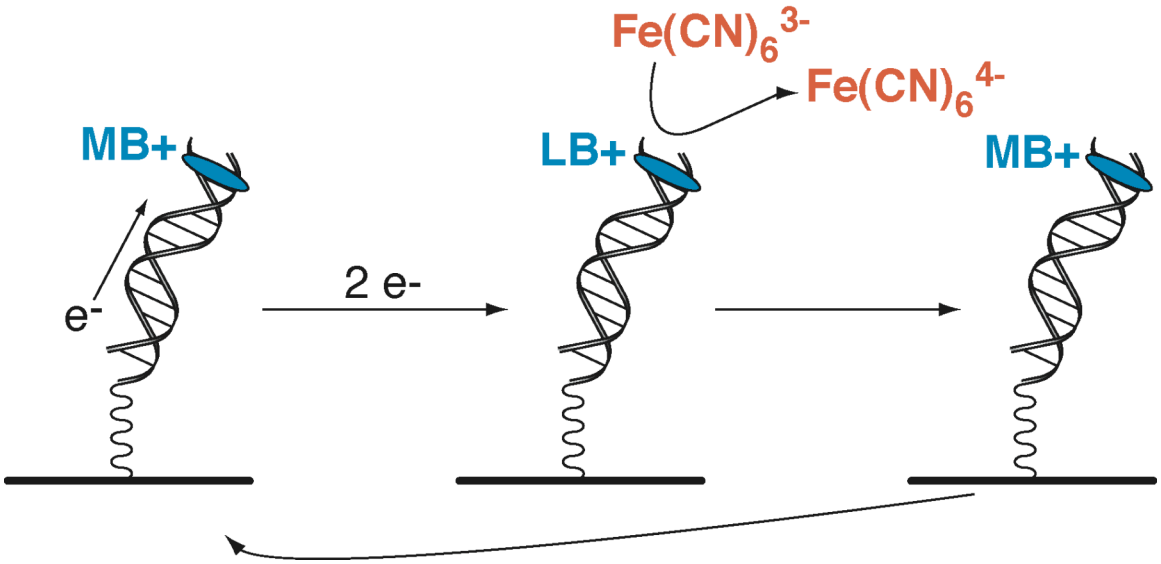

example, is this chemistry in detecting DNA methylation? Are base analogues utilized as probes of nucleic acid processes or as therapeutics readily detected? We have already observed that the conformational distortions in synthetic oligonucleotides containing constrained sugar-phosphate backbones can be detected electrochemically (*21*), and this may be an important consideration in their application in antisense therapeutics. Perhaps most importantly, our understanding of the sensitivity and scope of DNA CT chemistry in the detection of lesions provides a foundation for the consideration of possible roles for DNA CT in mechanisms of DNA repair.

MATERIALS AND METHODS

Materials

All reagents for DNA synthesis were purchased from Glen Research (including all unnatural DNA base phosphoramidites). Methylene blue, ferricyanide, and reagents used in the synthesis of thiol-modified DNA were purchased from Aldrich in the highest available purity and used as received. All buffers were prepared with Milli-Q water and filtered with a sterile, 0.2 μm filter.

Preparation of DNA-modified Electrodes

Oligonucleotides were prepared using standard phosphoramidite synthesis on an ABI 392 model DNA synthesizer. Oligonucleotide composition was verified by mass spectrometry. Thiol-modified duplexes were prepared using a solid-phase coupling procedure (*17*). The modified DNA was HPLC-purified on a semi-preparative C18 column after either the amino modification or attachment of the disulfide moiety and again after the thiol deprotection. Thiol-modified DNA and the appropriate

complementary strand were prepared in a 100 μM solution and annealed on a thermocycler. The resulting duplexes were self-assembled overnight (12-24 hours) on polished (0.3 μm, 0.05 μm alumina) and etched (CV from +1575 mV to -250 mV, 20 cycles in 1M H_2SO_4) bulk gold electrodes. $MgCl_2$ (100 mM) was added to the DNA solution prior to incubation to ensure a well-packed film. All DNA films were confirmed to be densely packed using a standard ferricyanide assay (*22*). At least three trials were performed for each base modification.

Electrochemical Analysis of DNA Films

Cyclic voltammetry and chronocoulometry experiments were carried out on a BAS CV50W model electrochemical analyzer. Experiments were executed in 50 mM NaCl, 5mM sodium phosphate, pH 7, at ambient temperatures under an inert atmosphere. A 3-compartment electrochemical cell was used with a Pt wire auxiliary electrode, 0.02 cm^2 gold working electrode, and saturated calomel reference electrode separated from the working electrode by a modified Luggin capillary.

Thermal Denaturation Studies

DNA duplexes (1.6 μM) were tested in 50 mM NaCl, 5 mM sodium phosphate, 100 mM $MgCl_2$, pH 7.0 in a quartz cell (with the exception of the lesions in group 4 which were analyzed in the absence of $MgCl_2$ and without the thiol tether). Absorbance at 260 nm was measured on a Beckman DU7400 spectrophotometer as the temperature decreased from 90 °C to 20 °C in a 0.5 °C/minute linear gradient. Melting curves were fit to a sigmoidal function using ORIGIN software. The T_m is defined as the midpoint of these sigmoidal curves.

RESULTS AND DISCUSSION

Methodology

Base lesions are incorporated into 15mer thiol terminated duplexes using standard phosphoramidite chemistry and the DNAs containing the base lesions are self-assembled into monolayers on gold electrodes. These DNA-modified electrodes are then investigated electrochemically using noncovalent methylene blue (MB) as a redox-active probe either directly or, in conjunction with ferricyanide, electrocatalytically. When MB is used as a direct probe, the DNA-modified electrodes are immersed in a buffered solution containing 2 μM MB. Note that it is the reduction of MB that is monitored using cyclic voltammetry from 0 to –650 mV; some of the lesions examined are easily oxidized but the conditions monitored here do not promote redox chemistry on the bases themselves. MB is also used as a catalytic reductive probe, when the DNA modified electrode is placed in a solution containing 2 mM ferricyanide and 0.5 μM MB. The redox activity of MB is then monitored primarily using chronocoulometry. In the experiments described here, charge is monitored for a period of 5s while the potential steps from 0 to –350 mV.

The lesions investigated here encompass a wide variety of modifications to DNA bases. Some of these lesions occur physiologically as a result of enzymatic modification to DNA or as a result of oxidative and/or hydrolytic damage. Other lesions represent synthetic modifications to DNA bases, damage to bases that is the result of exposure to alkylating agents, bases used as therapeutics, and fluorescent bases commonly used as synthetic probes of DNA.

Group 1 Lesions

The group 1 lesions are all associated with DNA damage processes. O4-methyl-thymine (OMT) and O6-methyl-guanine (OMG) are methylation damage products occurring at sites involved in hydrogen bonding, and 5-hydroxy-cytosine (OHC) and 8-oxo-guanine (OG) are common oxidative damage products (*23*). The structures of these lesions are shown in Figure 2.2. DNA films containing OMG base paired with cytosine can be distinguished electrochemically, either with or without electrocatalysis, from those containing well-matched unmodified base pairs (Figure 2.2). OMT base paired with adenine can also be detected with and without electrocatalysis, but detection is greatly enhanced using electrocatalysis. As illustrated in Table 2.1, incorporation of these lesions into DNA duplexes also leads to dramatically reduced T_m values. It is noteworthy, however, that duplexes containing OMG have a lower T_m than those containing OMT, yet show less attenuation in MB reduction.

The oxidative damage products OG and OHC can also be detected electrochemically both with and without electrocatalysis (Figure 2.2). OG is examined here base paired with both A and C (OG:A and OG:C, respectively). In both base pairing contexts, OG is detectable when MB is used as a direct probe. In the electrocatalysis experiments, OG is detectable when paired with C or A, but detection of OG:A is especially pronounced. OHC is also easily detectable with electrocatalysis. It is noteworthy that a higher background current is consistently observed in DNA films containing OHC; possibly this reflects a difference in film morphology. Note that all data, irrespective of film capacitance, were first background corrected.

Figure 2.2. Electrochemical detection of group 1 lesions. A. Cyclic voltammetry without electrocatalysis. B. Bar graph representing peak current attained in cyclic voltammetry experiments without electrocatalysis. C. Chronocoulometry with electrocatalysis. D. Structures of group 1 lesions. Deviations from standard base pairs are shown in red.

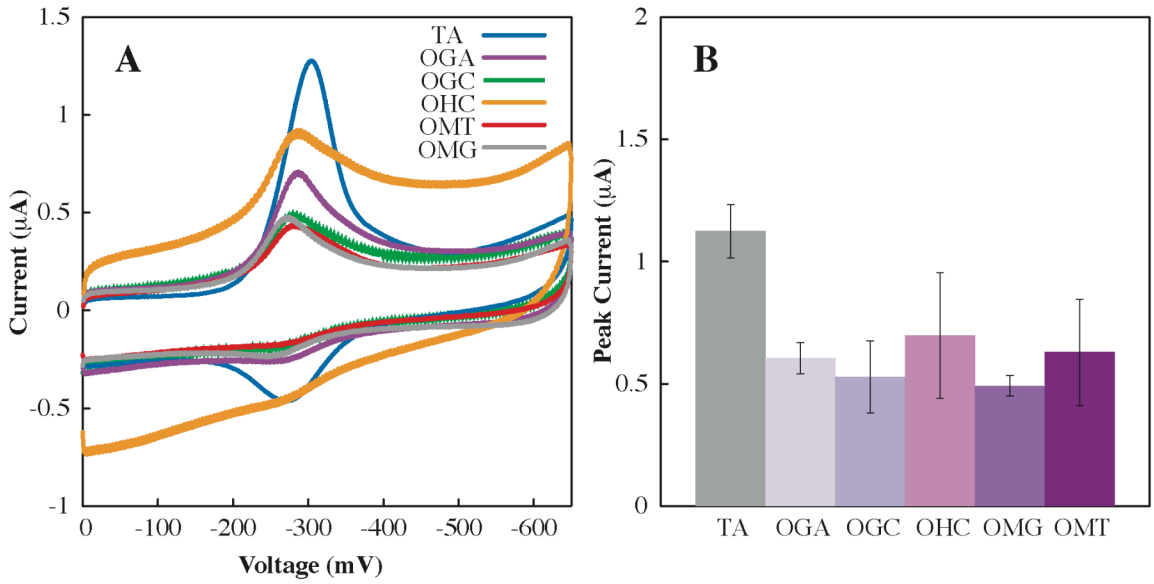

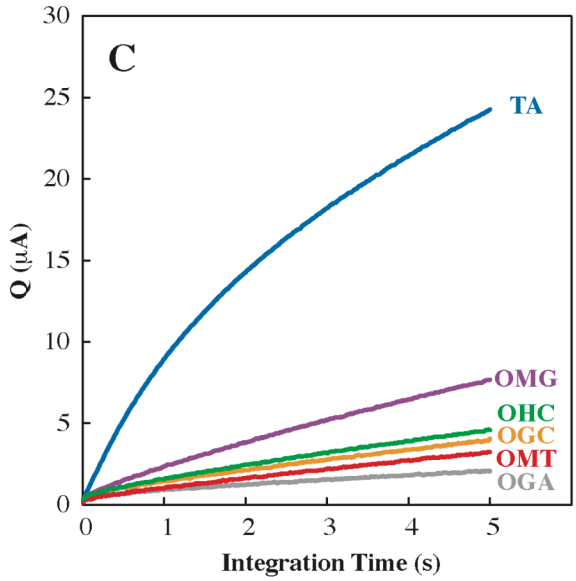

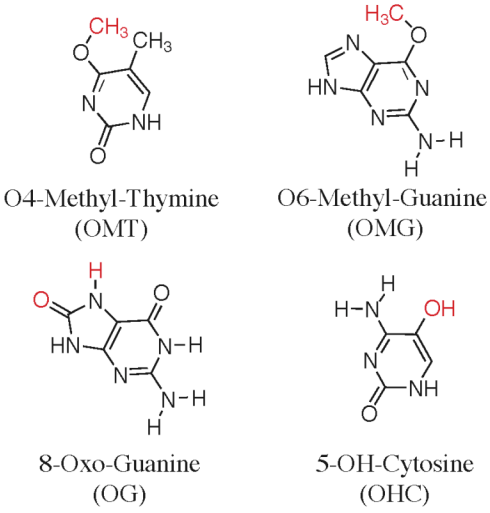

Table 2.1. Electrochemical detection of group 1 lesions.

Lesion	Sequence[a]	T_m (°C)	Q (μA) w/out electrocatalysis[b]	Q (μA) with electrocatalysis[c]
no lesion (TA)	SH - 5' - AGT ACA GTC ATC GCG 3' - TCA TGT CAG TAG CGC	60.0	1.27 ± 0.12	23.9 ± 1.7
O4-Methyl-Thymine (OMT)	SH - 5' - AGT ACA GTC ATC GCG 3' - TCA TG**T** CAG TAG CGC	49.4	0.63 ± 0.22	3.1 ± 1.0
O6-Methyl-Guanine (OMG)	SH - 5' - AGT ACA GTC ATC GCG 3' - TCA TGU CA**G** TAG CGC	47.8	0.492 ± 0.041	8.1 ± 2.4
5-Hydroxy-Cytosine (OHC)	SH - 5' - AGT ACA GTC ATC GCG 3' - TCA TGT **C**AG TAG CGC	54.9	0.70 ± 0.25	5.1 ± 1.1
8-Oxo-Guanine:C (OGC)	SH - 5' - AGT ACA GTC ATC GCG 3' - TCA TGT CA**G** TAG CGC	53.6	0.53 ± 0.15	4.1 ± 0.6
8-Oxo-Guanine:A (OGA)	SH - 5' - AGT ACA GTC ATC GCG 3' - TCA TG**G** CAG TAG CGC	52.3	0.604 ± 0.064	2.9 ± 0.5

[a] SH - 5' represents $SH(CH_2)_2CONH(CH_2)_6NHCO$ at 5'-OH
[b] Electrochemical detection using 2 μM methylene blue (MB) as redox probe. Q = current at CV peak.
[c] Electrochemical detection with electrocatalysis: 0.5 μM MB, 2 mM $Fe(CN)_6^{3-}$. Q = integrated current at 5s.

As evident in Table 2.1, these lesions are somewhat thermodynamically destabilizing; duplexes containing these modifications have lower melting temperatures than unmodified duplexes (TA). Nonetheless, incorporation of these lesions in DNA films leads to a dramatic attenuation in CT efficiency.

Group 2 Lesions

Group 2 includes the synthetic base analogues, P and K, that function as degenerate bases; they can pair with either purines (P) or pyrimidines (K) (*24*). Nebularine (Neb) is a natural product that also has greater base pairing degeneracy than the natural purines (*25*). As illustrated in Figure 2.3, each of these lesions causes a profound decrease in DNA-mediated CT monitored with electrocatalysis. Significantly, P and K base paired to each other results in a higher charge accumulation when compared to P or K base paired to a natural base. As evident in Table 2.2, it is also interesting that the duplex with the highest charge accumulation (Q) with electrocatalysis has the lowest T_m. This result provides another indication that CT attenuation does not correlate with duplex melting temperature.

Group 3 Lesions

This group includes the therapeutic base 5-fluoro-uracil (FIU) (*26*), fluorescent bases 2-amino-purine (2Ap) (*27*) and etheno-adenine (EA) (*28*), and synthetic base analogues 7-deaza-guanine (ZG) (*29*) and 7-deaza-adenine (ZA) (*30*). Group 3 represents structural modifications to DNA bases that are either completely synthetic (ZA, ZG, FIU, 2Ap) or the result of exposure to exogenous mutagens (EA).

Figure 2.4 illustrates, in DNA films containing these lesions, the reduction of MB without electrocatalysis as measured by cyclic voltammetry. None of these lesions are

Figure 2.3. Electrochemical detection of group 2 lesions. A. Cyclic voltammetry without electrocatalysis. B. Bar graph representing peak current attained in cyclic voltammetry experiments without electrocatalysis. C. Chronocoulometry with electrocatalysis. D. Structures of group 2 lesions. Deviations from standard base pairs are shown in red.

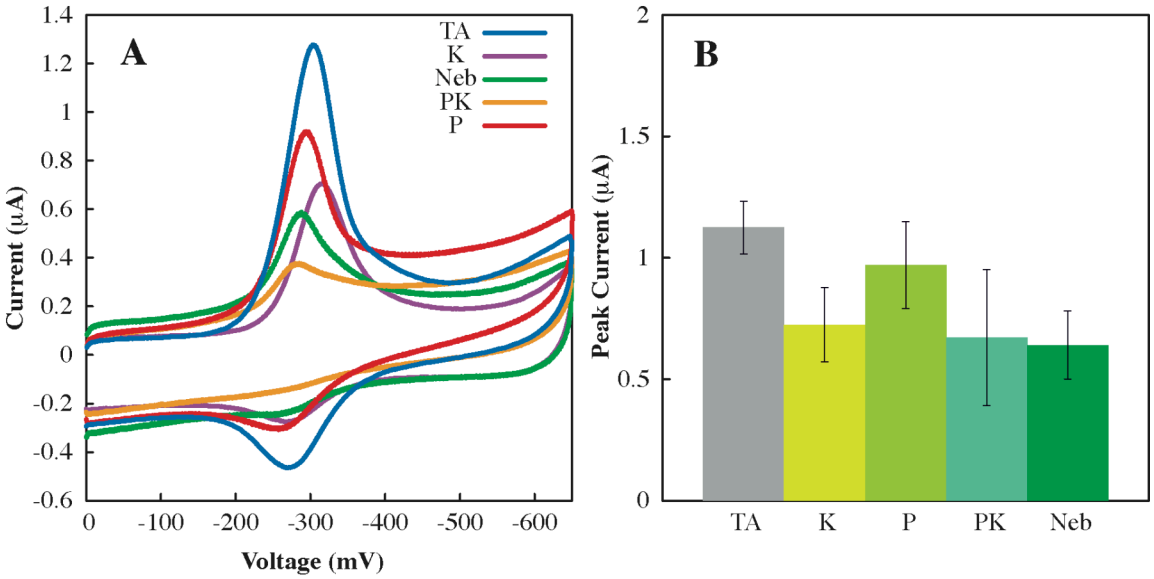

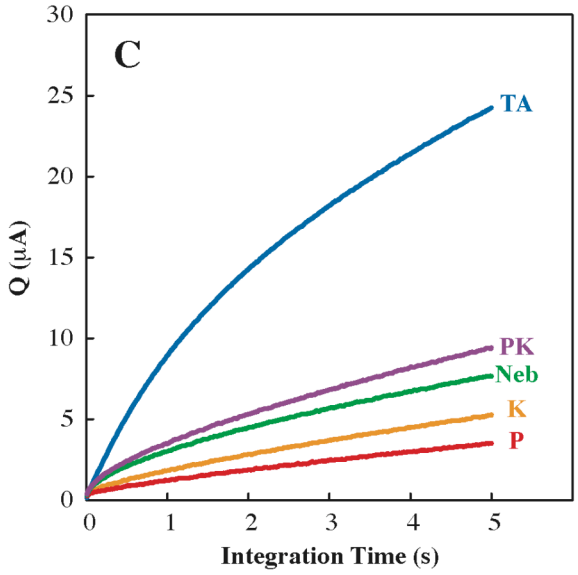

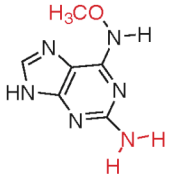

dK (K)

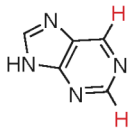

Nebularine (Neb)

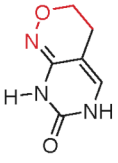

dP (P)

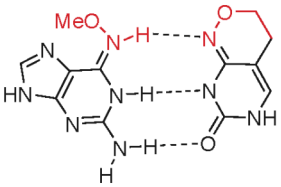

K:P (PK)

Table 2.2. Electrochemical detection of group 2 lesions.

Lesion	Sequence[a]	T_m (°C)	Q (μA) w/out electrocatalysis[b]	Q (μA) with electrocatalysis[c]
no lesion (TA)	SH – 5' – AGT ACA GTC ATC GCG 3' – TCA TGT CAG TAG CGC	60.0	1.27 ± 0.12	23.9 ± 1.7
dP (P)	SH – 5' – AGT ACA GTC ATC GCG 3' – TCA TG**P** CAG UAG CGC	56.8	0.97 ± 0.18	5.9 ± 2.2
dK (K)	SH – 5' – AGT ACA GTC ATC GCG 3' – TCA TGT C**K**G TAG CGC	53.4	0.73 ± 0.15	6.6 ± 2.5
P:K (PK)	SH – 5' – AGT ACA G**P**C ATC GCG 3' – TCA TGT C**K**G TAG CGC	50.2	0.67 ± 0.28	10.1 ± 2.1
Nebularine (Neb)	SH – 5' – AGT ACA GTC ATC GCG 3' – TCA TGT C**N**G TAG CGC	53.7	0.64 ± 0.14	9.7 ± 2.3

[a]SH - 5' represents $SH(CH_2)_2CONH(CH_2)_6NHCO$ at 5'-OH
[b]Electrochemical detection using 2 μM methylene blue (MB) as redox probe. Q = current at CV peak.
[c]Electrochemical detection with electrocatalysis: 0.5 μM MB, 2 mM $Fe(CN)_6^{3-}$. Q = integrated current at 5s.

appreciably distinguished without electrocatalysis. Figure 2.4 also shows these data in bar graph form, further demonstrating that these lesions, within error, all have the same ability to facilitate CT as a fully matched duplex (TA). When MB is used electrocatalytically, ZA, ZG, and 2Ap are still not distinguishable. Interestingly, FlU or EA incorporation, examined through electrocatalysis, does lead to some attenuation in CT. Table 2.3 summarizes these data and shows melting temperatures for each duplex. All group 3 lesions, with the exception of EA, also show little deviation in melting temperature from a fully matched duplex.

Group 4 Lesions

Group 4 lesions, 5-methyl-cytosine (MC), N6-methyl-adenine (NA), and uracil (UA) are biologically relevant bases that are the product of enzymatic methylation (MC and NA) or polymerase misincorporation (U base paired with A) (*31-33*). Each of these lesions is the result of the addition or subtraction of a methyl group in a location that does not appreciably hinder Watson-Crick hydrogen bonding ability.

Figure 2.5 shows the direct DNA-mediated reduction of MB (without electrocatalysis) measured by cyclic voltammetry. Without electrocatalysis, MB reduction is equivalent for DNAs containing these lesions when compared to a duplex that does not contain any lesions (TA). Figure 2.5 also shows these data as a bar graph, illustrating quantitatively that these lesions are not electrochemically detectable by this method. In addition, data from chronocoulometry experiments using electrocatalysis, our most sensitive assay, show that these lesions are not well detected even when MB is used as a catalytic probe. These data are summarized in Table 2.4. Also shown in Table 2.4 are melting

Figure 2.4. Electrochemical detection of group 3 lesions. A. Cyclic voltammetry without electrocatalysis. B. Bar graph representing peak current attained in cyclic voltammetry experiments without electrocatalysis. C. Chronocoulometry with electrocatalysis. D. Structures of group 3 lesions. Deviations from standard base pairs are shown in red.

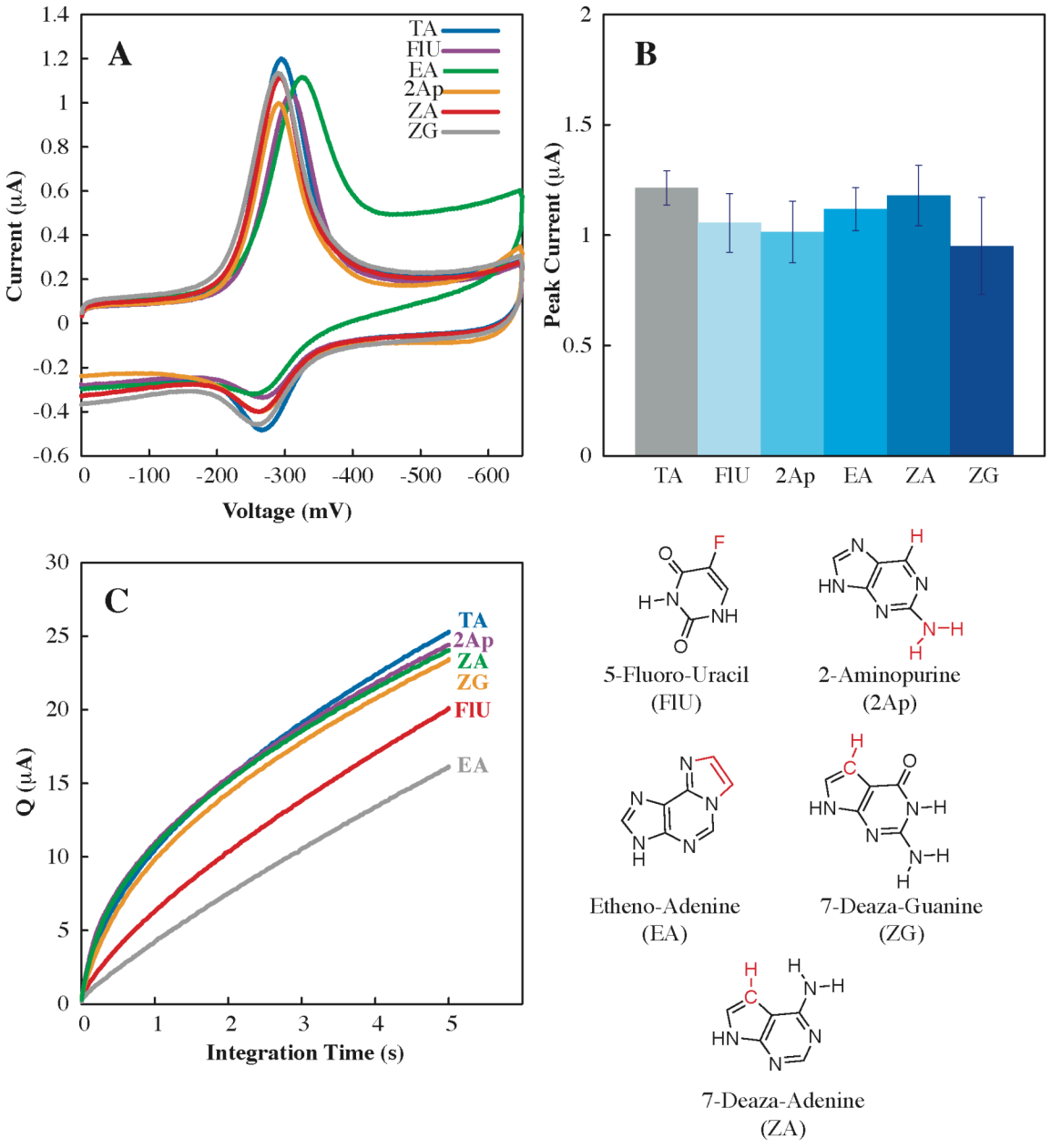

Table 2.3. Electrochemical detection of group 3 lesions.

Lesion	Sequence[a]	T_m (°C)	Q (μA) w/out electrocatalysis[b]	Q (μA) with electrocatalysis[c]
no lesion (TA)	SH – 5' – AGT ACA GTC ATC GCG 3' – TCA TGT CAG TAG CGC	60.0	1.27 ± 0.12	23.9 ± 1.7
5-Fluoro-Uracil (FlU)	SH – 5' – AGT ACA GTC ATC GCG 3' – TCA TGT CAG **U**AG CGC	59.9	1.06 ± 0.13	20.8 ± 0.93
2-Aminopurine (2Ap)	SH – 5' – AGT ACA GTC ATC GCG 3' – TCA TGU C**P**G TAG CGC	57.3	1.01 ± 0.14	20.6 ± 3.3
Etheno-Adenine (EA)	SH – 5' – AGT ACA GTC ATC GCG 3' – TCA TGT C**E**G TAG CGC	50.9	1.12 ± 0.10	18.8 ± 5.1
7-Deaza-Adenine (ZA)	SH – 5' – AGT ACA GTC ATC GCG 3' – TCA TGT C**Z**G TAG CGC	60.0	1.12 ± 0.14	24.5 ± 3.5
7-Deaza-Guanine (ZG)	SH – 5' – AGT ACA GTC ATC GCG 3' – TCA TGT CA**Z** TAG CGC	59.5	0.95 ± 0.22	24.0 ± 1.4

[a]SH - 5' represents $SH(CH_2)_2CONH(CH_2)_6NHCO$ at 5'-OH
[b]Electrochemical detection using 2 μM methylene blue (MB) as redox probe. Q = current at CV peak.
[c]Electrochemical detection with electrocatalysis: 0.5 μM MB, 2 mM $Fe(CN)_6^{3-}$. Q = integrated current at 5s.

Figure 2.5. Electrochemical detection of group 4 lesions. A. Cyclic voltammetry without electrocatalysis. B. Bar graph representing peak current attained in cyclic voltammetry experiments without electrocatalysis. C. Chronocoulometry with electrocatalysis. D. Structures of group 4 lesions. Deviations from standard base pairs are shown in red.

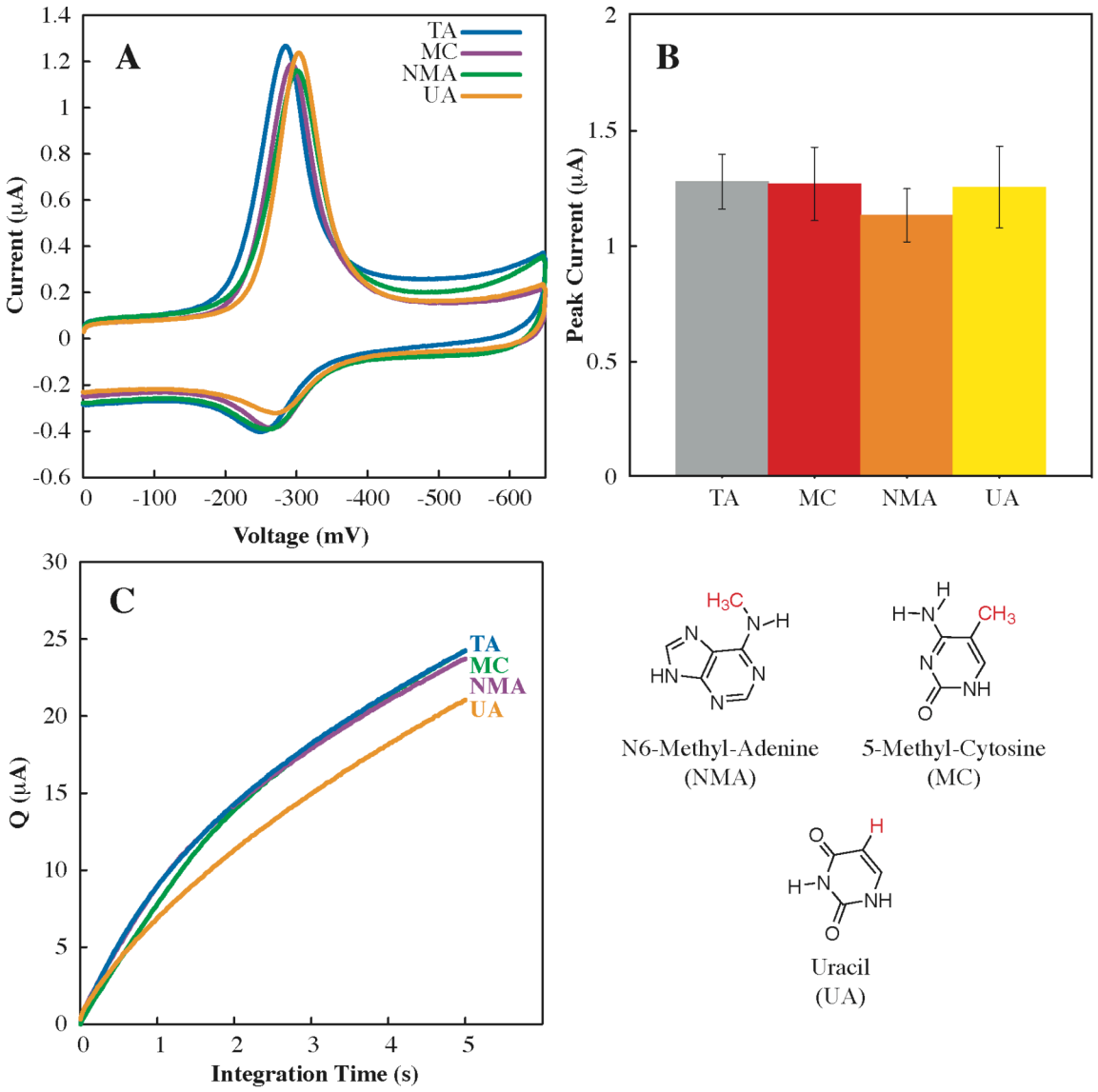

Table 2.4. Electrochemical detection of group 4 lesions.

Lesion	Sequence[a]	T_m (°C)	Q (μA) w/out electrocatalysis[b]	Q (μA) with electrocatalysis[c]
no lesion (TA)	SH – 5' – AGT ACA GTC ATC GCG 3' – TCA TGT CAG TAG CGC	54.3	1.27 ± 0.12	23.9 ± 1.7
5-Methyl-Cytosine (MC)	SH – 5' – AGT ACA GTC ATC GCG 3' – TCA TGT **C**AG TAG CGC	54.3	1.26 ± 0.16	22.8 ± 1.5
Uracil:A (UA)	SH – 5' – AGT ACA GTC ATC GCG 3' – TCA TG**U** CAG TAG CGC	53.2	1.25 ± 0.02	22.4 ± 1.0
N6-Methyl-Adenine (NA)	SH – 5' – AGT ACA GTC ATC GCG 3' – TCA TGT C**A**G TAG CGC	53.1	1.13 ± 0.12	23.47 ± 0.72

[a]SH - 5' represents $SH(CH_2)_2CONH(CH_2)_6NHCO$ at 5'-OH
[b]Electrochemical detection using 2 μM methylene blue (MB) as redox probe. Q = current at CV peak.
[c]Electrochemical detection with electrocatalysis: 0.5 μM MB, 2 mM $Fe(CN)_6^{3-}$. Q = integrated current at 5s.

Figure 2.6. Plot of Q versus ΔT_m based upon data in Tables 1–4. The best linear fit is shown, although $R^2 = 0.57$.

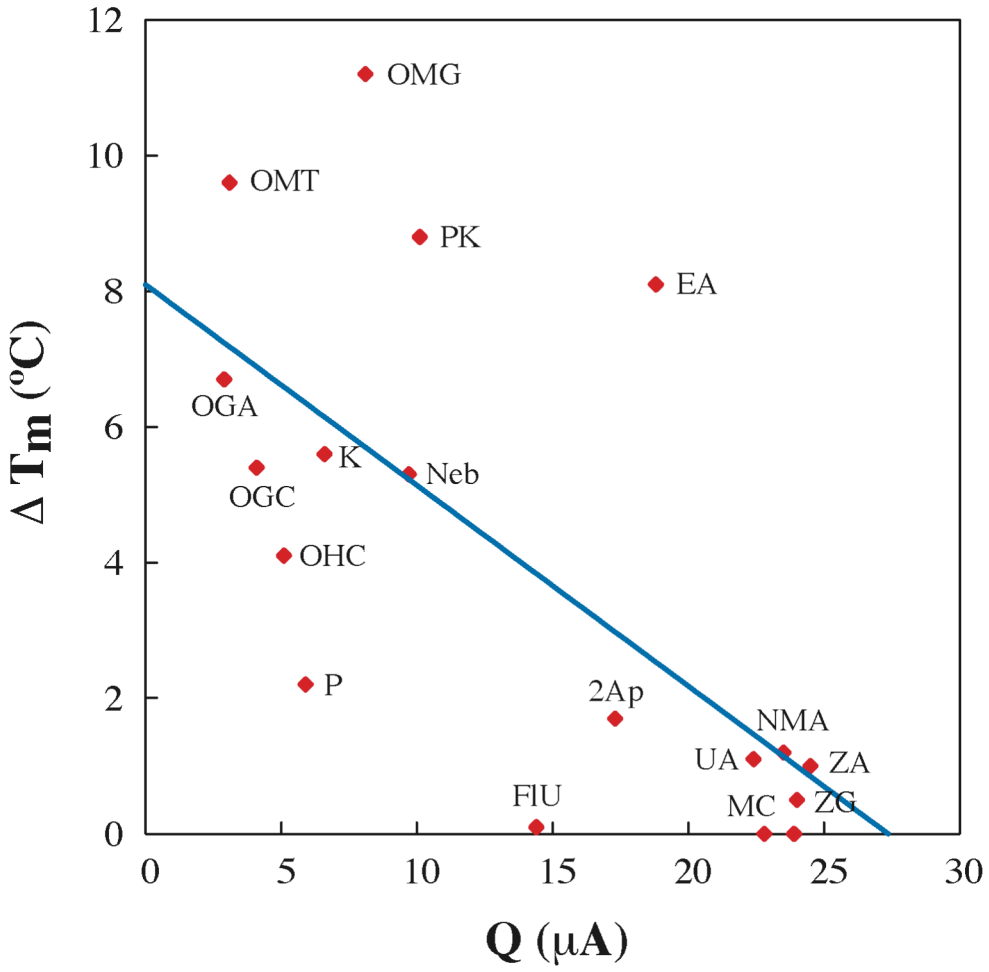

temperatures for these duplexes. It is noteworthy that these lesions do not promote a decrease in melting temperature.

Charge Transfer Efficiency versus Duplex Stability

Figure 2.6 shows a quantitative comparison of melting temperatures for the DNA duplexes, and charge accumulation in the DNA films, our measure of CT efficiency. Integrated charge accumulated after 5s (Q), as measured by our electrochemical assay, is plotted versus the absolute change in T_m from well-matched DNA (TA) for each duplex. The parameter ΔT_m, rather than absolute T_m, is used to account for any differences in experimental conditions among measurements on the lesion-containing DNAs (see Table 2.4). As evident in the plot, little statistical correlation is observed between the CT efficiency and the thermodynamic stability of the duplex; the squared correlation coefficient for these data (R^2) equals 0.57. The electrochemical assay used here depends upon different characteristics of the π-stacked DNA duplex rather than thermodynamic stability.

Discussion

Electrochemical DNA-based biosensors offer a sensitive method for detecting a range of modified bases in DNA. Many of the lesions examined here are implicated in a variety of cancers (*34-36*), so that new assays for low levels of lesions that employ electrocatalysis may provide a novel, early diagnostic tool.

The results presented here also establish the general trends in how base modifications affect CT efficiency. Alteration of the Watson-Crick hydrogen bonding interface yields a profound loss in CT efficiency (OMT, OMG, Neb, P, and K), as does

added steric bulk (P, K, OMT, and OMG). Base structure modifications that may induce base conformation changes (OG:A) also appear to diminish CT in DNA, as do those that place extra hydrophilic groups within the DNA helix (OHC). The presence or absence of methyl groups (MC, NMA, and UA) that do not disrupt hydrogen bonding interactions have little effect on CT efficiency. Little correlation between CT efficiency and thermal stability of duplex DNA containing a particular lesion is evident.

How are these lesions detected within the cell? The lesions examined here fall into three categories: oxidatively damaged bases, alkylated bases, and synthetic base analogues. The bases arising from oxidative or alkylation damage (OHC, OG, OMG, OMT) are all recognized by the cellular repair machinery. Enzymatic recognition by DNA repair systems is considered to involve similar factors to those that affect CT efficiency: hydrogen bonding patterns between the lesion and the opposite base, steric fit, the strength of the glycosidic bond, and base pair dynamics (*37*). OG is thought to be distinguished in part owing to protonation of the N7 nitrogen atom; N7 is not protonated in unmodified guanine (*38*). Repair of OG is also highly dependent on its base pairing environment. For instance, MutY, an enzyme that excises A from OG:A mispairs, can discriminate OG through stacking interactions involving an intercalated tyrosine coupled with hydrogen bonding of the OG to a serine (*39*). OHC is repaired by Endo III, a repair enzyme with a wide substrate specificity that targets oxidized pyrimidines (*40*). With this somewhat non-discriminate enzyme, recognition is thought to involve both the lability of the lesion glycosidic bond and hydrogen bonding of the enzyme with the base opposite the lesion (*41-42*). Direct damage reversal, where aberrant alkylation is transferred from DNA to a reactive cysteine in the repair protein, is the process that repairs O-methylation in DNA (*43*). OMT and OMG are recognized by methyltransferases and these enzymes likely recognize their substrates by sensing the instability of the lesion base pair (*44*). A

consensus has not yet been reached regarding the exact protein/DNA interactions that determine specificity, but structural studies indicate that hydrophobic residues near the reactive cysteine may be involved in recognizing the site of alkylation (*45-46*).

Many of these lesions associated with DNA damage have been previously reported as thermally destabilizing lesions (*47-49*), consistent with our findings here. Base modifications are also associated with dynamic changes in structure. OG is known to switch from the *anti* to the *syn* conformation while pairing with A (*50*). This conformational change is usually invoked as the basis for the mutagenic potential of OG (*51*), but it could also explain the drastic CT efficiency attenuation observed with the OG:A base pair. O-methylation (OMG, OMT) is also known to alter Watson-Crick hydrogen bonding patterns (*48-49*); OMG base paired with C does not form any hydrogen bonds unless C is protonated at the N3 position (*52*). OMT is similarly associated with increased flexibility at the lesion base pair (*49*), a property that, while linked to thermal instability and enzymatic recognition, may also be a factor in attenuation of CT efficiency. Synthetic lesions P, K, and Neb are not targeted by repair systems but can be thermally destabilizing (*24, 53*).

Among the lesions not well-detected in this assay are ZA and ZG, purines where the nitrogen atom at the 7 position is replaced by a carbon atom. This modification is known to lower the redox potential of the base, but the 7-deaza modification is not thought to cause destabilization or altered base pairing and stacking interactions (*54)*. 2-aminopurine base paired with thymine is similarly found to be thermodynamically stable and well stacked in the helix, thus it is not surprising that these three lesions are not easily detected using DNA CT (*5, 55*). FIU, when base paired with adenine, is also thermodynamically stable and not a source of structural distortion (*56*). EA, a sterically bulky lesion, is only marginally detected here. Structural studies indicate that EA forms

no hydrogen bonds with thymine and assumes a nonplanar conformation to accommodate the excess steric bulk of the lesion. Yet the lesion remains intrahelical, does not disrupt the structure of any flanking base pairs, and is purported to have stabilizing stacking interactions both with the bases above and below it and with the thymine opposite (*57*); perhaps these properties are sufficient to allow for some DNA-mediated reduction of MB in the presence of EA. Notably the poor coupling of EA in the base pair stack has been considered to account for the slow rate of base-base CT seen in other studies (*5*).

While O-methylation can be detected through CT, simple base alkylation, MC and NMA, cannot. Enzymatic methylation is generally thought to have a stabilizing effect on duplex DNA (*58-59*). MC can lead to a higher melting temperature for DNA duplexes (*59*) and methylation at the 5 position on the pyrimidine ring, in general, is purported to reduce base pair opening rates (*60*). NMA, also not significantly thermally destabilizing, exhibits more favorable stacking interactions with bases above and below (*58*). Since methylation, if anything, further stabilizes a well-stacked conformation, then, our inability to detect methylation through DNA CT should not be surprising.

Given that DNA CT offers a sensitive strategy to detect a variety of DNA base lesions, might DNA CT chemistry play some role in DNA repair? While recent crystal structures provide some insight into how lesions may be structurally discriminated, in most cases, it is not well understood how DNA damage is first located within the genome; this is especially true in the case of base excision repair, the process that is responsible for removing single instances of base damage (*37*). The results described here certainly support the idea that DNA-mediated CT could potentially provide the foundation for a method of long range detection of DNA damage by repair enzymes. In this context, the detection of 5-hydroxy-cytosine and 8-oxo-guanine is especially

significant as these are substrates for DNA repair glycosylases containing iron-sulfur cofactors that recently have demonstrated redox activity when bound to DNA (*16*).

SUMMARY

Electrochemical DNA-based sensors that exploit the inherent sensitivity of DNA-mediated charge transport (CT) to base pair stacking perturbations are capable of detecting base pair mismatches and some common base damage products. Here, using DNA-modified gold electrodes, monitoring the electrocatalytic reduction of DNA-bound methylene blue, we examine a wide range of base analogues and DNA damage products. Among those detected are base damage products O4-methyl-thymine, O6-methyl-guanine, 8-oxo-guanine, and 5-hydroxy-cytosine, as well as a therapeutic base, nebularine. The efficiency of DNA-mediated CT is found not to depend on the thermodynamic stability of the helix. However, general trends in how base modifications affect CT efficiency are apparent. Modifications of the hydrogen bonding interface in Watson-Crick base pairs yields a substantial loss in CT efficiency, as does added steric bulk. Base structure modifications that may induce base conformational changes also appear to attenuate CT in DNA as do those that bury hydrophilic groups within the DNA helix. Addition and subtraction of methyl groups that do not disrupt hydrogen bonding interactions do not have a large effect on CT efficiency. This sensitive detection methodology based upon DNA-mediated CT may have utility in diagnostic applications and implicates DNA-mediated CT as a possible damage detection mechanism for DNA repair enzymes.

REFERENCES

1. Friedberg, E. C., Walker, G. C., and Siede, W. (1995) *DNA Repair and Mutagenesis* ASM Press.

2. Lindahl, T. (1993) *Nature 362*, 709.

3. Cadet, J., Delatour, T., Douki, T., Gasparutto, D., Pouget, J. P., Ravanat, J. L., and Sauvaigo, S. (1999) *Mutat. Res. 424*, 9.

4. Hemminki, K., Koskinen, M., Rajeniemi, H., and Koskinen, M. (2000) *Regul. Toxicol. Pharmacol. 32*, 264.

5. Kelley, S. O., and Barton, J. K. (1995) *Science 283,* 375.

6. Kelley, S. O., Holmlin, R. E., Stemp, E. D. A., and Barton, J. K. (1997) *J. Am. Chem. Soc. 119*, 9861.

7. Holmlin, R. E., Dandliker, P. J., and Barton, J. K. (1997) *Angew. Chem., Int. Edn. Engl. 36*, 2715.

8. Schuster, G. B. (2000) *Acc. Chem. Res. 33*, 253.

9. Giese, B. (2002) *Annu. Rev. Biochem. 71*, 51.

10. Bhattacharya, P. K., and Barton, J. K. (2001) *J. Am. Chem. Soc. 123*, 8649.

11. Hall, D. B., and Barton, J. K. (1997) *J. Am. Chem. Soc. 119*, 5045.

12. Rajski, S. R., and Barton, J. K. (2001) *Biochemistry 40*, 5556.

13. Boon, E. M., Salas, J. E., and Barton, J. K. (2002) *Nat. Biotech. 20*, 282.

14. Rajski, S. R., Jackson, B. A., and Barton, J. K. (2000) *Mutat. Res. 447*, 49.

15. Friedman, K. A., and Heller, A. (2001) *J. Phys. Chem. B 105*, 11859.

16. Boon, E. M., Livingston, A. L., Chmiel, N. H., David, S. S., and Barton, J. K. (2003) *Proc. Natl. Acad. Sci. U.S.A. 100*, 12543; *ibid. 101,* 4718.

17. Kelley, S. O., Boon, E. M., Barton, J. K., Jackson, N. M., and Hill, M. G. (1999) *Nucleic Acids Res. 27*, 4830.

18. Boon, E. M., Ceres, D. M., Drummond, T. G., Hill, M. G., and Barton, J. K. (2000) *Nat. Biotech. 18*, 1096.

19. Drummond, T.G., Hill, M.G., and Barton, J.K. (2003) *Nature Biotechnology 21*, 1192.

20. Thorp, H. H. (2004) *Topics Curr. Chem. 237,* 159.

21. Boon, E. M., Barton, J. K., Pradeepkumar, P. I., Isaksson, J., Petit, C., and Chattopadhyaya, J. (2003) *Angew. Chem., Int. Ed. Engl. 41*, 3402.

22. Kelley, S. O., Barton, J. K., Jackson, N. M., and Hill, M. G. (1997) *Bioconjugate Chem. 8*, 31.

23. Bjelland, S., and Seeberg, E. (2003) *Mutat. Res. 531*, 37.

24. Hill, F., Loakes, D., and Brown, D. M. (1998) *Proc. Natl. Acad. Sci. U.S.A. 95*, 4258.

25. Brown, G. B., and Weliky, V. S. (1953) *J. Biol. Chem. 204*, 1019.

26. Pratt, W. B., Ruddon, R. W., Ensminger, W. D., and Maybaum, J. (1994) The Anticancer Drugs 2nd ed., Oxford University Press, New York.

27. Ward, D. C., Reich, E., and Stryer, L. (1969) *J. Biol. Chem. 244*, 1228.

28. Barrio, J. R., Secrist, J. A., and Leonard, N. J. (1972) *Biochem. Biophys. Res. Commun. 46*, 597.

29. Latimer, L. J., and Lee, J. S. (1991) *J. Biol. Chem. 266*, 13849.

30. Porello, S. L., Williams, S. D., Kuhn H., Michaels M. L., and David, S. S., (1996) *J. Am. Chem. Soc.118*, 10684.

31. Bird, A. (1992) *Cell 70,* 5.

32. Desrosiers, R., Friderici, K., and Rottman, F. (1974) *Proc. Natl. Acad. Sci. U.S.A. 71*, 3971.

33. Blount, B. C., Mack, M. M., Wehr, C. M., MacGregor, J. T., Hiatt, R. A., Wang, G., Wickramasinghe, S. N., Everson, R. B., and Ames, B. N. (1997) *Proc. Natl. Acad. Sci. U.S.A. 94*, 3290.

34. Goth, R., and Rajewsky, M. F. (1974) *Proc. Natl. Acad. Sci. U.S.A. 71*, 639.

35. Georgiadis, P., Xu, Y. Z., and Swann, P. F. (1991) *Biochemistry 30*, 11725.

36. Olinski, R., Gackowski, D., Rozalski, R., Fokinski, M., and Bialowski, K. (2003) *Mutat. Res. 531*, 177.

37. David, S. S., and Williams, S. D. (1998) *Chem. Rev. 98*, 1221.

38. Bruner, S. D., Norman, D. P. G., and Verdine, G. L. (2000) *Nature 403*, 859.

39. Fromme, C. J., Banarjee, A. A., Huang, S. L., and Verdine, G. L. (2004) *Nature*

427, 652.

40. Hatahett, Z., Kow, Y. W., Purmal, A. A., Cunningham, R. P., Wallace, S. S. (1994) *J. Biol. Chem. 269*, 18814.

41. Fromme, J. C., and Verdine, G. L. (2003) *EMBO J. 22,* 3461.

42. Berdal, K. G., Johansen, R. F., and Seeberg, E. (1998) *EMBO J. 17*, 363.

43. Sassanfar, M., Posanjh, M. K., Essigman, J. M., and Samson, L. (1991) *J. Biol. Chem. 266*, 2767.

44. Duguid, E. M., Mishina, Y., and He, C. (2003) *Chem. Biol. 10*, 827.

45. Daniels, D. S., Mol, C. D., Arvai, A. S., Kanugula, S., Pegg, A. E., and Tainer, J. A. (2000) *EMBO J. 19* 1719.

46. Moore, M. H., Gulbis, J. M., Dodson, E. J., Demple, B., and Moody, P. C. (1994) *EMBO J. 13*, 1495.

47. Oda, Y., Uesugi, S., Ikehara, M., Nishimura, S., Kawase, Y., Ishikawa, H., Inoue, H., and Ohtsuka, E. (1991) *Nucleic Acids Res. 19*, 1407.

48. Gaffney, B. L., and Jones, R. A. (1989) *Biochemistry 28*, 5881.

49. Cruzeiro-Hansson, L., and Goodfellow, J. M. (1994) *Carcinogenesis 15*, 1525.

50. Kouchakdjian, M., Bodepudi, V., Shibutani, S., Eisenberg, M., Johnson, F., Grollman, A. P., and Patel, D. J. (1991) *Biochemistry 30*, 1403.

51. Cheng, K. C., Cahill, D. S., Kasai, H., Nishimura, S., and Loeb, L. A. (1992) *J. Biol. Chem. 267*, 166.

52. Williams, L. D., and Shaw, B. R. (1987) *Proc. Natl. Acad. Sci. U.S.A. 84,* 1779.

53. Jiricny, J., Wood, S. G., Martin, D., and Ubasawa, A. (1986) *Nucleic Acids Res. 14*, 6579.

54. Baik, M., Silverman, J. S., Yang, I. V., Ropp, P. A., Szalai, V. A., Yang, W., and Thorp, H. H. (2001) *J. Phys. Chem. B 105,* 6437.

55. Law, S.M., Eritja, R., Goodman, M.F., and Breslauer, K.J. (1996) *Biochemistry 35*, 12329.

56. Kramer, A. B., Mikita, T., and Beardsley, G. P. (1987) *Biochemistry 26*, 391.

57. Kouchakdjian, M., Eisenberg, M., Yarema, K., Basu, A., Essigmann, J., and Patel, D. J. (1991) *Biochemistry 30*, 1820.

58. Engel, J. D., and von Hippel, P. H. (1977) *J. Biol. Chem. 253*, 927.

59. Marcourt, L., Cordier, C., Couesnon, T., and Dodin, G. (1999) *Eur. J. Biochem. 265*, 1032.

60. Warmlander, S., Sponer, J. E., Sponer, J., and Leijon, M. (2002) *J. Biol. Chem. 277*, 28491.

CHAPTER 3

DNA-bound Redox Activity of DNA Repair Glycosylases Containing [4Fe4S] Clusters

Adapted from Boal, A. K., Yavin, E., Lukianova, O. A., O'Shea, V. L., David, S. S., and Barton, J. K. (2005) *Biochemistry 44*, 8397.

E. Yavin performed EPR experiments. O. Lukianova and V. O'Shea prepared protein samples.

INTRODUCTION

Encoded in the sequence of DNA is all of the genetic information of a cell. Yet the primary structure of DNA is remarkably dynamic (*1*). Large scale rearrangements lead to gross changes in sequence, while chemical modifications to individual bases may lead to single base mutations. The consequences of large- and small-scale DNA sequence alterations can be beneficial, allowing for increased genetic diversity, but more often are deleterious, leading to mutation and disease. To counteract the harmful nature of DNA modification, organisms have developed diverse repair machinery aimed at protecting the genetic code (*2*).

Damage to a single DNA base is commonly repaired by two different pathways: direct damage reversal that repairs a damaged base without excising it, and base excision repair (BER), a pathway that removes a single damaged base and replaces it with a new one (*3*). The first step in the BER pathway involves the glycosylase enzyme, a protein that locates the damaged base and excises it from the helix. The excision reaction catalyzed by glycosylases is relatively well understood at the molecular level, but the mechanism by which these enzymes locate their substrates in the first place remains elusive (*4*). This detection challenge faced by glycosylases is formidable on two fronts. First, the base mismatches and modifications, the substrates for the glycosylases, often occur at low frequencies and are isolated among a vast amount of undamaged DNA (*1*). Second, the damage products detected by these enzymes represent very subtle deviations from the four natural DNA bases; often they vary by the addition or subtraction of a single functional group or even simply the mismatching of otherwise natural base pairs.

Some evidence suggests that glycosylases locate damage by processing along the DNA helix rather than randomly diffusing from site to site (*5*). Processive mechanisms offer some enhancement in rate and efficiency by reducing the dimensionality of the search process. However, it is not clear that procession alone would be sufficient to account for the remarkable repair efficiency of these enzymes. In addition, BER enzymes operate in a complicated cellular environment, one in which a simple processive search process may be impossible (*6*). High salt concentrations exist that prevent electrostatic interactions between proteins and DNA (*7*). DNA is highly compact and covered in proteins much of the time, preventing rapid translocation along the helix (*8*). Glycosylases are often present in very low copy numbers (*9*) and may be involved in intricate relationships with other proteins, including those related to other repair pathways, replication, and transcription processes (*10-17*). All of these facts indicate that damage detection by glycosylases is a highly complex process, one that may require more than one mechanism.

The base pair π-stack of double helical DNA has the unique ability to serve as a medium for charge transport over distances of at least 200 Å (*18-23*). This property of DNA is highly dependent on the integrity of the π-stack; perturbations that affect the structure and dynamics of DNA, including mismatched base pairs and damage products, greatly diminish the efficiency of DNA charge transport (*24-27*). In fact, devices based on DNA-mediated charge transport have proven to be powerful sensors of mutation in DNA (*28*). Additionally, evidence suggests that DNA charge transport can occur in biologically relevant environments; within a nucleosome core particle (*29*) and inside the nucleus of HeLa cells (*30*). While a biological role for DNA-mediated charge transport has not been definitively established, it has been proposed that DNA charge transport

may be involved in DNA damage and repair (*31-33*). The exquisite sensitivity of DNA-mediated charge transport to perturbations in the π-stack prompts one to ask: might DNA repair enzymes exploit this property of DNA in their search for damage in the genome?

MutY, one of many glycosylases containing a [4Fe4S] cluster (*34-37*), has recently displayed redox activity when investigated electrochemically on DNA-modified electrodes (*33*). MutY, containing 350 residues and the [4Fe4S] cofactor, acts as a glycosylase to remove adenine from G:A and 7,8-dihydro-8-oxo-2-deoxyguanonsine (8-oxo-G):A mismatches (*38-52*). Initial characterization of the [4Fe4S] cluster in MutY and Endonuclease III (EndoIII), a homologous enzyme with a substrate specificity instead for damaged pyrimidines (*53-62*), demonstrated that the cluster is in the 2+ oxidation state and is not readily oxidized or reduced within a physiologically relevant range of potentials; cluster decomposition occurs with oxidation but photoreduction does yield the $[4Fe4S]^{1+}$ cluster (*34*). In the presence of DNA, however, MutY has a midpoint potential of +90 mV versus NHE (*33*). This redox potential is typical of high-potential iron proteins (*63*) indicating that, when MutY is bound to DNA, the redox potential of the enzyme shifts such that the 3+ oxidation state of the cluster becomes accessible. Earlier redox studies on MutY and EndoIII conducted in the absence of DNA had argued for a structural rather than redox role for the ubiquitous cluster (*52, 61-62, 64*), yet it was demonstrated that the [4Fe4S] cluster in MutY was not required for protein folding but was essential for activity (*65*).

Given the redox activity for MutY now demonstrated with DNA activation, a model has been proposed describing a role for the cluster in damage detection by MutY (*33*). In this model, DNA-mediated charge transport between two MutY proteins would serve as a fast, efficient scanning mechanism for damage in DNA; in the absence of intervening lesions, DNA charge transport between proteins would be facile, permitting

reduction with concomitant dissociation of the protein from undamaged regions of the genome. Through this fast scanning and sorting process, MutY would quickly concentrate near sites of damage in DNA. Local procession on a slower timescale to a nearby site would then allow for efficient substrate recognition and repair.

EndoIII and *A. fulgidus* UDG (AfUDG), like MutY, are glycosylases that contain a [4Fe4S] cluster (*34-35*). EndoIII repairs a wide variety of oxidized pyrimidines in DNA. The cluster in EndoIII is well characterized spectroscopically (*34, 64*). EndoIII is of particular significance because, as with MutY, it is present in many organisms (*66-68*). AfUDG, on the other hand, is part of a special class of uracil glycosylases (*69*). These enzymes, known as family 4 UDGs, are present mostly in thermophilic bacteria and are the only family of UDGs to contain a [4Fe4S] cluster (*35, 69-74*). Cytosine deamination, the main process by which uracil is produced in DNA, is greatly enhanced at high temperatures (*75*). In spite of this fact, thermophiles do not exhibit a higher mutation rate than other organisms (*76*). BER enzymes in thermophiles therefore face an even greater challenge to efficiently eliminate base damage. Perhaps the [4Fe4S] cofactor in these enzymes is involved in enhancing the efficacy of repair?

Here we determine whether the DNA-bound redox activity seen with MutY is a more general characteristic of DNA glycosylases containing a [4Fe4S] cluster. EndoIII and AfUDG are both investigated electrochemically on DNA-modified electrodes to determine if the [4Fe4S] cluster in each is redox-active and if that redox activity is DNA-mediated. Furthermore, all three proteins are examined by EPR spectroscopy with a Co(III) oxidant to establish whether DNA binding can also promote oxidation of the cluster in solution. These experiments have implications for the further development of our model to include the possibility of collaborative searching for damage by redox-active glycosylases.

MATERIALS AND METHODS

Materials

All buffers were freshly prepared and filtered prior to use. Potassium ferricyanide was purchased from EM Science. Poly(dGC) (ε_{260} = 8,400 $M^{-1}cm^{-1}$) was purchased from Amersham Pharmacia and was passed through spin columns (BioRad) prior to use. All reagents for DNA synthesis were purchased from Glen Research.

$[Co(phen)_3]Cl_3$ was synthesized from $CoSO_4.7H_2O$ according to a literature procedure (*77*). The cobalt complex was precipitated first as the PF_6 salt by adding a solution of NH_4PF_6 in water (20% w/v) to the reaction. The Co(III) complex was then converted to its chloride salt by dissolving 200 mg $[Co(phen)_3]PF_6$ in 5 ml CH_3CN followed by the addition of $(tBu)_4NCl$ in 3 mL CH_3CN (20% w/v) and formation of a yellow precipitate. After filtration and washing with acetonitrile, the isolated complex $[Co(phen)_3]Cl_3$ was fully characterized by NMR and mass spectrometry.

Protein Preparation

EndoIII was generously donated by Professor T. R. O'Connor (City of Hope) (*78*). The purification of AfUDG was modified from the reported procedure (*74*). The pET28a-*afung* plasmid containing the gene encoding the AfUDG protein was provided by Dr. William A. Franklin (Albert Einstein). Rosetta(DE3)pLysS cells (Novagen) transformed with the pET28a-*afudg* plasmid were inoculated into LB media containing 34 μg/mL kanamycin and grown at 37 °C in 4L to an OD_{600} = 0.5-0.7. At this stage, 1 mM isopropyl-1-thio-β-D-galactopyranoside (IPTG) was added, and the cells were incubated

for an additional 6 hours at 30 °C. The cells were harvested by centrifugation (10000 rpm, 7 minutes, 4 °C), resuspended in 40 mL of ice-cold buffer L (25 mM Tris, 250 mM NaCl, pH 7.6) supplemented with 1 mM PMSF. The cells were disrupted by sonication (Branson Sonic Power CO., model 350, 70% pulse, 30 s on followed by 30 s off, repeated six times), and centrifuged to remove cellular debris (10000 rpm, 5 minutes, 4 °C). The proteins in the supernatant were batch-bound to Ni^{2+}-NTA resin (1.5 mL/40 mL supernatant) by gentle rocking at 4 °C for 1 hour. The protein-bound resin was poured into an empty column (10 mL) and washed with 25 mL of 2X buffer L, followed by 5 mL of 1X buffer L. Protein was eluted with 2-5 mL of 1X buffer L containing 250 mM imidazole and diluted 8-10 fold with Buffer A (25 mM Tris, pH 7.6). The protein solution was loaded onto a High S cartridge (BioRad), pre-equilibrated with 90% Buffer A and 10% Buffer B (25 mM Tris, pH 7.6, 1 M NaCl). The AfUDG protein was eluted by increasing the concentration of buffer B. Glycerol (10%) was added to the protein solution for storage at -80 °C. SDS-PAGE with Sypro Orange staining indicated the protein to be greater than 95% pure. Total protein concentrations were determined by the method of Bradford using BSA as the standard.

MutY was utilized fused to maltose binding protein to allow experiments to be carried out at high concentrations. JM101 *mutY- E. coli* cells containing a pMAL-c2x-*muty* vector encoding maltose binding protein fused to the N-terminus of MutY were used to inoculate LB media (200 mL) containing 100 μg/mL ampicillin, 15 μg/mL tetracycline, and 0.2 g/mL glucose (LBATG). After overnight incubation at 37 °C, the culture was added to 4 L LBATG which was further incubated with shaking at 37 °C until the OD at A_{600} was 0.6. IPTG (0.3 mM) was then added and the cells were incubated at 30 °C for 3.5 hours. After centrifugation (10,000 rpm for 7 minutes), the cells were

resuspended in 30 mL of 50 mM Tris-HCl pH 8 containing 2 mM EDTA, 5% glycerol, 250 mM NaCl, 5 mM DTT, and 1 mM PMSF. The cells were lysed using a French press, the process being repeated twice, followed by centrifugation to remove cellular debris. The cell lysate (~ 40 mL) was loaded onto two separate 20 mL amylose (New England BioLabs) columns pre-equilibrated with Buffer C (20 mM HEPES-KOH pH 7.5 at 4 °C, 200 mM NaCl, 1 mM EDTA, and 1 mM DTT). MutY was eluted using 50 mL buffer C containing 10 mM maltose. The protein-containing eluent was diluted twofold with buffer D (20 mM HEPES-KOH pH 7.5 at 4 °C, 1 mM EDTA, 5% glycerol, and 1 mM DTT), filtered with a 0.45 micron filter, and loaded onto a 5 mL heparin column (Amersham Biosciences) on a BioRad BioLogic. MutY was eluted using a gradient of 5 – 100% buffer D containing 1 M NaCl. Fractions containing pure MutY, as determined by SDS-PAGE with Sypro-orange staining, were concentrated and the buffer exchanged (20 mM Na-Phosphate pH 7.5, 100 mM NaCl, 10% glycerol, 1 mM EDTA) using an Amicon stirred ultrafiltration cell. The protein concentration was determined using an approximate ε(410 nm) of 17,000 $M^{-1}cm^{-1}$.

Preparation of DNA-modified Electrodes

Oligonucleotides were synthesized using standard phosphoramidite chemistry (*79*). Single strand oligonucleotides were modified at the 5' end with a thiol moiety to facilitate covalent attachment to a gold electrode surface, as described earlier (*80*). Oligonucleotides were purified by HPLC, hybridized to their complements and self-assembled into a loosely packed monolayer on a Au surface (*27*) in 50 mM NaCl, 5 mM sodium phosphate, pH 7.0. The electrode surface was then further passivated by incubation using mercaptohexanol (100 mM) in assembly buffer for 30 minutes.

Electrodes were then rinsed with protein storage buffer (MutY and EndoIII: 100 mM NaCl, 20 mM sodium phosphate, 1 mM EDTA, 10% glycerol, pH 7.0; AfUDG; 25 mM Tris-HCl, 500 mM NaCl, 5% glycerol, pH 7.6), and 50 μL protein (550 μM MutY, 150 μM EndoIII, or 360 μM AfUDG) in their storage buffers were added to the electrode surface and allowed to incubate for 10–15 minutes prior to measurement.

Electrochemistry Measurements

Low volume constraints necessitated the use of a specialized low-volume cell for protein electrochemistry experiments. The working electrode consisted of a Au(111) on mica chip and a Pt wire served as the auxiliary electrode. The reference electrode was a Ag/AgCl electrode modified with a tip containing 4% agarose in 3 M NaCl. This reference electrode was calibrated with ferrocene carboxylate and compared both to an unmodified Ag/AgCl reference electrode and a saturated calomel electrode. All measurements were made using a BAS CV50W model electrochemical analyzer.

EPR Spectroscopy

X-band EPR spectra were obtained on a Bruker EMX spectrometer equipped with a rectangular cavity working in the TE_{102} mode. Low temperature measurements (10K) were conducted with an Oxford continuous-flow helium cryostat (temperature range 3.6–300 K). A frequency counter built into the microwave bridge provided accurate frequency values. Solutions were prepared by adding the protein (50 μM) to a solution of oxidant (150 μM) (with the exception of EndoIII where the protein concentration was 10 μM and the oxidant concentration was 30 μM) in the presence or absence of poly(dGC) (1.5 mM in base pairs). Samples were incubated at ambient

temperature (10 min) or heated to 55 ºC (5 min) and cooled down to ambient temperature. All samples were frozen in liquid nitrogen prior to EPR measurement at low temperature. EPR parameters were as follows: receiver gain = 5.64×10^3, modulation amplitude = 4G, microwave power = 1.27 mW.

RESULTS AND DISCUSSION

Electrochemistry on DNA-modified Electrodes

The redox properties of each protein (MutY, EndoIII, and AfUDG) were investigated on a loosely packed DNA-modified electrode surface passivated with mercaptohexanol (MCH) (Figure 3.1). AfUDG and EndoIII both exhibit a redox signal using a DNA-modified electrode (Figure 3.2). The midpoint potential for AfUDG is 95 ± 3 mV versus NHE, while the midpoint potential for EndoIII is 58 ± 6 mV versus NHE. The measured midpoint potentials are similar to that previously measured for MutY of 90 mV versus NHE (*33*). The signals observed are quasi-reversible and robust over the course of the experiment. For each protein, the signal grows in over 5-10 minutes and remains at a constant intensity for up to 30 minutes after addition of the protein. No evidence of cluster degradation is observed during the experiment. Scan rate dependence measurements show a linear relationship between the peak current and the square root of the scan rate, an indication of a diffusion-limited process. However, measurements of electron transfer rates based on peak splitting (*81*) indicate a relatively slow rate of electron transfer (1–10 s^{-1}), consistent with earlier measurements of MutY (*33*). Importantly, as shown in Figure 3.2, each protein requires DNA for redox activity; at a MCH-modified surface lacking DNA, no signal is evident. In fact, even with 1 mM protein, no redox signal could be observed.

Figure 3.1. Schematic illustration of the electrochemical measurement of DNA-binding proteins containing [4Fe4S] clusters at a DNA-modified Au electrode surface.

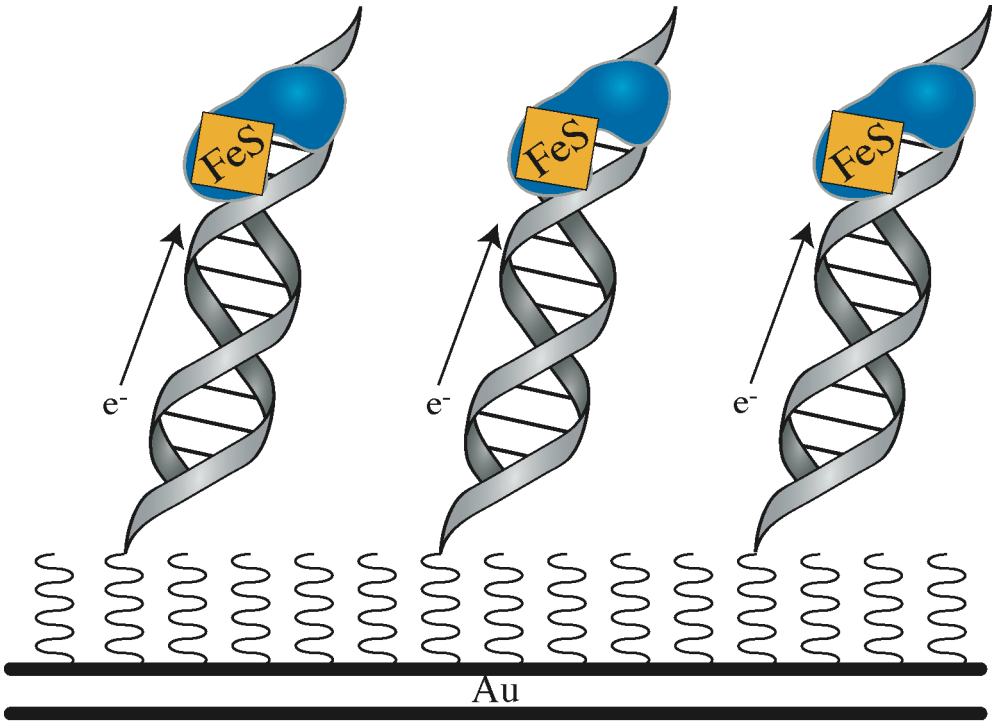

Figure 3.2. Cyclic voltammetry of MutY (left), EndoIII (middle), and AfUDG (right) at DNA-modified electrodes (shown in black) (Ag/AgCl reference electrode, Pt auxiliary electrode, 50 mV/sec scan rate). Buffer conditions for MutY and EndoIII are 100 mM NaCl, 20 mM sodium phosphate, 1 mM EDTA, 10% glycerol, pH 7.0. Buffer conditions for AfUDG are 25 mM Tris-HCl, 500 mM NaCl, 5% glycerol, pH 7.6. Average potentials, based on several trials, are 90 mV for MutY, 59 mV for EndoIII, and 95 mV for AfUDG, all versus NHE. DNA is required to observe the protein redox activity; proteins examined on a MCH-modified electrode (shown in grey) exhibit no electrochemical signal.

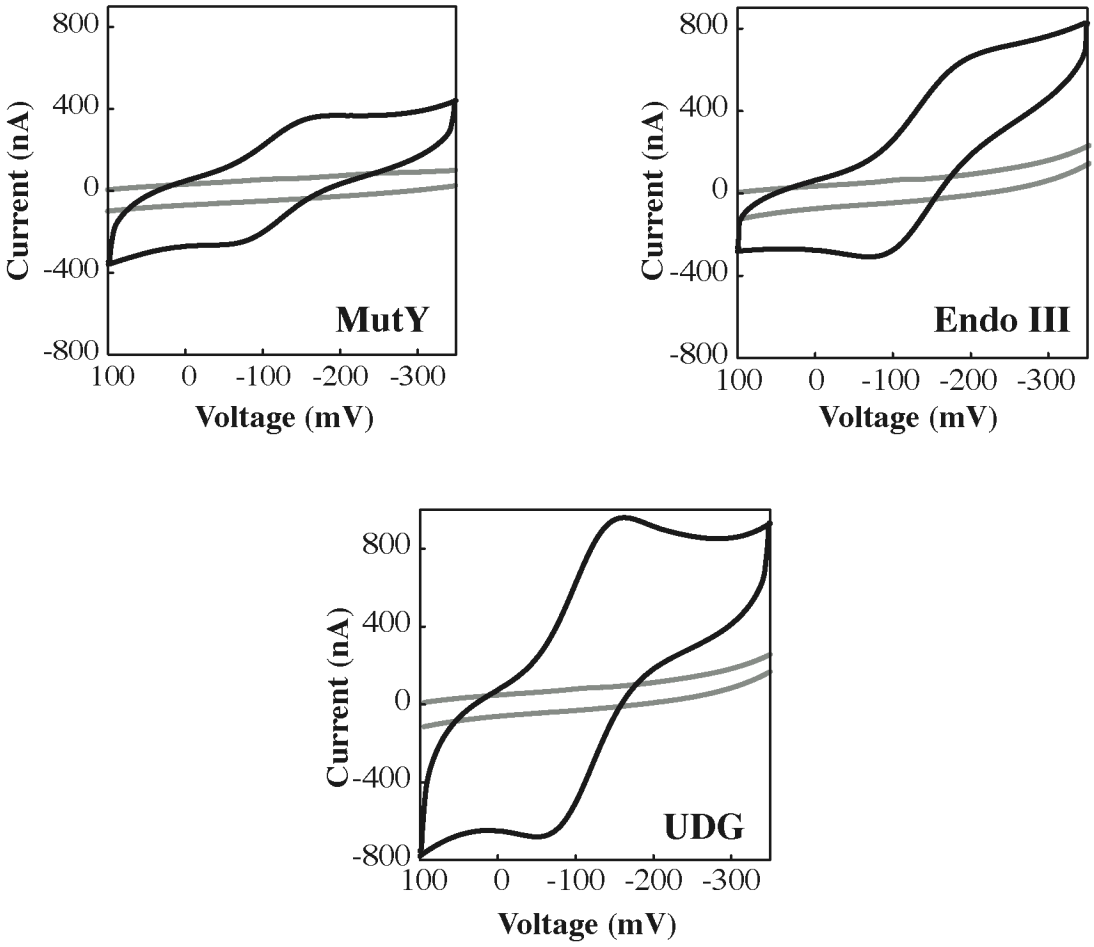

Covalent modification of electrodes is a technique commonly employed in protein electrochemistry both to concentrate proteins at the electrode surface and to properly orient buried redox centers for direct electron transfer with the electrode (*82-83*). To determine whether the redox activity observed here at a DNA-modified electrode is the result of direct interaction between the protein and the electrode surface or whether electron transfer to the cluster is mediated by the DNA π-stack, these proteins were investigated at a surface modified with a duplex containing an abasic site (thiol modified strand SH-5'-AGTACAGTCATCGCG hybridized to a complement containing an abasic site opposite the underlined thymine). We have determined previously that an intervening abasic site serves to diminish the redox signal from DNA-bound probes owing to the associated perturbation to the base pair stack (*28*). As evident in Figure 3.3, when each of these proteins is monitored electrochemically on a monolayer containing an abasic site, the redox signal is significantly attenuated. These observations support the idea that the redox chemistry obtained is DNA-mediated. The potential determined is therefore characteristic of the *DNA-bound* protein.

To test further that DNA binding promotes the shift in +3/+2 redox potential, activating the protein towards oxidation, we examined the protein electrochemistry on the DNA-modified surface before and after bulk electrolysis. Shown in Figure 3.4 are cyclic voltammograms for EndoIII bound to the DNA-modified electrode before and after shifts in applied potential. As is evident, when the sample is equilibrated and then the potential is held at –350 mV for a discrete time interval so as to reduce the DNA-bound protein, the signal is attenuated, consistent with reduced protein dissociating from the DNA-modified electrode. Similarly, as is also shown in Figure 3.4, when the potential is held at +50 mV, to promote oxidation, the signal increases, consistent with protein

Figure 3.3. Electrochemistry (clockwise from top right) of MutY, AfUDG, and EndoIII at an electrode modified with well matched DNA duplexes (TA DNA in black) or DNA duplexes containing an abasic site (Ab DNA in grey) as measured by cyclic voltammetry (Ag/AgCl reference electrode, Pt auxiliary electrode, 50 mV/sec scan rate). Buffer conditions for MutY and EndoIII are 100 mM NaCl, 20 mM sodium phosphate, 1 mM EDTA, 10% glycerol, pH 7.0. Buffer conditions for AfUDG are 25 mM Tris-HCl, 500 mM NaCl, 5% glycerol, pH 7.6.

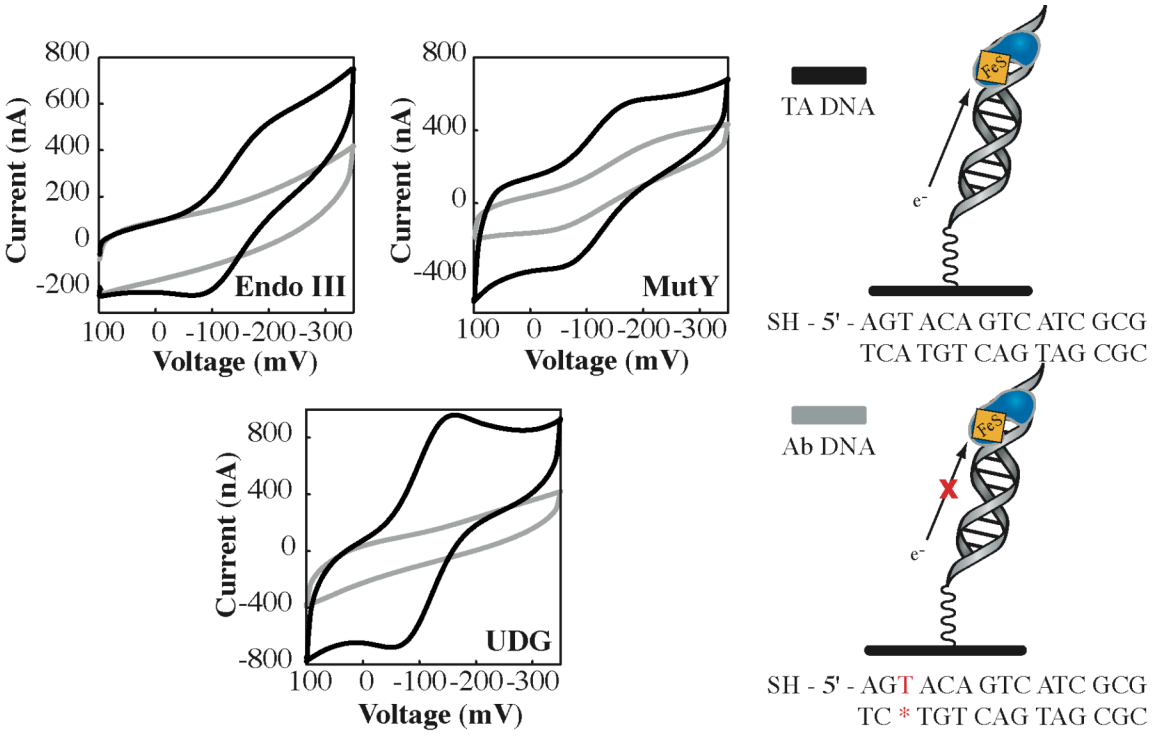

Figure 3.4. Cyclic voltammetry of EndoIII before and after bulk electrolysis. Left panel shows CV before (grey trace) and after (black trace) bulk electrolysis for 5 minutes at -350 mV (versus Ag/AgCl). Right panel shows CV before (grey trace) and after (black trace) bulk electrolysis for 5 minutes at +50 mV (versus Ag/AgCl). An increase in peak intensity is evident after electrolysis at +50 mV, whereas a corresponding decrease is observed after electrolysis at -350 mV.

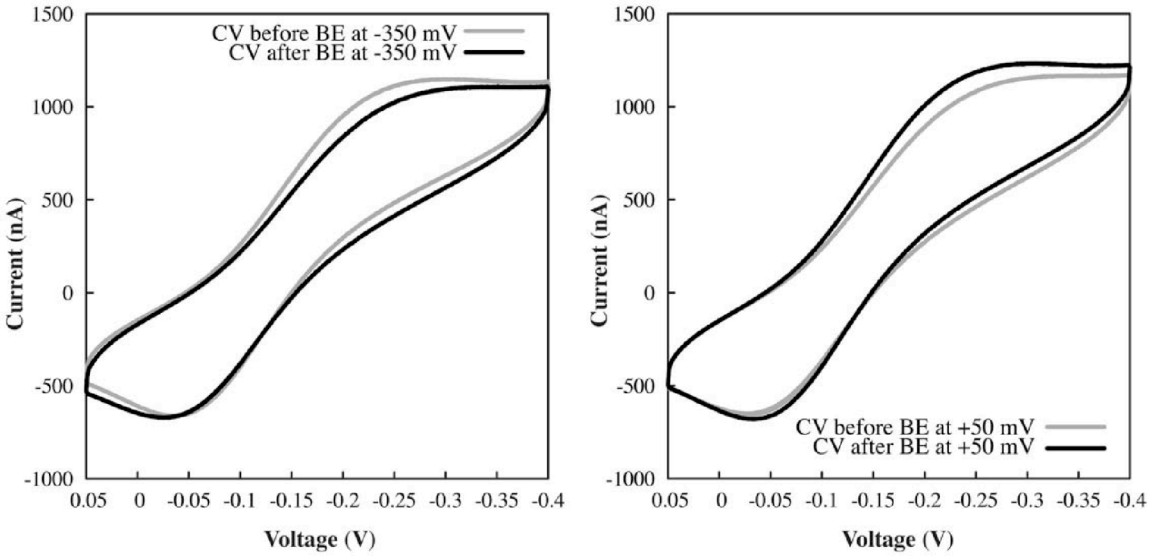

oxidation yielding association with DNA. Calculation of net changes in area under the cyclic voltammograms reveal a 14% difference in both directions as a result of electrolysis. Analogous results were found with the other BER enzymes examined. While these results cannot provide a quantitative determination of solution binding affinities, these data nonetheless provide support for a greater DNA affinity for the protein in the oxidized form versus the reduced +2 state.

Low Temperature EPR to Probe DNA-bound Redox Chemistry

All three proteins were investigated by EPR spectroscopy in the presence and absence of DNA using $Co(phen)_3^{3+}$ as the oxidant. EPR measurements were performed at 10K to observe any changes in the oxidation state of the [4Fe4S] cluster. The [4Fe4S] cluster in each of these proteins is in the 2+ oxidation state when free in solution, a configuration that is diamagnetic and EPR-silent (*34-35, 84*). However both the $[4Fe4S]^{3+}$ and $[3Fe4S]^{1+}$, a common damage product resulting from hydrolysis of the oxidized [4Fe4S] cluster (*63, 85-86*), are EPR-active and give rise to distinctive spectra (*84, 87-90*).

As expected, MutY, in the presence and absence of DNA, yields no EPR signal. The $[4Fe4S]^{2+}$ cluster in MutY is largely in the 2+ oxidation state and EPR-silent. When MutY (50 μM) is incubated with $[Co(phen)_3]^{3+}$ (150 μM), a small signal appears, that looks much like a [3Fe4S] cluster (*85, 89-90*) with g values at 2.02 and 1.99 (Figure 5). In the presence of DNA and $[Co(phen)_3]^{3+}$ (150 μM), this signal is also evident but the intensity is much greater (~ 4-fold by integration). It appears then that the presence of DNA enhances oxidation by Co(III). Since the cobalt complex binds DNA (*91-92*), albeit weakly, we also examined the oxidation reaction with an excess of $[Co(phen)_3]^{3+}$.

Figure 3.5. EPR spectroscopy at 10K of MutY in the presence of DNA (light grey), 150 μM $[Co(phen)_3]^{3+}$ without DNA (dark grey), 500 μM $[Co(phen)_3]^{3+}$ but no DNA (dotted line), and MutY with DNA and 150 μM Co(III) (black). Signal 1 shows g = 2.02, signal 2 shows g = 1.99.

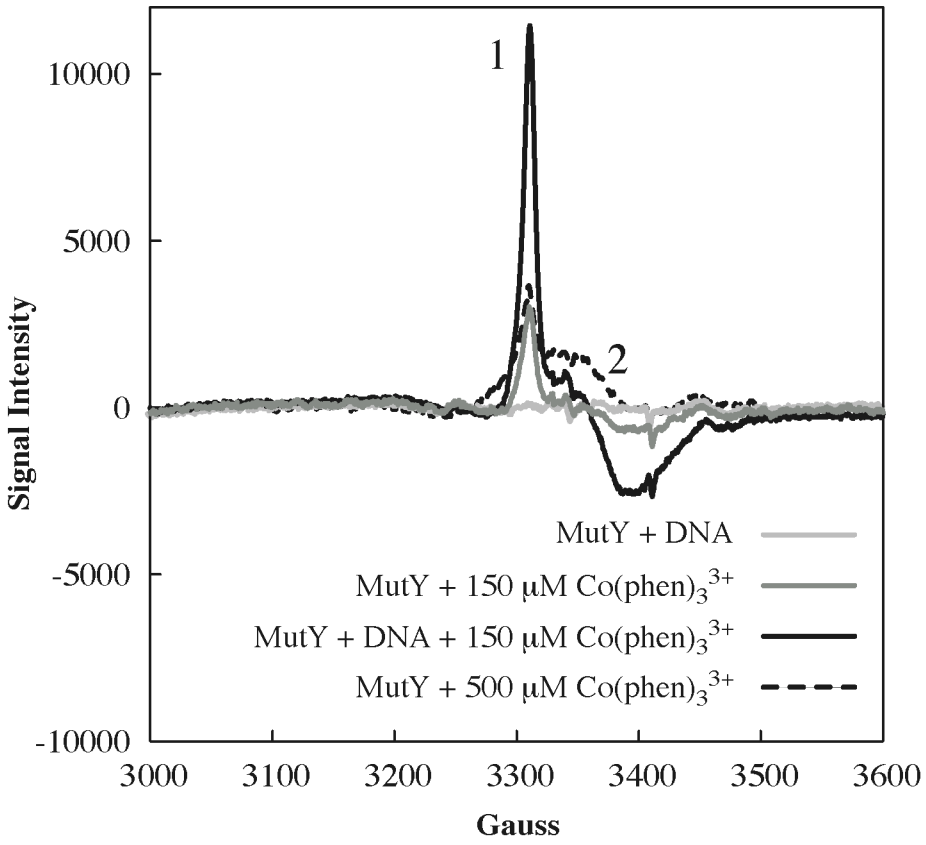

Addition of 500 μM $[Co(phen)_3]^{3+}$ in the absence of DNA results in a small increase in signal intensity; some interaction of the protein with the cobalt complex at these high concentrations is expected, yet without DNA little reaction occurs. These results are therefore consistent with DNA binding serving to shift the oxidation potential of the cluster, activating the cluster towards oxidation.

EndoIII also does not exhibit an EPR signal without oxidant in the presence or absence of DNA. Like MutY, upon addition of $[Co(phen)_3]^{3+}$ (30 μM) to EndoIII (10 μM), a signal appears with g = 2.03 and 2.01, consistent with formation of a $[3Fe4S]^{1+}$ cluster (Figure 3.6) (*89-90*). This signal also increases in intensity in the presence of DNA, although the enhancement is not as high as for MutY.

We also examined repair protein oxidation by ferricyanide in the presence and absence of DNA. A similar enhancement in cluster oxidation was observed in the presence of DNA (data not shown). However, ferricyanide is also known to promote oxidation of the cluster without DNA (*34-35*).

AfUDG in the presence or absence of DNA is EPR-silent as well. Unlike MutY and EndoIII, AfUDG (50 μM) in the presence of $[Co(phen)_3]^{3+}$ (150 μM) is also EPR silent in the absence of DNA. When DNA is included, however, a signal appears with g values at 2.13 and 2.04, typical of a $[4Fe4S]^{3+}$ cluster (*87-88*) (Figure 3.7). Since AfUDG is isolated from a thermophilic organism, these samples were also investigated following incubation at 55 ºC for five minutes. The same pattern is evident; AfUDG with DNA is EPR silent, as is AfUDG with $[Co(phen)_3]^{3+}$, while AfUDG with DNA and $[Co(phen)_3]^{3+}$ elicits a signal. However this signal has a g value of 2.02, indicating that the cluster is likely in the $[3Fe4S]^{1+}$ configuration. Previous studies examining oxidation

Figure 3.6. EPR spectroscopy at 10K of EndoIII in the presence of DNA (light grey), 150 μM $[Co(phen)_3]^{3+}$ without DNA (dark grey), and with both DNA and 150 μM Co(III) (black). Signal 1 shows g = 2.03, signal 2 shows g = 2.01.

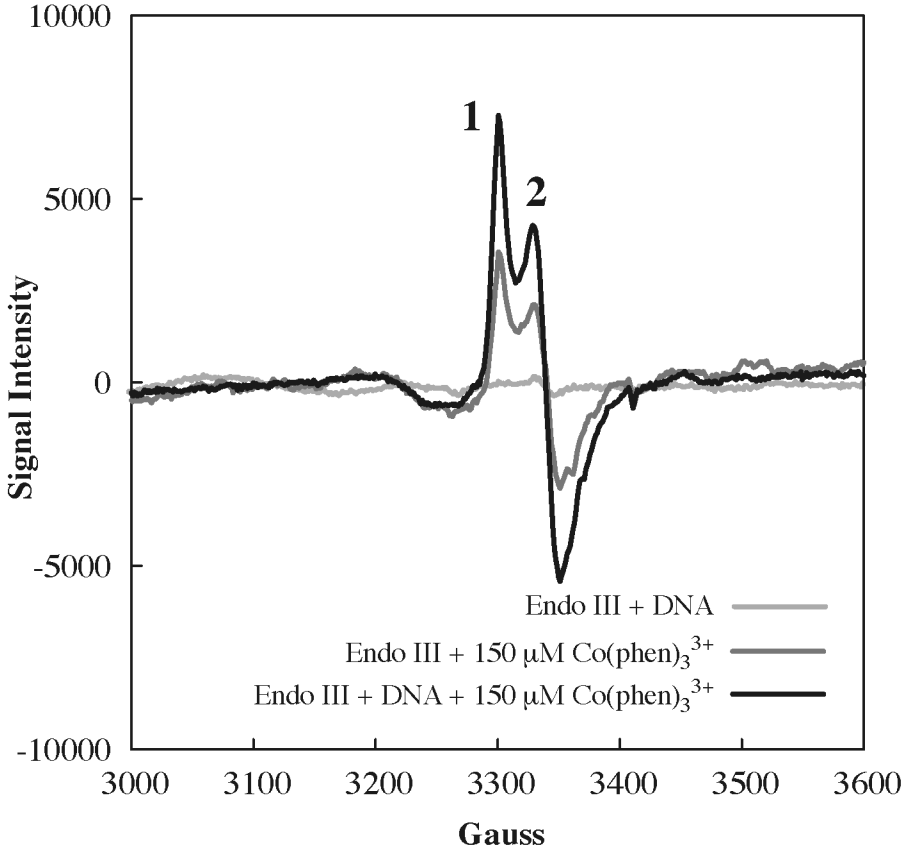

Figure 3.7. EPR spectroscopy at 10K in AfUDG in the presence of DNA (light grey), 150 μM $[Co(phen)_3]^{3+}$ without DNA (dark grey), and with both DNA and 150 μM Co(III) (black). Shown above after incubation at ambient temperature and below after incubation at 55 ºC. Signal 1 shows g = 2.13; signal 2 shows g = 2.04; signal 3 shows g = 2.02.

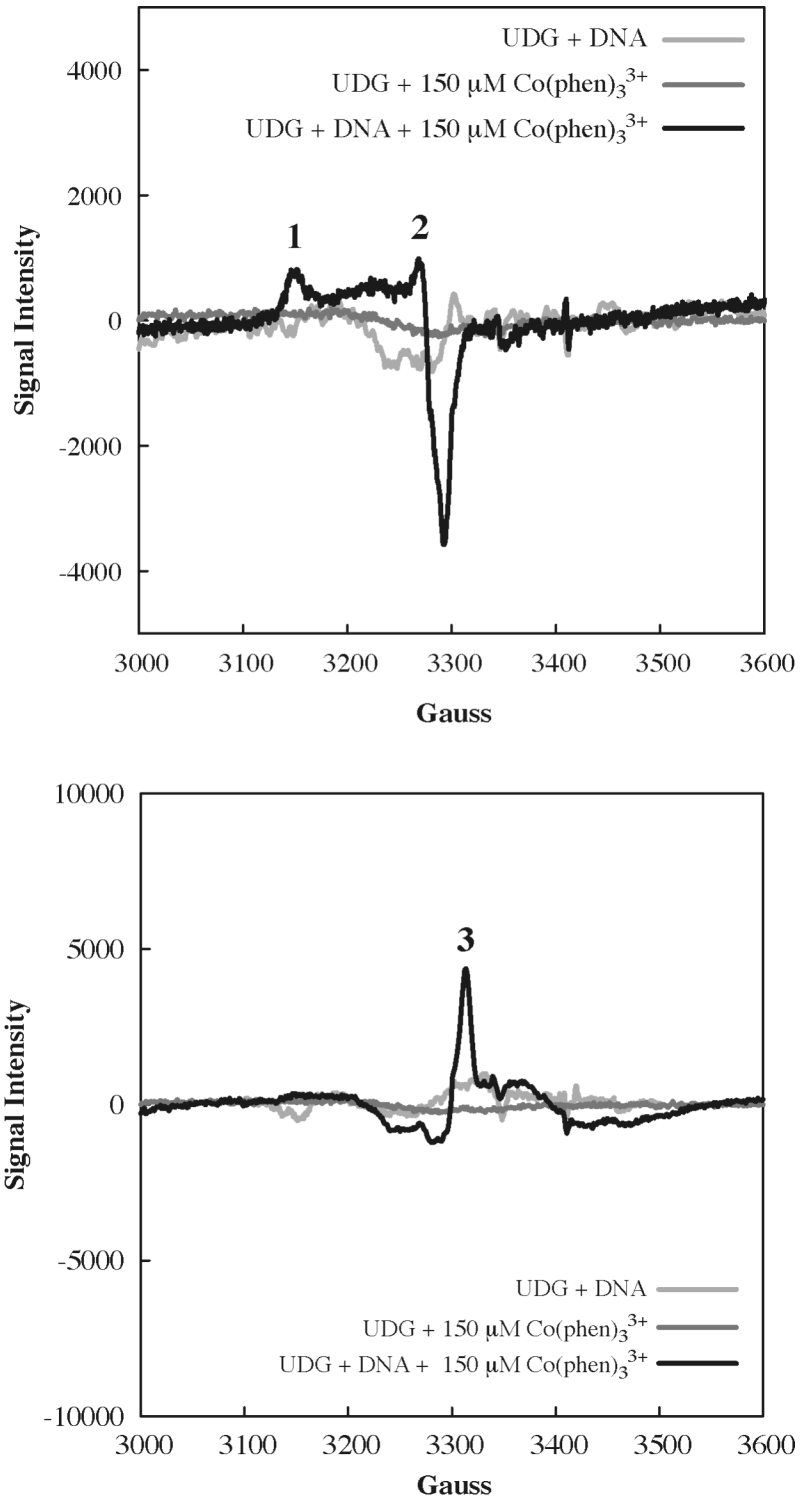

of the cluster in family 4 UDG from *Pyrobaculum aerophilum* by ferricyanide demonstrated that a mixture of $[4Fe4S]^{3+}$ and $[3Fe4S]^{1+}$ species are formed in the absence of DNA (*35*). It is therefore apparent that this repair enzyme also is activated toward oxidation of its [4Fe4S] cluster upon DNA binding.

Redox Activation of BER Enzymes upon DNA Binding

Electrochemical measurements of EndoIII and AfUDG using DNA-modified electrodes demonstrate that, like MutY, both of these enzymes that contain a [4Fe4S] cluster are redox-active when bound to DNA. Both BER enzymes have physiologically relevant redox properties when evaluated on DNA-modified electrodes, with potentials of ~ 100 mV versus NHE, typical of high-potential iron proteins (*63*), and similar to MutY (*33*). Solution studies with mediators have shown that the proteins could not be easily oxidized in the absence of DNA, and the more accessible 2+/1+ couple was estimated to be < -600 mV versus NHE (*34*). Without DNA attached to the gold electrodes, neither oxidation nor reduction of these proteins is observed electrochemically. Thus protein binding to DNA appears to shift the redox potential, activating the $[4Fe4S]^{2+}$ cluster towards oxidation.

Further support for this redox activation is apparent in monitoring changes in DNA-bound protein as a function of applied potential. When the DNA-modified electrodes are equilibrated with protein, but then the applied potential is shifted towards more negative potentials, reducing the protein, some protein dissociation from the electrode is evident. Similarly, shifting the potential to more positive values, to promote oxidation, increases the DNA-bound protein signal. While these data do not provide a quantitative measure of the difference in DNA binding affinity with protein in the reduced versus oxidized form, these data do qualitatively support an increase in binding affinity

for the protein with the [4Fe4S] cluster in the +3 state versus the +2 state. In other words, thermodynamically, DNA binding activates the protein towards oxidation. A quantitative determination of this difference in binding affinity for the protein with cluster in the +3 versus +2 form may not be possible technically, since cluster oxidation in the absence of DNA clearly leads to cluster decomposition. On the DNA-modified electrodes, however, the redox cycle appears to be reversible.

That DNA binding would shift the potential is reasonable to expect. The redox potentials of $[4Fe4S]^{2+}$ clusters are well known to vary considerably depending upon their environment (*63, 93*). Based on crystal structures of MutY (*94*) and EndoIII (*95*) bound to DNA, it is apparent that the iron-sulfur cluster is located near amino acid residues that contact DNA, so that DNA binding changes the environment for the cluster, taking it from an exposed and polar environment in the absence of DNA to a more hydrophobic environment in the presence of DNA. Moreover, the substrate binding affinity of MutY has been shown to be extremely sensitive to alterations of amino acids in the cluster coordination domain consistent with an intimate association of this region with DNA (*84*). It is reasonable to consider, then, that in the absence of DNA, the [4Fe4S] cluster is more ferredoxin-like, with the 2+/1+ couple being more accessible (*96*). Estimates for the reduction potential for the $[4Fe4S]^{2+}$ cluster of EndoIII of ~ -600 mV are consistent with this characterization. However, DNA binding may make the cluster environment more similar to high potential iron proteins, with the 2+/3+ couple being more accessible in the physiological regime (*96*). Indeed, the DNA-bound potentials of 100 mV we observe are characteristic of high potential iron proteins. Estimates based upon model studies for the difference in potential for the 3+/2+ couple versus the 2+/1+ couple are $\geq$ 1.0 V, both for ferredoxin-like clusters and high potential iron centers (*63,*

93, 96). Using a conservative value of 1.0 V for this difference, a value of –600 mV for the 2+/1+ cluster potential of EndoIII without DNA, and the measured potential of 90 mV for the DNA-bound 3+/2+ couple, suggests that DNA binding shifts the 3+/2+ potential 310 mV more negative. Thermodynamically this 300 mV shift would correspond to a change in binding affinity between the 2+ and 3+ states of more than 4 orders of magnitude.

The EPR results also are consistent with DNA binding activating the cluster towards oxidation. While some oxidation by $Co(phen)_3^{3+}$ in the absence of DNA is found, significant enhancements in oxidation are apparent in the presence of DNA. Earlier results had shown some evidence of irreversible oxidation of EndoIII by ferricyanide (*34*), but no enhancement with DNA binding was explored. Here it is noteworthy that $Co(phen)_3^{3+}$, an oxidant with potential similar to ferricyanide, binds to DNA (*91-92*). Hence the enhancement could reflect an increase in local concentration of the cobalt complex near the DNA-bound BER enzyme; ten times higher concentrations of $Co(phen)_3^{3+}$ without DNA showed no increased oxidation, however. Alternatively, the oxidation of the protein by $Co(phen)_3^{3+}$ might be DNA-mediated. $Co(phen)_3^{3+}$ binds DNA by partial intercalation (*92*), facilitating coupling into the base pair stack to enable a DNA-mediated reaction.

The electrochemical results using DNA-modified electrodes show clearly that the charge transport reaction to oxidize the cluster can be DNA-mediated. With all of these proteins, incubation at a DNA-modified surface containing an abasic site yields a drastically attenuated signal compared to that found with a well matched DNA duplex. This attenuation indicates that the DNA base pair stack must mediate electron transfer to the cluster, rather than simply serving to locally concentrate the enzyme at the electrode. DNA-mediated charge transfer to the cluster requires an intact base-pair π-stack.

Characteristics of the Oxidized Protein

EPR spectroscopy is used commonly to characterize [4Fe4S] clusters and their oxidation states. Based upon comparative g values, MutY, EndoIII, and AfUDG, upon DNA binding in the presence of an oxidant, primarily promote formation of the $[3Fe4S]^{1+}$ cluster. Some evidence for the $[4Fe4S]^{3+}$ cluster is also found, however, with AfUDG upon DNA binding.

High-potential iron proteins are known to be susceptible to degradation through reaction with water and oxygen (*63*);

$$[4Fe4S]^{2+} \xrightarrow[ox.]{DNA} [4Fe4S]^{3+} \quad (1)$$

$$[4Fe4S]^{3+} \xrightarrow[O_2]{H_2O} [3Fe4S]^{1+} \quad (2)$$

the $[4Fe4S]^{3+}$ cluster can lose an iron to form the $[3Fe4S]^{1+}$ cluster. This degradative process frequently occurs in [4Fe4S] proteins as a result of oxidative damage (*85*). While the electrochemistry results indicate that DNA activates the $[4Fe4S]^{2+}$ cluster towards oxidation in all three proteins and that oxidation can be reversed, MutY and EndoIII only show a signal typical of a $[3Fe4S]^{1+}$ cluster by EPR spectroscopy. With MutY and EndoIII, it is likely that the low temperature required to observe the cluster by EPR (10K) destabilizes the protein such that the cluster falls apart; electrochemistry results are obtained instead at ambient temperatures in buffer. Since this degradation process first requires oxidation of the $[4Fe4S]^{2+}$ cluster to the $[4Fe4S]^{3+}$ state (eq. 1, 2), the $[3Fe4S]^{1+}$ signal indicates, indirectly, oxidation of the cluster.

EPR experiments with AfUDG, furthermore, do show signals characteristic of a $[4Fe4S]^{3+}$ cluster in solution when the protein is incubated with DNA and $[Co(phen)_3]^{3+}$. Interestingly, when this same sample is first heated to 55 ºC, the degraded cluster ($[3Fe4S]^{1+}$) is observed instead. Oxidation of AfUDG with ferricyanide earlier had shown EPR evidence of both the $[4Fe4S]^{3+}$ and $[3Fe4S]^{1+}$ clusters (*35*), and here with DNA binding and oxidation with cobalt, a species with g values of 2.13 and 2.04, generally characteristic of a $[4Fe4S]^{3+}$ cluster (*83-84*), is observed. Noteworthy also are fluorescence studies of AfUDG as a function of temperature (*71*) which suggested that, above 50 ºC, AfUDG has a more "open" conformation, while the structure is more compact at lower temperature; this also was correlated with the higher activity of the enzyme above 50 ºC. It seems that this more "open" conformation is more susceptible to hydrolytic degradation of the $[4Fe4S]^{3+}$ cluster, leading to formation of the $[3Fe\text{-}4S]^{1+}$ cluster (based on the appearance of a species with a g-value of 2.01).

It is interesting in this context to consider recent results we have obtained for the DNA-mediated oxidation of MutY by guanine radical (*97*). Oxidized guanine radical in DNA, generated using a flash/quench technique, is found to promote oxidation of the $[4Fe4S]^{2+}$ cluster of MutY primarily to $[4Fe4S]^{3+}$ along with its decomposition product $[3Fe4S]^{1+}$ based upon EPR spectra with g values of 2.08, 2.06, and 2.02. Thus oxidation of the cluster in a rapid DNA-mediated reaction is far more likely to yield $[4Fe4S]^{3+}$ with minimum decomposition.

Model for Collaborative Scanning for DNA Lesions by BER Enzymes

While the enzymology of BER enzymes has been increasingly well established, little is understood about how BER repair enzymes first locate their substrates, often

single damaged bases in a vast array of undamaged DNA (*1*). The [4Fe4S] clusters are ubiquitous to these enzymes although a redox function for these clusters had been disregarded owing to the lack of redox activity seen with these proteins under physiological conditions (*34*). The data reported here, where DNA binding promotes a shift in redox potential to the physiological range, for all three BER enzymes, now requires that a redox role for these [4Fe4S] clusters be revisited.

We propose that the clusters serve as cofactors for DNA-mediated redox signaling among the BER enzymes. Through long range DNA-mediated charge transport, the BER enzymes may quickly become localized in regions of the genome containing DNA mismatches and lesions. This model is based upon the shift in potential we find for the BER enzymes associated with DNA binding. Thus our proposal reflects the electron exchange reaction among BER enzymes of similar potential bound to DNA so that

$$[4Fe4S]_A^{2+} + \{DNA\text{-}[4Fe4S]_B^{3+}\} \rightleftharpoons \{DNA\text{-}[4Fe4S]_A^{3+}\} + [4Fe4S]_B^{2+} \quad . \qquad (3)$$

Figure 3.8 illustrates this model for this cooperative BER detection strategy. A given BER enzyme, free in solution, contains the [4Fe4S] cluster in the 2+ state, as seen earlier (*34-35, 84*). As such, the protein is robust and insensitive to redox chemistry. As shown here, binding to DNA, however, shifts the redox potential, facilitating oxidation of the [4Fe4S] cluster to the +3 state. Oxidation, then, can involve a DNA-mediated charge transfer to an alternate BER enzyme bound at a distal site along the DNA with its cluster already in the +3 state. Reduction of this secondary BER enzyme could then facilitate its dissociation from the duplex. This process, as described, in actuality represents a scan

of one region of the genome: in the absence of an intervening lesion, mismatch, or other perturbation in base pair stacking, the DNA-mediated charge transfer process can proceed. The similarity in potentials for the different DNA-bound BER enzymes makes such a charge transfer process among DNA-bound $[4Fe4S]^{3+/2+}$ clusters near equilibrium plausible; a dynamic equilibrium between oxidized bound enzymes and reduced dissociated enzymes is expected. As also illustrated in Figure 3.8, the presence of a nearby perturbation in base pair stacking inhibits charge transfer. Under this circumstance, the BER enzyme remains associated with the DNA, allowing DNA-bound facilitated diffusion to the substrate site and repair. This model, then, provides a means to redistribute BER enzymes rapidly away from well matched DNA and preferentially onto genome sites in the vicinity of DNA lesions.

The results given here provide added support for this model. The shift in redox potential for BER enzymes upon DNA binding is now more widely demonstrated. Additionally, since each BER enzyme is in low copy number within the cell, this model provides a means for the enzymes to cooperate in locating their substrates. Some kinetic evidence for cooperativity in enzyme kinetics had been seen previously (*17*), yet there has been no structural evidence for protein dimerization in the bacterial forms of these enzymes. Our model provides for a cooperativity *among* BER enzymes. Indeed, irrespective of the specific substrate for the BER enzyme, none of the enzymes should populate well matched, unperturbed regions of the genome; this model provides a mechanism instead for the enzymes to redistribute onto damaged regions of the genome. Thus, by collaborating in their search for DNA damage, the BER enzymes can efficiently locate their substrates.

Figure 3.8. Proposed model for long range DNA signaling between BER enzymes using DNA-mediated charge transfer to detect base lesions. A collaboration among BER enzymes allows for more efficient sorting onto regions of DNA containing base lesions to facilitate substrate detection by these proteins.

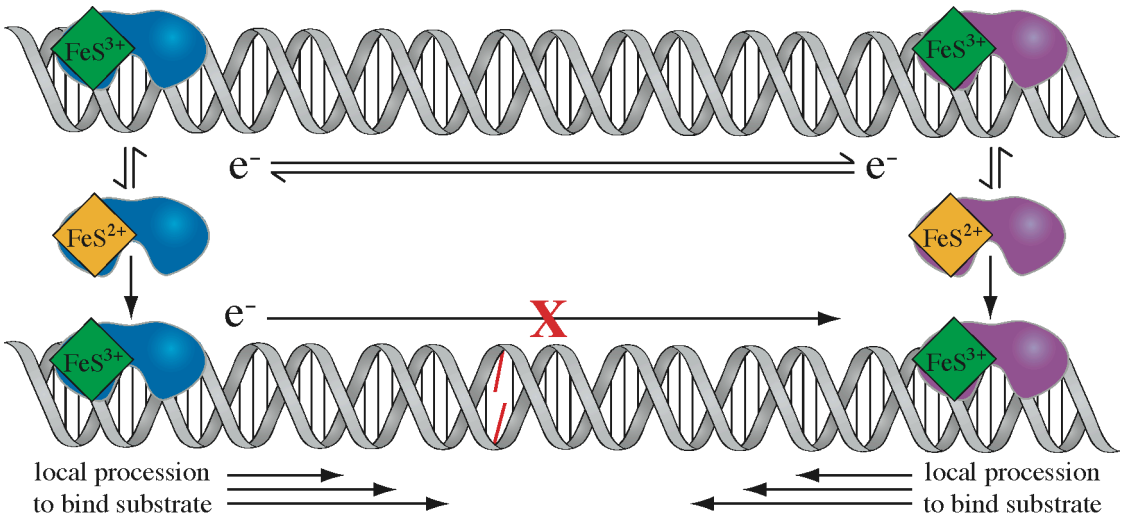

Implications

The [4Fe4S] clusters are ubiquitous in BER enzymes, present in homologues from bacteria to man. A clear functional role for these clusters has been lacking, however. Results here provide a basis for establishing a functional role for the [4Fe4S] clusters of BER enzymes that involves redox chemistry, the common chemistry utilized by most [4Fe4S] cluster-containing proteins within the cell. The role proposed, moreover, involves DNA-mediated charge transfer chemistry, a reaction that has been amply demonstrated to be sensitive to mismatches, lesions, and other perturbations in base pair stacking. Hence these results provide a framework for reconciling the frequency of [4Fe4S] clusters in repair enzymes as well as a strategy for effecting the rapid detection of DNA lesions by repair proteins in low copy number. Significantly, these results also provide a basis for considering how the DNA duplex may provide a medium for long range signaling within the cell.

SUMMARY

MutY and Endonuclease III, two DNA glycosylases from *Escherichia coli*, and AfUDG, a uracil DNA glycosylase from *Archeoglobus fulgidus*, are all base excision repair enzymes that contain the $[4Fe4S]^{2+}$ cofactor. Here we demonstrate that, when bound to DNA, these repair enzymes become redox-active; binding to DNA shifts the redox potential of the $[4Fe4S]^{3+/2+}$ couple to the range characteristic of high potential iron proteins and activates the proteins towards oxidation. Electrochemistry on DNA-modified electrodes reveals potentials for EndoIII and AfUDG of 59 mV and 95 mV versus NHE, respectively, comparable to 90 mV for MutY bound to DNA. In the absence of DNA modification of the electrode, no redox activity can be detected, and on electrodes modified with DNA containing an abasic site, the redox signals are dramatically attenuated; these observations show that the DNA base pair stack mediates electron transfer to the protein and the potentials determined are for the *DNA-bound* protein. In EPR experiments at 10K, redox activation upon DNA binding is also evident to yield the oxidized $[4Fe4S]^{3+}$ cluster and the partially degraded $[3Fe\text{-}4S]^{1+}$ cluster. EPR signals at g= 2.02 and 1.99 for MutY and g= 2.03 and 2.01 for EndoIII are seen upon oxidation of these proteins by $Co(phen)_3^{3+}$ in the presence of DNA and are characteristic of $[3Fe\text{-}4S]^{1+}$ clusters, while oxidation of AfUDG bound to DNA yields EPR signals at g= 2.13, 2.04, and 2.02, indicative of both $[4Fe4S]^{3+}$ and $[3Fe\text{-}4S]^{1+}$ clusters. Based upon this DNA-dependent redox activity, we propose a model for the rapid detection of DNA lesions using DNA-mediated electron transfer among these repair enzymes; redox activation upon DNA binding and charge transfer through well-matched DNA to an alternate bound repair protein can lead to the rapid redistribution of proteins onto genome sites in the vicinity of DNA lesions. This redox activation furthermore

establishes a functional role for the ubiquitous [4Fe4S] clusters in DNA repair enzymes that involves redox chemistry and provides a means to consider DNA-mediated signaling within the cell.

REFERENCES

1. Lindahl, T. (1993) *Nature 362*, 709.

2. Friedberg, E. C., Walker, G. C., and Siede, W. (1995) *DNA Repair and Mutagenesis* ASM Press.

3. Scharer, O.D. (2003) *Angew. Chem. Int. Ed. Engl. 42*, 2946.

4. David, S.S., and Williams, S.D. (1998) *Chem. Rev. 98*, 1221.

5. Verdine, G. L., and Bruner, S. D. (1997) *Chem. Biol. 4*, 329.

6. Stivers, J. T., and Jiang, Y. L. (2003) *Chem. Rev. 103*, 2729.

7. Hamilton, R.W., and Lloyd, R.S. (1989) *J. Biol. Chem. 264*, 17422.

8. Hildebrandt, E. R., and Cozzarelli, N. R. (1995) *Cell 81*, 331.

9. Demple, B., and Harrison, L. (1994) *Annu. Rev. Biochem. 63,* 915.

10. Bregeon, D., Doddridge, Z. A., You, H. J., Weiss, B., and Doetsch, P. W. (2003) *Mol. Cells 12*, 959.

11. Gu, Y., Parker, A., Wilson, T. M., Bai, H., Chang, D. Y., and Lu, A. L. (2002) *J. Biol. Chem. 277*, 11135.

12. Yang, H., Clendenin, W. M., Wong, D., Demple, B., Slupska, M. M., Chiang, J. H., and Miller, J. H. (2001) *Nucleic Acids Res. 29*, 743.

13. Pope, M. A., Porello, S. L., and David, S. S. (2002) *J. Biol. Chem. 277*, 22605.

14. Marenstein, D. R., Ocampo, M. T., Chan, M. K., Altamirano, A., Basu, A. K., Boorstein, R. J., Cunningham, R. P., and Teebor, G. W. (2001) *J. Biol. Chem. 276*, 21242.

15. Marenstein, D. R., Chan, M. K., Altamirano, A., Basu, A. K., Boorstein, R. J., Cunningham, R. P., and Teebor, G. W. (2003) *J. Biol. Chem. 278*, 9005.

16. Liu, X., Choudhury, S., and Roy, R. (2003) *J. Biol. Chem. 278*, 50061.

17. Wong, I., Bernards, A. S., Miller, J. K., and Wirz, J. A. (2003) *J. Biol. Chem. 278*, 2411.

18. Nunez, M. E., Hall, D. B., and Barton, J. K. (1999) *Chem. Biol. 6*, 85.

19. Kelley, S. O., and Barton, J. K. (1999) *Science 283,* 375.

20. Kelley, S. O., Holmlin, R. E., Stemp, E. D. A., and Barton, J. K. (1997) *J. Am. Chem. Soc. 119*, 9861.

21. Holmlin, R. E., Dandliker, P. J., and Barton, J. K. (1997) *Angew. Chem., Int. Edn. Engl. 36*, 2715.

22. Schuster, G. B. (2000) *Acc. Chem. Res. 33*, 253.

23. Giese, B. (2002) *Annu. Rev. Biochem. 71*, 51.

24. Bhattacharya, P. K., and Barton, J. K. (2001) *J. Am. Chem. Soc. 123*, 8649.

25. Hall, D. B., and Barton, J. K. (1997) *J. Am. Chem. Soc. 119*, 5045.

26. Rajski, S. R., and Barton, J. K. (2001) *Biochemistry 40*, 5556.

27. Boon, E. M., Salas, J. E., and Barton, J. K. (2002) *Nat. Biotechnol. 20*, 282.

28. Boon, E. M., Ceres, D. M., Drummond, T. G., Hill, M. G., and Barton, J. K. (2000) *Nat. Biotechnol. 18*, 1096.

29. Nunez, M. E., Noyes, K. T., and Barton, J. K. (2002) *Chem. Biol. 9*, 403.

30. Nunez, M. E., Holmquist, G. P., and Barton, J. K. (2001) *Biochemistry 23*, 12465.

31. Friedman, K. A., and Heller, A. (2001) *J. Phys. Chem. B 105*, 11859.

32. Rajski, S. R., Jackson, B. A., and Barton, J. K. (2000) *Mutat. Res. 447*, 49.

33. Boon, E. M., Livingston, A. L., Chmiel, N. H., David, S. S., and Barton, J. K. (2003) *Proc. Natl. Acad. Sci. U.S.A. 100*, 12543; *ibid. 101*, 4718.

34. Cunningham, R.P., Asahara, H., Bank, J.F., Scholes, C. P., Salerno, J. C., Surerus, K., Munck, E., McCracken, J., Peisach, J., and Emptage, M.H. (1989) *Biochemistry 28*, 4450.

35. Hinks, J.A, Evans, M.C.W., de Miguel, Y., Sartori, A.A., Jiricny, J., and Pearl, L.H. (2002) *J. Biol. Chem. 277*, 16936.

36. Rebeil, R., Sun, Y., Chooback, L., Pedraza-Reyes, M., Kinsland, C., Begley, T. P., and Nicholson, W. L. (1998) *J. Bacteriol. 180*, 4879.

37. Lee, C. H., Kim, S. H., Choi, J. I., Choi, J. Y., Lee, C. E., and Kim, J. (2002) *Mol. Cells 13*, 154.

38. Nghiem, Y., Cabrera, M., Cupples, C. G., and Miller, J. H. (1988) *Proc. Natl. Acad. Sci. U.S.A. 85*, 2709.

39. Michaels, M. L., Cruz, C., Grollman, A. P., and Miller, J. H. (1992) *Proc. Natl. Acad. Sci. U.S.A. 89*, 7022.

40. Michaels, M.L. and Miller, J. H. (1992) *J. Bacteriol. 174*, 6321.

41. Michaels, M. L., Tchou, J., Grollman, A. P., and Miller, J. H. (1992) *Biochemistry 17*, 10964.

42. Gogos, A., Cillo, J., Clarke, N. D., and Lu, A. L. (1996) *Biochemistry 35*, 16665.

43. Lu, A. L., Tsai-Wu, J. J., and Cillo, J. (1995) *J. Biol. Chem. 270*, 23582.

44. Manuel, R. C., Czerwinski, E. W., and Lloyd, R. S. (1996) *J. Biol. Chem. 271*, 16218.

45. Manuel, R. C., and Lloyd, R. S. (1997) *Biochemistry 36*, 11140.

50. Porello, S. L., Leyes, A. E., and David, S. S. (1998) *Biochemistry 37*, 14756.

51. Radicella, J. P., Clark, E. A., and Fox, M. S. (1998) *Proc. Natl. Acad. Sci. U.S.A. 85*, 9674.

52. Guan, Y., Manuel, R. C., Arvai, A. S., Parikh, S. S., Mol, C. D., Miller, J. H., Lloyd, S., and Tainer, J. A. (1998) *Nat. Struct. Biol. 5*, 1058.

53. Michaels, M. L., Pham, L., Nghiem, Y., Cruz, C., and Miller, J. H. (1990) *Nucleic Acids Res. 18*, 3841.

54. Demple, B., and Linn, S. (1980) *Nature 287*, 203.

55. Katcher, H. L., and Wallace, S. S. (1983) *Biochemistry 22*, 4071.

56. Breimer, L. H., and Lindahl, T. (1984) *J. Biol. Chem. 259*, 5543.

57. Duker, N. J., and Weiss, R. B. (1986) *Nucleic Acids Res. 26*, 6621.

58. Boorstein, R. J., Hilbert, T. P., Cadet, J., Cunningham, R. P., and Teebor, G. W. (1989) *Biochemistry 28*, 6164.

59. Wagner, J. R., Blount, B. C., and Weinfeld, M. (1996) *Anal. Biochem. 233*, 76.

60. Dizdaroglu, M., Laval, J., and Boiteux, S. (1993) *Biochemistry 32*, 12105.

61. Kuo, C. F., McRee, D. E., Fisher, C. L., O'Handley, S. F., Cunningham, R. P., and Tainer, J. A. (1992) *Science 258*, 434.

62. Thayer, M. M., Ahern, H., Xing, D., Cunningham, R. P, and Tainer, J. A. (1995) *EMBO J. 14*, 4108.

63. Cowan, J.A., and Lui, S.M. (1998) *Adv. Inorg. Chem. 45*, 313.

64. Fu, W., O'Handley, S., Cunningham, R. P., Johnson, M.K. (1992) *J. Biol. Chem. 267*, 16135.

65. Porello, S. L., Cannon, M. J., and David, S. S. (1998) *Biochemistry 37*, 6465.

66. Lu, A. L., and Fawcett, W. P. (1998) *J. Biol. Chem. 273*, 25098.

67. McGoldrick, J. P., Yeh, Y. C., Solomon, M., Essigmann, J. M., and Lu, A. L. (1995) *Mol. Cell. Biol. 15*, 989.

68. Ikeda, S., Biswas, T., Roy, R., Izumi, T., Boldogh, I., Kurosky, A., Sarker, A. H., Seki, S., Mitra, S. (1998) *J. Biol. Chem. 273*, 21585.

69. Pearl, L.H. (2000) *Mutat. Res.*, *460*, 165.

70. Hoseki, J., Okamoto, A., Masui, R., Shibata, T., Inoue, Y., Yokoyama, S., and Kuramitsu, S. (2003) *J. Mol. Biol. 333*, 515.

71. Knaevlsrud, I., Ruoff, P., Anensen, H., Klungland, A., Bjelland, S., and Birkeland, N. K. (2001) *Mutat. Res. 487*, 173.

72. Sartori, A. A., Schar, P., Fitz-Gibbon, S., Miller, J. H., Jiricny, J. (2001) *J. Biol. Chem. 276*, 29979.

73. Sandigursky, M., Faje, A., and Franklin, W. A. (2001) *Mutat. Res. 485*, 187.

74. Sandigursky, M., and Franklin, W. A. (2000) *J. Biol. Chem. 275*, 19146.

75. Lindahl, T., and Nyberg, B. (1974) *Biochemistry 13*, 3405.

76. Jacobs, K. L., and Grogan, D. W. (1997) *J. Bacteriol. 179*, 3298.

77. Thomas, N.C., Pringle, K., and Deacon, G.B. (1989) *J. Chem. Edu. 66*, 516.

78. Asahara, H., Wistort, P. M., Bank, J. F., Bakerian, R. H., and Cunningham, R. P. (1989) *Biochemistry 28*, 4444.

79. Beaucage, S. L., and Caruthers, M. H. (1981) *Tetrahedron Lett. 22*, 1859.

80. Kelley, S. O.; Boon, E. M.; Barton, J. K.; Jackson, N. M.; Hill, M. G. (1999) *Nucleic Acids Res. 27*, 4830.

81. Tender, L., Carter, M. T., and Murray, R. W. (1994) *Anal. Chem. 66*, 3173.

82. Armstrong, F. A., Heering, H. A., Hirst, J. (1997) *Chem. Soc. Rev. 26*, 169.

83. Guo, L. H., and Hill, H. A. O. (1991) *Adv. Inorg. Chem. 36*, 341.

84. Messick, T. E., Chmiel, N. H., Golinelli, M. P., Langer, M. R., Joshua-Tor, L., and David, S.S. (2002) *Biochemistry 41*, 3931.

85. Camba, R., and Armstrong, F. A. (2000) *Biochemistry 39*, 10587.

86. Roth, E. K. H., and Jordanov, J. (1991) *Inorg. Chem. 30*, 240.

87. Dilg, A. W. E., Mincione, G., Acterhold, K., Iakovleva, O., Mentler, M., Luchinat, C., Bertini, I., and Parak, F. G. (1999) *J. Biol. Inorg. Chem. 4*, 727.

88. Heering, H. A., Bulsink, Y. B. M., Hagen, W. R., and Meyer, T. E. (1995) *Eur. J. Biochem. 232*, 811.

89. Huynh, B. H., Moura, J. J. G., Moura, I., Kent, T. A., Legall, J., Xavier, A. V., and Munck, E. (1980) *J. Biol. Chem. 255*, 3242.

90. Ruzicka, F. J., and Beinert, J. (1978) *J. Biol. Chem. 253*, 2514.

91. Carter, M.T., Rodriguez, M., and Bard, A.J. (1989) *J. Am. Chem. Soc. 111*, 8901.

92. Rehmann, J. P., and Barton, J. K. (1990) *Biochemistry 29*, 1701.

93. Sticht, H., and Rosch, P. (1998) *Prog. Biophys. Mol. Biol. 70*, 95.

94. Fromme, J. C., Banerjee, A., Huang, S. J., and Verdine, G. L (2004) *Nature 427*, 652.

95. Fromme, J. C., and Verdine, G. L (2003) *EMBO J. 22*, 3461.

96. Carter, C.W., Kraut, J., Freer, S.T., Alden, R.A., Sieker, L.C., Adman, E. and Jensen, L.H. (1972) *Proc. Natl. Acad. Sci. USA 69,* 3526.

97. Yavin, E., Boal, A.K., Stemp, E.D.A., Boon, E.M., Livingston, A.L., O'Shea, V.L., David, S.S. and Barton, J.K. (2005) *Proc. Natl. Acad. Sci. USA, 102,* 3546.

CHAPTER 4

Electrochemical Investigation of Archaeal DNA Repair Proteins Containing [4Fe4S] Clusters

INTRODUCTION

Life on earth may be categorized by the division of organisms into three separate domains: eucarya, bacteria, and archaea (*1*). Some archaeal organisms are noted for their ability to exist and thrive in extreme environments and for their relatively evolutionarily close relationship to eukaryotes (*2*). Thus, the study of archaea, and of specific systems derived from archaea, can provide important clues about life under highly demanding conditions and in complex eukaryotic organisms that are otherwise difficult to study.

Given the unique properties of archaea, it is interesting to consider the question of how they protect their genomic material (*3, 4*). Some archaea can grow in the presence of radiation and other exogenous DNA damaging agents as well as at extremely high temperatures (*2*), which can greatly enhance the rate of spontaneous DNA damage reactions (*5*). Yet these organisms do not exhibit a higher mutation rate when compared with other microbes (*6*). While preliminary evidence indicates that archaea do harbor DNA repair systems, many of which bear sequence homology to eukaryotic or bacterial repair pathways, a full understanding of archaeal DNA repair has remained elusive (*3, 4*).

Base excision repair (BER) is the DNA repair pathway that is responsible for the excision of a variety of damaged DNA bases including uracil, oxidatively damaged bases (7,8-dihydro-deoxyguanosine and thymine glycol), methylated bases (3-methyl-adenine), and abasic sites (*7, 8*). Many archaeal organisms for which genomes have been sequenced, contain homologs of known BER enzymes from bacteria and eucarya (*3, 4*). Initially, one notable exception was the lack of any archaeal enzymes with homology to known enzymes that excise uracil in DNA in other organisms. Uracil in DNA arises via the misincorporation of uracil opposite adenine during replication or by the deamination

of cytosine to form G:U mispairs in DNA (*9*). Cytosine deamination is enhanced with increasing temperature (*5*), thus, it was surprising that archaea, especially hyperthermophilic archaea, did not possess a known uracil DNA glycosylase (UDG) homolog. Further examination of archaeal cell extracts revealed that archaea can, indeed, excise uracil from DNA (*10*) and it is now known that archaeal UDG enzymes constitute a new family of uracil excision enzymes termed family 4 UDGs. Several family 4 UDG genes have been isolated from archaea or expressed recombinantly in *Escherichia coli* (*11-13*). These are ~ 200 amino acid enzymes of extraordinary thermostability (enzyme activity can be maintained from 37–90°C) and the ability to remove uracil from G:U, A:U, and single stranded DNA environments.

Remarkably, many of these enzymes also contain [4Fe4S] clusters (*14*). Family 4 UDGs, as isolated, display a prominent absorption band between 370-400 nm and they lack any significant electron paramagnetic resonance (EPR) features at low temperature, an indication that the cluster exists in the $[4Fe4S]^{2+}$ state. Upon oxidation with ferricyanide, new EPR features arise at g values of 2.12 and 2.04, typical of a $[4Fe4S]^{3+}$ species. The cluster is ligated by a C-X_2-C-X_n-C-X_{14-17}-C sequence where n = 70–100. This sequence does not resemble any other known iron-sulfur cluster ligation motifs.

Figure 1 shows the location of the iron-sulfur cluster in a *Thermus thermophilus* family 4 UDG homolog (*15*). *T. thermophilus* UDG adopts a $\alpha/\beta/\alpha$ sandwich structure also found in the human UDG homolog. In Figure 1, the *T. thermophilus* UDG structure is aligned with that of human UDG bound to DNA (*16*). These alignments reveal that the [4Fe4S] cluster lies ~ 14 Å from the DNA backbone and ~ 10 Å from the active site uracil

Figure 4.1 A crystal structure of *Thermus thermophilus* uracil DNA glycosylase (UDG). *T. thermophilus* UDG adopts a $\alpha/\beta/\alpha$ fold highly similar to that found in the human UDG homolog. A bound uracil nucleotide is shown in grey and the [4Fe4S] cluster is shown in yellow and orange. A structural alignment with the DNA-bound structure of the human UDG homolog is shown below. Note that the [4Fe4S] cluster in *T. thermophilus* UDG is located ~ 14 Å from the DNA backbone in this model. Figure generated using 1UI0 and 1SSP PDB coordinates.

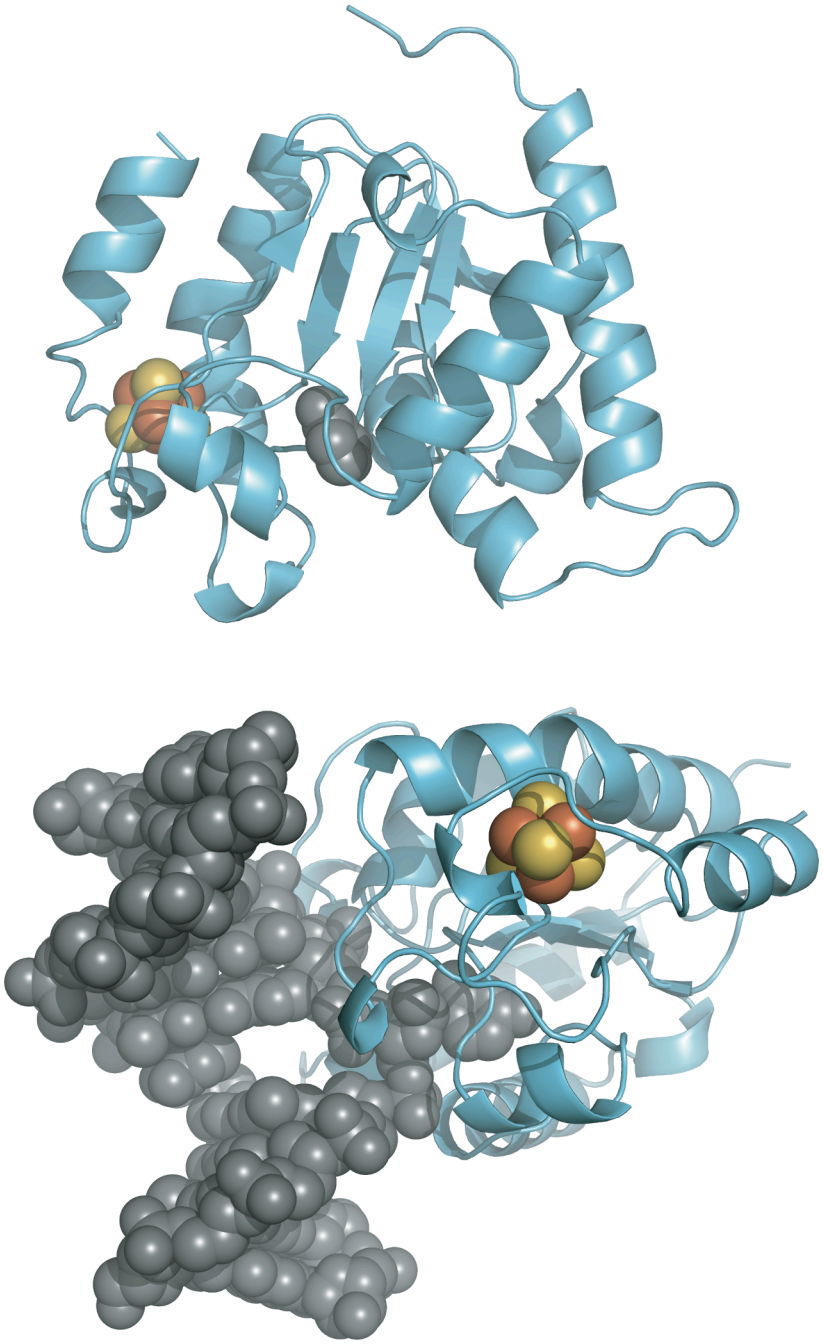

pocket. The role of the [4Fe4S] cluster remains unclear and the metal center has not been characterized in the DNA-bound form of the enzyme.

Another interesting feature of archaea is that they seem to lack the full complement of genes homologous to those involved in mismatch and nucleotide excision repair (NER) pathways in bacteria and eukaryotes (*3, 4*). NER is essential in bacteria and eukaryotes for the repair of DNA damage induced by UV light (*17, 18*). Archaeal organisms do possess some NER homologs that appear to be very similar to those present in eukaryotic NER systems (*3, 4*). In eukaryotes, global genomic NER is initiated by the XPC protein (Figure 2) which can recognize a wide range of lesions in DNA including UV damage products (thymine dimer, 6-4 photoproduct), DNA-protein crosslinks, and a variety of bulky DNA base adducts (*19*). XPC then recruits transcription factor IIH (TFIIH), replication protein A (RPA), and XPF-ERCC1. TFIIH is a multisubunit protein that contains the XPB and XPD helicases. XPB and XPD unwind the DNA around the damaged site, after which single strand DNA (ssDNA) binding proteins (RPA) are recruited as well as nucleases (XPG and XPF-ERCC1). These enzymes remove a 24–32 nucleotide swath of ssDNA containing the lesion. The last step in the pathway is the synthesis of new DNA. Understanding the biochemistry involved in eukaryotic NER poses specific challenges. Since many NER proteins exist as multiprotein complexes, it is difficult to isolate them individually and reconstitute NER *in vitro*. As with many other DNA repair pathways, it is also not well understood how NER enzymes very quickly and efficiently locate and repair damage in complex intracellular environments. It is generally accepted that XPC is the protein that initially detects damage inside the cell, but XPD and XPB helicases are also important for lesion recognition. Thus the discovery of archaeal NER homologs similar to eukaryotic NER enzymes could provide a much needed model system to understand this complex DNA

Figure 4.2 Global genomic nucleotide excision repair (NER) in eukaryotes. NER is initiated by the XPC protein which binds to a wide variety of bulky DNA lesions. XPC then recruits the multisubunit protein TFIIH, which is responsible for verification of the lesion followed by unwinding of the helix in the vicinity of the damaged site. ssDNA binding proteins RPA and XPA are then recruited, followed by nucleases. The final step is synthesis of new DNA.

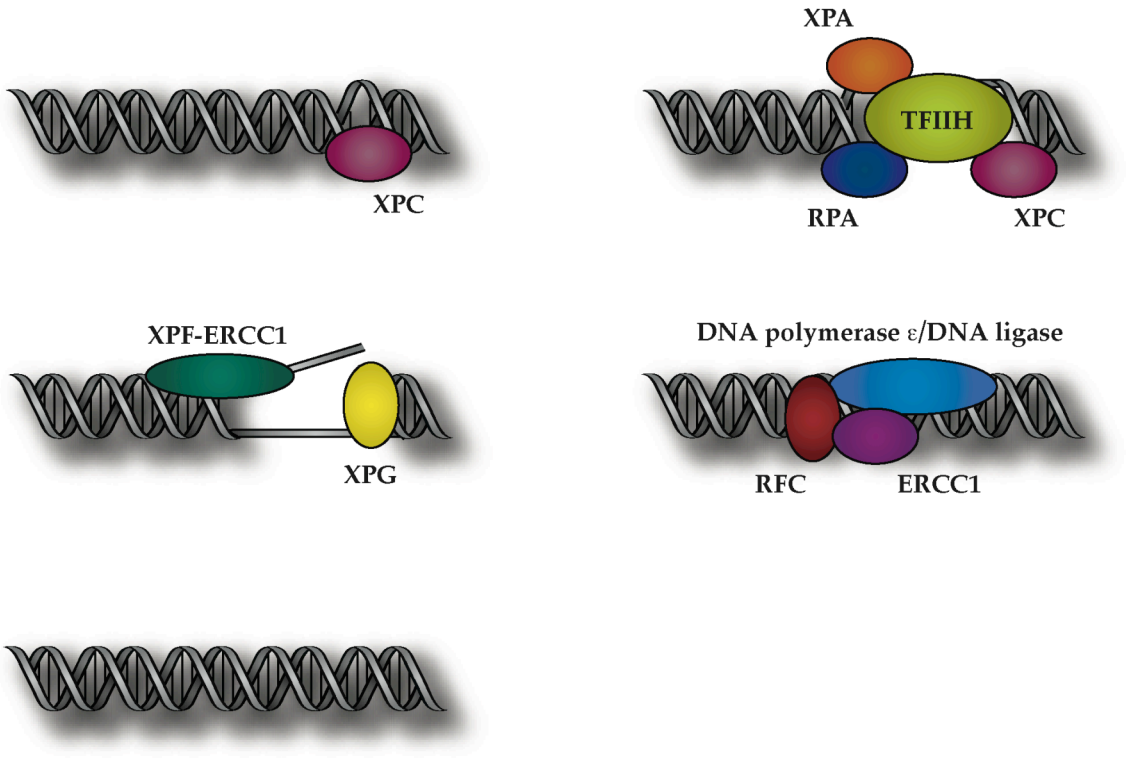

repair pathway. This is of the utmost importance since mutations in NER enzymes are associated with severe genetic disorders in humans including xeroderma pigmentosum, trichothiodystrophy, and Cockayne syndrome (*20*).

XPD homologs have been discovered in archaea through sequence analysis (*21, 22*). Initial characterization of *Sulfolobus acidocaldarius* XPD revealed that this archaeal XPD homolog harbors an iron-sulfur cluster (*21*). The purified protein has an absorbance maximum at ~ 410 nm and sequence alignments indicate that four cysteine residues are conserved across a large group of XPD homologs and related helicases, including several enzymes found in humans. EPR spectroscopy experiments show that exposure of *S. acidocaldarius* XPD to ferricyanide results in formation of a $[3Fe\text{-}4S]^{1+}$ cluster observed at 10K. These properties are quite similar to those observed with the iron-sulfur clusters present in MutY, EndoIII, and family 4 UDGs (*23, 24*). Thus, it is likely that archaeal XPD homologs also contain a $[4Fe\text{-}4S]^{2+}$ cluster. As with archaeal UDG, the iron-sulfur cluster in XPD has not been evaluated in the DNA-bound form of the enzyme.

MATERIALS AND METHODS

Materials

All chemicals were purchased from Sigma-Aldrich and used as received unless stated otherwise. All buffers were prepared immediately prior to use and filtered using a 0.2 μm sterile filter. All reagents for DNA synthesis were purchased from Glen Research.

Proteins

A. fulgidus UDG (AfUDG) variants were generously donated by Prof. Sheila David. *S. acidocaldarius* XPD was generously donated by Prof. Malcolm White (St. Andrews University).

Preparation of DNA-modified Electrodes

Oligonucleotides were synthesized using standard phosphoramidite chemistry (*25*). Single strand oligonucleotides were modified at the 5' end with a thiol moiety to facilitate covalent attachment to a gold electrode surface, as described earlier (*26*). Oligonucleotides were purified by HPLC, hybridized to their complements and self-assembled into a loosely-packed monolayer on a Au surface (*24*) in 50 mM NaCl, 5 mM sodium phosphate, pH 7.0. The electrode surface was then further passivated by incubation with mercaptohexanol (100 mM) in assembly buffer for 30 minutes. Electrodes were then rinsed with protein storage buffer (AfUDG; 25 mM Tris-HCl, 500 mM NaCl, 5% glycerol, pH 7.6; XPD; 20 mM sodium phosphate pH 7.6, 250 mM NaCl, 1 mM EDTA, 10% glycerol), and 50 μL protein (various concentrations) in the appropriate storage buffer was added to the electrode surface and allowed to incubate for 10–15 minutes prior to measurement.

Electrochemical Measurements

Low volume constraints necessitated the use of a specialized low-volume cell for protein electrochemistry experiments (*24*). The working electrode consisted of a Au(111) on mica chip and a Pt wire served as the auxiliary electrode. The reference electrode was a Ag/AgCl electrode modified with a tip containing 4% agarose in 3 M

NaCl. This reference electrode was calibrated with ferrocene carboxylate and compared both to an unmodified Ag/AgCl reference electrode and a saturated calomel electrode. All measurements were made using a BAS CV50W model electrochemical analyzer.

RESULTS AND DISCUSSION

A. fulgidus UDG Electrochemistry

A. fulgidus UDG was investigated electrochemically at DNA-modified electrode surfaces (Figure 4.3). These electrodes were prepared as described previously (*24, 26*) and were modified with the sequence SH-$(CH_2)_2$CONH$(CH_2)_6$NHCO-5`-AGTACAGTCATCGCG-3` plus the complementary strand. All proteins were analyzed on loosely packed surfaces backfilled with mercaptohexanol. *A. fulgidus* UDG displays a strong electrochemical signal at DNA-modified electrodes (Figure 4.4) that is not present at electrodes modified with mercaptohexanol (*24*). The midpoint potential measured for the DNA-bound protein is +95 mV versus NHE, typical of high potential iron proteins that can access the 2+/3+ redox couple of the [4Fe4S] cluster (Figure 4.4). We have also examined a suite of *A. fulgidus* UDG single site mutants at each of the cysteines that ligate the iron sulfur cluster in the protein. C14, C17, C85, and C101 were each mutated to histidine, serine, or alanine. These twelve proteins were also examined on DNA-modified electrodes. With the exception of C14S, all mutants display an electrochemical signal when evaluated on a DNA monolayer. Representative cyclic voltammograms are shown in Figure 4.5 and the data is summarized in Table 4.1. All electrochemical signals measured for *A. fulgidus* UDG mutants share the same general characteristics as wild-type UDG and other [4Fe4S] cluster DNA repair proteins. The signals are quasi-

Figure 4.3 Strategy for electrochemical analysis of iron-sulfur cluster DNA repair proteins at DNA-modified electrodes. DNA-modified electrodes are generated by self-assembly of thiol terminated DNA duplexes on a gold (Au) electrode surface to form a DNA monolayer. Electrodes are passivated with mercaptohexanol. Protein solutions are allowed to bind to the monolayer and evaluated with cyclic voltammetry.

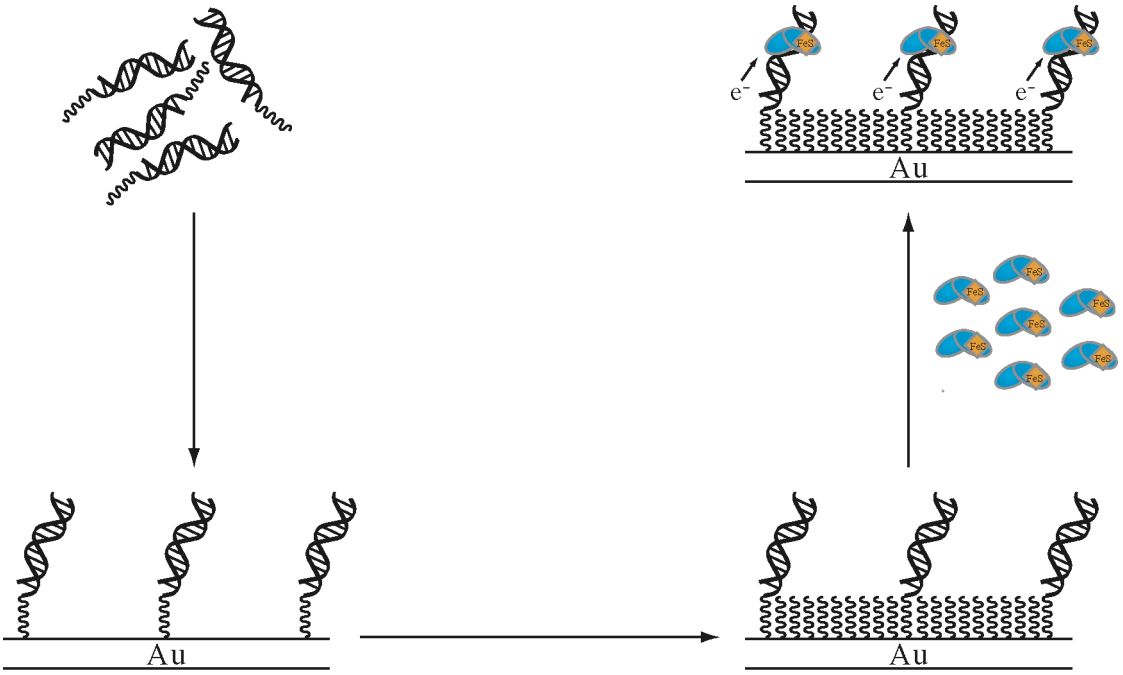

Figure 4.4 Electrochemical investigation of *A. fulgidus* UDG at DNA-modified electrodes.

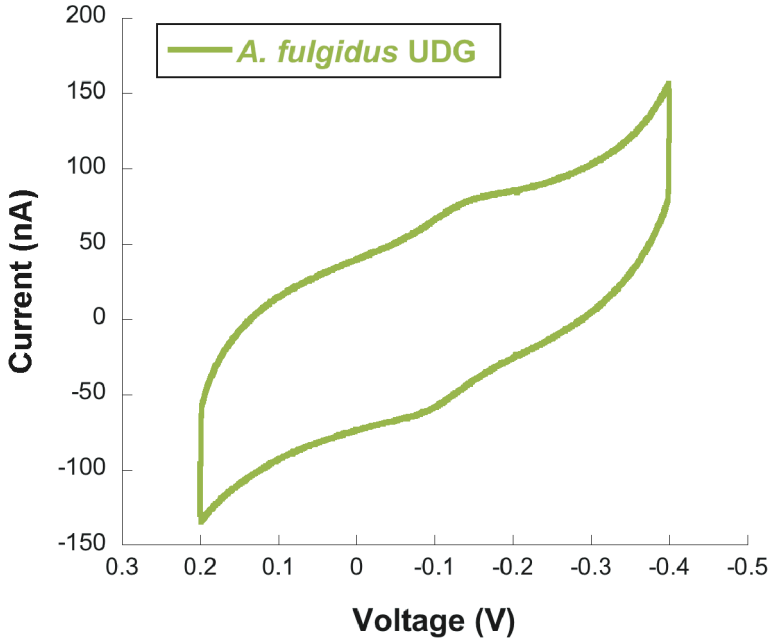

Figure 4.5. Cyclic voltammograms for the twelve *A. fulgidus* cysteine mutants evaluated electrochemically at DNA-modified electrodes.

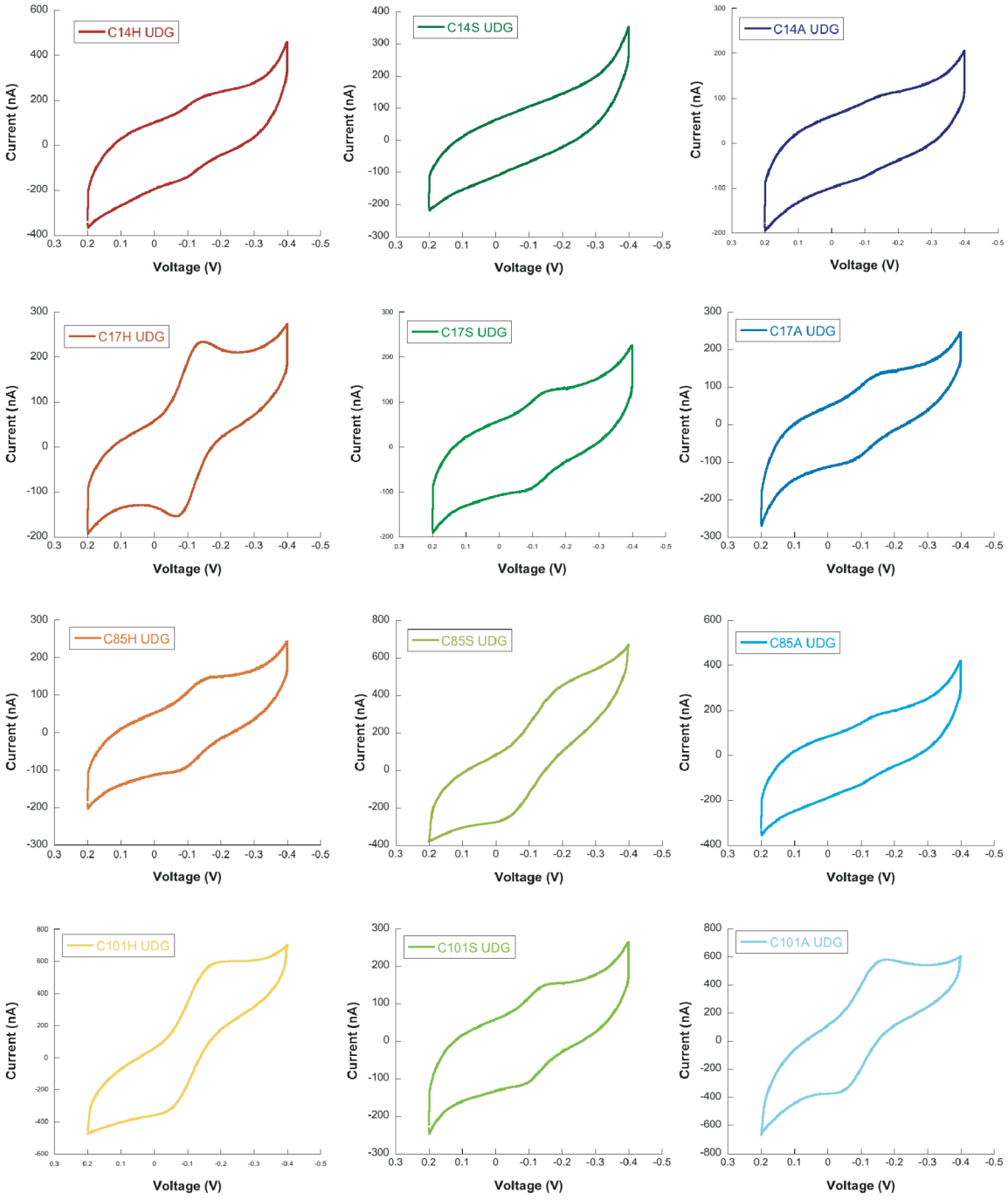

Table 4.1. Summary of electrochemical measurements for *A. fulgidus* UDG variants.

AfUDG mutant	E_m (mV vs. NHE)	Intensity	Concentration	Distance to DNA
wt	+95 ± 3	+	170 μM	
C14H	+89 ± 5	-	100 μM	24 Å
C14S	--	N/A	498 μM	
C14A	+82 ± 4	-	384 μM	
C17H	+92 ± 3	+	100 μM	12 Å
C17S	+79 ± 3	+	200 μM	
C17A	+93 ± 5	-	150 μM	
C85H	+86 ± 5	-	400 μM	12 Å
C85S	+104 ± 9	-	200 μM	
C85A	+88 ± 7	-	140 μM	
C101H	+96 ± 6	+	200 μM	17 Å
C101S	+84 ± 3	+	200 μM	
C101A	+97 ± 4	+	200 μM	

reversible, grow in on the order of 10−15 minutes, and have a linear relationship with respect to the square-root of the scan rate. Nearly all proteins display midpoint potentials similar to wild-type UDG with the notable exceptions of C17S, C101S, and C14A. Interestingly, the other serine ligated proteins either do not exhibit a signal (C14S) or have a slightly elevated midpoint potential (C85S). All of the alanine mutants examined, with the exception of C101A, display very weak signals, as might be expected since alanine cannot provide a ligation interaction to the iron-sulfur cluster. All of the histidine mutants have robust signals with midpoint potentials similar to that of wild-type UDG.

S. acidocaldarius XPD Electrochemistry

We have also examined *S. acidocaldarius* XPD on DNA-modified electrodes. XPD displays a quasi-reversible signal by cyclic voltammetry (Figure 4.6) when the protein is bound to DNA. The electrochemical signal associated with XPD also has many features in common with other [4Fe4S] cluster DNA repair proteins examined previously. The midpoint potential is +77 mV versus NHE, the XPD signal grows in over 10−15 minutes, and the peak current has a linear relationship with the square root of the scan rate. At an abasic site electrode, where DNA-mediated charge transport is hindered, XPD does not display a signal indicating that an intact π-stack is required for redox-activity of the enzyme (data not shown). Several mutant forms of XPD were also examined (Figure 4.7). C102S is an XPD mutant that still has an intact iron-sulfur cluster (*21, 22)* and it displays an electrochemical signal with similar properties to wt XPD. C88S, K84H, and F136P are mutants that do not appear to have an intact iron sulfur cluster (protein solutions are colorless) (*21*). These mutants exhibit electrochemical

Figure 4.6. Electrochemical investigation of XPD helicase at a DNA-modified electrode.

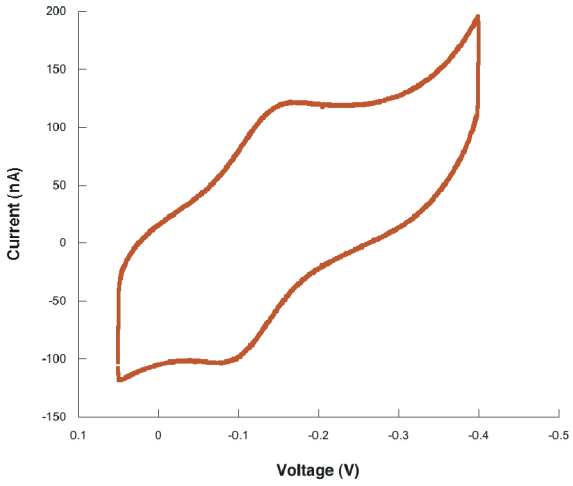

Figure 4.7. Electrochemical investigation of XPD variants.

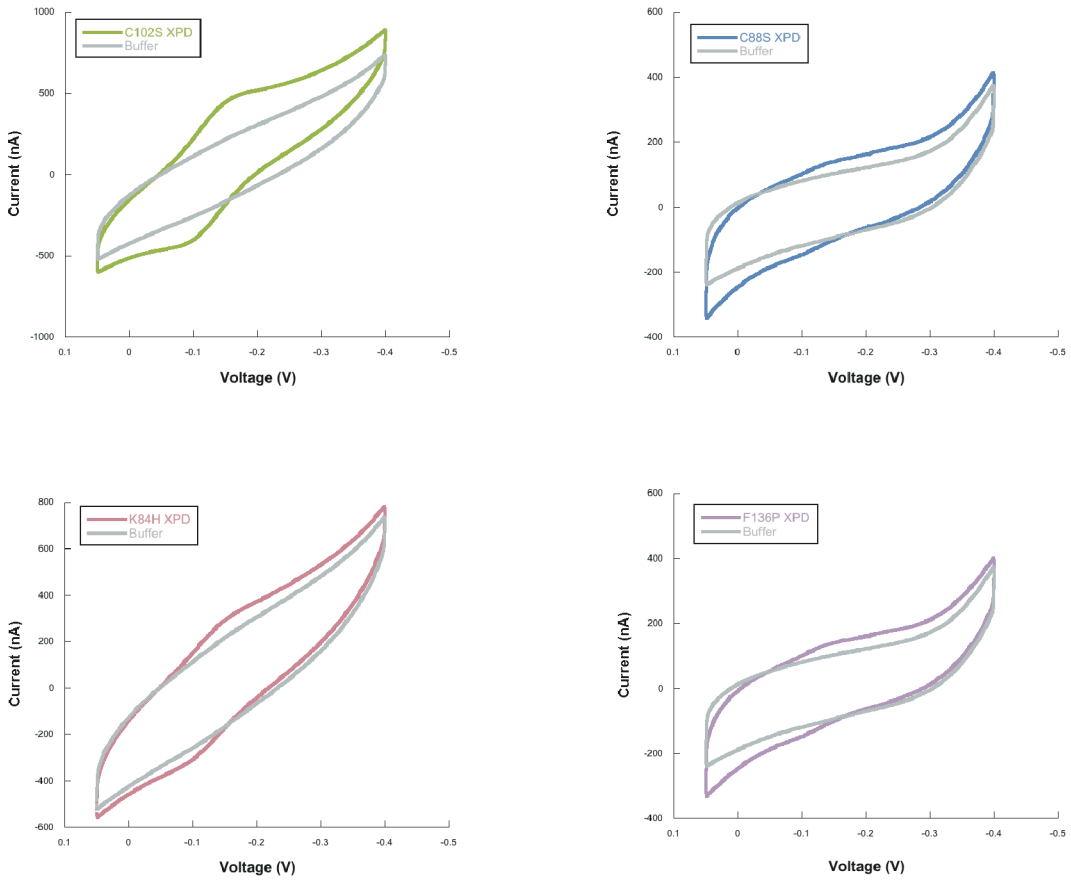

signals on DNA-modified electrodes, though the integrated intensities of these signals are markedly smaller than those associated with wt or C102S XPD.

Discussion

A. fulgidus UDG bears a [4Fe4S] cluster, much like the BER enzymes MutY and Endonuclease III (EndoIII) (*14, 24*). Though these enzymes all have a common cofactor, they are quite different in many other respects. *A. fulgidus* UDG has a very different overall fold when compared with MutY and EndoIII, as well as a different sequential spacing between the cysteines that ligate the iron sulfur cluster (*15, 27, 28*). MutY and EndoIII are members of the helix-hairpin-helix structural superfamily of DNA repair enzymes; they each have multiple domains and have a high degree of structural similarity to each other. The cysteines that ligate the iron-sulfur cluster in MutY and EndoIII are separated by a $CX_6CX_2CX_7C$ pattern that is unique to these enzymes. *A. fulgidus* UDG, however, is a single domain protein with a common $\alpha/\beta/\alpha$ fold that is observed in a wide variety of proteins. This overall structure is similar to many other members of the UDG superfamily (*15*). The iron sulfur cluster in *A. fulgidus* UDG is ligated by a $CX_2CX_{67}CX_{15}C$ motif, a ligation pattern not found among known iron-sulfur enzymes. *A. fulgidus* UDG also has a very different substrate specificity when compared with MutY and EndoIII (*11*). MutY and EndoIII repair substrates associated with oxidative DNA damage (*1*), while *A. fulgidus* UDG removes uracil from DNA (*11*). Lastly, MutY and EndoIII are enzymes found throughout phylogeny (*1*), while *A. fulgidus* UDG and other family 4 UDGs that contain an iron-sulfur cluster are found largely in archaea (*11-13*).

In spite of these differences, the [4Fe4S] cluster in *A. fulgidus* UDG has many characteristics in common with the clusters found in MutY and EndoIII. In their isolated

forms, all of these proteins appear to bear a [4Fe4S] cluster in the 2+ oxidation state (*24*) demonstrated by the lack of any significant signal when these proteins are analyzed by EPR. These proteins do not exhibit strong EPR signals after reduction with sodium dithionite (*14, 23*). Following oxidation by ferricyanide, however, strong EPR features are observed. With *A. fulgidus* UDG, signals at g = 2.12 and 2.04 indicate that both $[4Fe4S]^{3+}$ and $[3Fe4S]^{1+}$ species are formed upon oxidation. In MutY and EndoIII, ferricyanide treatment results in signals at g = 2.01–2.03 suggesting that only the $[3Fe4S]^{1+}$ species is present. This [3Fe4S] cluster is likely the result of oxidative degradation of the cluster or protein instability under the conditions required for EPR analysis (high protein concentration, extremely low temperature).

Electrochemical analysis of the [4Fe4S] cluster in DNA-bound *A. fulgidus* UDG also reveals similarities in the DNA-bound redox properties of *A. fulgidus* UDG and MutY/EndoIII (*24*). *A. fulgidus* UDG has a DNA-bound midpoint potential of +95 mV vs. NHE, comparable to those measured for MutY and EndoIII (+60–+90 mV versus NHE). *A. fulgidus* UDG redox activity is also sensitive to the integrity of the DNA π-stack, as are MutY and EndoIII. Thus, the pathway for electron transfer to the iron-sulfur cluster in these proteins is likely DNA-mediated.

A complete set of *A. fulgidus* UDG mutants at residues that ligate the iron-sulfur cluster were also evaluated electrochemically at DNA-modified electrodes. Substitution of histidine at these sites leads to very little change in the redox properties when compared to wt *A. fulgidus* UDG. Though histidine is occasionally found as a natural ligand in protein bound [4Fe4S] clusters (*29*), histidine substitution for a thiolate ligand is often found to shift the midpoint potential of the iron sulfur cluster (*30*). Histidine substitution can also lead to cluster instability (*31*). Thus, the robust signals observed

here with little to no potential shift compared to wt UDG are a bit unusual and may indicate that iron-sulfur clusters in archaeal proteins have unique properties with respect to ligand substitution and redox activity.

Equally surprising are the effects of serine and alanine substitution for the cysteine ligands to the [4Fe4S] cluster in *A. fulgidus* UDG. Serine is not a natural ligand for [4Fe4S] clusters in proteins, but the hydroxyl group in the serine side chain does have some ability to bond with iron (*30*). Serine ligated [4Fe4S] clusters generated by site directed mutagenesis are generally unstable and may result in cluster degradation (*32*). In *A. fulgidus* UDG, three of the four serine mutants examined exhibit electrochemical signals when bound to DNA. Notably, two of these mutants (C17S and C101S) have midpoint potentials significantly lower (> 10 mV) than that of wt *A. fulgidus* UDG. The remaining mutant, C85S, does not exhibit a significant potential shift. Alanine substitution at all cysteines evaluated leads to small signals across the board with the exception of C101A. The observation of even very tiny signals is unexpected with alanine substitution, though, since the alanine side chain cannot serve as a ligand for iron. This result might indicate some small amount of cluster ligation by a solvent molecule or structural rearrangement by the protein to provide a new amino acid as a fourth ligand to the cluster. Indeed, the observation that all C101 mutants display strong signals regardless of the nature of amino acid substitution perhaps indicates that structural rearrangement is particularly favorable upon loss of the C101 ligand. Note that C101 is oriented towards the interior of the protein (Figure 4.8) and is likely the least solvent exposed of the four ligating cysteines (*14*).

It is also important to note that all of the measurements reported here were accomplished at room temperature while *A. fulgidus* is an organism that grows at extremely high temperatures (70–95 °C) (*11*). *A. fulgidus* UDG is an active enzyme over

Figure 4.8. View of the iron-sulfur cluster in a thermophilic family 4 UDG. The cysteine residues in *A. fulgidus* UDG are shown in yellow and labeled appropriately.

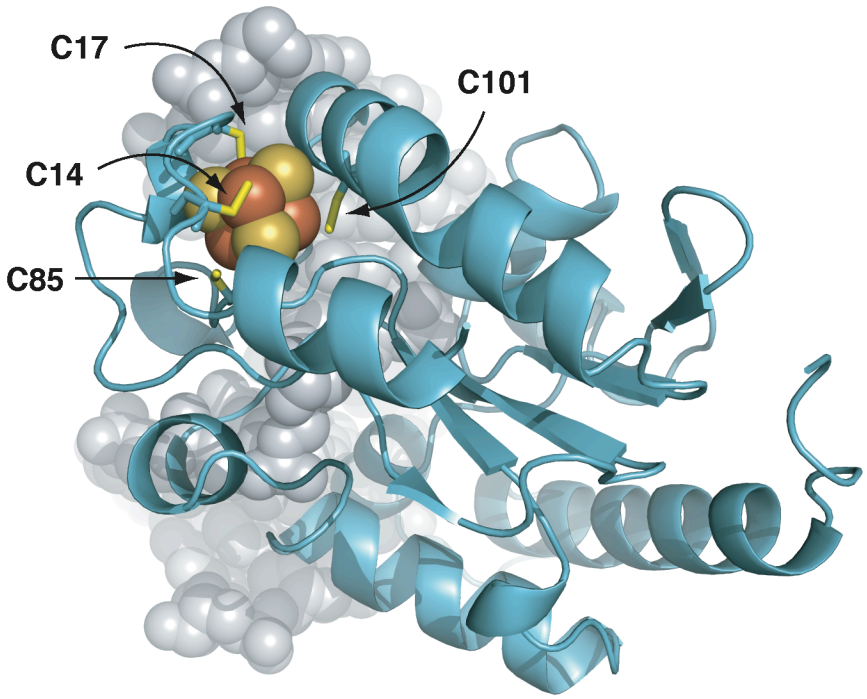

a wide range of temperatures, but it is certainly possible that observations made at room temperature may not reflect the properties of the protein in its native environment.

S. acidocaldarius XPD helicase is another iron-sulfur cluster enzyme found in archaea and involved in DNA repair (*21*). Sequence analysis indicates that iron-sulfur clusters are likely ubiquitous to many DNA helicases present in a broad range of organisms. While none of these helicases thought to contain iron-sulfur clusters have been structurally characterized, these enzymes likely have a very different structure and function from BER iron-sulfur cluster enzymes.

When evaluated at DNA-modifed electrodes, *S. acidocaldarius* XPD displays a signal similar to those observed with MutY, EndoIII, and *A. fulgidus* UDG (*24*). The midpoint potential observed for *S. acidocaldarius* XPD (+77 mV versus NHE) at a DNA-modified electrode is within the range of that observed for DNA-bound [4Fe4S] cluster BER enzymes and typical of high potential [4Fe4S] cluster enzymes (*32*). As with the other [4Fe4S] enzymes, XPD requires an intact base-pair stack for efficient charge transport to the iron-sulfur cluster (data not shown).

The role of the iron-sulfur cluster in these helicases is unknown though it appears that the presence of an intact cluster is required for functional enzyme activity (*21, 22*). XPD helicase functions in the nucleotide excision repair pathway to unwind DNA in the vicinity of damaged sites (*19*). The general function of helicases and DNA translocases is to hydrolyze ATP and use the resulting energy to drive movement along the DNA helix or strand separation or both (*33*). Thus, the activity of these enzymes is characterized both by their ability to hydrolyze ATP or their ability to separate double stranded DNA substrates. In the XPD helicases containing iron-sulfur clusters, ATP hydrolysis is unaffected by loss of the iron-sulfur cluster through site-directed mutagenesis of the

residues ligating the cluster (*21, 22*). The cluster is, however, required for efficient strand separation of forked or bifurcated DNA substrates.

We have also examined several *S. acidocaldarius* XPD mutants on DNA-modified electrodes. C102S XPD maintains an intact iron-sulfur cluster and near wt activity for both ATP hydrolysis and strand separation enzyme functions (*21, 22*). When analyzed electrochemically at DNA-modified electrodes, C102S XPD has many features in common with wt XPD. The signal intensity and midpoint potentials measured for each protein are nearly identical. As with the *A. fulgidus* serine substituted mutants, the robust nature of C102S XPD is remarkable given that serine ligated [4Fe4S] clusters are prone to cluster degradation (*32*).

K84H, F136P, and C88S XPD mutants were also evaluated at DNA-modified electrodes. Though these XPD variants are deficient in strand separation activity and appear to have compromised iron-sulfur clusters (protein solutions are colorless) (*21, 22*), they do exhibit very small signals when monitored by cyclic voltammetry at DNA-modified electrodes. It is possible that only a very small proportion of these proteins contain intact iron-sulfur clusters and we are able to selectively detect these metal-bound proteins at the DNA surface.

For MutY and EndoIII, our laboratory has proposed that the redox-active [4Fe4S] cluster present in these proteins might allow these enzymes to take advantage of DNA-mediated charge transfer as a long-range damage detection method (*24*). Furthermore, this damage detection scheme could facilitate cooperative lesion detection among MutY and EndoIII, thus increasing the efficiency of damaged site location (*34*). It is interesting to consider that archaeal DNA repair enzymes bearing [4Fe4S] clusters might employ the metal center to perform a similar function. This principle is easily transferred to *A. fulgidus* UDG, since this BER enzyme plays a role quite similar to that of MutY and

EndoIII within the cell. Notably, *A. fulgidus* contains an EndoIII homologue (though it does not contain a MutY homologue) (*35*), allowing for the possibility of cooperative damage detection with EndoIII. It is interesting that the [4Fe4S] cluster is unique to family 4 UDGs, enzymes present in organisms that thrive at high temperatures where the formation of uracil in DNA is enhanced, leading to a greater requirement for UDG activity. Does the iron-sulfur cluster in these proteins help fulfill this need for greater DNA repair?

It is perhaps a bit less clear how XPD might use a redox-active iron-sulfur cluster in its function. XPD is part of the NER pathway and has a very different enzymatic function from that of the BER glycosylase enzymes discussed here. XPD and BER glycosylases do share a similar molecular recognition challenge within the cell. While XPD is not the initial damage recognition enzyme in NER (XPC plays that role) (*19*), it is recruited by XPC to damaged sites and this colocalization process is not well understood. Perhaps the iron-sulfur cluster in XPD could be used to harness DNA-mediated charge transport to locate XPC-bound lesions? Since XPD has a similar potential when compared to [4Fe4S] cluster BER enzymes, it may be possible that XPD could also participate in cooperative damage detection with these enzymes. Importantly, the iron sulfur cluster could be present in a wide range of XPD-related helicases found in a variety of organisms (*21*). Most of these helicases are not well characterized, but many of them are believed to function in DNA repair processes (*33, 36*). Thus, these enzymes may all be charged with the task of locating lesions, forked, looped, and bubbled DNA structures in a fast and efficient manner, a task which could be accomplished via DNA-mediated charge transport.

SUMMARY

Several DNA repair enzymes from archaea have recently been discovered to contain iron-sulfur clusters. *A. fulgidus* UDG is a base-excision repair glycosylase, responsible for the excision of uracil in DNA, and the iron-sulfur cluster in this enzyme is unique to specific archaea. *S. acidocaldarius* XPD is a nucleotide excision repair helicase that unwinds DNA in the vicinity of bulky DNA lesions. The iron-sulfur cluster in this protein appears to be common to a large family of helicases present in many different organisms. *A. fulgidus* UDG and *S. acidocaldarius* XPD were both examined on DNA-modified electrodes to evaluate the DNA-bound redox properties of the proteins. *A. fulgidus* UDG displays an electrochemical signal at a DNA-modified electrode with a midpoint potential of +95 mV vs. NHE. A set of *A. fulgidus* UDG cysteine mutants were examined and nearly all of these variants have some DNA-bound redox activity indicating that this archaeal enzyme may be especially robust to ligand substitution at the iron-sulfur cluster. *S. acidocaldarius* XPD also exhibits DNA-bound redox activity with a midpoint potential of +77 mV versus NHE. The role of the [4Fe4S] cluster in these archaeal enzymes is unknown, but the redox properties of these proteins are quite similar to those of [4Fe4S] BER enzymes from *Escherichia coli*. For these *E. coli* enzymes, it has been proposed that the iron-sulfur cluster might allow BER enzymes to cooperatively search for damage via DNA charge transport. Perhaps the iron-sulfur cluster in archaeal UDG and DNA repair helicases has a similar function?

REFERENCES

1. Nealson, K. H., and Conrad, P. G. (1999) *Phil. Trans. R. Soc. Lond. B 354*, 1923.
2. Pace, N. R. (1997) *Science 276*, 734.
3. Kelman, Z., and White, M. F. (2005) *Curr. Op. Microbiol. 8*, 669.
4. Grogan, D. W. (2004) *Curr. Issues Mol. Biol. 6*, 137.
5. Lindahl, T., and Nyberg, B. (1974) *Biochemistry 13*, 3405.
6. Jacobs, K. L., and Grogan, D. W. (1997) *J. Bacteriol. 179*, 3298.
7. David, S. S., and Williams, S. D. (1998) *Chem. Rev. 98*, 1221.
8. David, S. S., O'Shea, V. L., and Kundu, S. (2007) *Nature 447*, 941.
9. Lindahl, T. (1993) *Nature 362*, 709.
10. Koulis, A., Cowan, D. A., Pearl, L. H., and Saava, R. (1996) *FEMS Microbiol. Lett. 143*, 267.
11. Sandigursky, M., and Franklin, W. A. (1999) *Curr. Biol. 9*, 531.
12. Sandigursky, M., and Franklin, W. A. (2000) *J. Biol. Chem. 275*, 19146.
13. Sartori, A. A., Schar, P., Fitz-Gibbon, S., Miller, J. H., and Jiricny, J. (2001) *J. Biol. Chem. 276*, 29979.
14. Hinks, J. A., Evans, M. C. W., de Miguel, Y., Sartori, A. A., Jiricny, J., and Pearl, L. H. (2002) *J. Biol. Chem. 277*, 16936.
15. Hoseki, J., Okamoto, A., Masui, R., Shibata, T., Inoue, Y., Yokoyama, S., and Kuramitsu, S. (2003) *J. Mol. Biol. 333*, 515.
16. Slupphaug, G., Mol, C. D., Kavli, B., Arvai, A. S., Krokan, H. E., and Tainer, J. A. (1996) *Nature 384*, 87.
17. Setlow, R. B., and Carrier, W. L. (1964) *Proc. Natl. Acad. Sci. USA 51*, 226.
18. Setlow, R. B., Regan, J. D., German, J., and Carrier, W. L. (1969) *Proc. Natl. Acad. Sci. USA 64,* 1035.
19. Dip, R., Camenisch, U., and Naegeli H. (2004) *DNA Repair 3*, 1409.
20. Lehmann A. R. (2001) *Genes Dev. 15*, 15.

21. Rudolf, J., Makrantoni, V., Ingledew, W. J., Stark, M. J., and White, M. F. (2006) *Mol. Cell 23*, 801.

22. Pugh, R. A., Honda, M., Leesley, H., Thomas, A., Lin, Y., Nilges, M. J., Cann, I. K. O., and Spies, M. (2008) *J. Biol. Chem. 283*, 1732.

23. Cunningham, R.P., Asahara, H., Bank, J.F., Scholes, C.P., Salerno, J.C., Surereus, K., Munck, E., McCracken, J., Peisach, J., and Emptage, M.H. (1989) *Biochemistry 28*, 4450.

24. Boal, A.K., Yavin, E., Lukianova, O.A., O'Shea, V.L., David, S.S., and Barton, J.K. (2005) *Biochemistry 44*, 8397.

25. Beaucage, S. L., and Caruthers, M. H. (1981) *Tetrahedron Lett. 22*, 1859.

26. Kelley, S. O.; Boon, E. M.; Barton, J. K.; Jackson, N. M.; Hill, M. G. (1999) *Nucleic Acids Res. 27*, 4830.

27. Fromme, J. C., and Verdine, G. L. (2003) *EMBO J. 22*, 3461.

28. Fromme, J. C., Banerjee, A., Huang, S. J., and Verdine, G. L. (2004) *Nature 427*, 652.

29. Volbeda, A., Charon, M. C., Piras, C., Hatchikian, E. C., Frey, M., and Fontecilla-Camps, J. C. (2002) *Nature 373*, 580.

30. Venkateswara, R. P., and Holm, R. H. (2004) *Chem. Rev. 104*, 527.

31. Messick, T. E., Chmiel, N. H., Golinelli, M. P., Langer, M. R., Joshua-Tor, L., and David, S. S. (2002) *Biochemistry 41*, 3931.

32. Cowan, J. A., and Lui, S. M. (1998) *Adv. Inorg. Chem. 45*, 313.

33. Singleton, M. R., Dillingham, M. S., and Wigley, D. B. (2007) *Annu. Rev. Biochem. 76*, 23.

34. Boal, A. K., Genereux, J. C., Sontz, P. A., Gralnick, J. A., Newman, D. K., and Barton, J. K. (2008) (*submitted for publication*).

35. Klenk, H. P., *et al.* (1997) *Nature 390*, 364.

36. Voloshin, O. N., and Camerini-Otero, R. D. (2007) *J. Biol. Chem. 282,* 18437.

CHAPTER 5

Protein-DNA Charge Transport: Redox Activation of a DNA Repair Protein by Guanine Radical

Adapted from Yavin, E., Boal, A. K., Stemp, E. D. A., Boon, E. M., Livingston, A. L., O'Shea, V. L., David, S. S., and Barton, J. K. (2005) *Proceedings of the National Acadamies of Sciences, U. S. A. 102*, 3546.

E. Yavin performed EPR experiments. E. Stemp and E. Boon performed transient absorption experiments. A. Livingston and V. O'Shea prepared protein samples.

INTRODUCTION

DNA-mediated charge transport (CT) from a distance to generate oxidative damage was first demonstrated in an assembly containing a tethered metallointercalator (*1*). In this assembly, photoinduced oxidative damage of the 5'-G of 5'-GG-3' sites was observed; this damage pattern has since become the hallmark of DNA CT chemistry and long range oxidative damage has been confirmed using a variety of pendant oxidants (*2-6*). Long range oxidative DNA damage has been demonstrated over a distance of at least 200 Å (*7, 8*). Indeed DNA either packaged in nucleosome core particles (*9*) or inside the cell nucleus (*10*) has been found to be susceptible to long range oxidative damage. Chemically well-defined assemblies, consisting of DNA duplexes with covalently bound oxidants, have been particularly useful in establishing the sensitivity of DNA CT to base stacking perturbation (*11-16*). Recently, analogous studies probing long range reductive chemistry on DNA has been probed both in solution (*17-20*) and on DNA-modified surfaces (*14, 15, 21*). As with oxidation chemistry, these reactions show only small variations in rate with distance but are remarkably sensitive to perturbations in the intervening base pair stack. Mechanistic descriptions for DNA CT focused first on a mixture of hopping and tunneling. A phonon-assisted polaron model has also been put forth (*22*). Studies in our laboratory as a function of temperature have shown the CT process to be gated by base pair dynamics; in fact base pair motions are required for CT (*23, 24*). We have therefore described DNA CT in the context of transport among delocalized DNA domains formed and dissolved based upon sequence-dependent DNA dynamics.

Given the exquisite sensitivity of DNA CT to DNA lesions and mismatches, we have recently explored a possible role for DNA CT in repair. We demonstrated that redox activity required DNA binding for MutY (*25*), a BER enzyme from *Escherichia coli* that

acts as a glycosylase to remove adenine from G:A and 7,8-dihydro-8-oxo-2-deoxyguanosine (8-oxo-G):A mismatches (*27-33*). Commonly considered a redox cofactor, $[4Fe4S]^{2+}$ clusters are ubiquitous to base excision repair (BER) enzymes (*27-37*), yet redox activity in these proteins could not be detected under physiological conditions. Electrochemistry on DNA-modifed electrodes showed a shift in potential for MutY to +90 mV versus NHE (*25, 26*), a potential characteristic of high potential iron proteins. Companion electrochemistry experiments showed furthermore that CT from the electrode surface to the [4Fe4S] cluster requires DNA and is DNA-mediated. Electrochemical studies on DNA-modified surfaces and EPR experiments in solution testing additional BER enzymes more recently showed that this DNA-dependent redox activity of BER enzymes is general. Bound to DNA, BER enzymes containing $[4Fe4S]^{2+}$ clusters show similar redox potentials; binding to DNA shifts the $[4Fe4S]^{3+/2+}$ potential, activating the proteins towards oxidation. Based on this DNA-dependent redox activity, we have proposed a model for how BER enzymes might more quickly redistribute onto regions of the genome containing DNA lesions (*25*). This model depends upon DNA-mediated CT among the BER enzymes and the sensitivity of DNA CT chemistry to intervening perturbations in base pair stacking, e.g. DNA mismatches and lesions.

Here we describe the redox activation of MutY by an oxidized base radical, the condition of oxidative stress. We generate guanine radicals using ruthenium flash/quench chemistry. This chemistry was first developed to probe long range electron transfer in proteins (*38*). Examining DNA CT using the flash/quench technique has been particularly advantageous in that the methodology permits both spectroscopic studies to monitor formation of DNA radicals on a short time scale (*16, 39-41*) and biochemical analysis to determine the yield of oxidative damage occurring on a longer time scale (*39-*

43). The flash/quench experiment for DNA typically is carried out with dipyridophenazine (dppz) complexes of Ru(II), complexes that bind avidly to DNA by intercalation (*44*). As illustrated in Figure 5.1, the cycle is initiated by visible light, which excites the intercalated Ru(II) complex. This excited Ru(II) complex, *Ru(II), is then quenched by a nonintercalating electron acceptor, Q, such as $[Ru(NH_3)_6]^{3+}$ or $[Co(NH_3)_5Cl]^{2+}$, so as to form Ru(III) *in situ*. It is this Ru(III) species that can oxidize guanines from a distance. The oxidized guanine radical can then undergo further reaction with H_2O and/or O_2 to form a family of oxidative products, G_{ox} (*45*). However, the lifetime of the guanine radical is relatively long (ms), and thus the guanine radical can also react with DNA-bound peptides (*46*) and proteins (*16*), or, as we demonstrate here, a BER glycosylase such as MutY.

MATERIALS AND METHODS

Materials

All chemical reagents and starting materials were purchased from commercial sources and used as received. Phosphoramidites were purchased from Glen Research. Poly(dGC) (ε_{260} = 8,400 $M^{-1}cm^{-1}$) and Poly(dAT) (ε_{260} = 6,600 $M^{-1}cm^{-1}$) were purchased from Amersham Pharmacia and were passed through spin columns (BioRad) prior to use. The ligands bpy' and dppz, as well as $[Ru(bpy')(dppz)(phen)]Cl_2$, were synthesized as described elsewhere (*47-51*).

Figure 5.1. Schematic illustration of the flash-quench technique utilized to generate Ru(III) *in situ* and subsequently to oxidize DNA-bound MutY. Back electron transfer reactions are represented as dotted lines.

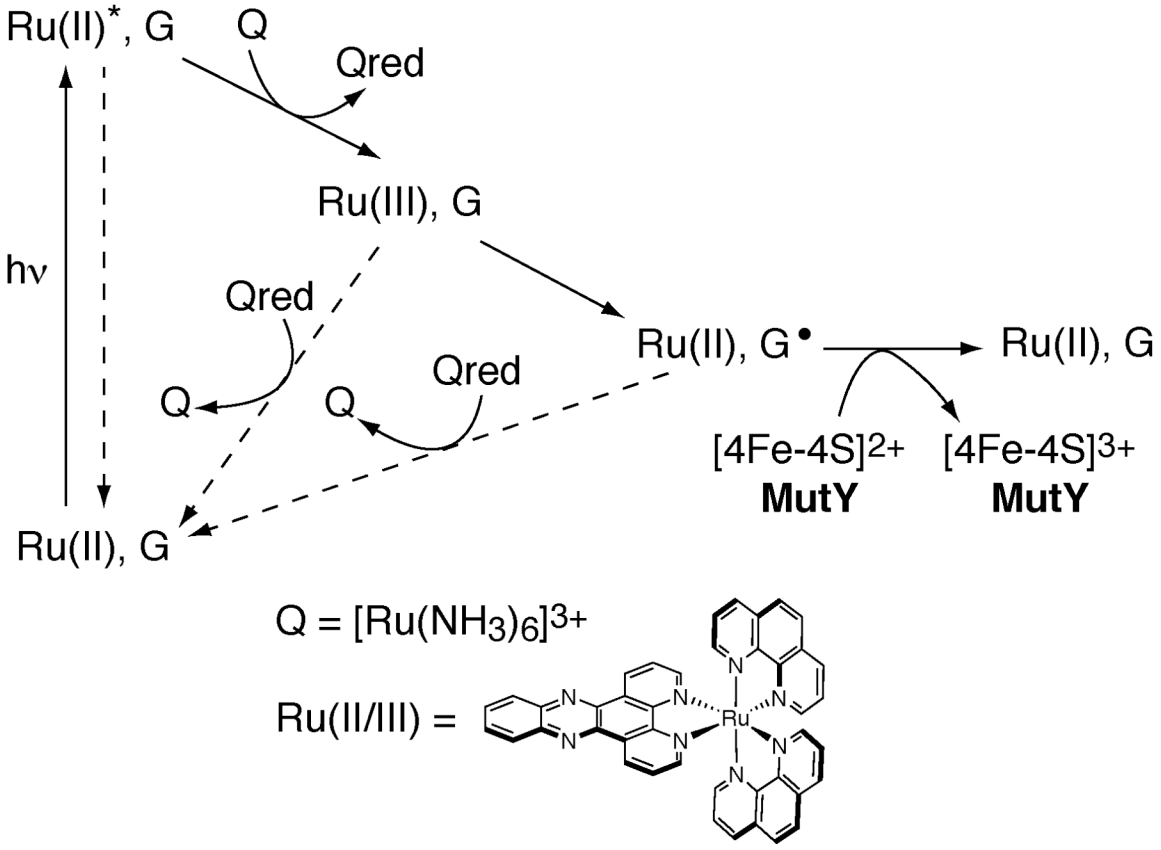

$Q = [Ru(NH_3)_6]^{3+}$

Ru(II/III) =

DNA Synthesis

The oligonucleotides were synthesized on an Applied Biosystems 394 DNA synthesizer (*52, 53*), purified by reverse-phase HPLC and characterized by mass spectrometry. The synthesis of ruthenium modified oligonucleotides was carried out with *rac*-[Ru(bpy')(dppz)(phen)]Cl_2 (*54*). Purification of the ruthenium modified DNA by reverse-phase HPLC yields four isomers, which were characterized by UV-vis spectroscopy and mass spectrometry; the mixture of diastereomers was used.

Protein Preparation

MutY was utilized in all experiments either fused to maltose binding protein or in a truncated form (Stop 225). Both forms are stable at concentrations much higher than the native form and thus are preferable for spectroscopic and EPR studies. Stop 225 was used in all transient absorption experiments and MutY-MBP was used in EPR and gel electrophoresis studies. Also, C199H-MutY was expressed as an MBP fusion and used for EPR experiments. All forms of MutY were purified as reported previously (*55*).

EPR Spectroscopy

X-band EPR spectra were obtained on a Bruker EMX spectrometer equipped with a rectangular cavity working in the TE_{102} mode. Low temperature measurements (10K) were conducted with an Oxford (ES9000) continuous-flow helium cryostat (temperature range 3.6–300 K). A frequency counter built into the microwave bridge provided accurate frequency values. Solutions were prepared by adding the protein (50

μM) or protein storage buffer (20 mM NaPi, 100 mM NaCl, 1 mM EDTA, 10% glycerol, pH = 7.5) to a solution of poly(dAT) (1 mM bp), poly(dGC) (1 mM bp) or Ru-tethered duplex (25 μM) in the presence of quencher ($Co(NH_3)_5Cl$, 125 μM). Samples were then irradiated in standard EPR quartz tubes while cooling in an un-silvered Dewar filled with liquid nitrogen; the excitation source was a focused beam from a xenon lamp (a suitable filter was used to remove light with $\lambda < 350$ nm). EPR parameters were as follows: receiver gain = 5.64×10^3, modulation amplitude = 4G, microwave power = 1.27 mW.

Assay of Oxidized Products

Unmetalated oligonucleotide strands were labeled at the 5' end with ^{32}P using standard procedures (*56*). DNA duplexes were formed by mixing equal concentrations of complementary strands (30- and 42-mers) in 50 mM NaCl, 10 mM sodium phosphate, pH 7, and heating to 90 °C followed by slow cooling to 20 °C over 120 min. The Ru-tethered DNA strand (12-mer) was then added to the duplex and the solution was heated to 37 °C followed by slow cooling to 4 °C. Samples containing 4 μM Ru-tethered DNA duplex and 80 μM quencher ($Co(NH_3)_5Cl^{2+}$) were irradiated for 15 minutes at 4 ºC using a He-Cd laser (~ 13 mW at 442 nm). After irradiation, all samples were treated with 10% (v/v) piperidine at 90 °C for 30 min, dried, and subjected to electrophoresis through a 20% denaturing polyacrylamide gel. The levels of damage were quantitated using phosphorimagery (Imagequant).

Laser Spectroscopy

Time resolved emission and transient absorption measurements used an excimer pumped dye (Coumarin 480) laser (λ = 480 nm) or a YAG-OPO laser (λ_{exc} = 470 nm)

(*40*). Laser powers ranged from 1 to 2.5 mJ/pulse. The emission of the dppz complexes was monitored at 610 nm, and the emission intensities were obtained by integrating under the decay curve for the luminescence. MutY (20 μM) was first incubated with poly(dGC) (1 mM bp) at ambient temperature for 20 minutes in 5 mM sodium phosphate buffer, pH 7.5, with $[Ru(NH_3)_6]^{3+}$ (400 μM) and $[Ru(phen)_2dppz]^{2+}$ (20 μM).

RESULTS AND DISCUSSION

Flash Quench Experiments Probed by EPR Spectroscopy

Solutions containing poly(dGC) or poly(dAT) (1 mM bp), $[Ru(phen)_2dppz]^{2+}$ (25 μM), and $[Co(NH_3)_5Cl]^{2+}$ (125 μM) were irradiated in the presence or absence of MutY (50 μM). Samples were irradiated in EPR tubes while freezing in liquid nitrogen. EPR spectra were then acquired at 10K. As shown in Figure 5.2, in the absence of MutY, irradiation of poly(dGC), $[Ru(phen)_2dppz]^{2+}$, and $[Co(NH_3)_5Cl]^{2+}$ results in an EPR signal with g = 2.004; we attribute this signal, found previously, to the guanine radical (*57, 58*). Also as seen earlier and in contrast, with poly(dAT), this signal is not observed; $[Ru(phen)_2dppz]^{3+}$ has been seen to promote formation of the guanine radical but not the adenine radical cation.

More interesting are our observations in the presence of MutY. Irradiation results in the appearance of EPR signals with primary g values of 2.02 and 2.08 and a feature at 2.06 for both poly(dGC) and poly(dAT) (Figures 5.2A and 5.2B, respectively). The peak at g = 2.02 is characteristic of the $[3Fe4S]^{1+}$ cluster (59). Earlier studies of MutY bound

Figure 5.2. EPR spectroscopy at 10K of DNA samples with and without protein after irradiation of $[Ru(phen)_2dppz]^{2+}$ (25 μM) with $[Co(NH_3)_5Cl]^{2+}$ (125 μM) as quencher and (A) poly(dGC) (1 mM bp) with and without MutY (50 μM); (B) poly(dAT) (1 mM bp) with and without MutY (50 μM); (C) poly(dGC) (1 mM bp) with native MutY or C199H mutant (50 μM).

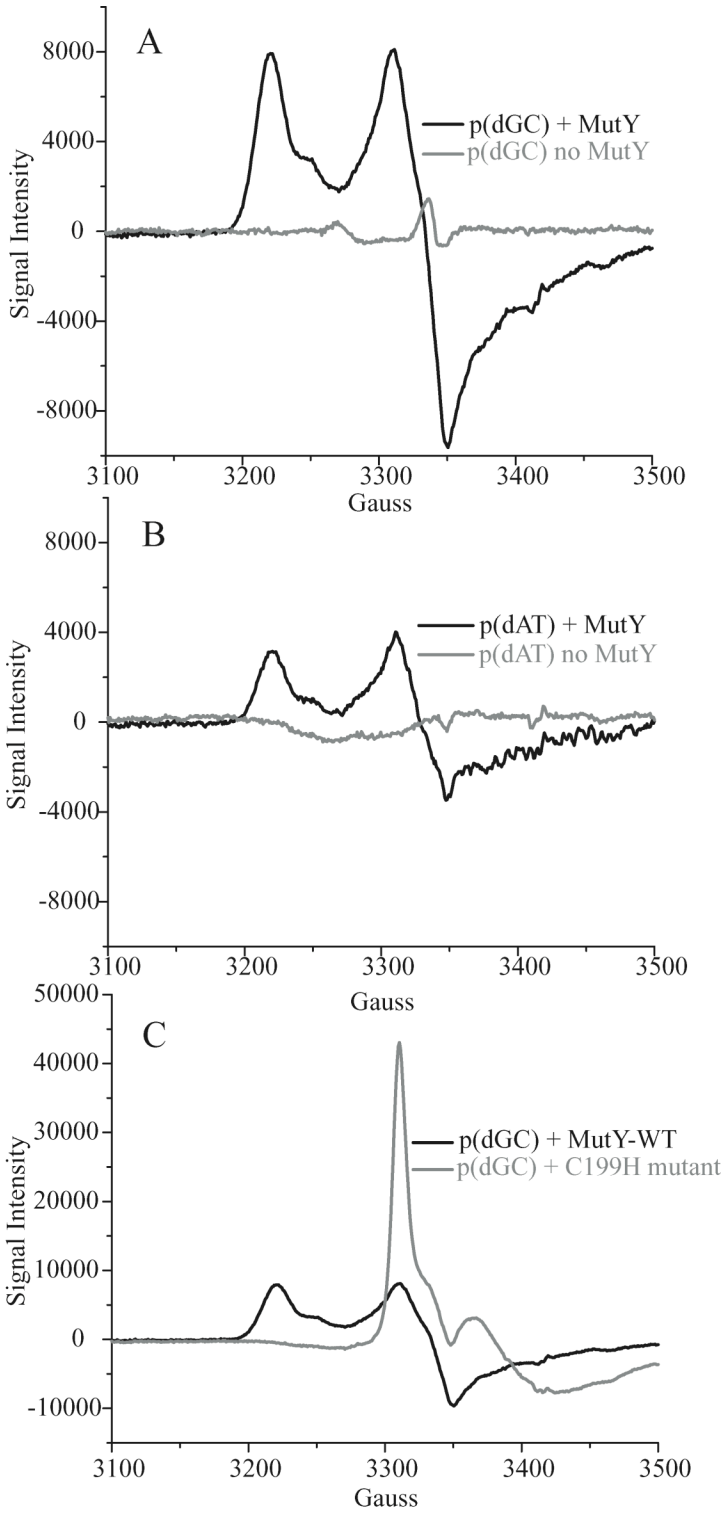

to DNA and oxidized by $Co(phen)_3^{3+}$ or MutY oxidized in the absence of DNA with ferricyanide (*60*) yielded the same EPR signal; the $[3Fe4S]^{1+}$ cluster can form as a decomposition product of $[4Fe4S]^{3+}$. Not seen earlier for MutY is the signal at g = 2.08 with a secondary feature at g = 2.06, and this g value is attributed to the fully intact, oxidized $[4Fe4S]^{3+}$ cluster (*59, 61*). In the absence of quencher, $[Co(NH_3)_5Cl]^{2+}$, or DNA, no EPR signal is observed. Noteworthy, additionally, is that with poly(dAT) and MutY, both signals are also apparent although at significantly lower intensity. Fluorescence experiments show that the concentration of excited Ru(II), and therefore Ru(III), is slightly lower for poly(dAT) compared to poly(dGC). Thus, MutY can be oxidized without guanine radical as an intermediate, but the formation of guanine radicals first may facilitate efficient MutY oxidation.

Also shown in Figure 5.2 is the flash/quench result for poly(dGC) in the presence of the C199H mutant of MutY (*60*). Interestingly, this mutant yields an EPR spectrum that is characteristic only of the $[3Fe4S]^{1+}$ cluster. In addition, the signal intensity is significantly larger. In this particular mutant, the cluster is more susceptible to decomposition (*60*); thus it is not unexpected that this mutant only exhibits formation of the degraded cluster.

Flash Quench Experiments Probed by Transient Absorption Spectroscopy

We also examined flash/quench reactions of $[Ru(phen)_2dppz]^{2+}$ bound to poly(dGC) with and without bound MutY on a faster time scale at ambient temperatures. Excitation of $[Ru(phen)_2dppz]^{2+}$ bound to poly(dGC) by nanosecond laser pulses leads to an emission decay at 610 nm that can be fit biexponentially. This excited state is oxidatively quenched by $[Ru(NH_3)_6]^{3+}$ in the presence (~ 70% quenched) and absence (~

90% quenched) of MutY. Quenching is less efficient with bound MutY, however, likely due to restricted access of the quencher to $[Ru(phen)_2dppz]^{2+}$ when MutY is bound to DNA. MutY alone does not quench the excited state of $[Ru(phen)_2dppz]^{2+}$, indicating the absence of direct electron transfer from the protein to the $[Ru(phen)_2dppz]^{2+}$ excited state.

We probed these assemblies by transient absorption spectroscopy to obtain the full absorption difference spectrum with and without MutY bound to poly(dGC). At each wavelength, the transient absorption signal was fit as follows ($A(t) = C_0 + C_1\exp(-k_1t)$) and the coefficients for the fast phase (C_1) and the slow phase (C_0) were plotted against wavelength. The spectrum of the fast phase resembles the spectrum of the guanine radical in duplex DNA, with broad maxima at 390 and 510 nm (*40*). There appears to be less of this product in the presence of MutY, however. The spectrum of the slow phase shows evidence of the formation of a new species with an absorption maximum at ~ 405 nm (Figure 5.3). It is noteworthy that a $[4Fe4S]^{3+/2+}$ difference spectrum should show an absorption maximum near 405 nm (*60, 62*). This long lived absorption is not observed with poly(dAT); the spectrum with poly(dAT) instead shows first a negative signal at 440 nm consistent with Ru(II) bleaching, with no long lived signal. This long lived signal is also not observed without inclusion of one or more of the necessary reagents: MutY, $[Ru(phen)_2dppz]^{2+}$, and $[Ru(NH_3)_6]^{3+}$. Thus, these transient absorption data are consistent with formation first of a guanine radical upon oxidative flash quench of $[Ru(phen)_2dppz]^{2+}$ bound to poly(dGC) in the presence of bound MutY, followed by a second species, likely $[4Fe4S]^{3+}$, that is very long lived.

Figure 5.3. Time-resolved transient absorption data for $Ru(phen)_2(dppz)^{2+}$ (20 μM) bound to poly(dGC) (1 mM bp) quenched by $[Ru(NH_3)_6]^{3+}$ (0.4 mM) with MutY (20 μM). Shown is the absorption difference spectrum of the long lived transient with data averaged over four experiments. Inset: Transient absorption at 405 nm in the presence (red) and absence (green) of MutY bound to poly(dGC) or without DNA (black).

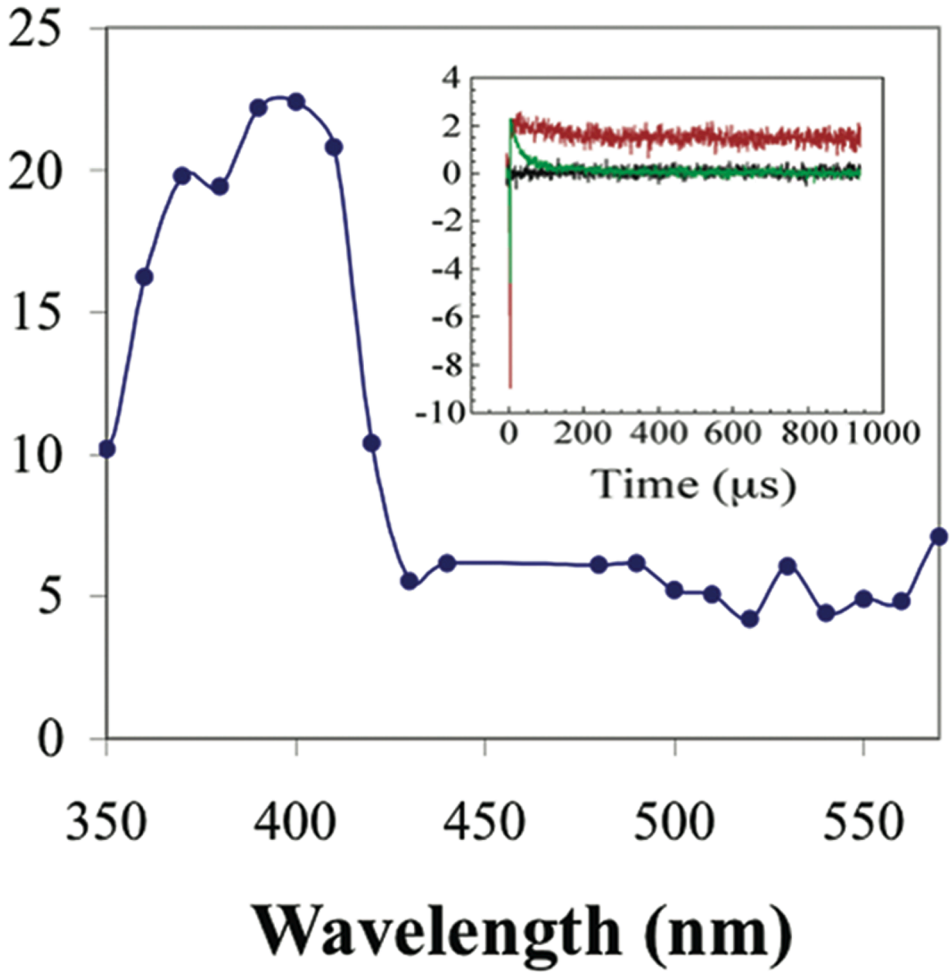

Figure 5.4. Autoradiogram after denaturing polyacrylamide gel electrophoresis of ^{32}P-5'- TTGGAATTATAATTTATAATATTAAATATT-3' after oxidation of the ruthenium-tethered oligonucleotide duplex by flash/quench. Lanes shown are Maxam-Gilbert sequencing reactions for C + T, and A + G respectively; lane 1 – lane 5: Ru-DNA irradiated in the presence of cobalt quencher and 8, 6, 4, 2, or 0 μM MutY; lane 6: Ru-DNA irradiated with 4 μM MutY but no quencher; lane 7: Ru-DNA without MutY or quencher; lane 8: DNA irradiated without Ru-tethered strand. Concentrations were [DNA] = 4 μM and $[Co(NH_3)_5Cl]^{2+}$ = 200 μM. Irradiations were for 15 min. Reactions were carried out in 5 mM sodium phosphate, 50 mM NaCl, pH = 7.

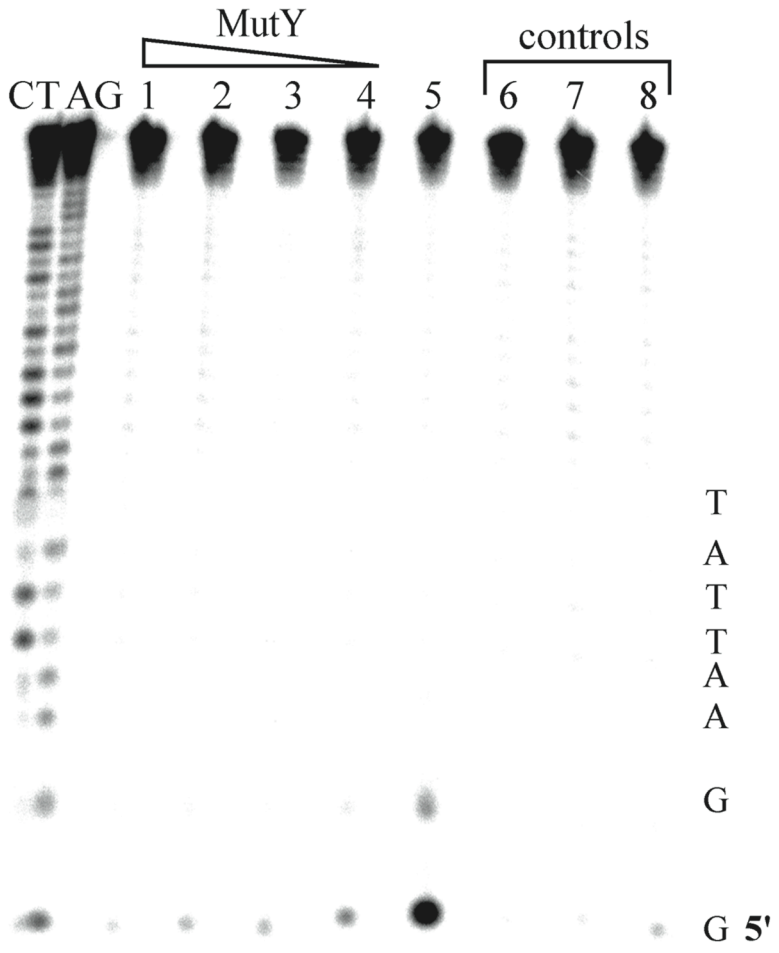

Figure 5.5 EPR spectroscopy at 10K of ruthenium-tethered DNA duplexes (25 μM, fully or partially hybridized) with MutY (50 μM) after irradiation in the presence of quencher ($[Co(NH_3)_5Cl]^{2+}$, 125 μM).

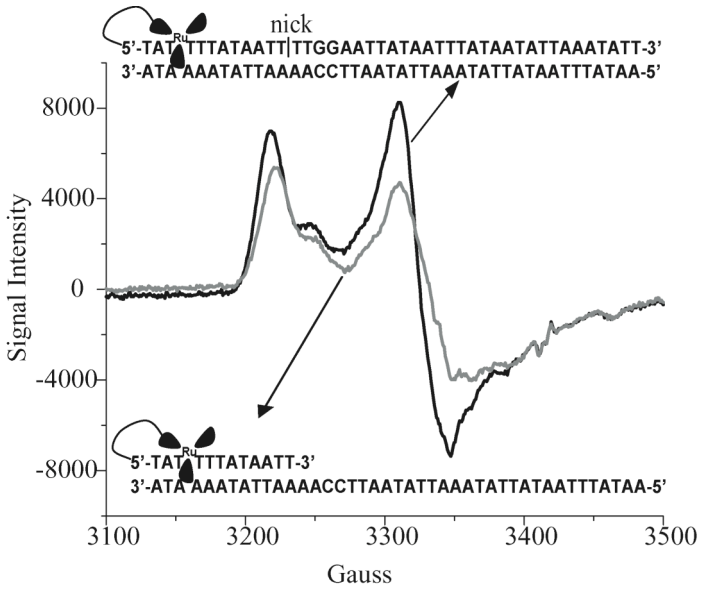

Flash Quench Experiments with Ruthenium-tethered Oligonucleotides

Shown in Figure 5.4 are autoradiographs after denaturing polyacrylamide gel electrophoresis of ^{32}P-5'-endlabeled DNA duplexes covalently linked to a ruthenium intercalator, irradiated in the presence or absence of MutY. The DNA duplex was assembled from a 12-mer ruthenium-tethered strand, a 30-mer strand ^{32}P-endlabeled containing a 5'-GG-3' doublet, and the full 42-mer complement. In the absence of MutY, the typical 5'-G damage on the 5'-GG-3' doublet guanine is observed; this guanine damage is expected upon oxidation from a distance *via* DNA-mediated charge transport from Ru(III) generated *in situ*. In the presence of 0.5–2 equivalents (2–8 μM) MutY, however, this damage is inhibited.

We also monitored the flash/quench reaction by EPR spectroscopy for the ruthenium-tethered oligonucleotide in the presence of MutY (Figure 5.5). As with poly(dGC), here too at 10K strong signals with g = 2.08, g = 2.06, and g = 2.02 are apparent, consistent with formation of the oxidized $[4Fe4S]^{3+}$ cluster as well as its decomposition product, $[3Fe4S]^{1+}$. Not apparent is any evidence of guanine radical formation in the absence of MutY; likely the lower concentration of guanine radical in this oligonucleotide assembly compared to poly(dGC) makes its detection by EPR more difficult.

In addition, we examined the flash/quench reaction of the Ru-tethered duplex lacking the 30-mer strand. This assembly, composed of a short duplex region and long single-stranded segment, contains no guanines but can generate Ru(III) by flash/quench with yields comparable to that for the fully duplexed oligomer above. Yet this assembly in the presence of MutY results in an attenuated EPR signal in comparison to the fully hybridized duplex containing the 5'-GG-3' doublet. Thus in the fully hybridized duplex,

oxidation of MutY mediated by the DNA duplex must occur, and here too guanine radical formation appears to facilitate efficient MutY oxidation.

Discussion

Results reported here show clearly that DNA-bound Ru(III) can promote oxidation of the $[4Fe4S]^{2+}$ cluster of MutY to $[4Fe4S]^{3+}$ and its decomposition product $[3Fe4S]^{1+}$. Flash/quench experiments monitored by EPR spectroscopy reveal spectra with g values characteristic of the oxidized clusters. Earlier studies had shown a resistance to oxidation of the $[4Fe4S]^{2+}$ cluster of BER enzymes in the absence of DNA but an enhancement in oxidation in the presence of DNA (*25, 63, 64*). We have attributed this facility in oxidation of the DNA-bound proteins to the shift in oxidation potential associated with DNA binding.

Interestingly, these data provide the first direct demonstration of the formation of $[4Fe4S]^{3+}$ in MutY. The signal with g = 2.08, 2.06 is characteristic of that seen for $[4Fe4S]^{3+}$ in high potential iron proteins (*59, 61*). We find some evidence for formation of the $[4Fe4S]^{3+}$ cluster in oxidation of DNA-bound uracil DNA glycosylase from *A. fulgidus* by $Co(phen)_3^{3+}$, but for EndoIII and MutY from *E. coli* both oxidation by ferricyanide and $Co(phen)_3^{3+}$ have produced only the oxidized but decomposed product, $[3Fe4S]^{1+}$ (*60, 64*).

It is useful in this context to consider our results for the C199H mutant. For this mutant, oxidative decomposition to $[3Fe4S]^{1+}$ is known to be facile owing to the poorer coordination of the cluster by the histidine ligand (*60*). Our finding of a signal at g = 2.02 for C199H, characteristic of the $[3Fe4S]^{1+}$ cluster, helps us to assign the signal at g =

2.08, 2.06 for wild type MutY to the one electron oxidized $[4Fe4S]^{3+}$. We suggest that this oxidation product is obtained by flash/quench, because this process is particularly fast. In this case, also, we utilize the tightly bound, well stacked DNA intercalator as oxidant rather than $Co(phen)_3^{3+}$ or ferricyanide, which do not bind deeply in the base pair stack by intercalation. Thus the direct, rapid formation of $[4Fe4S]^{3+}$ appears to be facilitated by the DNA-mediated oxidation of MutY.

The transient absorption data also provide a consistent picture. The long lived transient, with a maximum absorption at 405 nm, is attributed primarily to formation of $[4Fe4S]^{3+}$ and possibly also $[3Fe4S]^{1+}$; both absorb more in this region than does $[4Fe4S]^{2+}$ (*60-63*). The shape of the spectrum has some features that resemble that of a tyrosine radical, and several tyrosine residues surround the cluster in the enzyme (*36, 37*), but the extinction coefficient for $[4Fe4S]^{3+}$ is expected to be significantly higher in this region, so that tyrosine radical or even guanine radical may not be distinguishable. Some tyrosine radical formation at ambient temperatures on a short time scale, or even tyrosine radical as a second intermediate, cannot be ruled out, however.

Oxidation of DNA-bound MutY does not necessitate a DNA-mediated charge transfer, but the data here illustrate that the DNA-mediated reaction can occur and guanine radical formation may facilitate MutY oxidation. The oxidation potential of guanine is -1.25 V versus NHE (*65*), the midpoint potential of DNA-bound MutY ($[4Fe4S]^{2+/3+}$) is +0.1 V versus NHE (*26*), while the reduction potential of Ru(III) is 1.5 V versus NHE (*40*). Thus the net reaction for these charge transfer processes is thermodynamically favored. The biochemical data indicate that MutY inhibits long range oxidative damage to guanines. The EPR data show that the flash/quench reaction promotes oxidation of the $[4Fe4S]^{2+}$ cluster in DNA-bound MutY. Taken together, these

data show that MutY oxidation, the thermodynamic product, is formed at the expense of guanine radicals and accounts for the loss of irreversible oxidative DNA damage in the presence of MutY.

Cluster oxidation furthermore appears generally to occur in a DNA-mediated reaction. In the absence of DNA, no MutY oxidation occurs; DNA-binding is required to shift the $[4Fe4S]^{3+}/[4Fe4S]^{2+}$ potential of MutY, activating it towards oxidation. Moreover, the Ru(III) oxidant must also be DNA-bound to have been generated from excited Ru(II); there is no detectable formation of Ru(II) excited state unless the complex is intercalated. Thus both MutY and the ruthenium complex must be bound to DNA. In addition, MutY oxidation was found to be greater for the full ruthenated 42 bp duplex assembly versus that lacking the 30-mer strand. Ru(III) formation is equivalent in these assemblies and the shorter duplex region along with the single-stranded tail in this assembly might be expected to facilitate direct encounters between Ru(III) and DNA-bound MutY. Yet, oxidation is greater with the longer duplex that contains a guanine site. While some direct oxidation cannot be ruled out, oxidation mediated by a DNA duplex appears favored.

Is the cluster oxidized in competition with guanine oxidation or does guanine radical represent an intermediate in the charge transport process? The transient absorption spectroscopic data indicate that the guanine radical is formed on a fast time scale compared to the oxidized cluster formed in the presence of MutY. Low temperature EPR data for polyd(GC) also indicate that $[4Fe4S]^{3+}$ and $[3Fe4S]^{1+}$ form, and the sharp organic radical signal is no longer apparent. In the case of poly(dAT), no base radical in the absence of protein has been observed; an adenine radical, if formed, would be expected to be short lived, and the large negative bleach associated with Ru(III) makes

detecting any small positive transients in this wavelength region difficult. In any case, the transient absorption data with poly(dGC) indicate quite clearly that guanine radical is formed in the presence of MutY but is depleted, and instead the $[4Fe4S]^{2+}$ cluster is oxidized.

Indeed, while a guanine radical is not required as an intermediate in MutY oxidation, its presence appears to enhance oxidation. In the absence of any guanines, both for polyd(AT) and the assembly lacking the 30-mer strand that only contains adenines and thymines, Ru(III), once generated, does oxidize DNA-bound MutY. But the yield of oxidation per Ru(III) is clearly greater with polyd(GC) than polyd(AT). Furthermore, in the assembly with the extended duplex containing a guanine site, the yield of cluster oxidation seen by EPR spectroscopy is significantly greater than in the assembly containing only a 12-mer duplex region and no guanines.

Why does the presence of intervening guanines appear to enhance the efficiency of cluster oxidation? It is reasonable to consider that guanine radical formation serves to compete with fast back electron transfer to the DNA-bound ruthenium so that there is more time for oxidation of MutY. The guanine radical lifetime in the absence of MutY is on the millisecond time scale (*40*). Thus a DNA-mediated oxidation of MutY can occur with or without intervening guanines, but *guanine radical formation*, the first DNA product under oxidizing conditions, *facilitates the oxidation of DNA-bound MutY*.

Under conditions of oxidative stress, guanine radicals in DNA are generated and lead to the formation of 8-oxoG; note that 8-oxoG:A mismatches represent the primary substrate for MutY (*37*). The results presented here indicate that this first signal of the need for DNA repair may in fact activate the repair machinery through oxidation. Figure 5.6 shows our model for how DNA charge transport among BER enzymes may facilitate

the detection of DNA lesions. The data here describe MutY oxidation, but other BER enzymes containing $[4Fe4S]^{2+}$ clusters show equivalent DNA-bound redox potentials. In our model, the BER enzyme, robust to oxidation in solution has a $[4Fe4S]^{2+}$ cluster. DNA binding shifts the cluster potential, promoting its oxidation to $[4Fe4S]^{3+}$, with DNA-mediated charge transport to another oxidized repair protein bound at a distal site along the duplex; reduction of this distal DNA-bound repair protein then facilitates dissociation from DNA and relocation onto another site. In this model, charge transport occurs effectively among the repair proteins bound along well-matched, undamaged DNA and thus provides a strategy to scan the genome. However, when the protein binds to a region nearby a DNA lesion, DNA mediated charge transport cannot occur, and the repair protein processively moves on a slower time scale to the site of the lesion and carries out its repair. Thus, DNA charge transport provides a route to redistribute the repair proteins onto regions of the genome containing DNA lesions.

Also, as illustrated in Figure 5.6, guanine radicals, as effective oxidants of the repair proteins in a DNA-mediated reaction, may promote this redistribution. The guanine radicals, formed under oxidative stress, can essentially be “repaired” directly through DNA-mediated electron transfer from the repair protein. Significantly, oxidation of the repair protein through this process serves further to drive the redistribution of DNA repair proteins on genomic sites and hence preferentially onto sites near lesions. Thus guanine radicals, in oxidizing the DNA-bound repair proteins, can provide a signal to stimulate DNA repair.

DNA charge transport chemistry provides a route to carry out oxidative DNA damage from a distance. This chemistry is also exquisitely sensitive to the presence of

Figure 5.6. Model for detection strategy for BER enzymes using DNA mediated charge transport and stimulated by guanine radicals. The guanine radicals, formed under oxidative stress, are reduced and hence repaired through DNA-mediated electron transfer from the BER enzyme. Oxidation of the repair protein then drives charge transport to an alternate repair protein bound at a distal site, thereby promoting the redistribution of DNA repair proteins on genomic sites. Since no DNA charge transport can proceed through intervening lesions, the proteins are preferentially redistributed onto sites near lesions (below). Thus guanine radicals, in oxidizing the DNA-bound repair proteins, and driving the redistribution, provides a signal to stimulate DNA repair.

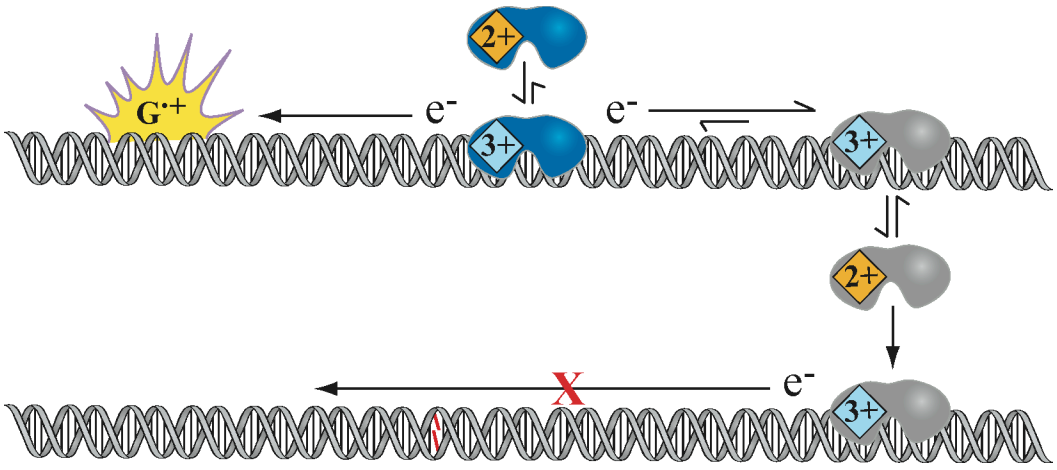

mismatches, lesions, and other perturbations to the structure of the base pair stack, and as a result, could serve as a sensor for mismatches and lesions in DNA. Here we see that this chemistry may also provide a unique biological signal within the cell. Oxidative damage from a distance may itself provide a stimulus for DNA charge transport among DNA-bound proteins and hence for activation of DNA repair.

SUMMARY

DNA charge transport chemistry provides a route to carry out oxidative DNA damage from a distance in a reaction that is sensitive to DNA mismatches and lesions. Here DNA-mediated charge transport also leads to oxidation of a DNA-bound base excision repair enzyme, MutY. DNA-bound Ru(III), generated through a flash/quench technique, is found to promote oxidation of the $[4Fe4S]^{2+}$ cluster of MutY to $[4Fe4S]^{3+}$ and its decomposition product $[3Fe4S]^{1+}$. Flash/quench experiments monitored by EPR spectroscopy reveal spectra with g of 2.08, 2.06, and 2.02, characteristic of the oxidized clusters. Transient absorption spectra of polyd(GC) and $[Ru(phen)_2dppz]^{3+}$ (dppz = dipyridophenazine), generated *in situ*, show an absorption characteristic of the guanine radical that is depleted in the presence of MutY with formation instead of a long lived species with an absorption at 405 nm; we attribute this absorption also to formation of the oxidized $[4Fe4S]^{3+}$ and $[3Fe4S]^{1+}$ clusters. In ruthenium-tethered DNA assemblies, oxidative damage to the 5'-G of a 5'-GG-3' doublet is generated from a distance but this irreversible damage is inhibited by MutY and instead EPR experiments reveal cluster oxidation. Using ruthenium-tethered assemblies containing duplex versus single-stranded regions, MutY oxidation is found to be mediated by the DNA duplex, with guanine radical as an intermediate oxidant; guanine radical formation facilitates MutY oxidation. A model is proposed for the redox activation of DNA repair proteins through DNA charge transport, with guanine radicals, the first product under oxidative stress, in oxidizing the DNA-bound repair proteins, providing the signal to stimulate DNA repair.

REFERENCES

1. Hall, D. B., Holmlin, R. E., and Barton, J. K. (1996) *Nature 382,* 731.

2. Hall, D. B., Kelley, S. O., and Barton, J. K. (1998) *Biochemistry 37*, 15933.

3. Gasper, S. M., and Schuster, G. B. (1997) *J. Am. Chem. Soc. 119,* 12762.

4. Meggers, E., Kusch, D., Spichty, M., Wille, U., and Giese, B. (1998) *Angew. Chem., Int. Ed. 37,* 460.

5. Nakatani, K., Dohno, C., and Saito, I. (1999) *J. Am. Chem. Soc. 121,* 10854.

6. Núñez, M. E., Noyes, K. T., Gianolio, D. A., McLaughlin, L. W., and Barton, J. K. (2000) *Biochemistry 39,* 6190.

7. Núñez, M. E., Hall, D. B., and Barton, J. K. (1999) *Chem. Biol. 6,* 85.

8. Ly, D., Sanii, L., and Schuster, G. B. (1999) *J. Am. Chem. Soc. 121,* 9400.

9. Núñez, M. E., Noyes, K. T., and Barton, J. K. (2002) *Chem. Biol. 9,* 403.

10. Núñez, M. E., Holmquist, G. P., and Barton, J. K. (2001) *Biochemistry 40,* 12465.

11. Rajski, S. R., Kumar, S., Roberts, R. J., and Barton, J. K. (1999) *J. Am. Chem. Soc. 121,* 5615.

12. Bhattacharya, P. K., and Barton, J. K. (2001) *J. Am. Chem. Soc. 123,* 8649.

13. Hall, D. B., and Barton, J. K. (1997) *J. Am. Chem. Soc. 119,* 5045.

14. Boon, E. M., Ceres, D. M., Drummond, T. G., Hill, M. G., and Barton, J. K. (2000) *Nat. Biotechnol. 18,* 1096.

15. Boon, E. M., Salas, J. W., and Barton, J. K. (2002) *Nat. Biotechnol. 20,* 282.

16. Wagenknecht, H.-A., Rajski, S. R., Pascaly, M., Stemp, E. D. A., and Barton, J. K. (2001) *J. Am. Chem. Soc. 123,* 4400.

17. Giese, B., Carl, B., Carl, T., Carell, T., Behrens, C., Hennecke, U., Schieman, O. , and Feresin, E. (2004) *Angew. Chem., Int. Ed. 43,* 1848.

18. Breeger, S., Hennecke, U. , and Carell, T. (2004) *J. Am. Chem. Soc. 126,* 1302.

19. Ito, T. , and Rokita, S. E. (2004) *J. Am. Chem. Soc. 126,* 15552.

20. Lewis, F. D., Liu, X., Miller, S. E., Hayes, R. T. , and Wasielewski, M. R. (2002) *J. Am. Chem. Soc. 124,* 11280.

21. Kelley, S. O., Jackson, N. M., Hill, M. G. , and Barton, J. K. (1999) *Angew. Chem. Int. Ed. 38,* 941.

22. Barnett, R. N., Cleveland, C. L., Joy, A., Landman, U. , and Schuster, G. B. (2001) *Science 294,* 567.

23. O'Neill, M. A. , and Barton, J. K. (2004) *J. Am. Chem. Soc. 126,* 11471.

24. O'Neill, M. A. , and Barton, J. K. (2004) *J. Am. Chem. Soc. 126,* 13234.

25. Boon, E. M., Livingston, A. L., Chmiel, N. H., David, S. S. , and Barton, J. K. (2003) *Proc. Natl. Acad. Sci. USA 100,* 12543.

26. Boon, E. M., Livingston, A. L., Chmiel, N. H., David, S. S. , and Barton, J. K. (2004) *Proc. Natl. Acad. Sci. USA 101,* 4718.

27. Radicella, J. P., Clark, E. A. , and Fox, M. S. (1998) *Proc. Natl. Acad. Sci. USA 85,* 9674.

28. Porello, S. L., Cannon, M. J. , and David, S. S. (1998) *Biochemistry 37,* 6465.

29. Nghiem, Y., Cabrera, M., Cupples, C. G. , and Miller, J. H. (1998) *Proc. Natl. Acad. Sci. USA 85,* 2709.

30. Michaels, M. L., Cruz, C., Grollman, A. P. , and Miller, J. H. (1992) *Proc. Natl. Acad. Sci. USA 89,* 7022.

31. Michaels, M. L. , and Miller, J. H. (1992) *J. Bacteriol. 174,* 6321.

32. Michaels, M. L., Tchou, J., Grollman, A. P. , and Miller, J. H. (1992) *Biochemistry 17,* 10964.

33. Manuel, R. C., Czerwinski, E. W. , and Lloyd, R. S. (1996) *J. Biol. Chem. 271,* 16218.

34. McGoldrick, J.P., Yeh, Y.C., Solomon, M., Essigmann, J.M., Lu, A.L. (1995) *Mol. Cell Biol. 15,* 989.

35. Desiraju, V., Shanabruch, W., Lu, A. (1993) *J. Bacteriol. 175,* 541.

36. Guan, Y., Manuel, R. C., Arvai, A. S., Parikh, S. S., Mol, C. D., Miller, J. H., Lloyd, S. , and Tainer, J. A. (1998) *Nat. Struct. Biol. 5,* 1058.

37. Fromme, J. C., Banerjee, A., Huang, S. J. , and Verdine, G. L. (2004) *Nature 427,* 652.

38. Chang, I.-J., Gray, H. B., , and Winkler, J. R. (1991) *J. Am. Chem. Soc. 113,*

7056.

39. Yoo, J., Delaney, S., Stemp, E. D. A. , and Barton, J. K. (2003) *J. Am. Chem. Soc. 125,* 6640.

40. Stemp, E. D. A., Arkin, M. R. , and Barton, J. K. (1997) *J. Am. Chem. Soc. 119,* 2921.

41. Delaney, S., Yoo, J., Stemp, E. D. A. , and Barton, J. K. (2004) *Proc. Natl. Acad. Sci. USA 101,* 10511.

42. Delaney, S., Pascaly, M., Bhattacharya, P. K., Han, K. , and Barton, J. K. (2002) *Inorg. Chem. 41,* 1966.

43. Arkin, M. R., Stemp, E. D. A., Coates Pulver, S. , and Barton, J. K. (1997) *Chem. Biol. 4,* 389.

44. Freidman, A. E., Chambron, J.-C., Sauvage, J.-P., Turro, N. J. , and Barton, J. K. (1990) *J. Am. Chem. Soc. 112,* 4960.

45. Burrows, C. J. , and Muller, J. G. (1998) *Chem. Rev. 98,* 1109.

46. Wagenknecht, H.-A., Stemp, E. D. A. , and Barton, J. K. (2000) *Biochemistry 39,* 5483.

47. Anderson, P. A., Deacon, G. B., Haarman, K. H., Keene, F. R., Meyer, T. J., Reitsma, D. A., Skelton, B. W., Strouse, G. F., Thomas, N. C. , and Treadway, J. A. (1995) *Inorg. Chem. 34,* 6145.

48. Amouyal, E., Homsi, A., Chambron, J.-C. , and Sauvage, J.-P. (1990) *J. Chem. Soc., Dalton Trans.* 1841.

49. Della Ciena, L., Hamachi, I. , and Meyer, T. J. (1989) *J. Org. Chem. 54,* 1731.

50. Dupueur, C. M. , and Barton, J. K. (1997) *Inorg. Chem. 36,* 33.

51. Strouse, G. F., Anderson, P. A., Schoonover, J. R., Meyer, T. J. , and Keene, F. R. (1992) *Inorg. Chem. 31,* 3004.

52. Goodchild, J. (1990) *Bioconjugate Chem. 1,* 165.

53. Beaucage, S. L. , and Caruthers, M. H. (1981) *Tetrahedron Lett. 22,* 1859.

54. Holmlin, R. E., Dandliker, P. J. , and Barton, J. K. (1999) *Bioconjugate Chem. 10,* 1122.

55. Chmiel, N. H., Golinelli, M.-P., Francis, A. W. , and David, S. S. (2001) *Nucl. Acid Res. 29,* 553.

56. Sambrook, J., Fritsch, E. F. , and Maniatis, T. (1989) *Molecular Cloning: A Laboratory Manual* Cold Spring Harbor Laboratory, New York.

57. Schiemann, O., Turro, N. J. , and Barton, J. K. (2000) *J. Phys. Chem. B 104*, 7214.

58. Cullis, P. M., Malone, M. E. , and Merson Davies, L. A. (1996) *J. Am. Chem. Soc. 118***,** 2775.

59. Cowan, J. A. , and Lui, S. M. (1998) *Adv. Inorg. Chem. 45***,** 313.

60. Messick, T. E., Chmiel, N. H., Golinelli, M.-P., Langer, M. R., Joshua-Tor, L. , and David, S. S. (2002) *Biochemistry 41***,** 3931.

61. Dilg, A. W. E., Mincione, G., Achterhold, K., Iakovleva, O., Mentler, M., Luchinat, C., Bertini, I. , and Parak, F. G. (1999) *J. Biol. Inorg. Chem. 4***,** 727.

62. Johnson, M. K., Duderstadt, R. E. , and Dunn, E. C. (1999) *Adv. Inorg. Chem. 47,* 1.

63. Rogers, P. A., Eide, L., Klungland, A. , and Ding, H. (2003) *DNA Repair 2,* 809.

64. Cunningham, R. P., Asahara, H. , and Bank, J. F. (1989) *Biochemistry 28,* 4450.

65. Steenken, S., and Jovanovic, S. V. (1997) *J. Am. Chem. Soc. 119,* 617.

CHAPTER 6

Direct Electrochemistry of Endonuclease III in the Presence and Absence of DNA

Adapted from Gorodetsky, A. A., Boal, A. K., and Barton, J. K. (2005) *Journal of the American Chemical Society 18*, 12082.

A. Gorodetsky performed electrochemical measurements.

INTRODUCTION

In vivo, DNA is constantly being assaulted and damaged (*1, 2*). To protect the integrity of the genome, an impressive repair network has evolved. Macromolecular crowding, low repair enzyme copy number, and small structural differences in DNA base lesions are, however, challenges in detecting damage. Processive searches along DNA may represent one component of detection (*3-5*). We have proposed DNA-mediated charge transport as the first step in detection since it provides a means to redistribute base excision repair (BER) proteins in the vicinity of damage rapidly and efficiently (*6-9*).

EndoIII is a DNA glycosylase that repairs damaged pyrimidines (*10-14*). Much like the closely related BER enzyme MutY, EndoIII features a [4Fe4S] cluster (*10-20*). In MutY, the [4Fe4S] cluster is not required for protein folding but is crucial *in vivo* (*21-24*). We have demonstrated for both proteins that the cluster is activated towards oxidation upon enzyme binding to DNA, and this DNA-dependent redox activity promotes charge transport through DNA (*6-9*). Electrochemistry of MutY and EndoIII on DNA-modified gold electrodes shows a redox potential of ~ 60 mV versus NHE for the $[4Fe4S]^{3+/2+}$ couple; DNA binding appears to shift the potential, so that the protein bound to DNA is more similar to a HiPIP than a ferredoxin (*25-27*).

Here we demonstrate this shift in potential associated with DNA binding directly using highly oriented pyrolytic graphite HOPG electrodes to compare the electrochemical properties of EndoIII bound to DNA and free (Figure 6.1). Previous work had shown that, without DNA binding, the $[4Fe4S]^{2+}$ cluster is not readily oxidized or reduced within a physiological range of potentials (*11*).

Figure 6.1. Schematic representation of electrochemistry for Endonuclease III on HOPG with and without modification with DNA.

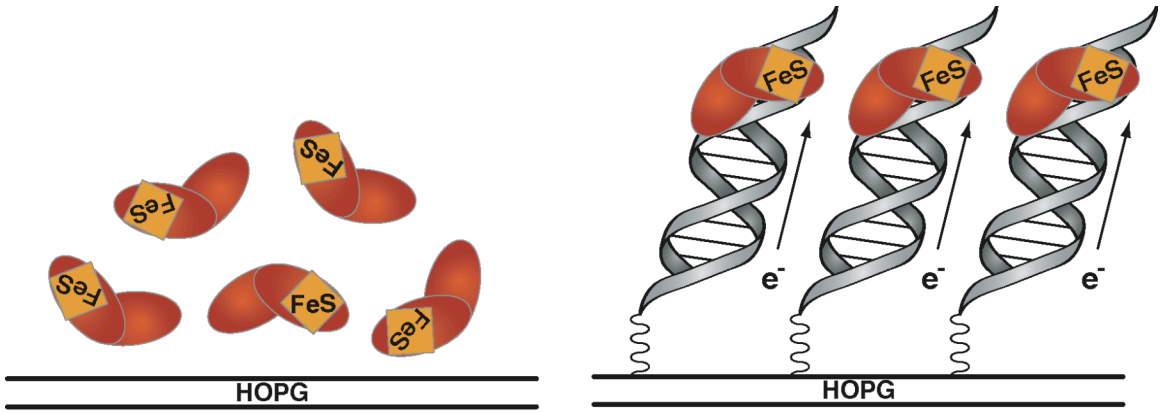

We have recently explored the electrochemical properties of HOPG modified with pyrenated DNA (*28*). The DNA monolayers formed are quite similar to thiolated DNA films on gold (*29-31*), but the accessible potential window is significantly larger. Graphite electrodes, moreover, are particularly useful for protein electrochemistry (*32-37*).

MATERIALS AND METHODS

Protein Purification

EndoIII was expressed and purified according to published procedures, slightly modified (*38, 39*).

Electrochemical Measurments

In a typical protein experiment, a loosely packed DNA film is self-assembled in the absence of Mg^{2+} (*6, 7*). After incubation with protein and cooling of the electrodes, electrochemical experiments are performed using the inverted drop cell electrode configuration (*40*). Protein samples are analyzed at graphite electrodes modified with the sequence pyrene-$(CH_2)_4$-Pi-5'-AG*T* ACA GTC ATC GCG-3' plus complement with or without an abasic site opposite the italicized base. Protein samples are also evaluated on bare HOPG. EndoIII was measured electrochemically at 50 μM EndoIII in 20 mM Na phosphate, 100 mM NaCl, 1 mM EDTA, 20% glycerol, pH 7.5. Cyclic voltametry was performed at 50 mV/s and square wave voltammetry at 15 Hz with a Ag/AgCl reference electrode and a platinum wire auxiliary electrode.

RESULTS AND DISCUSSION

Electrochemical Investigation of EndoIII on Graphite

Figure 6.2 shows cyclic voltammetry (CV) and square wave voltammetry (SWV) of EndoIII on HOPG with and without DNA modification. For the DNA-modified electrode, a quasi-reversible redox couple is observed with a midpoint potential of 20 mV versus NHE. Backfilling the DNA electrode with octane has no effect on this signal, while backfilling HOPG without DNA leads to the loss of any protein signal (data not shown). To establish that this signal is DNA-mediated, we examined also an electrode modified with DNA featuring an abasic site prepared under identical conditions; DNA-mediated charge transport has been shown to be inhibited by the abasic site, owing to the disruption in base stacking (*6, 7, 30*). As seen in Figure 6.2, a complete loss of signal for EndoIII is observed at the electrode modified with DNA containing an abasic site. Thus the DNA does not serve to locally concentrate the protein on the graphite surface; the duplex with an abasic site would serve a similar function. Instead it is the *DNA-bound* protein that is probed electrochemically on HOPG in a DNA-mediated reaction, as long as the DNA duplex is well stacked.

Note that at the DNA-modified surface, we observe only one redox signal, with no other peaks evident in the range of 600 mV to -400 mV versus NHE. The only couple we observe features a cathodic peak at -30 ± 20 mV versus NHE whose shape and magnitude indicates slow diffusive kinetics, as found for MutY (3). Indeed in all respects, this couple resembles that found for EndoIII at a DNA modified Au surface (*7*) and is assigned to the $[4Fe4S]^{3+/2+}$ couple (*8*).

Figure 6.2. CV (left, 50 mV/s scan rate) and SWV (right, 15 Hz) of 50 μM EndoIII in 20 mM sodium phosphate, 100 mM NaCl, 1 mM EDTA, 20% glycerol, pH 7.5. The top two panels show electrochemistry of EndoIII at an electrode modified with the sequence pyrene-$(CH_2)_4$-Pi-5'-AG*T* ACA GTC ATC GCG-3' plus complement. Cyclic voltammetry of an electrode modified with DNA featuring an abasic site is in red (top left), where the abasic position corresponds to the complement of the italicized base. The bottom two panels show electrochemistry of EndoIII on bare HOPG. All runs were taken using the inverted drop cell electrode configuration versus Ag/AgCl reference and Pt auxiliary.

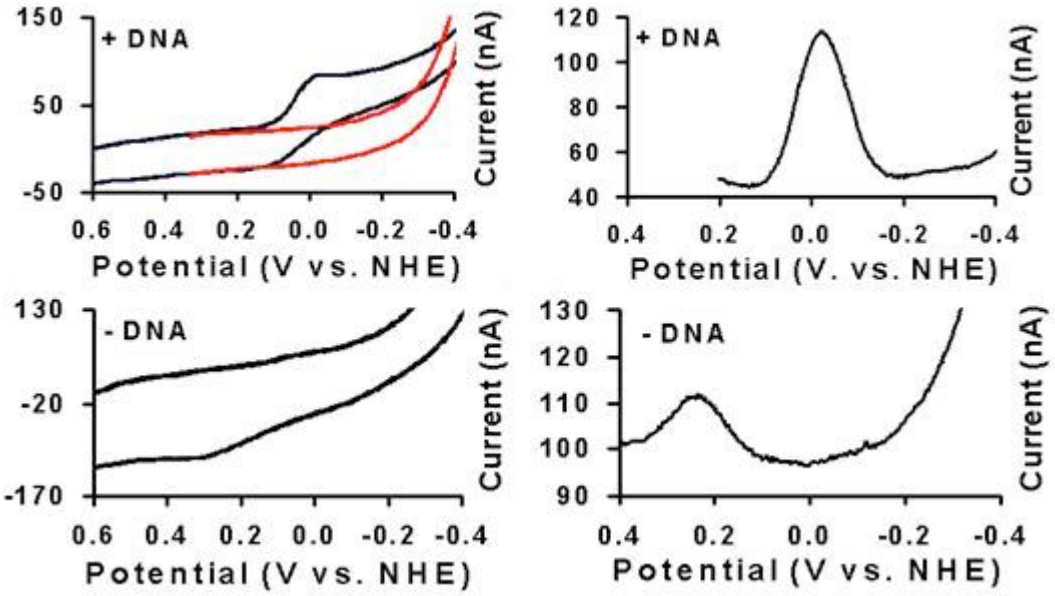

Significantly, on HOPG versus Au, we may explore the electrochemistry of EndoIII at a larger range of applied biases (*28*), and thus we may directly compare the electrochemistry of EndoIII in the presence and absence of DNA. Oxidative scans of EndoIII on bare HOPG reveal an irreversible anodic peak at 250 ± 30 mV versus NHE and no couple at 20 mV as with DNA (Figure 6.2). At higher protein concentrations, a quasi-reversible wave is observed (data not shown). Successive positive scans lead to new broad, irregular signals at ~ -80 mV and ~ -710 mV versus NHE; additionally, the yellow color of the protein solution is lost. These results are fully consistent with oxidative decomposition of the cluster in EndoIII without DNA. Indeed, these redox signals are commonly associated with [3Fe4S] clusters (*25-27, 41*). It is noteworthy that on bare HOPG, we observe also the 2+/1+ couple of the [4Fe4S] cluster during reductive scans with a cathodic peak at ~ -300±80 mV versus NHE (Figure 6.3). The peak is near the edge of our potential window, and this redox signal also contains a small oxidative wave at slow scan rates. The potential difference between the 3+/2+ and 2+/1+ couples is somewhat smaller than expected (*11*) and may be an underestimate since we are at the edge of the potential window.

Figure 6.4 summarizes the potentials we have observed for EndoIII on HOPG over several trials. A significant negative shift in potential occurs for the 3+/2+ couple on DNA binding; the shift in 2+/1+ couple cannot be determined. DNA binding clearly stabilizes the oxidized 3+ form of the cluster, whereas without DNA, it is $[4Fe4S]^{2+}$ that is more stable. This shift is understandable based upon the sensitivity of [4Fe4S] cluster potentials to their environment (*25-27*). Crystal structures of EndoIII with and without DNA reveal that the cluster is located near amino acid residues that contact DNA

Figure 6.3 Cyclic voltammetry (20mV/s scan rate) of 50 μM EndoIII on bare HOPG showing the 2+/1+ couple (top). A plot of peak current as a function of scan rate is inset. Square wave voltammetry (15 Hz frequency) of 50 μM EndoIII on bare HOPG showing the same couple (bottom). An electrode backfilled with octane showing the loss of the signal is in blue.

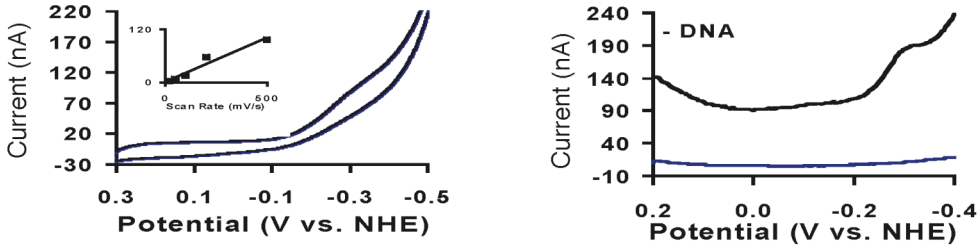

Figure 6.4. Illustration of the potentials versus NHE for the redox couples of Endonuclease III in the presence and absence of DNA. These values are based upon SWV on HOPG and are averages of at least four trials each.

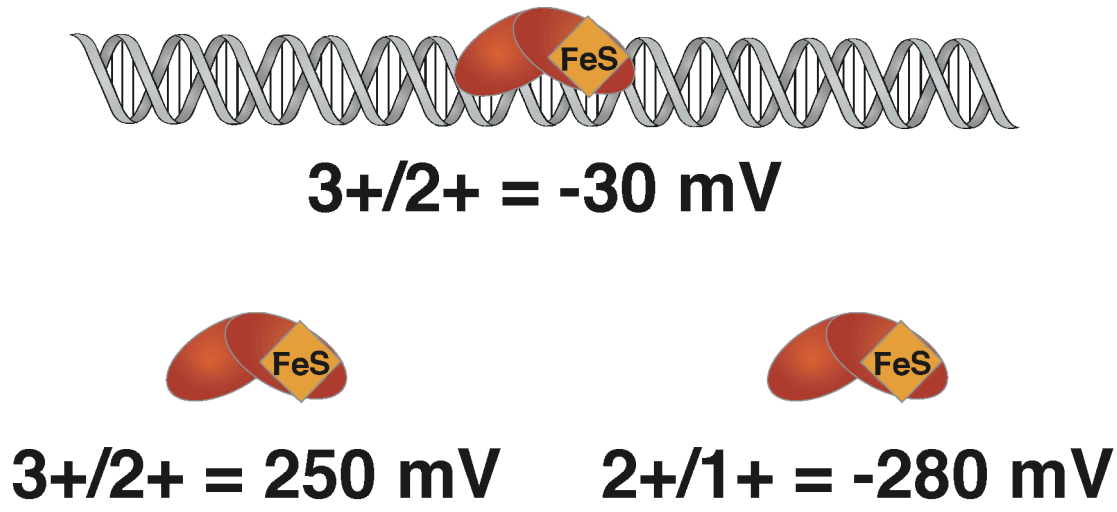

(*21-23*). DNA binding takes the cluster to a more hydrophobic environment compared to the exposed and polar environment in the absence of DNA. Importantly, the resultant shift in potential is not associated with significant conformational changes in the protein; the structures of the bound and free proteins are remarkably similar. Instead, then, the ~ 200 mV shift in potential must correspond to a decrease in DNA binding affinity of more than three orders of magnitude between the 2+ and 3+ forms of the cluster. Square wave voltammetry gives a shift of 280 mV between the cathodic DNA-bound potential and the anodic potential on bare HOPG. The shift in midpoint potentials should be slightly smaller. While previous evidence qualitatively indicated a lessened DNA binding affinity for the reduced protein (*7*), these data provide a more quantitative estimate. In the context of our model of DNA-mediated signaling for damage detection, it is this difference in DNA binding affinity for the reduced versus oxidized state that leads to the dissociation of protein from the DNA upon reduction and thus the redistribution of BER proteins onto sites near damage.

SUMMARY

We have now identified the electrochemistry of EndoIII both with and without DNA on HOPG electrodes. DNA binding clearly promotes a shift in redox potential, activating the protein towards oxidation; subsequent reduction of the cluster to the 2+ form leads to dissociation from the duplex. These results provide strong support for the detection strategy we have proposed for BER enzymes. Furthermore, these data underscore the importance of the outer sphere environment in regulating potentials of [4Fe4S] proteins (9, 12), as well as the utility of DNA-modified electrodes in probing the redox characteristics of proteins that bind to DNA.

REFERENCES

1. Friedberg, E. C., Walker, G. C., and Siede, W. (1995) *DNA Repair and Mutagenesis* ASM Press.

2. Krokan, H. E., Standal, R., and Slupphaug, G. (1997) *Biochem. J. 325*, 1.

3. Roberts, R. J., and Cheng, X. (1998) *Annu. Rev. Biochem. 67*, 181.

4. Verdine, G. L., and Bruner, S. D. (1997) *Chem. Biol. 4*, 329.

5. Francis, A.W., and David, S. S. (2003) *Biochemistry 42*, 801.

6. Boon, E. M., Livingston, A. L., Chmiel, N. H., David, S. S., and Barton, J. K. (2003) *Proc. Natl. Acad. Sci. U. S. A. 100*, 12543.

7. Boal, A. K., Yavin, E., Lukianova, O. A., O'Shea, V. L., David, S. S., and Barton, J. K. (2005) *Biochemistry 44*, 8397.

8. Yavin, E., Boal, A. K., Stemp, E. D. A., Boon, E. M., Livingston, A. L., O'Shea, V. L., David, S. S., and Barton, J. K. (2005) *Proc. Natl. Acad. Sci. U. S. A. 102*, 3546.

9. Yavin, E., Stemp, E. D. A., O'Shea, V. L., David, S. S., and Barton, J. K. (2006) *Proc. Natl. Acad. Sci. U. S. A. 103*, 3610.

10. Asahara, H., Wistort, P. M., Bank, J. F., Bakerian, R. H., and Cunningham, R. P. (1989) *Biochemistry 28*, 4444.

11. Asahara, H., Bank, J. F., Cunningham, R. P., Scholes, C. P., Salerno, J. C., Surerus, K., Munck, E., McCracken, J., Peisach, J., and Emptage, M. H. (1989) *Biochemistry 28*, 4450.

12. Fu, W., O'Handley, S., Cunningham, R. P., and Johnson, M. K. (1992) *J. Biol. Inorg. Chem. 267*, 16135.

13. O'Handley, S., Scholes, C. P., and Cunningham, R. P. (1995) *Biochemistry 34*, 2528.

14. Xing, D., Dorr, R., Cunningham, R. P., and Scholes, C. P. (1995) *Biochemistry 34*, 2537.

15. Michaels, M. L., Pham, L., Nghiem, Y., Cruz, C., and Miller, J. H. (1990) *Nucleic Acids Res. 18*, 3841.

16. Tsai-Wu, J. J., Liu, H. F., and Lu, A. L. (1992) *Proc. Natl. Acad. Sci. U.S.A. 89*, 8779.

17. Lu, A. L., Tsai-Wu, J. J., and Cillo, J. (1995) *J. Biol. Chem. 270*, 23582.

18. Bulychev, N. V., Varaprasad, C. V., Dorman, G., Miller, J. H., Eisenberg, M., Grollman, A. P., and Johnson, F. (1996) *Biochemistry 35*, 13147.

19. Porello, S. L., Williams, S. D., Kuhn, H., Michaels, M. L., and David, S. S. (1996) *J. Am. Chem. Soc*. *118*, 10684.

20. David, S.S., and Williams, S.D. (1998) *Chem. Rev. 98*, 1221.

21. Kuo, C. F., McRee, D. E., Fisher, C. L., O'Handley, C. F., Cunningham, R. P., and Tainer, J. A. (1992) *Science 258*, 434.

22. Thayer, M. M., Ahern, H., Xing, D. C. F., Cunningham, R. P., and Tainer, J. A. (1995) *EMBO J. 14*, 4108.

23. Fromme, J. C., and Verdine, G. L. (2003) *EMBO J. 22*, 3461.

24. Porello, S. L., Cannon, M. J., and David, S. S. (1998) *Biochemistry 37*, 6465.

25. Cowan, J.A., and Lui, S.M. (1998) *Adv. Inorg. Chem. 45*, 313.

26. Beinert, H. (2000) *J. Biol. Inorg. Chem. 5*, 2.

27. Carter, C.W., Kraut, J., Freer, S.T., Alden, R.A., Sieker, L.C., Adman, E. and Jensen, L.H. (1972) *Proc. Natl. Acad. Sci. U.S.A. 69,* 3526.

28. Gorodetsky, A. A., and Barton, J. K. (2006) *Langmuir 22*, 7917.

29. Kelley, S. O., Boon, E. M., Barton, J. K., Jackson, N. M., and Hill, M. G. (1999) *Nucleic Acids Res*. *27*, 4830.

30. Boon, E. M., Ceres, D. M., Drummond, T. G., Hill, M. G., and Barton, J. K. (2000) *Nat. Biotechnol*. *18*, 1096.

31. Boal, A. K., and Barton, J. K. (2005) *Bioconjug. Chem. 16*, 312.

32. Guo, L. H., and Hill, H. A. O. (1991) *Adv. Inorg. Chem. 36*, 341.

33. Armstrong, F. A. (1992) *Adv. Inorg. Chem. 38*, 117.

34. Armstrong, F. A., Heering, H. A., and Hirst, J. (1997) *Chem. Soc. Rev. 26*, 169.

35. Camba, R., and Armstrong, F. A. (2000) *Biochemistry 39*, 10587.

36. Armstrong, F.A., and Wilson, G.S. (2000) *Electrochem. Acta 45*, 2623.

37. Nassar, A.F., and Rusing, J.F. (1996) *J. Am. Chem. Soc. 118*, 3043.

38. Boiteux, S., O'Connor, T. R., and Laval, J. (1987) *EMBO J. 6*, 3177.

39. O'Connor, T.R. (1993) *Nucleic Acids Res*. *21*, 5561.

40. Bowler, R., Davies, T.J., Hyde, M.E., and Compton, R.G. (2005) *Anal. Chem. 77*, 1916.

41. Thomson, A. J., Breton, J., George, S. J., Butt, J. N., Armstrong, F. A., and Hatchikian, E. C. (1991) *Biochem. Soc. Trans. 19*, 594.

CHAPTER 7

Investigating the Role of the *Rnf* Operon in DNA Repair

INTRODUCTION

MutY and Endonuclease III (EndoIII) are DNA repair glycosylases in the base excision repair (BER) pathway that are responsible for excising oxidatively damaged DNA bases from the genome (*1*). Though EndoIII and MutY do not remove the same lesions from DNA (MutY removes adenine mispaired with 8-oxo-guanine and EndoIII excises a variety of oxidized pyrimidines), these enzymes are related by their similar structures and the [4Fe4S] cluster cofactor harbored by each protein (*1-3*). The role of the iron-sulfur cluster in these enzymes is not fully understood, but it has been demonstrated that the [4Fe4S] cluster is redox active when the enzyme is bound to DNA (*4-8*). Thus, it is proposed that the iron-sulfur cluster might be used to quickly and efficiently detect damage in the genome via DNA-mediated charge transport (CT), a reaction modulated by both the structural and dynamic integrity of the DNA base-pair stack (*9-13*). Furthermore, similar redox potentials measured for MutY and EndoIII indicate that DNA CT may occur between MutY and EndoIII protein molecules; DNA CT could allow for cooperative damage detection among [4Fe4S] DNA repair glycosylases (*14*).

The discovery that MutY and EndoIII are transcribed as part of complex operons in *Escherichia coli* brings up additional questions about the role of the [4Fe4S] cluster in these proteins. The gene encoding MutY (*mutY*) is a member of an operon consisting of four genes (Figure 7.1) (*15*). The gene immediately 5` to *mutY* is *yggX*, a gene that encodes the 91aa protein YggX (*16*). YggX may function in oxidative stress protection in *Salmonella enterica* and *E. coli* (*17-19*). YggX can also sequester iron in solution and has been shown to protect DNA from damage via Fenton chemistry *in vitro*. The structure of YggX, as determined by NMR, consists of one small helical domain as well

Figure 7.1. The chromosomal arrangement of *mutY* in *E. coli*. *MutY* is the first gene in a four gene operon followed by *yggX*, which encodes a protein involved in iron trafficking and oxidative stress protection, *mltC,* the gene for a lytic membrane-bound glycosylase, and *nupG*, a gene encoding a nucleoside transport protein. Putative promoters are represented as arrows and attenuators and terminators as bars.

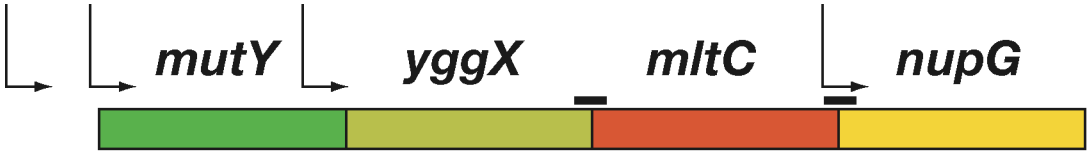

soluble BER 4Fe-4S glycosylase	soluble Fe transport protein	membrane bound lytic trans-glycosylase	nucleoside transport protein

as a relatively unstructured region. The binding site for iron is not revealed in these structures, and it is postulated that YggX may bind to a partner protein inside the cell (*16*). The other two genes in the MutY operon appear to be less related in function (*15*). *mltC* encodes a membrane-bound lytic glycosylase that can hydrolyze peptidoglycans. *nupG* is the gene for a high-affinity nucleoside transporter. This genomic arrangement is conserved among many bacterial organisms, though in some bacteria only *mutY* and *yggX* are transcribed together (*15*).

The gene encoding EndoIII (*nth*) is the terminal gene in an eight-gene operon in *E. coli* (Figure 7.2) (*20*). The other seven genes have not been characterized in *E. coli*, but some of them bear sequence homology to a set of genes required for nitrogen fixation in purple photosynthetic bacteria (i. e., *Rhodobacter capsulatus*) (*21*). In *R. capsulatus*, *nth* is replaced by *rnfH*. The remaining genes are termed *rnfABCDGE* and are believed to form a membrane-bound complex probably involved in electron transport to nitrogenase or nitrogenase reductase (*22-24*). It has also been proposed that the *rnf* operon could be involved in protein-bound iron-sulfur cluster maturation in organisms that fix nitrogen.

RnfA, rnfD, and *rnfE* are predicted to encode transmembrane proteins while *rnfB, rnfC,* and *rnfG* encode largely soluble proteins. *RnfB* and *rnfC* are also predicted to bind iron-sulfur clusters. The *rnfC* gene product may contain up to two [4Fe4S] clusters while *rnfB* encodes 12 cysteine residues with potential binding sites for two [4Fe4S] clusters and one [2Fe2S] cluster. Attempts to overexpress the *R. capsulatus rnf* genes in *E. coli* have met with limited success. RnfA, RnfB, and RnfC were all able to be expressed heterologously, but they appear to associate strongly with the cell membrane, may not contain all of their iron-sulfur cofactors, and lose stability in the absence of the rest of their *rnf* counterparts.

Figure 7.2. The chromosomal arrangement of *nth* in *E. coli. Nth* is the terminal gene in an eight gene operon. The remaining genes are uncharacterized in *E. coli* but are homologous to a set of genes found in *R. capsulatus* and other nitrogen fixing organisms. These genes, termed *rnfABCDGE,* are required for nitrogen fixation and are believed to form a membrane-bound complex. Putative promoters are represented by arrows and terminators are indicated by bars.

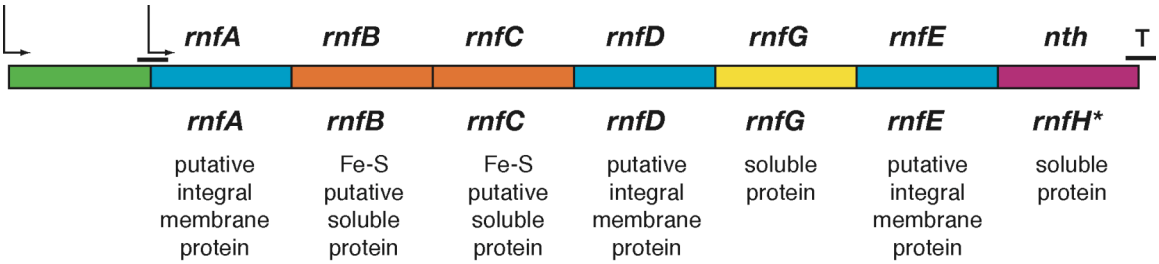

Though the *E. coli rnf* genes have not been biochemically characterized, it has been demonstrated that inactivation of these genes has an effect on SoxR mediated *soxS* expression (*25*). The *soxRS* system senses oxidative stress and activates transcription of a wide variety of genes to protect against and repair oxidative damage (interestingly, one of the genes targeted is *yggX* (*19*)) (*26*). Activation of the *soxRS* regulon is mediated by SoxR, a [2Fe2S] cluster transcription factor (*27-29*). Upon oxidation of the cluster in SoxR from the 1+ to the 2+ state, transcription of *soxS* is initiated. *SoxS* transcription is transient; within minutes after administration of oxidants has ceased, SoxR is rereduced and *soxS* is no longer transcribed (*29*). The pathways for oxidation and rereduction of SoxR are not fully understood, though SoxR is activated within the cell by administration of paraquat (*29*) and it has been demonstrated *in vitro* that SoxR can be oxidized from a distance, in a DNA-mediated fashion, by guanine radicals or electrochemical methods (*30, 31*). Inactivation of the *E. coli rnf* genes slows the deactivation of *soxS* expression, indicating that the *rnf* gene products may be involved in the rereduction of SoxR (*25*).

The relationship between the *rnf* gene products and EndoIII (or other [4Fe4S] cluster DNA repair enzymes) is unknown, though it is theorized that genes that are transcribed together often perform similar or related functions within the cell (*32*). To examine the possibility that the *E. coli rnf* genes might affect the activity of EndoIII within the cell, we have knocked out the *rnf* operon in an *E. coli* strain that serves as a reporter for EndoIII repair activity. Inactivation of the *rnf* operon leads to a suppression of EndoIII-associated mutations, a surprising result given that knockout of the *rnf* operon should eliminate EndoIII expression as well. Thus, further studies will be required to fully understand the relationship between the *rnf* operon and DNA repair.

MATERIALS AND METHODS

Materials

All vectors for gene inactivation were generously donated by Prof. Dianne Newman. Oligonucleotides were purchased from IDT or synthesized in-house. All enzymes were purchased from Stratgene or Roche. All strains used were derivatives of CC102 (*33*) and generated as described below. Luria-Bertani (LB) broth was used as the rich medium while NCE (*34*) medium supplemented with $MgSO_4$ (100 μM) and glucose (11 mM) or lactose (6 mM) was used as the minimal medium.

Genetic Inactivation of rnf Genes

CC102 strains were generously donated (*33*) and *RnfA* was replaced by a kanamycin resistance cassette (*kan*) in CC102 using a previously described deletion method (*35*). Primer sequences are as follows: (*rnfA* homology regions are shown in regular text and *kan* priming regions are highlighted in boldface) 5`-CTGCTCTGGATTAACGGATAATAGGCGGCTTTTTTATTTCAGGCCGAAAA**GTGTAGGCTGGAGCTGCTTC**-3`, 5`-CGCCAGGCCCAGCAGGCTCACGGCGGCAACGGCAATCCAGATAGCATTCA**CATATGAATATCCTCCTTAG**-3`. Inactivation was verified with colony PCR.

Lac$^+$ Reversion Assays

Strains were streaked to LB medium and incubated overnight at 37°C. For *rnfA* knockouts, strains were streaked to LB+kanamycin (17 mg/mL). 1 mL LB cultures were started from single colonies and grown overnight in a shaking incubator at 37°C, 220 rpm. 20 mL of each starter culture was used to inoculate a 10 mL NCE+glucose culture

which was then grown to a density of 10^9 cells/mL at 37°C, 250 rpm. Cell density was determined by dilution plating a 10 mL aliquot of the NCE+glucose culture onto NCE+glucose solid medium followed by incubation at 37°C for 36 hours. 5 mLs of this culture was centrifuged in a clinical tabletop centrifuge at 4°C and plated on NCE+lactose solid medium and then incubated at 37°C for 36 hours. Colonies arising are reported as *lac*$^+$ revertants/mL cells plated.

RESULTS AND DISCUSSION

Effect of rnfA Inactivation on EndoIII Activity

The CC102 strain uses an engineered *lacZ* mutation to report the frequency of GC:AT transition mutations in a population of *E. coli* cells (*33*). EndoIII prevents these mutations through enzymatic excision of 5-hydroxy-cytosine (*1*) which will mispair with adenine if allowed to go unrepaired and to undergo replication (*36*). In the CC102 strain, a base-pair substitution has been introduced in the codon for Glu461 in *lacZ,* the gene encoding β-galactosidase, an enzyme required for lactose metabolism (*33*). Glu461 is essential for enzyme activity and the *lacZ* mutation introduced to generate the CC102 strain renders these cells *lac-* or unable to grow in lactose-containing media. A GC:AT transition mutation in the *lacZ* Glu461 codon is required for growth on lactose by CC102, thus the number of *lac*$^+$ revertant colonies reflects the GC:AT mutation rate. Inactivation of *nth* in CC102 increases the GC:AT mutation rate as shown in Figure 7.3. Note that the error bar for the CC102/*nth-* strain is large, a common phenomenon with the CC102 strain since it relys on the spontaneous oxidation of cytosine, a process that happens with somewhat low frequency inside the cell (*36*), to revert to *lac*$^+$. Inactivation of *rnfA* in CC102 does not increase the number of *lac*$^+$ revertants. Knockout of *rnfA* should

Figure 7.3. Genetic inactivation of *rnfA* in CC102. All revertants are reported as *lac*$^+$ colonies per mL (10^8 cells/mL). Inactivation of *nth* in CC102 leads to a large number of revertants, but *rnfA* inactivation suppresses the reversion rate to a level similar to the CC102 control.

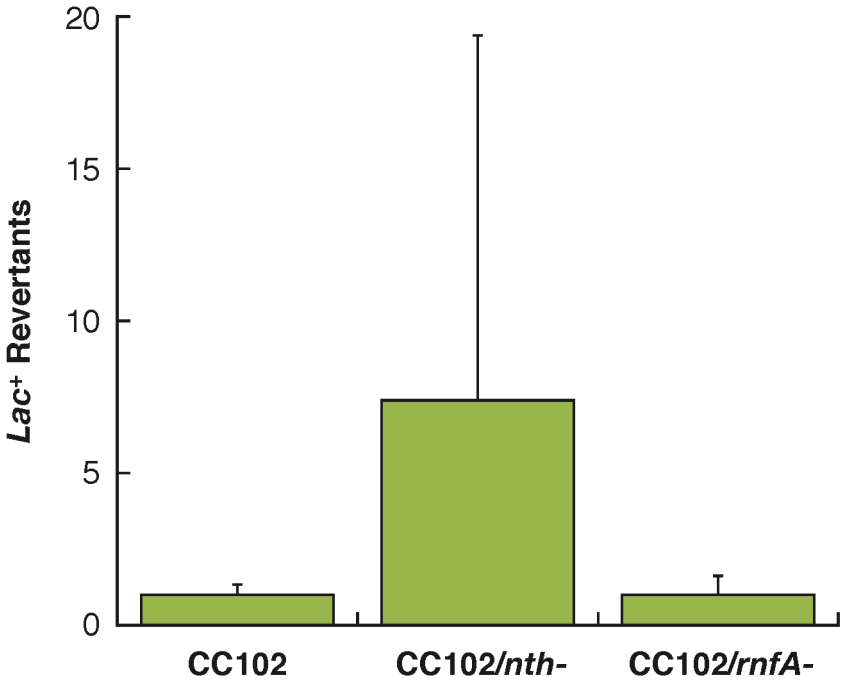

inactivate the entire *rnf* operon, including *nth*. Thus, this result suggests that knockout of the *rnf* operon has a mutation suppression effect on the cell, despite the loss of the DNA repair protein EndoIII.

Discussion

It is interesting to consider the result reported here in the context of the only other proposed role for the *rnf* proteins in *E. coli*, as a reducing system for SoxR (*25*). Knockout of the *rnf* genes has been demonstrated to slow deactivation of *soxS* transcription (*25*), perhaps resulting in a more constituitive oxidative stress response state. Thus, the result observed here, that *rnf* inactivation suppresses the GC:AT mutation rate, might support the hypothesis that the *rnf* genes are involved in SoxR rereduction since a lower rate of oxidative DNA damage might be expected with a less efficient *soxS* deactivation state.

It is clear from these initial experiments that the relationship between the *rnf* genes and *nth* is complicated and will not be fully elucidated by the simple experiments performed here. Future work in this area will include experiments to determine if the mutation suppression observed with CC102 is specific to GC:AT mutations or if *rnf* inactivation reduces the general mutation rate. It must be verified, in a more rigorous manner, that inactivation of *rnfA* eliminates transcription of the downstream genes (including *nth*). Lastly, in-frame deletion of each of the *rnf* genes may reveal some of the specific roles of the individual genes.

It may also be interesting to examine the role of *yggX*, the gene immediately 5` to *mutY* in *E. coli*, in DNA repair. Reduced expression of *yggX* in *S. enterica* causes a 20–50-fold increase in the rate of GC:TA transversion mutations (the type of mutation prevented by MutY) (*18*). While YggX has been overexpressed and characterized as a

purified protein, it has not been determined if YggX binds to DNA or to MutY, or whether the iron bound by YggX is redox active.

SUMMARY

In *E. coli*, the genes encoding MutY and EndoIII, two [4Fe4S] DNA repair glycoslyases, are transcribed as operons. Each of these operons contains other putative iron-binding proteins that are currently uncharacterized in *E. coli*. Of particular interest are the *rnf* genes that precede the gene encoding EndoIII; several of the *rnf* proteins are predicted to contain multiple iron sulfur clusters and it is suggested that these proteins might play a role in reduction of SoxR, another DNA-binding [4Fe4S] cluster protein. To examine the relationship between the *rnf* proteins and EndoIII, we inactivated the entire *rnf* operon in an EndoIII activity reporter strain of *E. coli*. Interestingly, the *rnf* knockout strain displays a near wild-type level of mutations (as opposed to the elevated mutation level observed with an EndoIII genetic knockout). While this result would be consistent with the prediction that the *rnf* gene products are involved in deactivation of SoxR mediated oxidative stress protection, the relationship between the *rnf* genes and [4Fe4S] DNA repair enzymes is still not well understood and requires further examination.

REFERENCES

1. David, S. S., and Williams, S. D. (1998) *Chem. Rev. 98,* 1221.

2. Fromme, J. C., and Verdine, G. L. (2003) *EMBO J. 22*, 3461.

3. Fromme, J. C., Banerjee, A., Huang, S. J., and Verdine, G. L. (2004) *Nature 427*, 652.

4. Boon, E. M., Livingston, A. L., Chmiel, N. H., David, S. S., and Barton, J. K. (2003) *Proc. Natl. Acad. Sci. USA 100*, 12543.

5. Boal, A. K., Yavin, E., Lukianova, O. A., O'Shea, V. L, David, S. S., and Barton, J. K. (2005) *Biochemistry 44*, 8397.

6. Yavin, E., Boal, A. K., Stemp, E. D. A., Boon, E. M., Livingston, A. L., O'Shea, V. L., David, S. S., and Barton, J. K. (2005) *Proc. Natl. Acad. Sci. USA 102*, 3546.

7. Gorodetsky, A. A., Boal, A. K., and Barton, J. K. (2006) *J. Am. Chem. Soc. 128*, 12082.

8. Yavin, E., Stemp, E. D. A., O'Shea, V. L., David, S. S., and Barton, J. K. (2006) *Proc. Natl. Acad. Sci. USA 103*, 3610.

9. Bhattacharya, P. K., and Barton, J. K. (2001) *J. Am. Chem. Soc. 123*, 8649.

10. Rajski, S. R., and Barton, J. K. (2001) *Biochemistry 40*, 5556.

11. Boon, E. M., Ceres, D. M., Drummond, T. G., Hill, M. G., and Barton, J. K. (2000) *Nat. Biotechnol. 18*, 1096.

12. Boon, E. M., Salas, J. E., and Barton, J. K. (2002) *Nat. Biotechnol. 20*, 282.

13. Boal, A. K., and Barton, J. K. (2005) *Bioconjug. Chem. 16*, 312.

14. Boal, A. K., Genereux, J. C., Sontz, P. A., Gralnick, J. A., Newman, D. K., and Barton, J. K. (2008) (*submitted for publication*).

15. Gifford, C. M., and Wallace, S. S. (1999) *J. Bacteriol. 181*, 4223.

16. Cui, Q., Thorgersen, M. P., Westler, W. M., Markley, J. L., and Downs, D. M. (2006) *Proteins 62*, 578.

17. Gralnick, J., and Downs, D. (2001) *Proc. Natl. Acad. Sci. USA 98*, 8030.

18. Gralnick, J., and Downs, D. (2003) *J. Biol. Chem. 278*, 20708.

19. Pomposiello, P. J., Koutsolioutsou, A., Carrasco, D., and Demple, B. (2003) *J. Bacteriol. 185*, 6624.

20. Gifford, C. M., and Wallace, S. S. (2000) *Nucleic Acids Res. 28*, 762.

21. Schmehl, M., Jahn, A., Meyer zu Vilsendorf, A., Hennecke, S., Masepohl, B., Schuppler, M., Marxer, M., Oelze, J., and Klipp, W. (1993) *Mol. Gen. Genet. 241*, 602.

22. Kumagai, H., Fujiwara, T., Matsubara, H., and Saeki, K. (1997) *Biochemistry 36*, 5509.

23. Jouanneau, Y., Jeong, H. S., Hugo, N., Meyer, C., and Willison, J. C. (1998) *Eur. J. Biochem. 251*, 54.

24. Curatti, L., Brown, C. S., Ludden, P. W., and Rubio, L. M. (2005) *Proc. Natl. Acad. Sci. USA 102*, 6291.

25. Koo, M. S., Lee, J. H., Rah, S. Y., Yeo, W. S., Lee, J. W., Lee, K. L., Koh, Y. S., Kang, S. O., and Roe, J. H. (2003) *EMBO J. 22*, 2614.

26. Storz, G., and Imlay, J. A. (1999) *Curr. Op. Microbiol. 2*, 188.

27. Amabile-Cuevas, C. F., and Demple, B. (1991) *Nucleic Acids Res. 19*, 4479.

28. Ding, H., Hidalgo, E., and Demple, B. (1996) *J. Biol. Chem. 271*, 33173.

29. Ding, H., and Demple, B. (1997) *Proc. Natl. Acad. Sci. USA 94*, 8445.

30. Gorodetsky, A. A., Dietrich, L. E., Lee, P. E., Demple, B., Newman, D. K., and Barton, J. K. (2008) *Proc. Natl. Acad. Sci. USA 105*, 3684.

31. Lee, P. E., and Barton, J. K. (2008) (*unpublished data*).

32. Stryer, L. (1995) *Biochemistry, 4th Ed.* W.H. Freeman, New York.

33. Cupples, C. G., and Miller, J. H. (1989) *Proc. Natl. Acad. Sci. USA 86*, 5345.

34. Davis, R. W., Botstein, D., and Roth, J. R. (1980) *Advanced Bacterial Genetics: A Manual for Genetic Engineering.* Cold Spring Harbor Laboratory Press, New York.

35. Datsenko, K. A., and Wanner, B. L. (2000) *Proc. Natl. Acad. Sci. USA 97*, 6640.

36. Kreutzer, D. A., and Essigmann, J. M. (1998) *Proc. Natl. Acad. Sci. USA 95*, 3578.

CHAPTER 8

Redox Signaling between DNA Repair Proteins for Efficient Lesion Detection: DNA Charge Transport within the Cell

Adapted from Boal, A. K., Genereux, J. C., Sontz, P. A., Gralnick, J. A., Newman, D. K., and Barton, J. K. (2008) (*submitted for publication*).

J. C. Genereux performed calculations. P. A. Sontz performed AFM experiments. J. A. Gralnick performed strain construction and aided in the design of genetics experiments.

INTRODUCTION

Base excision repair (BER) proteins, from bacteria to man, are challenged with combing the genome for DNA base lesions in order to maintain the integrity of our genetic material (*1-4*). This challenge is more remarkable to consider given the low copy number of these proteins and that they must discriminate among small differences between the modified and natural bases. In the case of MutY, a BER repair protein in *E.coli* with a human homolog, there are 30 proteins in the *E.coli* cell (*2*) to interrogate 4.6 million bases (*5*); the ratio of binding affinities for the target lesion, an 8-oxoguanine:adenine mismatch, versus well-matched native GC or AT base pairs is $\leq$ 1000 (*6*). Endonuclease III (EndoIII), another BER enzyme in the same protein family (*1-4*), recognizes a less prevalent lesion, hydroxylated pyrimidines, with equally low specificity; the copy number of EndoIII within *E.coli* is estimated as 500 (*2*). The enzymology has been well characterized regarding how MutY and EndoIII, as glycosylases, fix their substrate lesions once found (*1-4*), and the structures of MutY and EndoIII bound to DNA have been elucidated (*7, 8*), revealing the basis for substrate recognition. Yet how these lesions are efficiently detected remains to be determined.

Current models for genome scanning to detect lesions involve protein sliding along the DNA, squeezing the backbone, slipping bases out to allow for interrogation, or finding transiently opened sites (*9-13*). However, a simple sliding model, involving facilitated diffusion along the strand where each base is contacted and the interrogation is assumed to be instantaneous, yields a genome interrogation time, T, of 46 minutes for MutY, wholly insufficient given the doubling time in *E.coli* of 20 minutes. The time for sliding to scan the genome is calculated from a one-dimensional random walk (*9*). The one-dimensional diffusion (sliding) constant has been measured (*10*) *in vitro* for the DNA repair proteins hOGG1 and *Bacillus stearothermophilus* MutM as 5×10^6 bp^2/sec and

$3.5x10^5$ bp^2/sec respectively. Taking the more generous (faster) value for the diffusion constant, a genome size of $5x10^6$ base pairs, and the MutY copy number of 30 yields a scanning time of 46 minutes.

The higher copy number for EndoIII yields a significantly shorter interrogation time of 10 seconds for a much less prevalent lesion. These estimates for T significantly understate the problem, since the interrogation time cannot be instantaneous in the sliding model, and to slide along the strand, proteins, even water, must be displaced, which takes time. Some sliding models for facilitated movements of proteins along DNA incorporate hopping and intersegment transfer to locate a target (*9, 14*), but in a repair process, each base must be interrogated; hopping leads to an incomplete search.

DNA-mediated charge transport (CT) offers an alternative strategy to localize BER proteins in the vicinity of lesions. Ubiquitous to these low copy number BER proteins are [4Fe4S] clusters, common redox cofactors in proteins (*2-4*). While the mechanisms responsible for DNA CT chemistry are still being debated, it is now generally accepted that DNA-mediated CT can proceed over long molecular distances on a very short timescale (*15*). Oxidative damage to DNA has been demonstrated with oxidants covalently tethered and spatially separated from oxidized sites in the DNA duplex at distances of > 200 Å with negligible loss in efficiency (*16-18*). Previous studies have also established that CT through DNA is possible in biological environments that include nucleosomes (*19, 20*) and isolated HeLa cell nuclei (*21*). DNA CT is, however, extremely sensitive to perturbations in the intervening base pair stack (*22-24*). DNA mismatches, base lesions, and the binding of proteins that distort the DNA all serve to inhibit long range CT. Recently we have found that well-matched DNA covalently attached within a nanotube device can conduct charge through the π-stack

similarly to graphite through its π-stack, but the device resistance increases by 300-fold upon introduction of a single base mismatch (*25*). Given that this chemistry occurs at a distance and is modulated by the structural integrity of the base pair stack, we have considered that these reactions may be useful within the cell for long range signaling (*26-28*).

Our model for lesion detection involves cooperative DNA-mediated redox signaling among BER proteins containing [4Fe4S] clusters (Figure 8.1) (*26-28*). When not bound to DNA, these proteins are found in the $[4Fe4S]^{2+}$ state and are not easily oxidized or reduced under physiological conditions (*29*). The estimated potential for the $[4Fe4S]^{2+/1+}$ couple in EndoIII is -300 mV versus NHE while the potential for the $[4Fe4S]^{3+/2+}$ couple is estimated to be +250 mV versus NHE (*30*). Notably, the $[4Fe4S]^{3+}$ form of the protein is especially unstable in solution (*29, 30*). However, for MutY and EndoIII, we have demonstrated using DNA-modified electrodes that DNA binding shifts the 3+/2+ cluster potential more negative by > 200 mV (*26, 27, 30*); DNA-binding stabilizes the protein in the +3 form (*30*). Furthermore, the protein can be oxidized in a DNA-mediated reaction (*26, 27, 30, 31*). Thus we have proposed that these BER proteins bearing [4Fe4S] clusters exploit DNA-mediated CT as a very fast and sensitive method to detect damage inside the cell. As illustrated in Figure 8.1 (*b-d*), this DNA-mediated redox signaling model involves binding to DNA by one protein in the 2+ state (donor), which would promote electron transfer from the donor protein to a distal protein (acceptor), already bound to the helix and in the 3+ state. The donor protein is now oxidized and remains bound to DNA while the acceptor becomes reduced and diffuses away. Integral to this model is a differential DNA affinity for the $[4Fe4S]^{3+}$ and $[4Fe4S]^{2+}$ forms of the protein. In fact, the 200 mV potential

Figure 8.1. A model for DNA-mediated CT in DNA repair where DNA repair proteins, for example EndoIII (green) and MutY (orange), containing $[4Fe4S]^{2+}$ clusters bind DNA, activating them towards oxidation to the $[4Fe4S]^{3+}$ state. The sequence of events is as follows: Guanine radical formation can oxidize a repair protein in a DNA-mediated reaction, stabilizing the oxidized protein bound to DNA (*a*). A second protein binds in the vicinity of the first protein (*b, e*). Electron transfer to a distally bound protein can occur through the DNA p-stack if the intervening DNA is undamaged (*c, f*). The newly reduced protein has a diminished affinity for DNA and diffuses away (*d*). If, instead, a lesion site is present between the proteins (*g*), the DNA-mediated CT step is inhibited and the oxidized protein remains bound to DNA. In this search mechanism the sum of the DNA-mediated electron transfer steps between proteins constitutes a full search of the genome with the end result being a redistribution of low abundance DNA repair proteins in the vicinity of lesions.

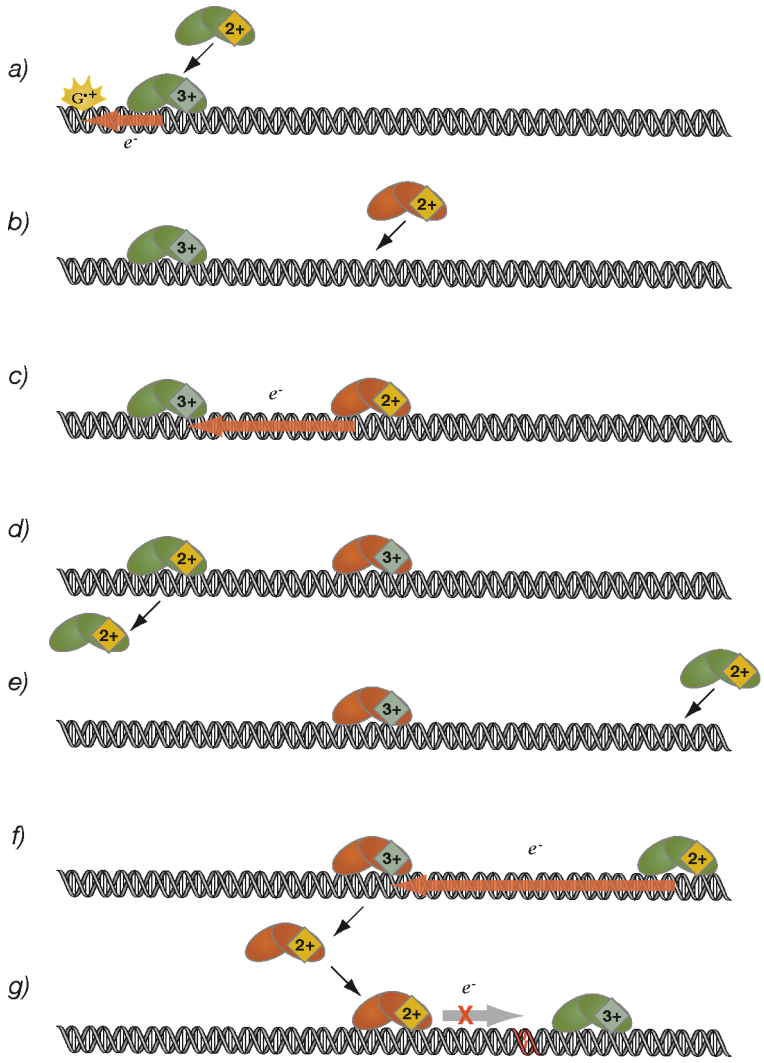

shift associated with DNA binding corresponds thermodynamically to a thousand-fold difference in DNA affinity between the oxidized and reduced proteins (*30*).

Importantly, this DNA-mediated CT process can be considered as a scan of the integrity of intervening DNA, since DNA-mediated CT can only proceed through a well stacked duplex. It should be noted that, although the DNA-mediated reduction occurs at potentials insufficient to damage the DNA (*32*), we have used a modified base to serve as a trap for the electron in this process and have found that binding of either MutY or EndoIII to the DNA promotes rapid reduction of the modified base (*31*). Thus DNA-mediated CT provides a means to distinguish whether the intervening DNA is intact or damaged. As illustrated in Figure 8.1 (*g*), when the repair protein, already oxidized, is bound in the vicinity of a base lesion, DNA-mediated CT does not provide a pathway for reduction and subsequent dissociation of the protein. The protein remains bound to the duplex so that on a slower timescale the protein can processively diffuse to the target site; now, however, sliding is needed only across a small region and the low specificity of the protein for its substrate (*33, 34*) is sufficient for recognition. Essentially, then, our proposal for base lesion detection based upon DNA CT involves redistributing the BER enzymes onto local regions of the genome that contain lesions. Critical to this mechanism is DNA-mediated signaling among proteins bound at long range so that the proteins, despite their low abundance, cooperate with one another in localizing onto target sites.

In order for the BER enzymes to exploit DNA-mediated CT to detect lesions, some of the proteins must exist in the oxidized state. Many agents in the cellular milieu could oxidize these DNA-bound proteins, and the level of oxidative stress within the cell could govern the proportion of oxidized protein present at any time. Indeed, these proteins can be oxidized by guanine radicals, the first genomic signal of oxidative stress (*35*), via DNA-

mediated CT. We have demonstrated the DNA-mediated oxidation of both MutY and p53, a cell cycle regulatory protein, with guanine radicals as intermediates (*28, 36*).

MATERIALS AND METHODS

Materials

All chemicals were purchased from Sigma Aldrich. All enzymes were purchased from New England Biolabs unless otherwise specified. All buffers were freshly prepared and filtered prior to use. Mica surfaces were purchased from SPI supplies. Silicon AFM probes were purchased from Nanoscience Instruments. Oligonucleotides were purchased from IDT or synthesized on a 3400 DNA synthesizer (ABI). All strains used were derivatives of CC104 or CC102 (*37*) and generated as described below. Luria-Bertani (LB) broth was used as the rich medium while NCE (*38*) medium supplemented with $MgSO_4$ (100 μM) and glucose (11 mM) or lactose (6 mM) was used as the minimal medium.

Generation of DNA Samples for AFM

Four primers were synthesized with the following sequences, 5'-GTACAGAGTTCAGTCGGCATCCGCTTACAGACAAGC-3' (forward), 5'-CCGGTAACTATCGTCTTGAGTCC-3' (reverse), 5'-GACTGAACTCTGTACCTGGCACGACAGGTTTCCCG-3' (forward), and 5'-GACTGAACTCTATACCTGGCACGACAGGTTTCCCG-3' (forward). The underlined bases highlight the location of a 2'-*O*-methyl residue. These primers were used in separate PCR reactions using pUC19 as a template to generate three duplexes 1610bp, 2157bp (matched), or 3767bp (mismatched) long and each containing one 14 nt single-

strand overhang. These PCR products were purified by ethanol precipitation and resuspended in 50 mM NaCl, 5mM sodium phosphate, pH 7 buffer and quantitated by OD_{260}. Duplexes were phosphorylated using 100 U PNK in 10% T4 DNA ligase buffer for 1 hour at 37°C and deactivated for 10 minutes at 65°C. Separate duplexes were then annealed at 65°C for 8 minutes then cooled to 20°C over 2 hours. The resulting larger duplexes were then ethanol precipitated and resuspended in 100 μL 50 mM NaCl/ 5mM phosphate buffer. 15 U T4 DNA ligase and 10% T4 ligase buffer were added (total reaction volume ~ 150 μL) and incubated overnight at 16°C followed by deactivation for 10 minutes at 65°C. We did not bring the ligation reaction to completion, so as to obtain a mixture of DNA samples that were equivalent other than the presence of the mismatch at the ligation site. The DNA duplexes (ligated and unligated) were then purified from a 0.6% agarose gel using a QiaQuick gel extraction kit (Qiagen).

AFM Deposition Conditions

Mica surfaces were freshly cleaved with scotch tape. Wild-type EndoIII (0.4 μM) was added to the stock DNA solution containing 50–100 ng total DNA composed of the mixture of ligated 3.8 kb duplexes and the two unligated duplexes (1.6 and 2.2 kb) in 6 mM $MgCl_2$/Tris-EDTA buffer. This protein-DNA solution was incubated at 4°C overnight and deposited (5 μL) on the mica surface for 2 minutes, rinsed with 2 mL water, and dried under argon. Two of the five wild-type EndoIII samples analyzed were deposited onto the mica surface in 5 ng quantities followed by immediate addition of 3.7 μM EndoIII (1 μL volume). This difference in deposition conditions did not result in any significant differences in the trends observed. Mutant protein (Y82A) was added to a stock solution

of 50 ng DNA for a final protein concentration of 0.4 μM. After incubation at 4°C overnight, deposition conditions were identical to that for wt EndoIII-DNA samples.

AFM Instrument Setup

Silicon AFM Probes purchased from Nanoscience Instruments (BudgetSensors), with a spring constant of 3 N/m and a resonance frequency of 75 kHz, were used in a Digital Instruments Multimode SPM. Images with scan areas of 2x2 μm^2 or 1x1 μm^2 were acquired in tapping mode, using an amplitude of 0.5416–0.200 V at a scan rate of 3.05 Hz. Scan rates of 3.05 Hz were used to obtain images of higher quality. Data analysis was performed using the WSxM program (*39*).

Strain Construction

CC104 and CC102 strains were generously donated (*37*), as was CC104 *mutY-* (CC104 *muty::*mini-tn 10) (*40*). *Nth* was replaced by a chloramphenicol resistance cassette (*cm*) in CC104 and CC104 *mutY-* using a previously described in-frame deletion method (*41*). See Table 8.1 for primer sequences; *nth* homology regions are shown in regular text and *cm* priming regions are highlighted in boldface. CC102 strains were constructed using P1 transduction (*42*). Inactivation in all strains was verified with colony PCR.

Lac^+ Reversion Assays

Strains were streaked to LB medium and incubated overnight at 37°C. For *nth* knockouts, strains were streaked to LB+chloramphenicol (17 μg/mL), and for *mutY* knockouts, strains were streaked to LB+tetracycline (50 μg/mL). 1 mL LB cultures were

Table 8.1. Primer sequences used for *nth* inactivation, cloning, and mutagenesis.

Function	Primer Sequence
Wanner inactivation of *nth*	5'-gaagcagctgcagaacgtgcattgccaaacggtgaaacagggaatgtctg**gtgtaggctggagctgcttc**-3'
	5'-agaggataaagaaaggttatcaatggggtaatcggtgttacccctttttct**catatgaatatcctccttag**-3'
Cloning *nth* into pBBR1MCS-4	5'-**ggaattc**gcaatggcacattgtttgac-3'
	5'-**aggttcc**tcaatggggtaatcggtgtt-3'
D138A mutant generation	5'-cggctggccgactattgctgtc**gcc**acgcacattttccgcg-3' + complement
Y82A mutant generation	5'-ggggtgaaaacctatatcaaaactattgggcttgctaacagcaaagc-3' + complement

started from single colonies and grown overnight in a shaking incubator at 37°C, 220 rpm. 20 μL of each starter culture was used to inoculate a 10 mL NCE+glucose culture which was then grown to a density of 10^9 cells/mL at 37°C, 250 rpm. Cell density was determined by dilution plating a 10 μL aliquot of the NCE+glucose culture onto NCE+glucose solid medium followed by incubation at 37°C for 36 hours. 5 mLs of this culture was centrifuged in a clinical tabletop centrifuge at 4°C and plated on NCE+lactose solid medium and then incubated at 37°C for 36 hours. Colonies arising are reported as *lac*$^+$ revertants/mL cells plated. In experiments incorporating plasmid vectors, CC104 and CC102 strains were made electrocompetent (*43*) and transformed via electroporation at 1.8 kV. Transformants were selected on LB+ampicillin (amp) (100 μg/mL) solid medium after incubation overnight at 37°C. Single colonies were restreaked to LB+amp (100 μg/mL) solid media and incubated 12 hours at 37°C. 1 mL LB+amp (100 μg/mL) cultures were started from these colonies and grown overnight at 37°C, 220 rpm. 20 μL of this starter culture was used to inoculate a 10 mL NCE+glucose+amp (40 μg/mL) culture which was grown to a density of 10^9 cells/mL at 37°C, 250 rpm. 5 mLs of this culture was plated onto NCE+lactose+amp (40 μg/mL) and incubated at 37°C for 36 hours. *Lac*$^+$ revertants were reported as described above.

Mutagenesis

Nth was cloned into pBBR1MCS-4 (p) using standard techniques (*43*). Primer sequences are given in Table S1; restriction sites are highlighted in boldface. Gene incorporation was verified by PCR and sequencing (Laragen) using KS/SK (pBBR1MCS-4 derived vectors) or M13 (pNTH10 derived vectors) sequencing primers. Mutants were generated using a QuikChange site-directed mutagenesis kit (Stratagene) and verified

by 3 independent sequencing reactions (Laragen). Primers used are shown in Table S1; the altered codon site is highlighted in boldface.

Protein Expression and Purification

EndoIII and Y82A EndoIII were expressed from the pNTH10 expression vector and purified as described previously (*44*). Protein concentrations were determined using the UV-visible absorbance of the [4Fe4S] cluster (410 nm, e = 17,000) (*29*).

Glycosylase Assays

Oligonucleotides were synthesized containing a 5-OH-dU lesion site (purchased as a phosphoramidite from Glen Research), HPLC purified, and verified with MALDI-TOF mass spectrometry. The following sequences were used: 5'-TGTCAATAGCAAGXGGAGAAGTCAATCGTGAGTCT-3' + complementary strand where X = 5-OH-dU base-paired with G. The strand containing the lesion was 5'-^{32}P endlabelled as previously described (*43*) and annealed to its complement. Reactions were run at 37°C for 15 minutes with 10 nM DNA and 100 or 10 nM protein and quenched with 1M NaOH (*45*). Samples were analyzed by denaturing 20% PAGE and imaged by autoradiography. Band intensity was quantified using ImageQuant software.

Electrochemistry at DNA-modified Electrodes

DNA-modified electrodes for protein electrochemistry experiments were prepared as described (*27*) using the following sequences: thiol-modified strand, 5'-AGTACAGTCATCGCG-3', TA complementary strand, 5'-CGCGATGACTGTACT-3', and abasic site (Ab) complementary strand, 5'-CGCGATGACTGTXCT-3', where X = dSpacer (Glen Research). Surfaces were backfilled with 100 mM mercaptohexanol for

30 minutes and rinsed at least 3 times with protein storage buffer (20 mM sodium phosphate, 100 mM NaCl, 0.5 mM EDTA, 20% glycerol, pH 7.5). Protein solution was introduced to the electrode surface and allowed to incubate for ~ 20 minutes until signal reached full intensity. Cyclic voltammetry experiments were performed on a CH Instruments 760 potentiostat using a 50 mV/s scan rate, Ag/AgCl reference electrode, and Pt wire auxiliary electrode in an electrochemical cell modified for protein experiments (*27*).

RESULTS AND DISSCUSSION

Genome Scanning Calculations

Using our CT scanning model, we can predict the genome interrogation time, T, for MutY in *E.coli*. In the CT scanning model, the DNA is essentially scanned by the electron with the repair proteins facilitating electron migration (Figure 8.1). Since an injected charge equilibrates on the nanosecond timescale (*15*), and protein diffusion occurs in micro- to milliseconds (*9*), the rate-limiting step in this process is the diffusion of a reduced protein within CT range of the oxidized DNA-bound protein. Hence scanning can be modeled as a random walk of the electron on the DNA, where the step time, *t*, for the walk is the average time for a reduced protein to approach within range to carry out DNA-mediated CT to the oxidized protein. We can calculate the step time for three dimensional diffusion of the reduced protein to the DNA as

$$t = \frac{V}{k_a C_p (1 - \Theta)}$$

where V is the cell volume, $C_p(1-\Theta)$ is the number of reduced repair proteins in the volume (Θ = fraction oxidized), and k_a is the bimolecular rate constant for protein association with the DNA target within the cellular volume. The bimolecular rate constant can be determined using a modified Smoluchowski equation for protein collision with a rod of DNA within the cell volume, where the length of the rod reflects the number of bases, *N*, over which DNA-mediated CT can proceed. The Smoluchowski equation is constructed with two terms: one describes the ballistic 3-dimensional diffusion of the protein to the DNA and the second (*46*) considers the gyrations of a rod with persistence length of 150 base pairs and the ends fixed as part of the chromosome.

$$k_a = 4\pi\kappa f D_p(r_{DNA} + r_p) + D_a a\sqrt[3]{\frac{r_{DNA} + r_p}{a}}$$

The protein diffusion constant (D_p) is determined from the Stokes-Einstein equation using the 10 cP viscosity of *E. coli* cytoplasm (*47*) and the measured Stokes radius of EndoIII (r_p) (*48*). DNA diffusion is considered to be negligible. The persistence length of DNA (150 bp) is defined as *a*. The electrostatic (*f*) and orientational (κ) constants are taken as unity (*49*), in keeping with the high ionic strength *in vivo* environment. The dissociation rate of the protein is not included in our model because charge equilibration should occur on a much faster timescale than dissociation of the reduced protein. Any contact of the reduced protein within the DNA rod allows electron transfer to the DNA-bound oxidized protein. We assume DNA is a rod, N base pairs long, but clearly the organization of the bacterial nucleoid is more complex (*50*). We can calculate the overall time to search the genome of *Z* bases through the random walk of the electron as

$$T_{ox} = t\left(\frac{4Z}{N}\right)^2$$

.

Since there is equal probability of reduced protein associating with each base in the CT-active target region, and N represents that maximum distance of interprotein charge transfer, the average distance of interprotein CT is N/2. Self-exchange decreases the average step distance by a further factor of 2. This represents the scanning time for a single oxidized protein. Each oxidized protein provides a separate nucleation site for CT scanning, but drawing from the same reservoir of reduced protein to scan different portions of the genome,

$$T_{CT} = t\left(\frac{4Z}{\Theta C_p N}\right)^2.$$

Scanning through sliding without a CT search represents a boundary condition, so that the total time is

$$T = (T_{CT}^{-1} + T_D^{-1})^{-1}$$

where T_D is the diffusion scanning time. It is also important to note that, since this model involves cooperation among the repair proteins, we can utilize the *total* concentration of these proteins within the cell, rather than copy numbers for MutY or EndoIII individually. Thus MutY benefits from help from the 500 copies of EndoIII (*2*).

This model assumes that DNA-mediated interprotein CT is much faster than protein diffusion, and that the oxidized repair proteins have higher nonspecific DNA affinity than the reduced proteins; both assumptions have experimental support (*15, 30*). We assume also that intervening DNA-binding proteins do not inhibit DNA-mediated CT, consistent with *in vivo* (*21*) and nucleosome (*19, 20*) experiments. We make no distinction between 5' to 3' versus 3' to 5' transport, although subtle differences have been observed (*51, 52*). In our model, reduced proteins are not allowed to exploit facilitated diffusion to find their DNA target containing oxidized protein, although this

would enhance the efficiency of the search. The possibility of other proteins participating in helper function, which would also substantially speed the search process, is neglected; other DNA-binding proteins at similar potentials could aid in helping MutY find its site (*53*). As formulated, there is an inverse cube dependence of scanning time on total copy number. Hence, the presence of even a hundred more redox-active repair proteins with this helper function would halve the overall scanning time. These conditions lead to an estimate for CT scanning that is conservative and therefore represents an overestimate for the amount of time necessary to search for lesions by DNA-mediated CT.

Figure 8.2 shows how the interrogation time varies as a function of N, the distance over which DNA-mediated CT proceeds and ox, the percentage of proteins that are oxidized. Remarkably, permitting DNA CT over 500 bp with 10% oxidized protein yields an interrogation time of 5 minutes, while DNA CT over only 200 bp with 20% oxidized protein results in an interrogation time of 8 minutes. These values are well within the 20 minute doubling time of *E. coli*. While we have not yet constructed long DNA sequences to establish the limits for long range DNA CT, we have demonstrated substantial long range oxidative damage in tethered DNA assemblies *in vitro* over 60 bp and in DNA within mitochondria over ~ 100 bp (*17, 54*). We and others have also found the distance dependence of CT to be remarkably shallow (*16-18, 55*). Long range CT has furthermore been demonstrated in nucleosomes with tethered photooxidants (*19, 20*). In fact, one advantage of DNA CT over other search mechanisms is that the electron travels *through* the DNA base pairs and no proteins need to be displaced.

The dependence of interrogation time on the percentage of proteins oxidized is also interesting to consider (Figure 8.2). There is a sharp decrease in the needed interrogation time at low levels of protein oxidized, and with higher oxidation levels the

Figure 8.2. Scanning time as a function of maximum distance of DNA-mediated interprotein CT (N) and the fraction of repair proteins that are in the 3+ state (% ox) is calculated using the CT scanning model. Note that at 10% oxidized protein with a maximum CT distance of 500 bp, the time required to interrogate the genome is ~ 5 minutes.

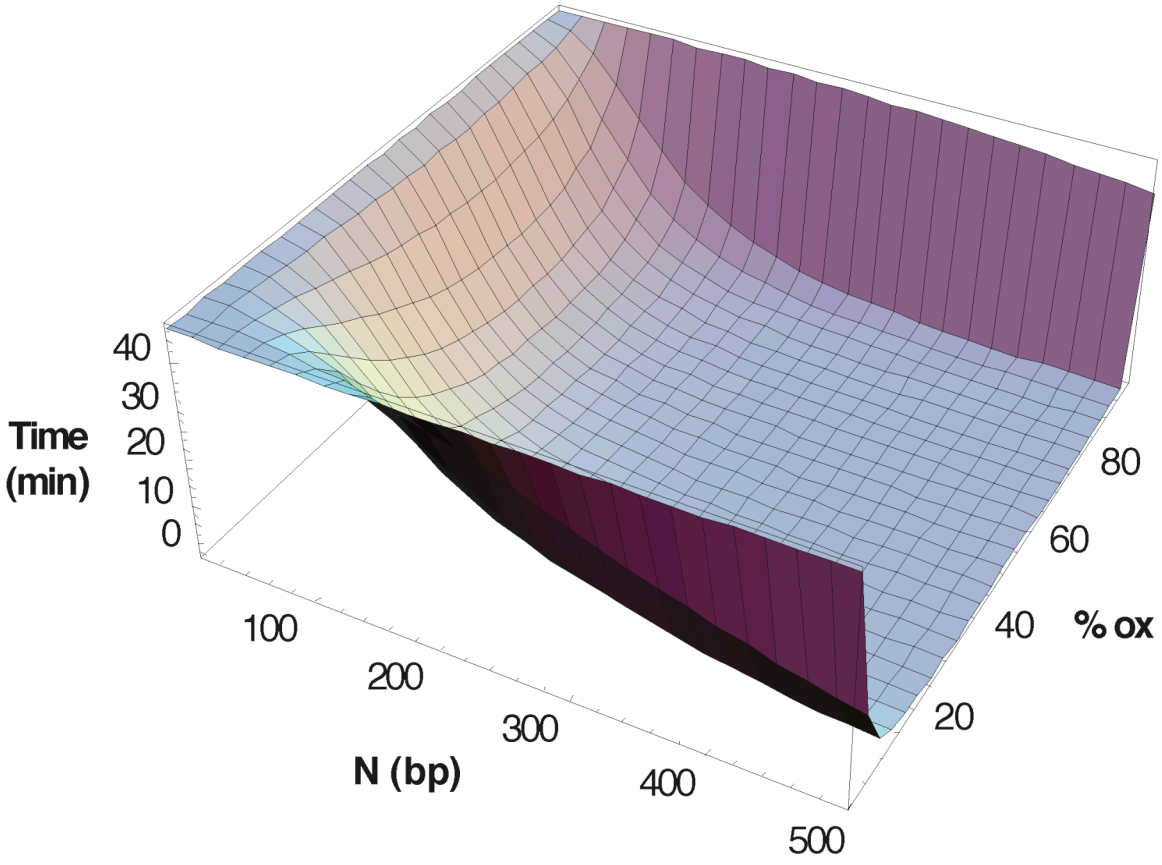

variation in interrogation time is quite small (Figure 8.3). The scanning efficiency resembles a switch that is turned on at low levels of oxidation, when DNA repair is needed. Activation of this switch could be influenced by the redox buffering capacity of the cell and by the level of oxidative DNA damage present. This would allow DNA repair proteins to sense oxidative assaults both locally and far away and to tune the repair response to fit the needs of the cell.

Atomic Force Microscopy Measurements

We can test this model directly using atomic force microscopy (AFM). A mixture of DNAs, both long (3.8 kilobase) DNA duplexes containing a single CA mismatch and short (2.2 and 1.6 kilobases) well-matched duplexes of the same total sequence were prepared; the longer sequence was obtained by ligation of the two shorter sequences. This mixture of matched and mismatched DNA strands was incubated with EndoIII and examined using established AFM techniques (*56*) (Figure 8.4). At least 5 images and > 100 strands were counted using 5 preparations of protein/DNA samples. We assume some adventitious oxidation of DNA-bound EndoIII, but have not yet carried out AFM measurements as a function of the percentage protein oxidized. The CA mismatch is a lesion that effectively inhibits DNA CT (*17, 23*). Since the CA mismatch is not a lesion that is preferentially bound by EndoIII, without DNA CT between bound EndoIII molecules, one might expect an equal density of proteins on the short and long strands. However, we find that EndoIII shows a small but significant preference for the longer strands containing the CA mismatch. Examination of the number of proteins bound to 187 long strands and 206 short strands reveals an average of 0.16±0.01 proteins bound per kilobase long strand and 0.12±0.02 proteins bound per kilobase short strand. Only clearly identifiable long or short strands were counted. Protein assignments were

Figure 8.3. Plot showing the contour from Figure 2 that corresponds to a genome scanning time (*T*) of 20 minutes, the doubling time of an *E. coli* cell.

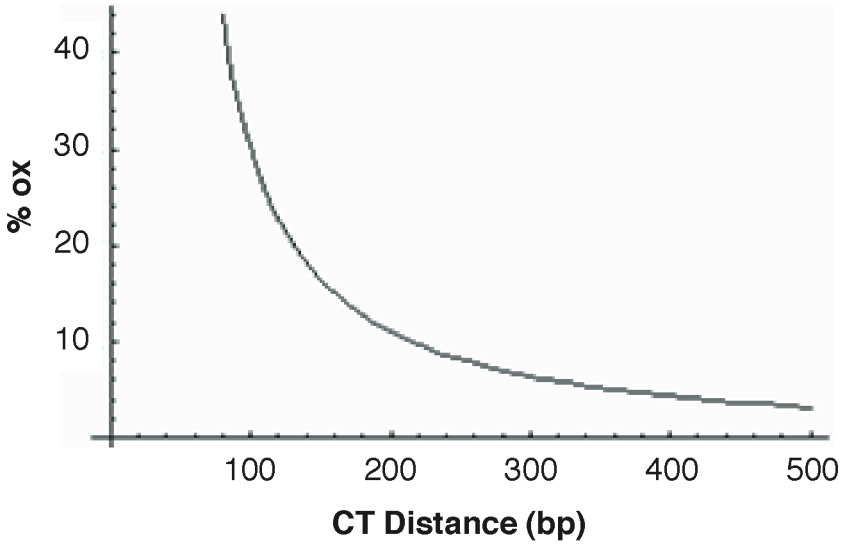

Figure 8.4. Measurements of repair protein distributions on DNA by AFM. A zoomed-in view (A) and a zoomed-out view (B) of representative AFM images of DNA strands incubated overnight with wild-type EndoIII. A higher density of proteins is apparent on the longer DNA strands containing the single base CA mismatch. Densities of 0.16±0.01 proteins bound per kilobase long strand and 0.12±0.02 proteins bound per kilobase short strand are observed where the error reflects the total number of bound proteins counted. Clumped DNAs and clumping at strand ends were excluded from the dataset.

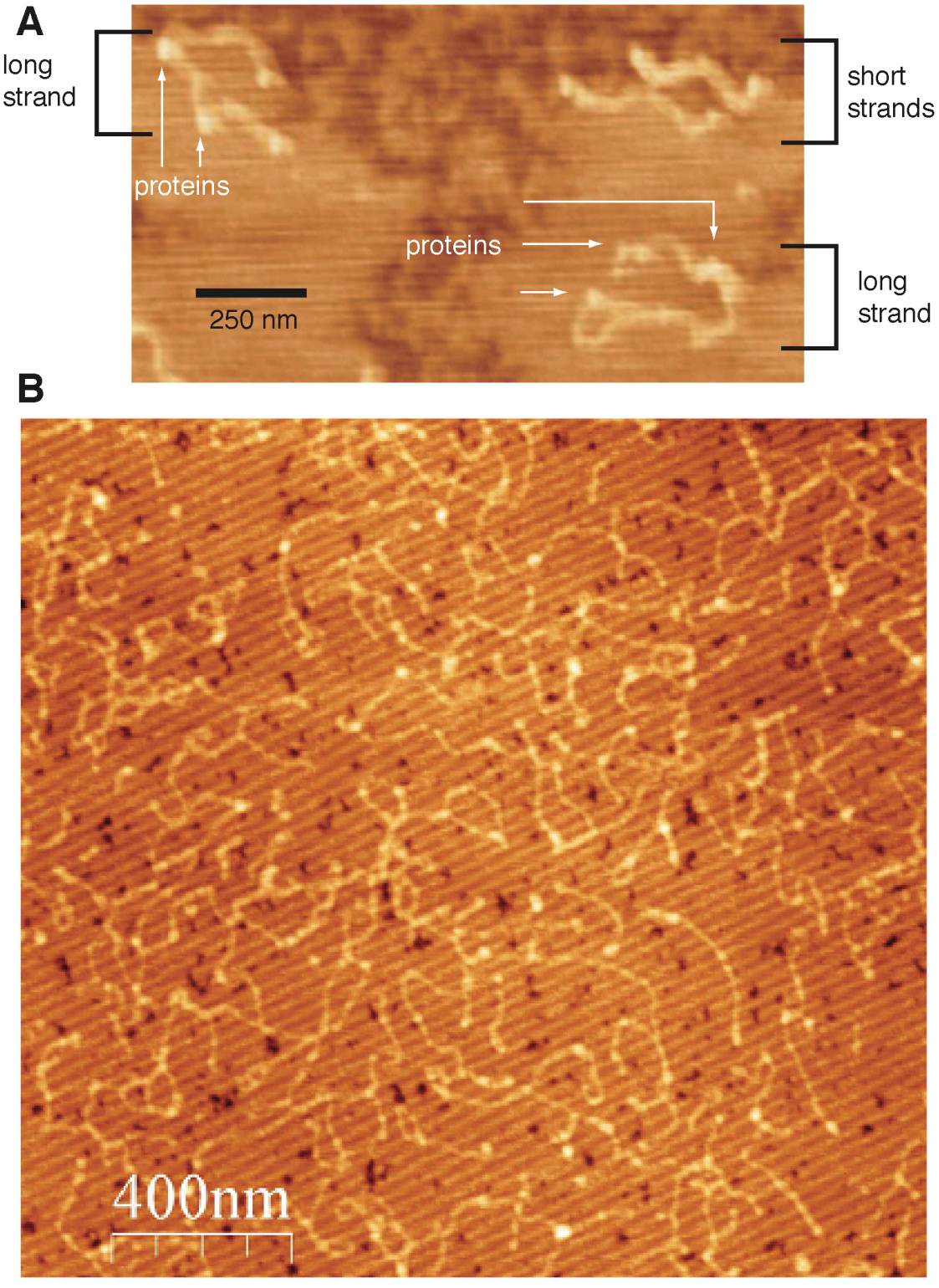

verified through analysis of their 4 nm heights in the images; without protein, features of this dimension are not observed. These results are consistent with the outcome predicted by our model. DNA-mediated CT will drive the redistribution of repair proteins away from undamaged regions such that the proteins will cluster near damaged sites. As a result, we see the proteins redistribute preferentially onto the DNA strand containing the mismatch.

Helper Function Assays in Escherichia coli

This CT scanning model can also be tested *in vivo* by assaying for the cooperation among the repair proteins in DNA-mediated signaling. If these proteins are able to help each other in their search for damage using DNA CT, upon knocking out the gene for EndoIII, for example, or reducing its capability to carry out electron transfer, one should be able to observe a decrease in the *in vivo* activity of MutY. Established assays for MutY and EndoIII activity inside *E. coli* cells have already been developed (*37*). The assay for "helper function" used here employs engineered mutations in the *lacZ* gene (encoding β-galactosidase, the enzyme that allows cells to grow in lactose-containing media) to report the frequency of a particular base pair substitution. The strain that serves as an assay for MutY activity, CC104, substitutes a cytosine for an adenine in the Glu 461 codon in *lacZ*, an amino acid essential for β-galactosidase activity. Since MutY prevents GC to TA transversion mutations (*57*), reversion of this original mutation back to wild-type (wt) *lacZ* can reflect a deficiency in MutY activity. Similarly, the CC102 strain serves as an assay for EndoIII activity by replacing an adenine with a guanine in the Glu 461 codon (*37*). EndoIII prevents GC to AT transition mutations (*58*); thus reversion back to wt *lacZ* indicates deficiency in EndoIII activity. In these experiments we

inactivated the gene encoding EndoIII (*nth*) in CC104, the MutY activity reporter strain, and looked for an increase in the reversion frequency from *lac-* to *lac+*. The reciprocal experiment, where the gene for MutY (*mutY*) is knocked out in the CC102 reporter strain, was also performed.

As illustrated in Table 8.2, in the CC104 MutY activity reporter strain, 20 ± 9 *lac+* revertants are observed per 10^9 cells, while inactivation of *mutY* in CC104 (CC104 *mutY-*) causes the number of *lac+* revertants to increase by a factor of 15 (300 ± 33), as expected (*37, 57*). When *nth* is inactivated in CC104 (CC104 *nth-*), the *lac+* reversion frequency observed is 54 ± 5, representing more than a factor of two increase over CC104. Thus, loss of EndoIII does have a small but significant effect on the *in vivo* activity of MutY. This loss in activity is consistent with a loss in helper function by EndoIII, as predicted by our model; the lower activity of MutY without EndoIII could reflect the lack of cooperative searching via DNA CT. An alternative explanation, however, is that MutY and EndoIII share some overlapping ability to repair the same lesions in genomic DNA. In this case, one would expect the *lac+* reversion frequency of the CC104 *mutY-/nth-* strain (270 ± 29) to be greater than that of CC104 *mutY-*, but they are, within error, equivalent.

We also performed the opposite experiment where *mutY* is inactivated and the resulting effect on the *in vivo* activity of EndoIII is observed using CC102, the EndoIII activity reporter strain (Table 8.2). An average of 14 ± 4 *lac+* revertants were found for the CC102 EndoIII activity reporter strain. Upon knocking out *nth* in CC102 (CC102 *nth-*), the reversion frequency becomes 34 ± 8. Removal of *mutY* (CC102 *mutY-*) leads to 27 ± 9 *lac+* revertants. In the double mutant (CC102 *nth-/mutY-*) 48 ± 16 revertants are observed. Note that the reversion frequency after inactivation of EndoIII is much

smaller for this assay than for the equivalent experiment (CC104 *mutY-*) using the MutY activity

Table 8.2. Assay for *in vivo* DNA repair by EndoIII (CC102) and MutY (CC104). *Lac+* revertants are reported as the average number *lac+* colonies that arise per 10^9 cells plated on minimal lactose media.

Strain	*lac*+ Revertants (*lac*+ colonies/ 10^9 cells plated)	Increase (x/CC104 or CC102)
CC104	20 ± 9	--
CC104 *nth-*	54 ± 5	2.7
CC104 *mutY-*	300 ± 33	15
CC104 *mutY-/nth-*	270 ± 29	13.5
CC102	14 ± 4	--
CC102 *mutY-*	27 ± 9	1.9
CC102 *nth-*	34 ± 8	2.4
CC102 *mutY-/nth-*	48 ± 16	3.4

assay and thus associated uncertainties are higher. In the CC102 assay, the mutagenesis pathway is likely initiated by damage to cytosine whereas in the CC104 assay the pathway likely begins with oxidative guanine damage. Given that the oxidation potential of guanine is substantially lower than that of cytosine, oxidized guanine lesions should be much more prevalent inside the cell (*35*), leading to a higher mutation frequency as observed with CC104. Nevertheless, the trend is the same: MutY appears to have a helper function in the EndoIII assay, just as EndoIII appears to have a helper function in the MutY assay. Indeed, just as the model predicts, MutY needs more help from EndoIII than *vice versa*.

This *in vivo* relationship between EndoIII and MutY has been observed previously by others, although in different experimental contexts. Small increases in mutational frequency have been detected when *mutY* is inactivated in CC102 (*37*) or when *nth* is inactivated in CC104 (*59*). In the latter case, it was proposed that this could be due to some intrinsic ability of EndoIII to repair oxidatively damaged guanine residues. However, biochemical evidence available on the substrate specificity of EndoIII (*34, 60*) indicates that the enzyme excises pyrimidine damage, which does not lead to GC to TA transversion mutations (*58*) and thus EndoIII would not be expected to exhibit MutY-like activity.

We can furthermore test directly whether the loss of MutY activity in the CC104 assay is the result of overlapping glycosylase activities by determining whether the number of *lac+* revertants is still suppressed by an EndoIII mutant that is biochemically incompetent to carry out the glycosylase reaction. As a control, we test for loss of EndoIII activity in the CC102 assay. Thus a mutant of EndoIII (D138A) that is known to be deficient in glycosylase activity (*61*) was introduced on a plasmid into both the CC102 and CC104 strains along with appropriate vector controls (an empty vector, p, and a

vector containing wt *nth*, pnth). Because this mutant cannot perform the base excision reaction, D138A also fails to reduce the high reversion frequency observed with CC102 *nth*- (Table 8.3). However, D138A is able to complement the CC104 *nth*- strain (Table 8.4). Thus, the glycosylase activity of EndoIII is not required to perform the helper function that EndoIII assumes to aid MutY in its repair of lesions inside the cell. Nonetheless, it appears that EndoIII lacking D138 can bind DNA and contains an intact [4Fe4S] cluster (*61*). Based upon our model, D138A should be competent to carry out DNA-mediated electron transfer and thus serve as a helper to MutY, as we observe.

In the context of our model, it is clearly not the glycosylase activity of EndoIII that is critical to its helper function, but its ability to carry out DNA-mediated CT. Thus, perturbing the path for electron transfer to the DNA would interfere with this helper function. Studies of protein electron transfer show that aromatic tyrosine and tryptophan residues often facilitate long range electron transfers in proteins (*62*), and EndoIII contains many of these residues. In particular, Y82 is a residue that is conserved in most species containing an *nth* homolog (in the human gene for EndoIII, *hNTH*, a W is present in this position, a relatively conservative substitution) as well as in many *mutY* homologs (*63*). In the crystal structure of *Bacillus stearothermophilus* EndoIII trapped in complex with DNA, the position equivalent to Y82 is located very close to the DNA backbone and directly adjacent to a residue that intercalates into the DNA base pair stack (*7*). Y82A EndoIII was thus introduced on a plasmid into both reporter strains (CC102 and CC104) and their *nth* knockouts to explore whether this mutation attenuates helper function. We find that Y82A is able to complement CC102 *nth*-. The observation that Y82A complements CC102 *nth*- further establishes that the glycosylase activity is not a source of helper function. Moreover the fact that Y82A complements CC102 *nth*- is understandable in the context of our model, because of the higher copy number of EndoIII in *E. coli* cells than MutY (*2*). MutY, therefore, is necessarily

Table 8.3. EndoIII activity assay (CC102) with an enzymatic EndoIII mutant (D138A). *Lac+* revertants are reported as the average number *lac+* colonies that arise per 10^9 cells plated on minimal lactose media with ampicillin (40 μg/mL). These data represent a single set of experiments with 10 replicates per strain assayed concurrently.

Strain	*lac*+ Revertants (*lac*+ colonies/ 10^9 cells plated)	Increase (x/CC102p)
CC102/p	10 ± 4.2	--
CC102 *nth-/p*	68 ± 26	6.8
CC102 *nth-*/pnth	18 ± 5.4	1.8
CC102 *nth-*/D138A	62 ± 31	6.2

Table 8.4. MutY activity assay (CC104) with an enzymatic EndoIII mutant (D138A). *Lac+* revertants are reported as the average number *lac+* colonies that arise per 10^9 cells plated on minimal lactose media with ampicillin (40 μg/mL). These data represent a single set of experiments with 10 replicates per strain assayed concurrently.

Strain	***lac*⁺ Revertants** (*lac*⁺ colonies/ 10^9 cells plated)	**Increase** (x/CC104p)
CC104/p	33 ± 2.0	--
CC104 *nth-/p*	64 ± 7.4	1.9
CC104 *nth-*/pnth	36 ± 3.3	1.1
CC104 *nth-*/D138A	32 ± 3.2	1.0

more dependent on a fast, efficient CT damage detection scheme to locate its lesions than EndoIII. In addition, oxidized guanine lesions, such as those excised by MutY, are much more abundant than the oxidized cytosine lesions repaired by EndoIII (*35*). Thus, the role of EndoIII in helping MutY search for lesions may more important than the ability of EndoIII to search for its own lesions.

Significantly, Y82A in the CC104 *nth-* strain shows an increase in mutation rate versus the CC104/Y82A and CC104/p controls (Figure 8.5). The data shown in Figure 8.5 is based on five sets of experiments with the CC104 strains. The number of *lac+* revertants is found to increase by 53±16% when comparing CC104 *nth-*/ Y82A to CC104/p. When comparing CC104 *nth-*/Y82A to CC104/Y82A, the number of *lac+* revertants increases by 68±13%. Similarly, for these trials, the ratio of the number of *lac+* revertants for CC104 *nth-*/ p versus CC104/p is 65±13%. If Y82A were attenuated but not completely defective in its electron transfer ability, we might expect that the number of *lac+* revertants measured in the CC104 assay would be lower on average for strains carrying this allele in the presence or absence of *nth* relative to their counterparts without it; this is what we observe (Figure 8.5). Together, these results indicate that Y82A is unable to restore helper function.

To check directly the biochemical characteristics of Y82A EndoIII, the protein was purified and its redox and glycosylase activities examined. Importantly, the mutant enzyme does contain the [4Fe4S] cluster, characterized by its distinctive spectrum with a maximum absorption at 410 nm (Figure 8.6). Y82A EndoIII also maintains glycosylase activity against a 5-OH-dU lesion in a ^{32}P-5'-endlabelled 35-mer duplex (Figure 8.7) as monitored by denaturing polyacrylamide gel electrophoresis; the activity of the mutant in this assay is equivalent (10% uncertainty) to that of the wild type enzyme. Note that this experiment on a 35-mer duplex measures only the base excision reaction, not the search process. To test for DNA-bound redox activity, Y82A was examined on a Au

Figure 8.5. Characterization of Y82A EndoIII, a mutant in DNA-mediated CT capability. Bar graph showing *lac+* revertants for CC102/p, CC102 *nth-*/p, CC102/Y82A, CC102 *nth-*/Y82A (left), CC104/p, CC104 *nth-*/p, CC104/Y82A, and CC104 *nth-*/Y82A strains (right). *Lac+* revertants are reported as the average number *lac+* colonies that arise per 10^9 cells plated on minimal lactose media containing ampicillin. Data for the CC104 strains are shown based upon five sets of independent biological experiments, each containing 10 replicates per strain. A statistically significant increase in the number of *lac+* revertants is observed in the CC104 *nth-*/Y82A strain (52±6) when compared to either the CC104/p (34±4) or the CC104/Y82A strain (31±2) indicating that Y82A does not restore helper function.

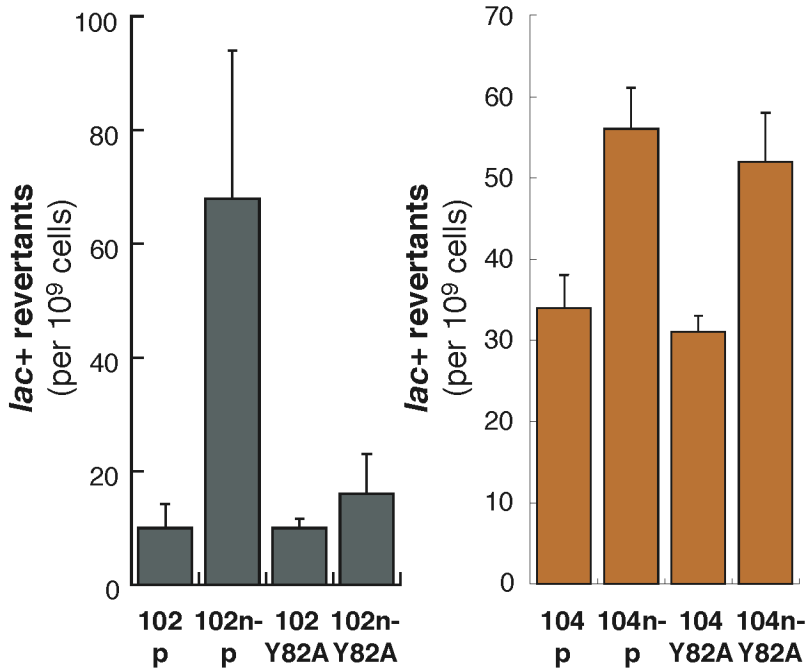

Figure 8.6. The UV-visible spectrum of Y82A EndoIII. A peak in the visible region is observed at 410 nm characteristic of a [4Fe4S] cluster.

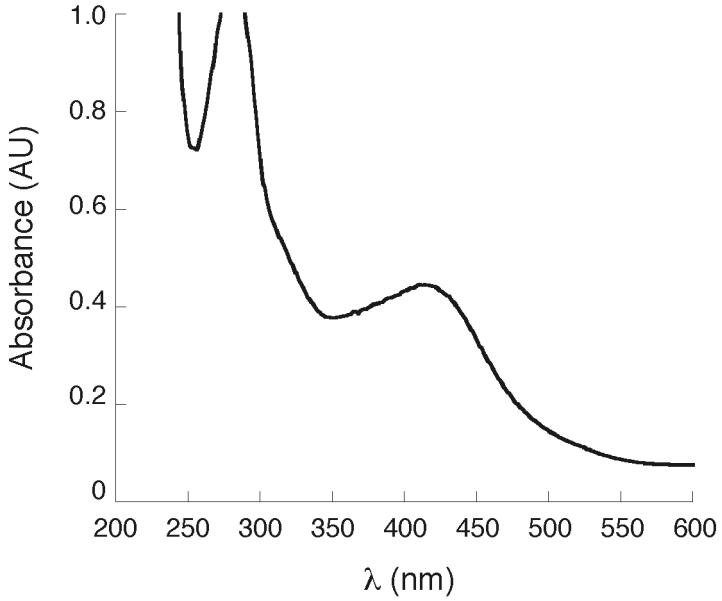

Figure 8.7. Autoradiogram after denaturing PAGE of ^{32}P-5'-TGTCAATAGCAAGXGGAGAAGT-CAATCGTGAGTCT-3' where X = 5-OH-dU base-paired with G. Protein samples (100 or 10 nM) were incubated with duplexes for 15 min at 37°C and quenched with 1 M NaOH. No significant difference in glycosylase activity is observed between Y82A and wt EndoIII.

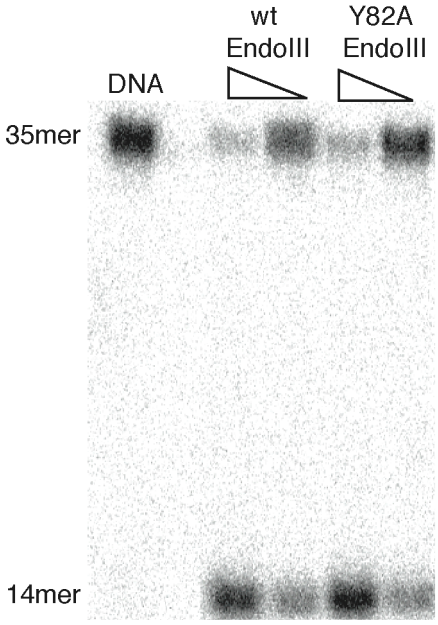

electrode surface modified with thiol-terminated DNA duplexes. Significantly, the potential for the DNA-bound mutant resembles that seen for the wild type protein (*27*), but the signal intensity is diminished (Figure 8.8). Note that, here, the protein concentrations are determined based on the 410 nm absorbance of the [4Fe4S] cluster; the smaller electrochemical signal observed with Y82A does not reflect a lower concentration of [4Fe4S] clusters. Over three trials, Y82A EndoIII exhibits a signal that is 50±13% smaller than that for wt EndoIII (per [4Fe4S] cluster). This lowered signal intensity would be expected with an attenuated efficiency of electron transfer from the cluster to the DNA. Y82A was also investigated at an electrode modified with a duplex containing an abasic site (Ab), a modification known to attenuate DNA-mediated CT to species bound above this lesion (*23*). Y82A does not exhibit a signal at this electrode modified with Ab (Figure 8.9) indicating that, as with wt EndoIII (*27, 30*), oxidation of the 4Fe4S cluster is DNA-mediated and requires an intact base pair stack. Significantly, and consistent with these results, examination of the distribution of Y82A on mismatched and matched strands by AFM shows no preference for the mismatched strand; 0.16±0.01 proteins per kilobase long strand and 0.18±0.02 proteins per kilobase short strand are observed (Figure 8.10). Thus Y82A not only is a mutant in “helper” function, but it also shows a compromised ability to carry out DNA-mediated CT. These results, considered together, demonstrate a distinct connection between DNA-mediated CT to the [4Fe4S] cluster and the *in vivo* relationship observed between MutY and EndoIII.

These experiments therefore indicate that MutY and EndoIII cooperate in their search for damage in the genome and redistribute in the vicinity of lesions consistent with our model for CT scanning. It is demonstrated that this cooperation, or helper function, does not involve the glycosylase reaction. Based on their chromosomal arrangement, the expression of MutY and EndoIII also do not appear to be linked (*64,*

Figure 8.8. Cyclic voltammetry of Y82A EndoIII at a Au electrode modified with $SH(CH_2)_2CONH(CH_2)_6NHOCO$-5'-AGTACAGTCATCGCG-3' + complementary strand. Scans were performed at 50 mV/s using a Ag/AgCl reference electrode and Pt wire auxiliary electrode. DNA-modified surfaces were prepared, backfilled with mercaptohexanol, and wt or Y82A EndoIII was tested. Surfaces were then rinsed and the other protein analyzed on the same surface. Over several trials, the electrochemical signal associated with Y82A is 50±13% smaller per [4Fe4S] cluster compared with wt EndoIII.

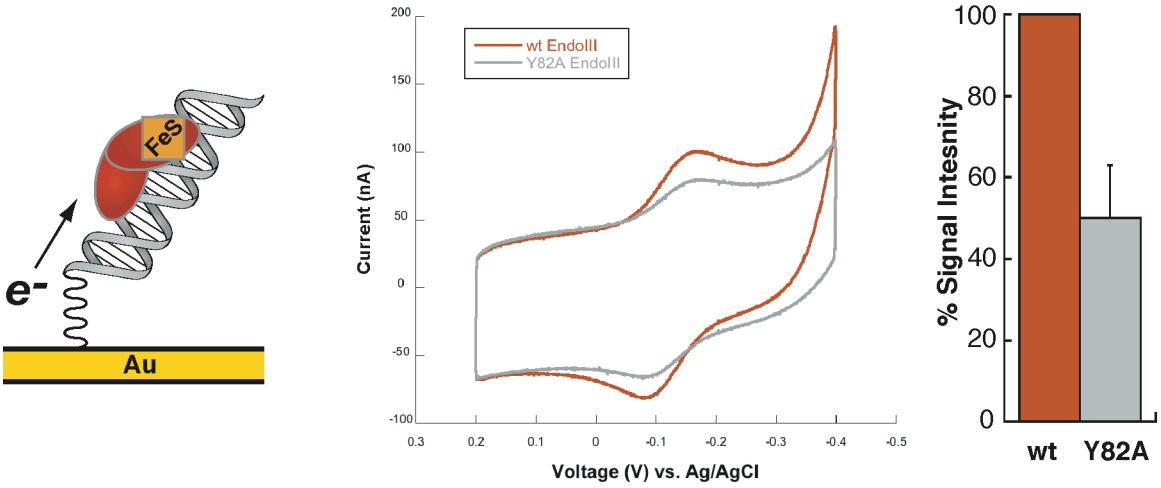

Figure 8.9. Y82A EndoIII examined by cyclic voltammetry at a Au electrode surface modified with DNA containing an abasic site. No peak is evident, indicating that CT to the [4Fe4S] cluster in Y82A EndoIII requires an intact DNA π-stack. See Materials and Methods section for further experimental details.

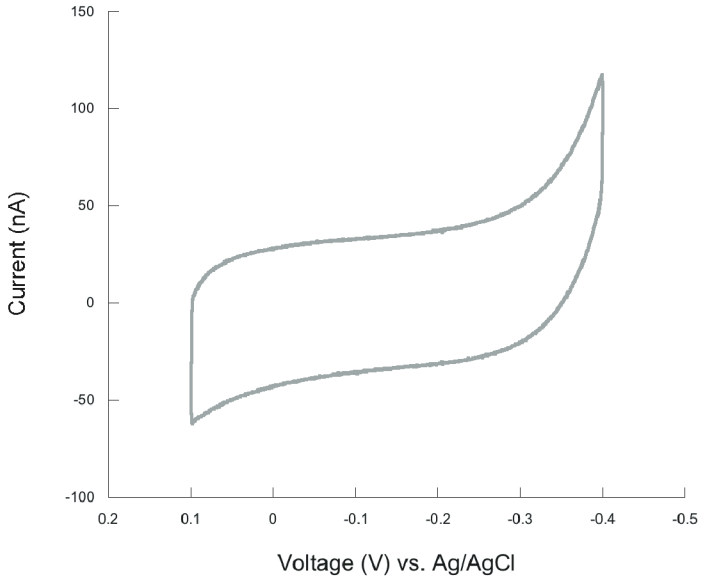

Figure 8.10. Comparative densities for wt (left) and Y82A (right) EndoIII bound to matched versus mismatched (CA) strands measured by AFM. Although wt EndoIII preferentially redistributes onto the mismatched strand, Y82A shows no preference.

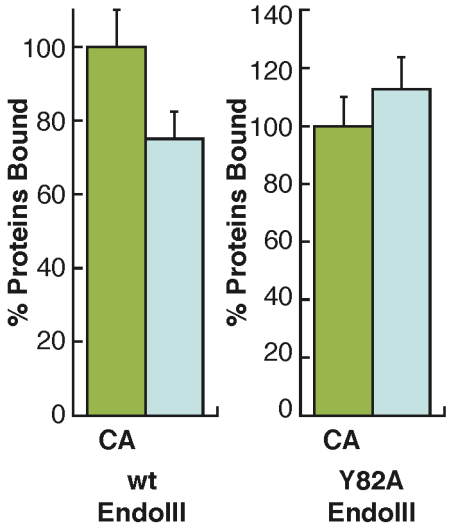

65). There is also no chemical evidence that the proteins physically bind to one another, and their low abundance within the cell makes random associations improbable. This cooperation thus arises from a distance. Importantly, what does appear to be required for helper function is an intact [4Fe4S] cluster, as well as an electroactive protein-DNA interface. Mutation of an aromatic amino acid residue near the DNA binding site, Y82A, leads to a decrease in CT efficiency *in vitro*, the inability of the protein to redistribute near lesions, and to diminished helper function *in vivo*. It is noteworthy that an analogous mutation (Y166S) in the human homolog of *mutY* is associated with cancer (*66*). While the detailed electron transfer pathway from this mutant to the DNA remains to be delineated, these experiments establish a link between DNA-mediated CT and the cooperative search for damage carried out by these repair proteins. These results thus provide biological support for our model of long range DNA-mediated signaling between repair proteins (Figure 8.1).

DNA-mediated CT chemistry serves as a fast and efficient reaction that is exquisitely sensitive to lesions and perturbations in the base pair stack. This chemistry helps to explain how these repair glycosylases locate their lesions efficiently in the cell, a key function since mutations in these enzymes in humans are implicated in colorectal cancer (*66*). This mechanism furthermore provides a rationale for iron-sulfur clusters in DNA repair proteins. More generally, these experiments illustrate the importance of DNA-mediated CT in long range signaling among proteins in low abundance that are bound to DNA. Other roles for DNA-mediated CT in biological signaling must now be considered.

SUMMARY

Given the remarkable sensitivity of DNA-mediated charge transport (CT) to mismatched and damaged base pairs, we have proposed that DNA repair glycosylases containing a redox active [4Fe4S] cluster (EndoIII and MutY) could use DNA CT in signaling one another to search cooperatively for damage in the genome. Here we examine this model for efficient CT scanning, where we estimate that electron transfers over a few hundred base pairs are sufficient for rapid interrogation of the full genome. Using atomic force microscopy, we find a redistribution of EndoIII onto DNA strands containing a single base mismatch, consistent with our model for CT scanning. We also demonstrate, using an *in vivo* assay for MutY activity in *Escherichia coli*, a cooperativity between EndoIII and MutY that is predicted by the CT scanning model. This helper function of EndoIII does not depend upon the enzymatic activity of the glycosylase but does depend upon its CT properties; Y82A EndoIII, a mutation that renders the protein deficient in DNA-mediated CT, as assayed with DNA electrochemistry, inhibits helper function. These results indicate a strategy for how these repair proteins efficiently locate DNA lesions and demonstrate a biological role for DNA-mediated CT within the cell.

REFERENCES

1. E. C. Friedberg, *et al.* (2006) *DNA Repair and Mutagenesis* ASM Press.

2. Demple, B., and Harrison, L. (1994) *Annu. Rev. Biochem. 63*, 915.

3. David, S. S., and Williams, S. D. (1998) *Chem. Rev. 98*, 1221.

4. David, S. S., O'Shea, V. L., and Kundu, S. (2007) *Nature 447,* 941.

5. Blattner, F. R., *et al.* (1997) *Science 277*, 1453.

6. Francis, A. W., Helquist, S. A., Kool, E. T., and David, S. S. (2003) *J. Am. Chem. Soc. 125,* 16235.

7. Fromme, J. C., and Verdine, G. L. (2003) *EMBO J. 22*, 3461.

8. Fromme, J. C., Banerjee, A., Huang, S. J., and Verdine, G. L. (2004) *Nature 427*, 652.

9. Berg, O. G., Winter, R. B., and von Hippel, P. H. (1981) *Biochemistry 20*, 6929.

10. Blainey, P. C., van Oijen, A. M., Banerjee, A., Verdine, G. L., and Xie, X. S. (2006) *Proc. Natl. Acad. Sci. U. S. A. 103*, 5752.

11. Parikh, S. S., *et al.* (1998) *EMBO J. 17*, 5214.

12. Wong, I., Lundquist, A. J., Bernards, A. S., and Mosbaugh, D. W. (2002) *J. Biol. Chem. 277*, 19424.

13. Parker, J. B., *et al.* (2007) *Nature 449*, 433.

14. Murugan, R. (2004) *Phys. Rev. E 69*, 011911 (2004).

15. Wagenknecht, H. A., Ed. (2005) *Charge Transfer in DNA: From Mechanism to Application,* Wiley-VCH.

16. Hall, D. B., Holmlin, R. E., and Barton, J. K. (1996) *Nature 382*, 731.

17. Nunez, M. E., Hall, D. B., and Barton, J. K. (1999) *Chem. Biol. 6,* 85.

18. Ly, D., Sanil, L., and Schuster, G. B. (1999) *J. Am. Chem. Soc. 121*, 9400.

19. Nunez, M. E., Noyes, K. T., and Barton, J. K. (2002) *Chem. Biol. 9*, 403.

20. Bjorklund, C. C., and Davis, W. B. (2006) *Nucleic Acids Res. 34,* 1836.

21. Nunez, M. E., Holmquist, G. P., and Barton, J. K. (2001) *Biochemistry 40*, 12465.

22. Boal, A. K., and Barton, J. K. (2005) *Bioconjug. Chem 16*, 312.

23. Boon, E. M., Salas, J. E., and Barton, J. K. (2002) *Nat. Biotechnol. 20,* 282.

24. Boon, E. M., Ceres, D. M., Drummond, T. G., Hill, M. G., and Barton, J. K. (2000) *Nat. Biotechnol. 18*, 1096.

25. Guo, X., Gorodetsky, A. A., Hone, J., Barton, J. K., and Nuckolls, C. (2008) *Nat. Nanotechnol. 3*, 163.

26. Boon, E. M., Livingston, A. L., Chmiel, N. H., David, S. S., and Barton, J. K. (2003) *Proc. Natl. Acad. Sci. U. S. A. 100*, 12543.

27. Boal, A. K. *et al.* (2005) *Biochemistry 44*, 8397.

28. Yavin, E., *et al.* (2005) *Proc. Natl. Acad. Sci. U. S. A. 102*, 3546.

29. Cunningham, R. P., *et al.* (1989) *Biochemistry 28*, 4450.

30. Gorodetsky, A. A., Boal, A. K., and Barton, J. K. (2006) *J. Am. Chem. Soc. 128*, 12082.

31. Yavin, E., Stemp, E. D. A., O'Shea, V. L., David, S. S., and Barton, J. K. (2006) *Proc. Natl, Acad. Sci. U. S. A. 103*, 3610.

32. Hickerson, R. P., Prat, F., Muller, J. G., Foote, C. S., and Burrows, C. J. (1999) *J. Am. Chem. Soc. 121*, 9423.

33. Porello, S. L., Leyes, A. E., and David, S. S. (1998) *Biochemistry 37*, 14756.

34. O'Handley, S., Scholes, C. P., and Cunningham, R. P. (1995) *Biochemistry 34*, 2528.

35. Burrows, C. J., and Muller, J. G. (1998) *Chem. Rev. 98*, 1109.

36. Augustyn, K. E., Merino, E. J., and Barton, J. K. (2007) *Proc. Natl. Acad. Sci. USA 104*, 18907.

37. Cupples, C. G., and Miller, J. H. (1989) *Proc. Natl. Acad. Sci. USA 86,* 5345.

38. Davis, R. W., Botstein, D., and Roth, J. R. (1980) *Advanced Bacterial Genetics: A Manual for Genetic Engineering* Cold Spring Harbor Laboratory.

39. Horcas, I., *et al.* (2007) *Rev. Sci. Instrum. 78*, 013705.

40. Golinelli, M. P., Chmiel, N. H., and David, S. S. (1999) *Biochemistry 38*, 6997.

41. Datsenko, K. A., and Wanner, B. L. (2000) *Proc. Natl. Acad. Sci. USA 97*, 6640.

42. Miller, J. H. (1992) *A Short Course in Bacterial Genetics: A Laboratory Manual and Handbook for Escherichia coli and Related Bacteria* Cold Spring Harbor Laboratory.

43. Sambrook, J., and Russell, D. W. (2001) *Molecular Cloning: A Laboratory Manual* Cold Spring Harbor Laboratory.

44. Boiteux, S., O'Connor, T. R., and Laval, J. (1987) *EMBO J. 6*, 3177.

45. Watanabe, T., Blaisdell, J. O., Wallace, S. S., and Bond, J. P. (2005) *J. Biol. Chem. 280*, 34378.

46. Berg, O. G. (1986) *Biopolymers 25*, 811.

47. Mullineaux, C. W., Nenninger, A., Ray, N., and Robinson, C. (2006) *J. Bacteriol. 188*, 3442.

48. Asahara, H., Wistort, P. M., Bank, J. F., Bakerian, R. H., Cunningham, R. P. (1989) *Biochemistry 28*, 4444.

49. Berg, O. G., and von Hippel, P. H. (1985) *Ann. Rev. Biophys. Chem. 14,* 131.

50. Thanbichler, M., Wang, S. C., and Shapiro, L. (2005) *J. Cell. Biochem. 96*, 506.

51. O'Neill, M. A., and Barton, J. K. (2002) *Proc. Natl. Acad. Sci. USA 99*, 16543.

52. O'Neill, M. A., Becker, H. C., Wan, C., Barton, J. K., and Zewail, A. H. (2003) *Angew. Chem. Int. Ed. 42*, 5896.

53. Gorodetsky, A. A., *et al.* (2008) *Proc. Natl. Acad. Sci. USA 105*, 3684.

54. Merino, E. J., and Barton, J. K. (2007) *Biochemistry 46*, 2805.

55. Kelley, S. O., Jackson, N. M., Hill, M. G., and Barton, J. K. (1999) *Angew. Chem. Int. Ed. 38*, 941.

56. Chen, L., Haushalter, K. A., Lieber, C. M., and Verdine, G. L. (2002) *Chem. Biol. 9*, 345.

57. Nghiem, Y., Cabrera, M., Cupples, C. G., and Miller, J. H. (1988) *Proc. Natl. Acad. Sci. USA 85*, 2709.

58. Kreutzer, D. A., and Essigmann, J. M. (1998) *Proc. Natl. Acad. Sci. USA 95*, 3578.

59. Tano, K., Iwamatsu, Y., Yasuhira, S., Utsumi, H., and Takimoto, K. (2001) *J. Radiat. Res. 42*, 409.

60. Dizdaroglu, M., Laval, J., and Boiteux, S. (1993) *Biochemistry 32*, 12105.

61. Thayer, M. M., Ahern, H., Xing, D., Cunningham, R. P., and Tainer, J. A. (1995) *EMBO J. 14*, 4108.

62. Stubbe, J., Nocera, D. G., Yee, C. S., and Chang, M. C. (2003) *Chem. Rev. 103*, 2167.

63. Watanabe, T., Blaisdell, J. O., Wallace, S. S., and Bond, J. P. (2005) *J. Biol. Chem. 280*, 34378.

64. Gifford, C. M., and Wallace, S. S. (2000) *Nucleic Acids Res. 28*, 762.

65. Gifford, C. M., and Wallace, S. S. (1999) *J. Bacteriol. 181*, 4223.

66. Cheadle, J. P., and Sampson, J. R. (2007) *DNA Repair 6*, 274.

CHAPTER 9

Summary and Perspective

The efficiency of DNA-mediated charge transport (CT) is influenced by the structure and dynamics of the base-pair π-stack. Specifically, the presence of mismatched or damaged bases in the duplex can dramatically hinder charge migration through the base-pair stack (*1, 2*). This property of DNA CT has been exploited to develop electrochemical devices for biosensing applications (*1*). In addition, we have proposed that the natural machinery for sensing DNA damage inside the cell, DNA repair enzymes, may employ DNA CT as an expedient method for the detection of lesions (*3*).

In exploring the role of DNA CT in DNA repair, we have focused on a class of base-excision repair (BER) glycosylases that contain [4Fe4S] clusters. In these enzymes, the function of the cluster is not well understood. Experimental methods relying on DNA-mediated CT reveal that the [4Fe4S] cluster in these enzymes is redox-active when the protein is DNA-bound (*3*). Indeed, DNA-mediated oxidation of these enzymes is a more favorable process and results in a more stable product than oxidation in the absence of DNA (*4*). A ~ 280 mV potential shift is observed for the 2+/3+ redox couple of the [4Fe4S] cluster upon DNA binding and this difference could translate into a differential DNA binding affinity for the oxidized and reduced forms of the enzyme. These experiments, and others (*5, 6*), demonstrate that methods employing DNA-mediated CT are a valuable tool when studying the properties of redox-active proteins that bind DNA.

Might redox activity in [4Fe4S] cluster BER glycosylases allow them to use DNA CT to search for damage? We have put forth a model describing how this process might happen (*3, 7*). A protein, the acceptor, in the $[4Fe4S]^{3+}$ state is bound to DNA. If this protein is surrounded by undamaged DNA, other [4Fe4S] cluster DNA-binding enzymes may bind nearby and reduce the acceptor protein in a DNA-mediated electron transfer reaction. If, instead, the acceptor protein is in the vicinity of damaged DNA, it is less

likely to be accessible for reduction *via* the π-stack of DNA. Thus the protein would remain bound near the lesion site. These reactions, when considered in the highly complex and dynamic environment present inside a cell, provide a viable explanation for how repair enzymes might swiftly locate damage. Furthermore, DNA-mediated CT as a damage detection mechanism also allows for the possibility of cooperative searching among different [4Fe4S] DNA repair enzymes, as long as they are of the appropriate redox potential.

MutY and Endonuclease III (EndoIII) are the most widespread [4Fe4S] cluster DNA repair enzymes; both are found in organisms ranging from *Escherichia coli* to humans and both repair oxidatively damaged bases in DNA (*8*). The recent discovery of [4Fe4S] clusters in several DNA repair enzymes from archaeal organisms may expand the scope of our model (*9, 10*). The discovery of a [4Fe4S] uracil DNA glycosylase (UDG) in a number of hyperthermophilic organisms, where the rate of uracil production in DNA is greatly enhanced, may indicate that the presence of an [4Fe4S] center could help fulfill a need for greater DNA repair in extreme environments. Perhaps the [4Fe4S] cluster could allow these UDGs to exploit a fast and efficient lesion detection mechanism based on DNA-mediated CT. An iron-sulfur cluster in an archaeal nucleotide excision repair (NER) helicase (XPD) is of great interest because sequence analyses suggest that it may be a universal cofactor present in helicases from a broad range of organisms. Though these helicases have a very different enzymatic function than [4Fe4S] BER glycosylases, they do face a common challenge in that they must locate lesions or forked structures in DNA and, subsequently, catalyze strand separation at these sites. As proposed for BER glycosylases, these helicases could use DNA-mediated CT to locate these unusual DNA structures cooperatively (Figure 9.1).

Figure 9.1. Proposed mechanisms of interaction between MutY and YggX. YggX may interact directly with MutY and prevent oxidation and degradation (*a*). Or YggX could bind DNA and transfer electrons to MutY in a DNA-mediated fashion (*b*).

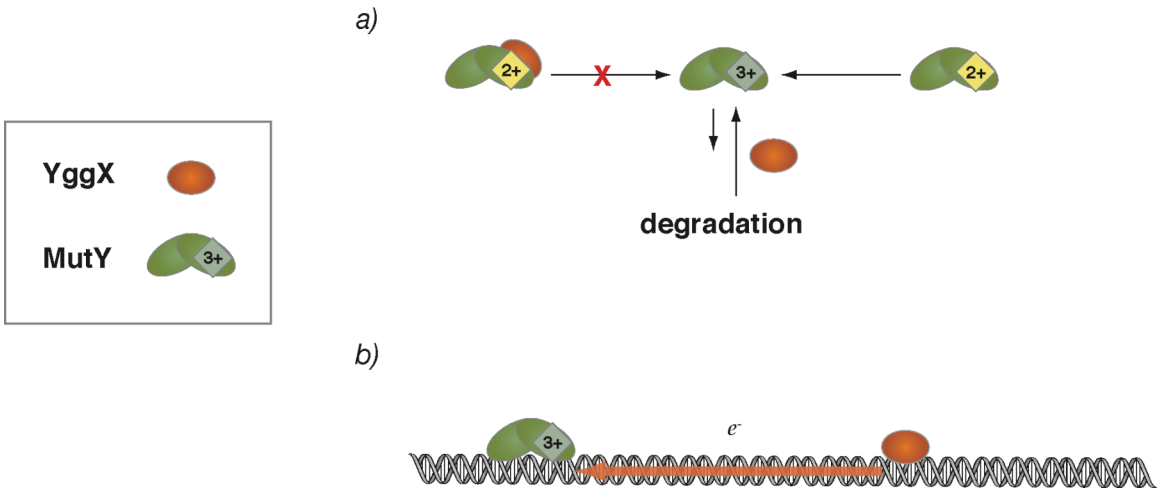

MutY and EndoIII are expressed as part of multigene operons in *E. coli* and other bacterial species (*11, 12*). MutY is expressed along with YggX, a protein proposed to be involved in iron trafficking and oxidative stress protection. The interaction between these proteins is currently uncharacterized, though there is some evidence that they might functionally interact inside the cell (*13*). YggX may serve as a signaling partner for MutY or as a protective or restorative element for the [4Fe4S] cluster in MutY (Figure 9.2). EndoIII is expressed as the final gene in an eight gene operon in *E. coli*. Several of the other genes in this operon are postulated to contain multiple iron-sulfur clusters, while others are predicted to be transmembrane proteins (*14*). These proteins have not been biochemically characterized in *E. coli* but are homologous to a set of genes, termed *rnf*, that are required for nitrogen fixation in *Rhodobacter capsulatus* and other diazotrophs. In *R. capsulatus*, the *rnf* gene products are proposed to form a membrane bound complex that may deliver reducing equivalents to nitrogenase or nitrogenase reductase. It is also postulated that they may be involved in iron-sulfur cluster maturation (*15*). It is possible that the *E. coli rnf* homologs may play a similar role, but instead, providing reducing equivalents to DNA-binding iron-sulfur cluster proteins. The *E. coli rnf* proteins might (either as the membrane-bound complex or in concert with soluble redox shuttle proteins) reduce EndoIII and other DNA-binding proteins (perhaps in a DNA-mediated fashion) or they could play a role in general iron-sulfur cluster assembly or repair (Figure 9.2). In fact, it has already been suggested that the *E. coli rnf* homologs may be involved in reduction of SoxR, a redox-sensitive transcription factor. In any case, further investigation of YggX and the *rnf* proteins in *E. coli* may allow us to learn more about the role of iron-sulfur clusters in DNA repair enzymes, since genes that are transcribed together as operons in prokaryotes often perform similar or related functions.

In the course of investigating the cooperative nature of DNA-mediated CT among DNA repair enzymes MutY and EndoIII we have discovered an EndoIII mutant (Y82A) that hinders the efficiency of DNA-mediated CT as measured at DNA-modified electrodes (*7*). This result could provide an important clue about the requirements for effective charge transport across a protein-DNA interface, a reaction that is not well understood. Experimental studies of DNA-mediated CT with small molecules indicate that strong coupling of the donor and acceptor entities into the base-pair stack is required for rapid and efficient reactions. The [4Fe4S] cluster in EndoIII is located relatively close (~ 15–20 Å) to the DNA (*16*) making it possible that protein-DNA CT could occur in a simple tunneling reaction (*17*). Many aspects of this reaction remain elusive, though. We do not know if the protein must be in a particular conformation for the reaction to occur or if there are amino acids residues that serve as intermediates in the CT process. We also do not understand which elements of the protein are required for coupling into the DNA π-stack or appropriate positioning of the protein relative to the DNA base-pair stack for efficient CT. Furthermore, it is not yet known if protein-DNA CT has universal features or if this reaction occurs by a different mechanism for different proteins. Our observation that Y82A EndoIII displays a diminished CT efficiency implies that aromatic residues may be important for effective protein-DNA CT, but further experimentation will be required to understand these reactions in full.

The human homolog of MutY has been recently implicated in inherited colorectal cancer (*18*). The mutational spectrum identified in cancer patients includes frameshift, truncating, splice-site, and missense variants. Of these, the over 50 different missense, or single amino acid, mutations that have been identified reveal some interesting

Figure 9.2. Proposed role for *rnf* gene products in *E. coli*. The membrane bound complex may deliver electrons to redox-active DNA-binding proteins. This could happen through a direct interaction between the complex and the DNA-binding protein (left) or *via* soluble shuttle proteins (right).

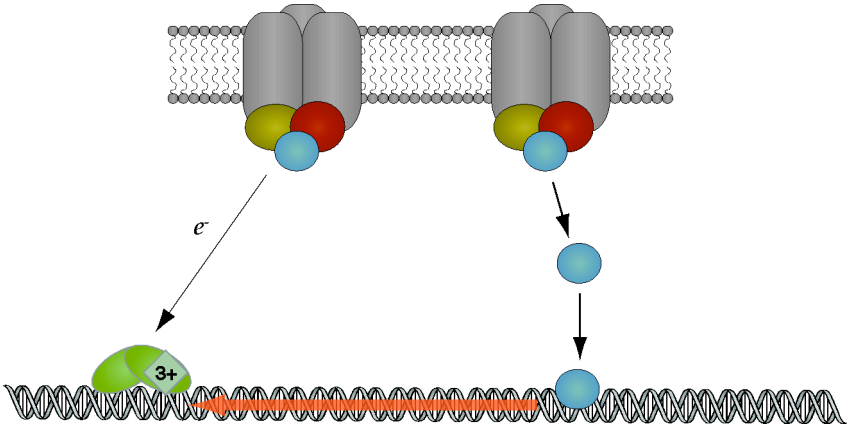

patterns. One of the most common disease-associated variants found is Y165C, which results in substitution of an intercalated tyrosine for a cysteine residue. It will be interesting to examine the redox properties of this variant. Does eradication of the intercalated tyrosine affect the efficiency of protein-DNA CT? Will introduction of a cysteine in its place result in increased DNA-protein crosslinking as a result of DNA CT? Another interesting pattern is the large number of mutations in positively charged residues that map to the DNA-binding interface. Many of these residues are mutated to bulky aromatic residues. While these mutations could result in disrupted protein structure, they might also result in misalignment of the protein for efficient protein-DNA CT, formation of inappropriate radical intermediates, or increased DNA-protein crosslinking. In general, investigation of cancer-associated MutY variants may offer an important opportunity for our laboratory to learn more about the relationship between the metal center in these enzymes and impaired function *in vivo*.

Clearly, base-excision repair by glycosylase enzymes within the complex environment of a cell is a complicated process and the first step of damage detection by these enzymes within the genome is not well understood. The importance of this step in the repair pathway is highlighted by the growing body of evidence indicating that damage detection is likely the rate-limiting step for repair inside the cell (*19*). Thus, a better understanding of lesion recognition by DNA repair enzymes will not only allow us to understand how nature solves an exceedingly complex molecular recognition problem but it could also inspire more creative and effective therapeutic solutions for the problems that arise when DNA repair goes awry.

REFERENCES

1. Boon, E. M., Ceres, D. M., Drummond, T. G., Hill, M. G., and Barton, J. K. (2000) *Nat. Biotechnol. 18*, 1096.

2. Boal, A. K., and Barton, J. K. (2005) *Bioconjug. Chem. 16*, 312.

3. Boal, A.K., Yavin, E., Lukianova, O.A., O'Shea, V.L., David, S.S., and Barton, J.K. (2005) *Biochemistry 44*, 8397.

4. Gorodetsky, A. A., Boal, A. K., and Barton, J. K. (2006) *J. Am. Chem. Soc. 128*, 12082.

5. Gorodetsky, A. A., Dietrich, L. E., Lee, P. E., Demple, B., Newman, D. K., and Barton, J. K. (2008) *Proc. Natl. Acad. Sci. USA 105*, 3684.

6. Augustyn, K. E., Merino, E. J., and Barton, J. K. (2007) *Proc. Natl. Acad. Sci. USA 104*, 18907.

7. Boal, A. K., Genereux, J. C., Sontz, P. A., Gralnick, J. A., Newman, D. K., and Barton, J. K. (2008) (*submitted for publication*).

8. David, S. S., and Williams, S. D. (1998) *Chem. Rev. 98*, 1221.

9. Hinks, J. A., Evans, M. C. W., de Miguel, Y., Sartori, A. A., Jiricny, J., and Pearl, L. H. (2002) *J. Biol. Chem. 277*, 16936.

10. Rudolf, J., Makrantoni, V., Ingledew, W. J., Stark, M. J., and White, M. F. (2006) *Mol. Cell 23*, 801.

11. Gifford, C. M., and Wallace, S. S. (1999) *J. Bacteriol. 181*, 4223.

12. Gifford, C. M., and Wallace, S. S. (2000) *Nucleic Acids Res. 28*, 762.

13. Gralnick, J., and Downs, D. (2003) *J. Biol. Chem. 278*, 20708.

14. Jouanneau, Y., Jeong, H. S., Hugo, N., Meyer, C., and Willison, J. C. (1998) *Eur. J. Biochem. 251*, 54.

15. Curatti, L., Brown, C. S., Ludden, P. W., and Rubio, L. M. (2005) *Proc. Natl. Acad. Sci. USA 102*, 6291.

16. Fromme, J. C., and Verdine, G. L. (2003) *EMBO J. 22*, 3461.

17. Gray, H. B., and Winkler, J. R. (2005) *Proc. Natl. Acad. Sci. USA 102*, 3534.

18. Cheadle, J. P., and Sampson, J. R. (2007) *DNA Repair 6*, 274.

19. Livingston, A.L., O'Shea, V.L., Kim, T., Kool, E.T., and David, S.S. (2008) *Nat. Chem. Biol. 4*, 51.

APPENDIX I

Purification of Endonuclease III from *Escherichia coli*

INTRODUCTION

The procedures here are modified from those published previously (*1, 2*).

MATERIALS AND METHODS

Materials

JM101 *E. coli* stock was obtained from New England Biolabs and maintained as a 50% glycerol stock at -80°C thereafter. pNTH10 EndoIII expression vector was obtained from Prof. O'Connor at City of Hope (Duarte, CA) (*2*). All buffers and culture media were prepared using standard procedures and sterilized by autoclave or sterile filter techniques (*3*).

Transformation

JM101 was freshly transformed with pNTH10 prior to each protein preparation. JM101 cells were streaked from a freezer stock to Luria-Bertani (LB) agar and incubated at 37°C overnight. A 1 mL LB culture was started from a single colony and grown up overnight at 37°C. 50 μL of the starter culture was used to inoculate a 10 mL LB culture. This culture was grown to the appropriate density at 37°C and made competent according to standard procedures (*3*). pNTH10 was transformed by electroporation at 1.7 kV or heat shock at 42°C. Transformed cells were allowed to recover at 37°C for 0.75-2 hours. Transformants were selected by plating on LB+ampicillan (amp) (50 μg/mL) followed by overnight incubation at 37°C.

Expression Test

From a single colony of JM101/pNTH10, a 1 mL LB+amp (50 μg/mL) culture was grown overnight at 37°C. 50 μL of the starter culture was used to inoculate a 50 mL LB+amp (50 μg/mL) culture. This culture was grown to an OD_{600} ~ 0.6-0.8. Isopropyl-β-*D*-thiogalactopyranoside (IPTG) was added to induce protein expression (125 μL, 0.2 M IPTG stock). 1 mL aliquots were removed at 2, 4, 5, and 6 hours postinduction. Cells were pelleted from these aliquoted and the pellet was resuspended in water and 2X SDS-PAGE buffer (0.09M Tris-Cl, pH 6.8, 20% glycerol, 2% SDS, 0.05% bromophenol blue, 0.1 M DTT). These samples were loaded onto a 4-15% Tris-HCl gradient gel and electrophoresed for 35 minutes at 200V. Gel was stained for 1 hour with BioSafe Comassie (BioRad) stain, destained overnight in water, and imaged.

Large-Scale Expression

A 1 mL LB+amp (50 μg/mL) culture was started from a single JM101/pNTH10 colony and grown up overnight at 37°C. This culture was used to start a 500 mL LB+amp (50 μg/mL) which was grown up overnight at 37°C. 50 mLs of this culture was used to start a 1L LB+amp (50 μg/mL) culture. This 1L culture was grown shaking at 220 rpm at 37°C until it reached an OD_{600} of 0.6-0.8. IPTG was added to each liter (0.5 mLs, 1M IPTG stock) and the cultures were grown an additional 4-6 hours at 37°C. 1 mL aliquots were removed before induction and at the end of the 4-6 hour induction period. These were analyzed as described above for successful induction of protein expression. Cells were transferred to centrifuge bottles and centrifuged at 3000 rpm for 20 minutes at 4°C. Supernatant is discarded and the pellet is resuspended in wash buffer (10 mM Tris, pH 7-8, 100 mM NaCl, 1 mM EDTA) and centrifuged again. The

pellet may be stored temporarily at -20°C. A typical yield is ~5g cell pellet/L culture. A typical protein prep is usually 8-16 L.

Cell Lysis

Cells are thawed on ice and resuspended in lysis buffer (250 mM KCl, 50 mM Tris, pH 8.0, 0.5 mM EDTA, 5% glycerol, 10 mM β-mercaptoethanol) at 4X the wet weight of the cell pellet (i.e., 25g cells in 100 mL lysis buffer). Note that in later preparations, the β-mercaptoethanol was omitted from all buffers without any adverse effects. Lysozyme was added at a final concentration of 1 mg/mL and phenylmethylsulfonyl fluoride (PMSF) was added at a final concentration of 0.14 mM (stock is 50 mM in isopropanol prepared just prior to use). This mixture is incubated on ice for 15 minutes. DNaseI and RNaseA are added at final concentrations of 5 μg/mL and 10 μg/mL, respectively. Solutions are incubated a further 30 minutes at room temperature and then centrifuged at 4°C for 20 minutes at 15,000 rpm in an SS-34 rotor. The supernatant is retained and stored on ice. From this point on, all manipulations are performed at 4°C or on ice unless otherwise specified.

Anion Exchange Chromatography

Quanternary methylammonium (QMA) resin (Sigma) was used to remove excess nucleic acids from the cell lysate. A QMA column was equilibrated with QMA buffer (250 mM NaCl, 10 mM Tris-Cl, pH 7.5, 0.5 mM EDTA, 5 mM β-mercaptoethanol, and 5% glycerol). Lysate was loaded onto the column and all fractions containing protein were collected.

Dialysis

QMA fractions are pooled and loaded into 10,000 MWCO dialysis tubing (Pierce) and dialyzed in dialysis tubing against the cation exchange column loading buffer (150 mM NaCl, 10 mM Tris, pH 7.5, 0.1 mM EDTA, 5% glycerol) overnight.

Cation Exchange Chromatography

Sulfopropyl sepharose (SP) resin (Sigma) was used to perform the main purification step. The column volume used was 10% of the dialysate volume (i.e., if 300 mLs dialysate must be loaded, then a 30 mL column should be prepared). The SP resin was equilibrated with loading buffer and the dialysate was loaded onto the column. The loaded column was then rinsed with 5-10 column volumes loading buffer to remove any nonspecifically bound proteins. A gradient was run from 150 mM NaCl to 800 mM NaCl. All yellow bands were collected in 1-2 mL fractions.

Ammonium Sulfate Precipitation

SP column fractions were pooled in a beaker on ice over a stir plate. Ammonium sulfate was added to a final concentration of 1 g/mL (saturated) slowly over 20 minutes. The solution was stirred an additional 20 minutes on ice and then centrifuged at 15,000 rpm at 4°C for 30 minutes in an SS-34 rotor. Resulting pellet should be brown and the supernatant should be clear. Pellet was retained and resuspended in 1-3 mLs gel filtration loading buffer (1M NaCl, 10 mM Tris, pH 7.5, 0.5 mM EDTA, 10 mM β-mercaptoethanol).

Size Exclusion Chromatography

AcA54 resin (Sigma) was equilibrated with gel filtration loading buffer. The resuspended pellet from the previous step was loaded onto the AcA54 column and eluted with the loading buffer. All dark yellow fractions were retained. Purity was evaluated by SDS-PAGE (Figure A1.1).

Concentration and Storage

Protein solutions were concentrated by either reverse dialysis with polyethylene glycol (PEG) in gel filtration loading buffer or by Centriprep 10 (Amicon) devices. Concentrated solutions are dialyzed into storage buffer (20 mM sodium phosphate, pH 7.5, 100 mM NaCl, 1 mM EDTA, 20% glycerol) and stored in working aliquots at -80°C.

Summary

Figure A1.1 shows a representative SDS-PAGE gel after completion of the purification steps outlined here.

Figure A1.1. Purification of *E. coli* Endonuclease III.

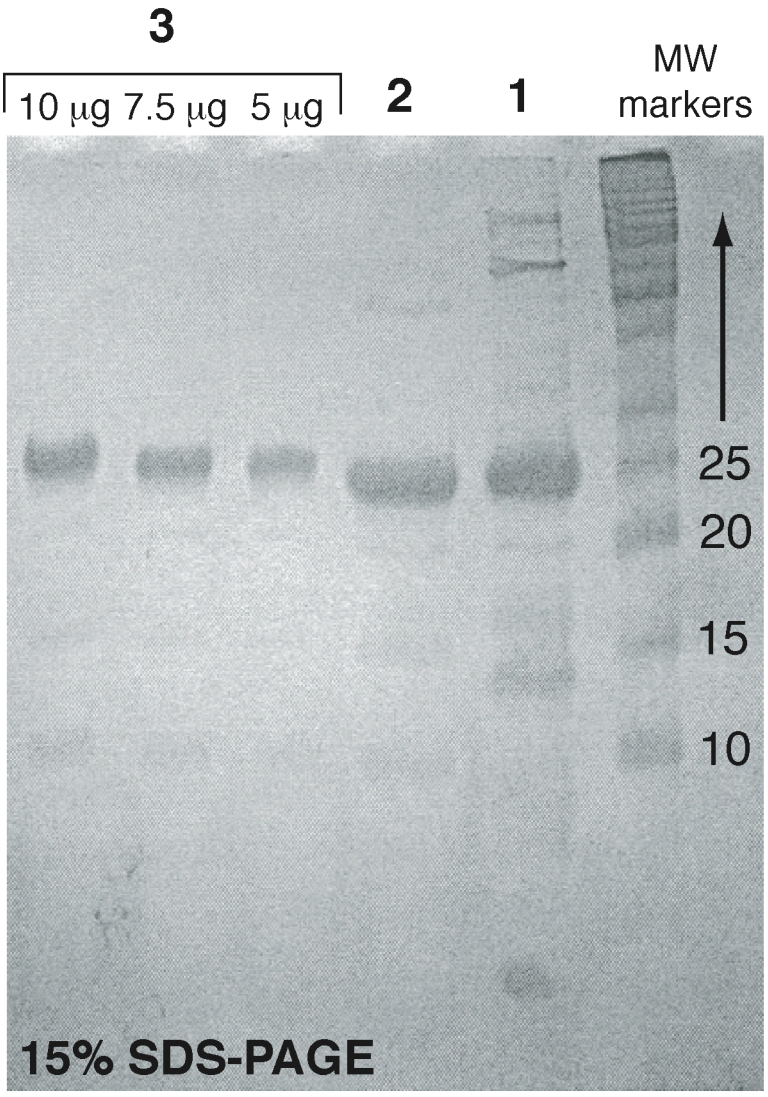

1. After Phosphoultrogel cation exchange column

2. After AcA54 size exclusion column

3. After concentration and dialysis (MWCO ~ 10,000)

Yield = 2 mLs of ~ 200 μM

12 L synthesis

REFERENCES

1. O'Connor, T.R. (1993) *Nucleic Acids Res*. *21*, 5561.

2. Boiteux, S., O'Connor, T. R., and Laval, J. (1987) *EMBO J. 6*, 3177.

3. Sambrook, J., and Russell, D. W. (2001) *Molecular Cloning: A Laboratory Manual* Cold Spring Harbor Laboratory Press, Cold Spring Harbor.

APPENDIX II

Inactivation of genes in *Escherichia coli*

INTRODUCTION

The methods described here are adapted from those published previously (*1*).

MATERIALS AND METHODS

Materials

The CC104 strain was obtained from Prof. Jeffrey Miller at UCLA (Los Angeles, CA), CC104 *mutY-* and CC104 *mutY-/mutM-* strains were obtained from Prof. Sheila David at UC Davis (Davis, CA), and the CC102 strain was obtained from the *E. coli* Genetic Stock Center at Yale University (New Haven, CT). pKD3, pKD4, and pKD46 were obtained from Prof. Dianne Newman at MIT (Boston, MA). Enzymes were purchased from New England Biolabs or Stratagene. All media and buffers were prepared according to standard procedures (*2*).

Generation of FRT-flanked Resistance Gene

Figure A2.1 shows the overall experimental strategy developed by Wanner *et al.* for gene inactivation in *E. coli*. Primers containing priming regions for amplification of pKD3 as well as sequences flanking the *nth* or *rnfA* region in *E. coli* were designed and these are shown in Table A2.1. These were purchased HPLC purified from Qiagen (or IDT) and dissolved in 10 mM Tris, pH 7.5 at a final concentration of 100 μM. These were used in a PCR reaction using purified pKD3 as the template where each reaction contained 85 μL sterile water, 10 μL *Pfu* buffer (Stratagene), 2 μL dNTPs, 0.5 μL each primer, 1 μL template, and 1 μL of a 9:1 mixture of *Taq* and *PfuTurbo* polymerases

Figure A2.1. Scheme for gene inactivation via the Wanner method.

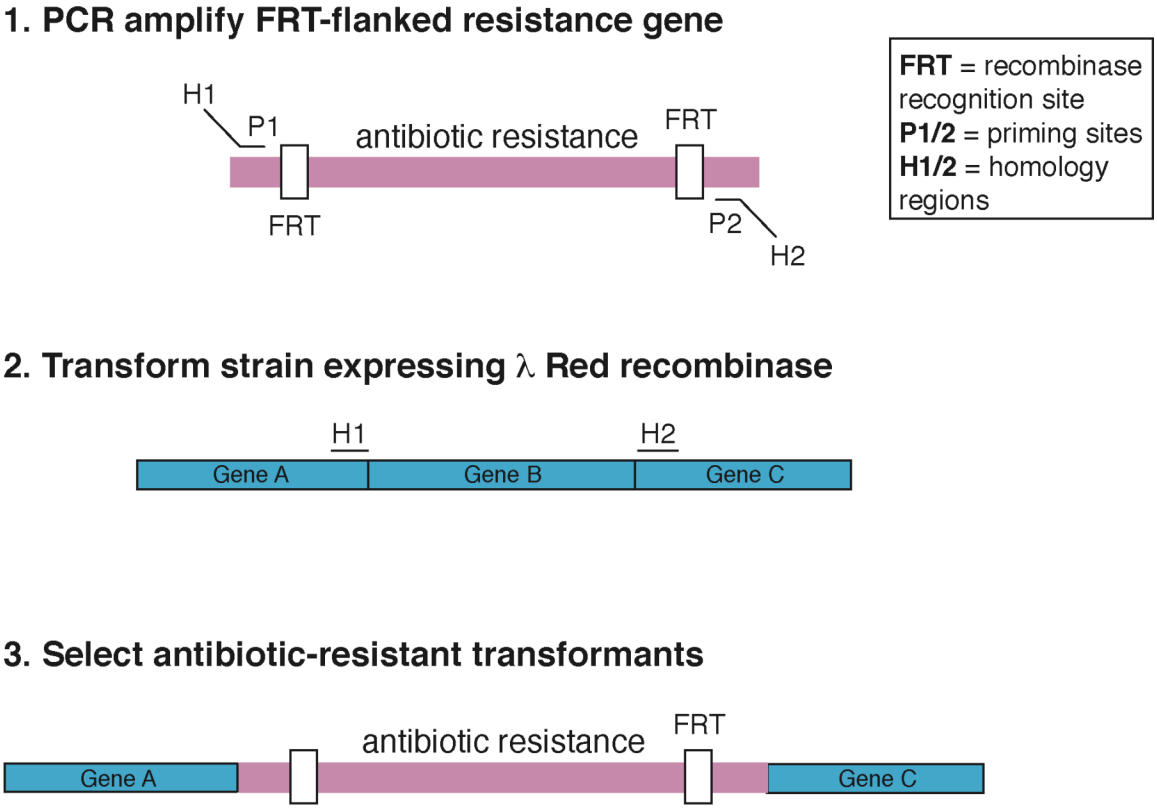

Table A2.1. Primers for Wanner inactivation of *nth* and *rnfA*.

Function	Primer Sequence
Wanner inactivation of *nth*	5'-gaagcagctgcagaacgtgcattgccaaacggtgaaacagggaatgtctg**gtgtaggctggagctgcttc**-3'
	5'-agaggataaagaaaggttatcaatggggtaatcggtgttacccctttttct**catatgaatatcctccttag**-3'
Wanner inactivation of *rnfA*	5'-ctgctctggattaacggataataggcggctttttttatttcaggccgaaaa**gtgtaggctggagctgcttc**-3'
	5'-cgccaggcccagcaggctcacggcggcaacggcaatccagatagcattca**catatgaatatcctccttag**-3'

(Stratagene). A standard 35 cycle PCR method was used with an annealing temperature of 50°C and an extension temperature of 72°C. Reaction products were loaded onto a 1.5% agarose gel and electrophoresed at 1.5 hours at 100V. Bands were excised and purified using a gel extraction kit (Qiagen). Samples were then treated with DpnI (1 μL in 50 μL total volume) for 1 hour at 37°C to remove any remaining template, purified with a QiaQuick kit (Qiagen), and concentrated.

Gene Inactivation

The target strain (CC104) was streaked to LB media and incubated overnight at 37°C. A 1 mL LB culture was started from a single colony and incubated overnight at 37°C. 200 μL of the starter culture was used to inoculate a 20 mL LB culture which was grown to OD_{600} ~ 0.4. The cells were harvested and made electrocompetent and transformed with pKD46. The transformed cells were recovered at 30°C in 1 mL LB for 3 hours. Transformants were selected on LB+amp (50 μg/mL) at 30°C. A 1 mL LB+amp (50 μg/mL) culture was grown overnight at 30°C. 200 μL of this starter culture was used to inoculate a 50 mL LB+amp (50 μg/mL) culture containing 20 mM arabinose to induce expression of the λ Red recombinase genes. Cultures were grown to OD_{600} ~ 0.4 at 30°C and harvested via centrifugation. Cells were made electrocompetent (*2*) and 15 μL of the FRT flanked resistance gene PCR product was transformed by electroporation at 2.5 kV. Cells were recovered in 1 mL LB for 3 hours at 37°C or 42°C. Recombinants were selected at on LB+kan (10 μg/mL) at 42°C. Any resulting colonies were restreaked to LB+kan and verified by colony PCR (Figure A2.2, A2.3).

Figure A2.2. PCR verification of *nth* inactivation in CC104 and CC104 *muty*-.

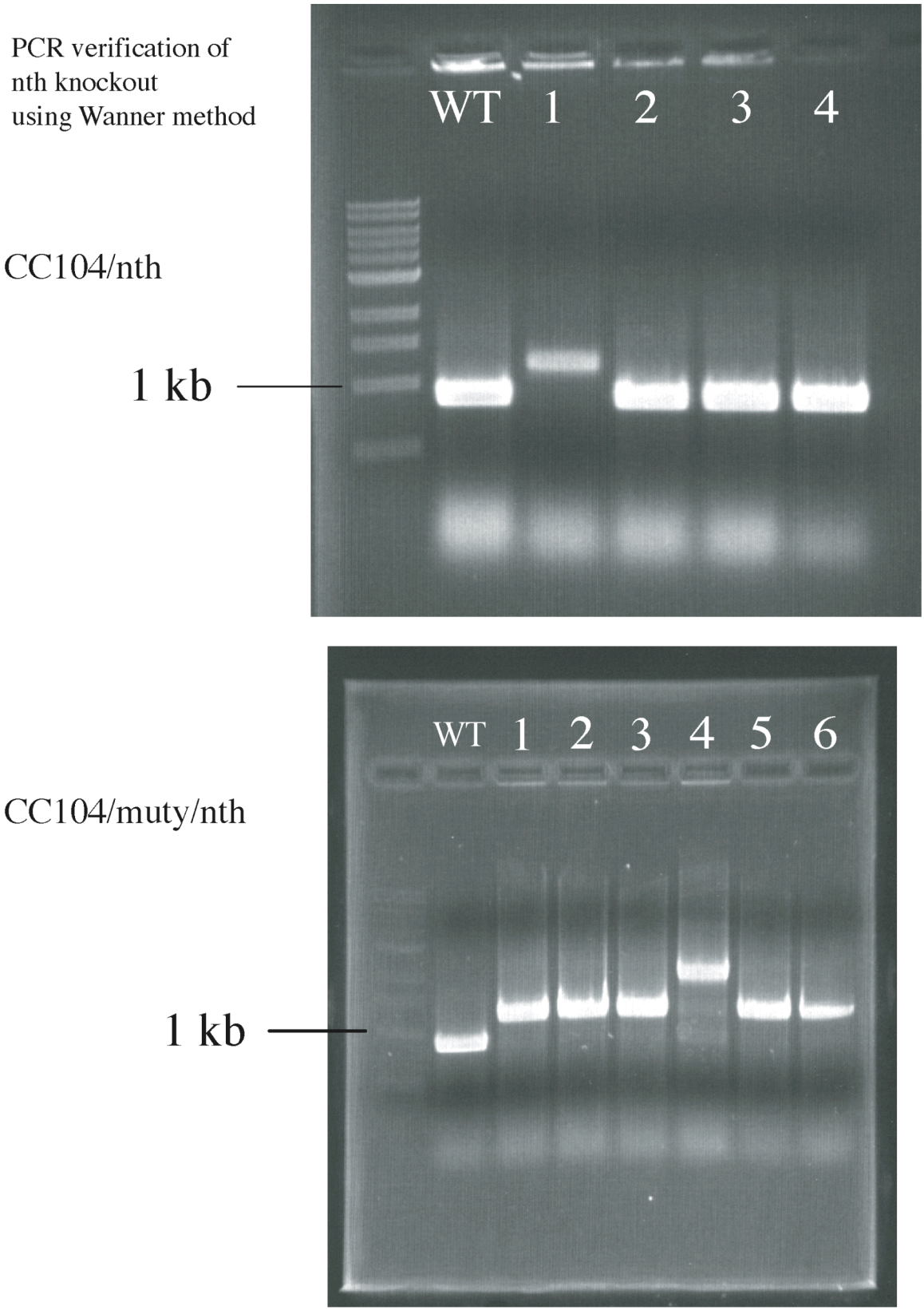

Figure A2.3. PCR verification of *rnfA* inactivation in CC102.

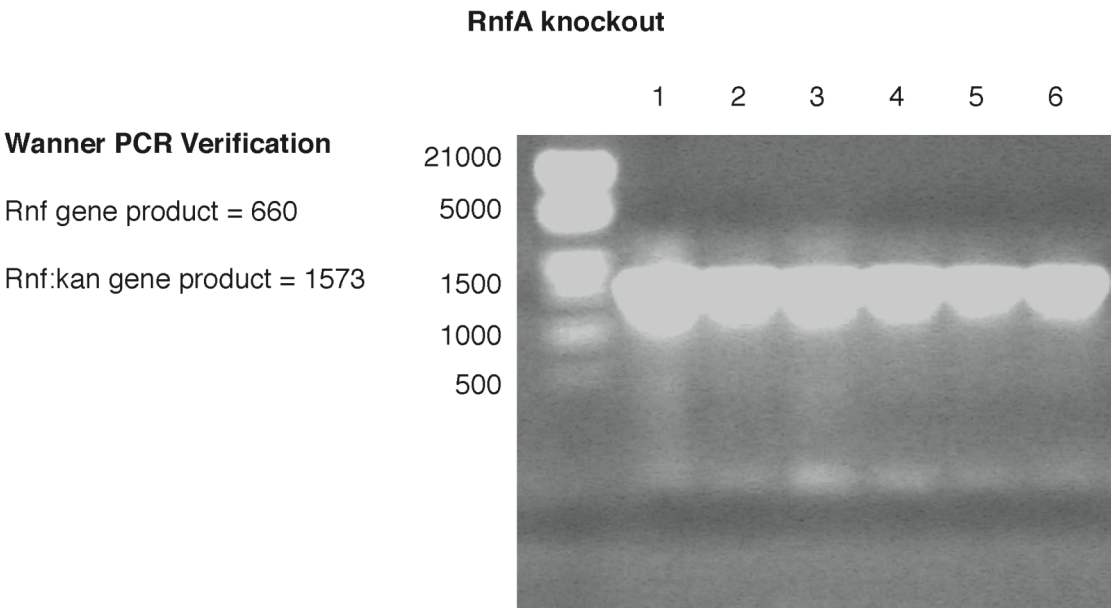

REFERENCES

1. Sambrook, J., and Russell, D. W. (2001) *Molecular Cloning: A Laboratory Manual* Cold Spring Harbor Laboratory Press, Cold Spring Harbor.

2. Datsenko, K. A., and Wanner, B. L. (2000) *Proc. Natl. Acad. Sci. USA 97*, 6640.